PNICTOGEN-ASSISTED SELF-ASSEMBLY OF ORGANIC MACROCYCLES, CAGES, AND CYCLOPHANES

by

TREVOR A. SHEAR

A DISSERTATION

Presented to the Department of Chemistry and Biochemistry
and the Division of Graduate Studies of the University of Oregon
in partial fulfillment of the requirements
for the degree of
Doctor of Philosophy

June 2021

DISSERTATION APPROVAL PAGE

Student: Trevor A. Shear

Title: Pnictogen-Assisted Self-Assembly of Organic Macrocycles, Cages, and Cyclophanes

This dissertation has been accepted and approved in partial fulfillment of the requirements for the Doctor of Philosophy degree in the Department of Chemistry and Biochemistry by:

Ramesh Jasti	Chairperson
Darren W. Johnson	Advisor
Michael Haley	Core Member
Benjamín Alemán	Institutional Representative

and

Andy Karduna	Interim Vice Provost for Graduate Studies

Original approval signatures are on file with the University of Oregon Division of Graduate Studies.

Degree awarded June 2021.

DISSERTATION ABSTRACT

Trevor A. Shear

Doctor of Philosophy

Department of Chemistry and Biochemistry

June 2021

Title: Pnictogen-Assisted Self-Assembly of Organic Macrocycles, Cages, and Cyclophanes

Cyclophanes are a venerable class of macrocyclic and cage compounds that often include unique properties owing to their unusual conformations and high strain. Due to these traits, synthesis of new, complex cyclophanes has remained difficult because of the need for harsh reaction conditions, difficult purification steps, and often resulting in low yields. Utilizing the error-correcting nature of dynamic covalent chemistry in conjunction with the directing ability of self-assembly, thiol-disulfide exchange has been used for the facile synthesis of discrete disulfide, thioether, sulfone, and hydrocarbon cyclophanes using pnictogen-assisted self-assembly. This dissertation expands on this synthetic method and explores its full capability in synthesizing a wide variety of new cyclophanes while using ‘design of experiments’ to quickly and efficiently optimize reaction conditions.

Chapter I is a review covering two key synthetic methods required for the formation of discrete disulfide cyclophanes: 1) the self-editing ability of dynamic covalent chemistry which often leads to the most stable thermodynamic products and 2) the use of self-assembly to form complex structures without outside manipulation. In Chapter II, the synthetic tolerance of this method to form disulfide cyclophanes with the

presence of reactive functional groups is explored. The utility of ‘design of experiments’ is also demonstrated by considerably increasing the yield of targeted cyclophanes from two different disulfide systems with minimal experimental effort. Chapter III discusses the discovery of a trithioorthoformate capped cage compound and its yield optimization. The utility of this pnictogen-assisted self-assembly method is fully explored in Chapter IV resulting in 21 new disulfide and thioether cyclophanes, ranging from large extended aromatic systems to linear alkene/alkyne to highly twisted heterocyclic spiro compounds. In Chapter V, the current synthetic progress towards disulfide and thioether perylene diimide cyclophane chromophores is discussed. Chapter VI includes conclusions and future directions of the project.

This dissertation includes co-authored material and previously published results.

CURRICULUM VITAE

NAME OF AUTHOR: Trevor A. Shear

GRADUATE AND UNDERGRADUATE SCHOOLS ATTENDED:

University of Oregon, Eugene, Oregon
Oregon State University, Corvallis, Oregon

DEGREES AWARDED:

Doctor of Philosophy, Chemistry, 2021, University of Oregon
Master of Science, Chemistry, 2017, University of Oregon
Bachelor of Science, Chemistry, 2016, Oregon State University

AREAS OF SPECIAL INTEREST:

Supramolecular Main Group Chemistry
Organic Chemistry
Polymer Chemistry

PROFESSIONAL EXPERIENCE:

Graduate Research Assistant, Department of Chemistry and Biochemistry
University of Oregon, Eugene, 2017-2021

Synthetic Chemist Intern, Cascade Chemistry, Eugene, 2019

Graduate Research Assistant, Los Alamos National Lab, Los Alamos, 2016-2017

Mass Spectrometry Lab Tech, Oregon State University, Corvallis, 2014-2016

GRANTS, AWARDS, AND HONORS:

National Science Foundation Graduate Research Fellow, 2018-2021

Knight Campus Transitioning Scholar Fellow, 2019-2021

PUBLICATIONS:

Shear, T. A.; Mayhugh, J. T.; Demachkie, I. S.; Zochhi, L. J.; Trubenstein, H. J.; Zakharov, L. N.; Johnson, D. W. *Angewandte Chemie International Edition* **2021**, manuscript in preparation.

Shear, T. A.; Johnson, D. *Synlett* **2021**, (AAM).

Shear, T. A.; Lin, F.; Zakharov, L. N.; Johnson, D. W. *Angewandte Chemie International Edition* **2020**, 59, (4), 1496-1500.

Patterson, B. M.; Kuettner, L.; Shear, T.; Henderson, K.; Herman, M. J.; Ionita, A.; Chawla, N.; Williams, J.; Sun, T.; Fezzaa, K. *Journal of Materials Science* **2020**, 55, 11353-11366.

Phan, N. M.; Shear, T. A.; Zakharov, L. N.; Johnson, D. W. *European Journal of Organic Chemistry* **2020**, 2020, (43), 6795-6800.

Collins, M. S.; Shear, T. A.; Smith, E. K.; Strain, S. M.; Zakharov, L. N.; Johnson, D. W. *Chemistry – A European Journal* **2019**, 25, (58), 13290-13293.

Lohrman, J. A.; Deng, C.-L.; Shear, T. A.; Zakharov, L. N.; Haley, M. M.; Johnson, D. W. *Chemical Communications* **2019**, 55, (13), 1919-1922.

ACKNOWLEDGMENTS

As my time here in graduate school comes to an end, I find myself reflecting on the accomplishments I have achieved and the people who helped me get here. I only now realize it took an army. First, I would like to thank Prof. Darren W. Johnson for being an outstanding mentor and guide during my time at the University of Oregon. Darren took a chance on me after I returned from completing my Master of Science in Chemistry through the Knight Campus Graduate Internship Program, allowing me to directly join his lab and start my PhD, for which I will be forever grateful. Darren has set an excellent example for me and every graduate student around him on how to be an outstanding leader. It was an honor to work with him during my graduate career and I am grateful to have made a lifelong friend in the process.

I would also like to thank the wonderful professors and leadership I have met along the way. Prof. Ramesh Jasti and Prof. Michael Haley, thank you for providing me with great feedback and guidance whenever I need it. Prof. Benjamín Alemán, thank you for agreeing to be my outside member. Stacey York and Lynde Ritzow, thank you for all the amazing opportunities you have given me access too and believing in my abilities as a scientist. To Dr. Brian Patterson, thank you so much for your mentorship during my time at Los Alamos National Lab.

Without the support of the amazing facility managers, I would not have been nearly as successful as I have been. Dr. Nanette Jarenwattananon, thank you for all your help with me NMR questions and guidance on complex problems. Dr. Lev Zakharov, aka “The Crystal Wizard”, thank you for using your expect knowledge and providing me with all my crystallographic needs.

I would like to thank all past and current members of our lab. First, I would like to deeply thank Dr. Ngoc Minh Phan who immediately took me under her wing and taught me the basics of synthetic organic chemistry. I also would like to thank all the lab members who have been instrumental to my success through stimulating scientific conversations and hours of laughter: Thaís de Faría, Hazel Fargher, Dr. Jess Lorhman, Jordan Levine, Hannah Bates, Kiana Kawamura, Jacob Mayhugh, Henery Trubenstein, Bella Demachkie, and Jeremy Bard. You are all dear friends to me and working through graduate school would not have been possible without all your support.

Most of all, I want to thank my family. Since the start of my schooling, my mother has been my biggest supporter. Without her help, I wouldn't be where I am today and I can't say how grateful I am for her. Right behind my mother from day one has always been my grandparents. They've always encouraged me to follow me dreams, no matter how crazy they were or where they took me. I've always sought their advice and know that I wouldn't be the man I am today without their love and support.

Lastly, to my wonderful, amazing, loving, caring, and especially patient wife. You've always encouraged me to chase my dreams and you've never once hesitated or tried to stop me, and for that I will be forever grateful. You've always been there for me, through the good and bad, the ups and downs, supporting me in every way without complaint. You've made more sacrifices than I can count so that I could follow my aspirations and I only hope that I can do the same for you. I couldn't ask for a better partner in life and can't wait to see what the future holds for us. Love you always.

TABLE OF CONTENTS

Chapter Page

Chapter Page

Chapter Page

Chapter Page

LIST OF FIGURES

Figure Page

CHAPTER III

Figure Page

Figure Page

LIST OF TABLES

LIST OF SCHEMES

Scheme Page

CHAPTER III

CHAPTER V

CHAPTER VI

CHAPTER I

PNICTOGEN-ASSISTED SELF-ASSEMBLY OF ORGANIC MACROCYCLES, CAGES, AND CYCLOPHANES

Contributions

This dissertation describes the pnictogen-assisted self-assembly of organic macrocycles, cages and cyclophanes. Chapter I introduces the significance of supramolecular chemistry, dynamic covalent chemistry, and self-assembly. The history and current state of the Darren W. Johnson laboratory research is also discussed. This manuscript was requested and published in *Synlett*.[1] Prof. Darren W. Johnson provided intellectual input and editorial feedback.

Introduction to Dynamic Covalent Chemistry

Through the contributions of Cram, Lehn, and Pedersen in the field of molecular recognition, for which they were awarded the 1987 Nobel Prize in Chemistry, the groundwork for supramolecular chemistry was laid. Supramolecular chemistry studies the chemistry beyond the singular molecule; it looks at the behavior and utilization of non-covalent intramolecular interactions. Through these non-covalent interactions, large and complex structures can easily be formed and is the basis for many biological and material science applications. Subsequently, taking this dynamic principle back down to the molecular level, dynamic covalent chemistry (DCC) emerged. While supramolecular chemistry is complex at scales beyond the single molecule, DCC is a powerful process

that allows for the formation and breaking of chemical bonds within molecules, establishing the most thermodynamically stable products of the system (Figure 1.1).[2] The facile reversibility of these covalent bonds led to the exploration of new types of building blocks and gave rise to dynamic combinatorial libraries (DCL), where dynamic covalent interactions are used to form libraries of compounds.[3]

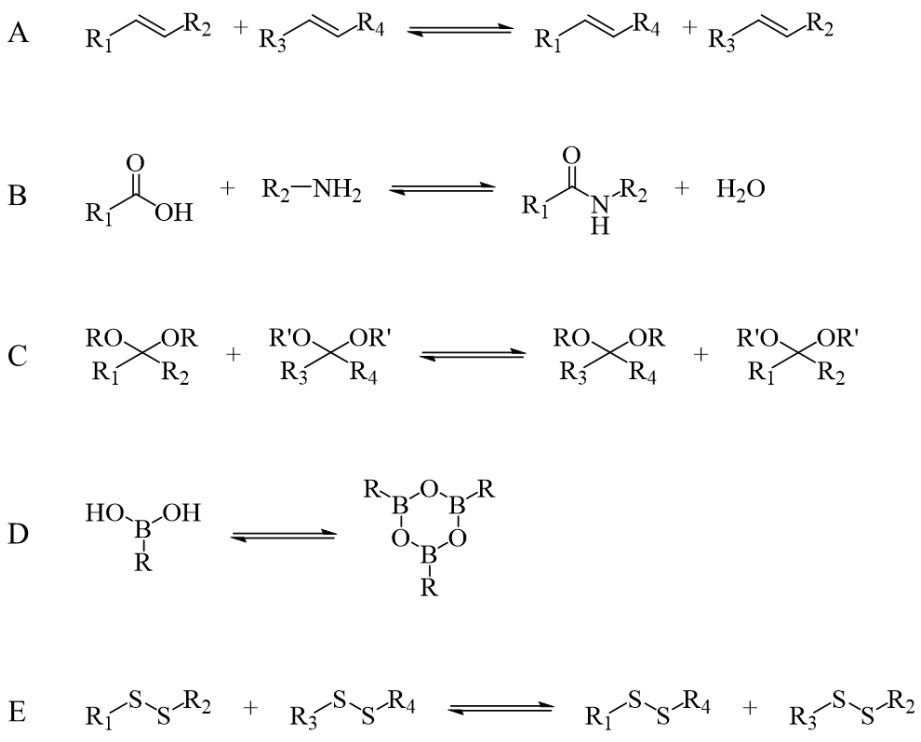

Figure 1.1: Selected examples of dynamic covalent reactions, including A) olefin metathesis, B) amide formation/exchange, C) acetal formation/exchange, D) boronic acid condensation, and E) disulfide exchange.

The reversibility, and thereby product formation, of DCC reactions can be affected in many different ways and is often dependent on the local chemical environment (i.e., solvent, temperature, concentration, light, metal ions, pH, etc.). Typically, the minimum energy path over an activation barrier is responsible for the formation or breaking of the chemical bond while the relative energy barriers in opposite

directions account for the forward and reverse reaction rates.[4] Ideally, DCC reactions occur under thermodynamic control, and the distribution of possible products is a result of their relative thermodynamic stabilities at equilibria. However, there are often 'kinetic traps' that occur which result in non-dynamic members, such as insoluble oligomers and polymers (Figure 1.2).

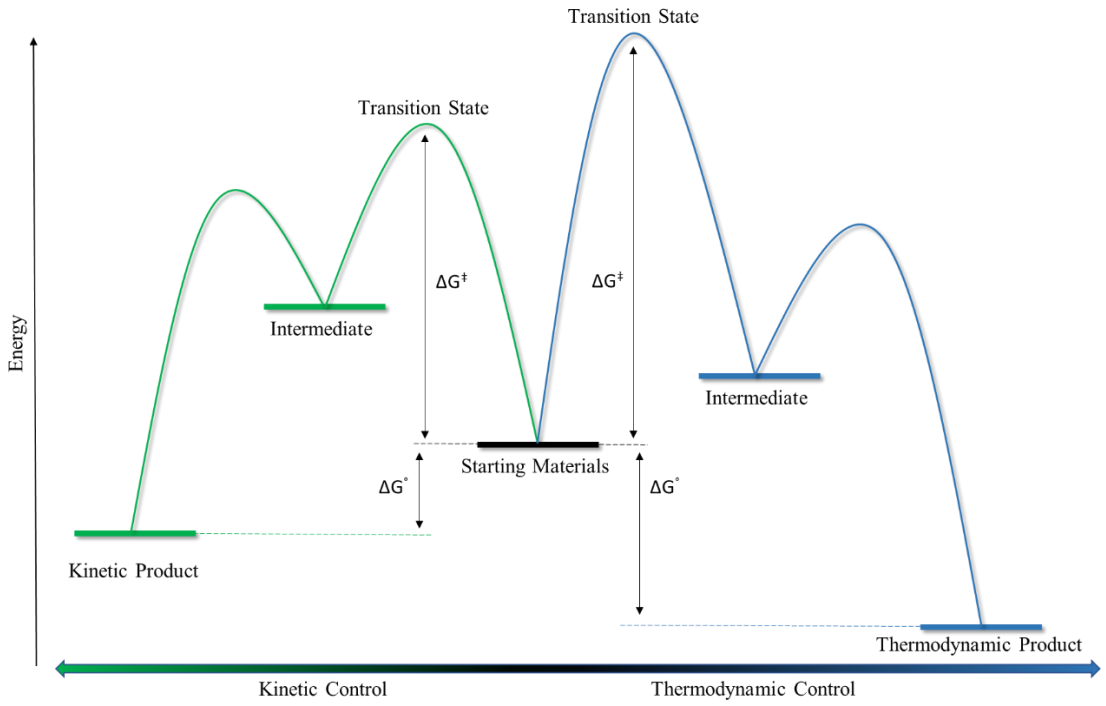

Figure 1.2: Reaction coordinate diagram representing a kinetic and thermodynamic path of a given reaction. Initial formation of kinetic intermediates (green) will occur due to the lower activation barrier ($\Delta G^{\ddagger}$). If the reaction proceeds via DCC, the intermediates will tend to equilibrate towards the global minimum with the lowest overall Gibb's free energy ($\Delta G°$) resulting in the thermodynamic product (blue).

To avoid these traps, building blocks are thoughtfully chosen to help avoid irreversible bond formation/precipitation and ensure free exchange between members of the library. One such functional group is the thiol-disulfide bond, which is of significant interest to the DCC community due to its highly reversible nature and its ubiquity

throughout biological systems. In proteins, the disulfide bridge of the cystine residue plays an important role in oxidative protein folding which lowers the unfolded entropy of the tertiary and quaternary structure.[5] If these disulfide bonds do not form correctly or undergo intramolecular shuffling due to external stimuli, incorrect protein folding can occur, leading to improper function.[6]

However, the use of thiol-disulfide exchange in DCC has allowed for the formation of complex libraries of new macrocycles. For example, in 2012 Sanders *et. al.* produced a stereoselective molecular trefoil knot using disulfide bonds in high yield.[7] The building blocks were comprised of three hydrophobic and electron-deficient naphthalenediimide (NDI) groups connected via a flexible amino acid spacer (L-β-alanine) and terminated at both ends with a thiol (L-cysteine).

The synthesis of the resulting DCL was achieved in water under basic conditions, utilizing the hydrophobic nature of the NDI core while still using the pendant carboxylate anions for water solubility. This reaction yielded three main products: a monomer, dimer, and the trefoil trimer. Under initial conditions (1mM dithiol) the monomer and dimer dominated product formation. However, when the concentration was increased (5mM), the trefoil knot yield increased dramatically, and when the solvent polarity was increased with various salts, the trefoil knot yield was near quantitative (Figure 1.3A). These results were the consequence of two principles: hydrophobic effects and thiol-disulfide exchange within an equilibrating DCC system.

The inherent hydrophobic character of the NDI core has a thermodynamic driving force to be isolated from water as efficiently as possible while keeping the hydrophilic side chains exposed to the aqueous environment (Figure 1.3B). This leads to a dramatic

increase in formation of the knot when the dithiol concentration is increased (Le Chatelier's principle) and the polarity of the water is increased and why very little to none of the un-knotted macrocyclic trimer is formed. The authors reported that full oxidation was achieved after only four hours, indicating that kinetic pathways may play an important role in this. They showed via LC-MS that intermediate macrocycles and oligomers form and break during the early stages of oxidation and shows the conversion of these species into the trefoil knot, which can maximize hydrophobic stabilization. This fast thiol-disulfide interchange essentially stops once the knot is formed; once the knot is formed, cleavage of a disulfide bond would rapidly re-close due to the unfavorability and slow unfolding and re-exposure of the hydrophobic cores (Figure 1.3C). Due to these mechanisms, the authors conclude that the trefoil knot is not only thermodynamically favorable, but kinetically preferred as well. This study showcases the facile synthesis of a complex disulfide structure using DCC and has also inspired additional research.[8]

The use of DCC to form complex structures is not limited to thiol-disulfide exchange. The "proof reading" ability of DCC through repeated bond breaking and forming allows for unfavorable side products to be re-introduced to the reaction and maximize product yield. These types of syntheses can be further enhanced by external stimuli, templates, or careful starting material design to selectively produce a single, targeted structure. Thus, many functional motifs, such as cyclobenzoins,[9] orthoesters,[10] imines,[11] and alkynes[12] have been investigated to expand this toolkit in the synthesis of large, complex structures.

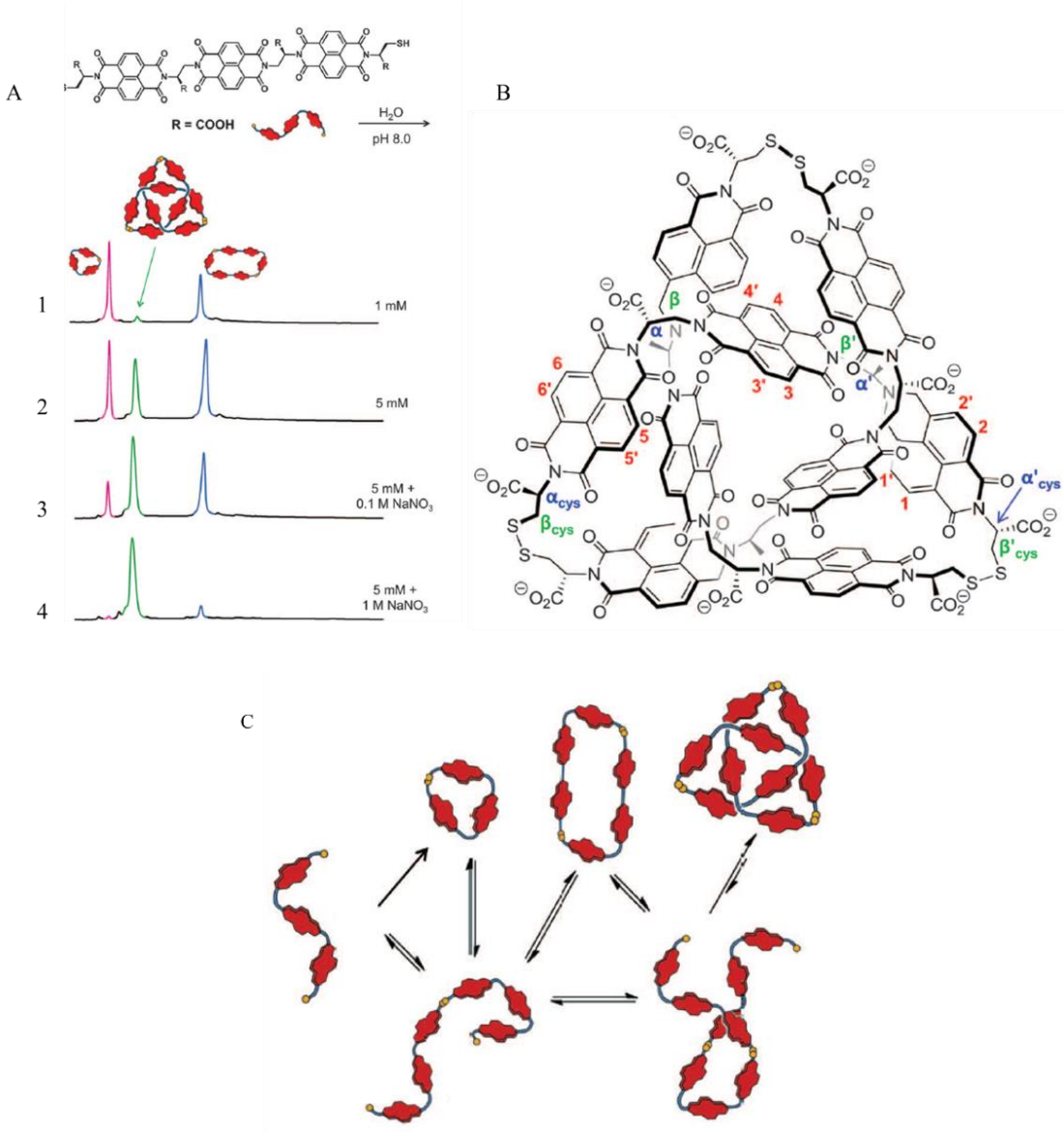

Figure 1.3: Selected example of DCC, forming a trefoil knot. A) Library analysis at 1mM and 5mM dithiol concentrations (1 and 2) and in the presence 0.1M and 1M concentration of $NaNO_3$ (3 and 4). B) Chemical structure of the trefoil knot. C) Proposed mechanism of the DCC equilibrium with the trefoil knot as the end thermodynamic product. From *Science* **2012**, 338, (6108), 783-785. Reprinted with permission from AAAS.

Introduction to Self-Assembly in Supramolecular Chemistry

As a complementary tool to DCC in the synthesis of large structures, self-assembly lends itself as a powerful ally. Self-assembly is the process by which a disordered system comprised of simple building blocks comes together to form large aggregates without the need for outside interaction or assistance. The interactions that allow for this spontaneous process to occur are predominantly non-covalent in nature, involving van der Waals, hydrophobic and electrostatic forces as well as hydrogen and coordination bonds.[13] Nature has used self-assembly to a masterful degree. For example, the ds-DNA found in all organisms is based around the double-helix formation, which is self-assembled with extremely high specificity by two individual strands of DNA and is bound together with hydrogen bonds (Figure 1.4A).[14] Phospholipid bilayers are another great example of self-assembly in biological systems. The two-layered structure is self-assembled using the hydrophobic effect, where the hydrophobic tails point internally to be secluded from water and the hydrophilic heads point externally for solvation by the aqueous environment to form the double-layer structure (Figure 1.4B).[15]

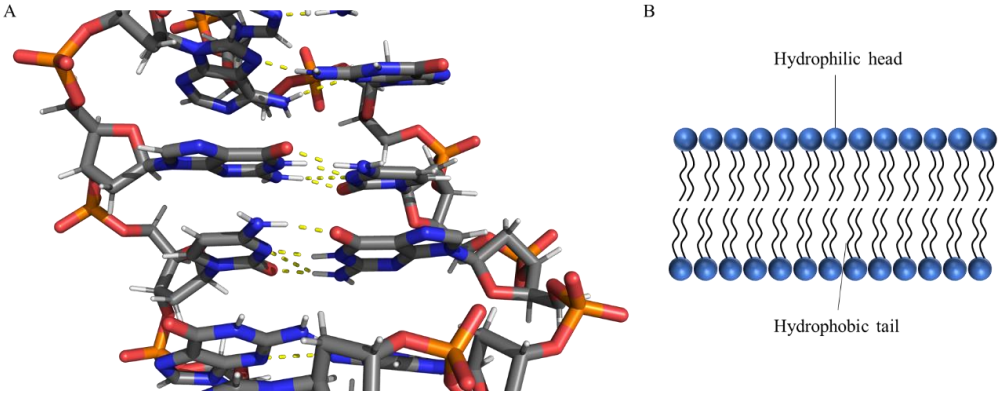

Figure 1.4: Selected natural self-assembled systems. A) DNA double helix formed via hydrogen bonding between adjacent base pairs. B) Phospholipid bilayer assembled through the hydrophobic effect. DNA image adapted from NDB 1D69.

In an attempt to mimic nature's ability to self-assemble complex systems, chemists usually use ligands that are coordinated to a metal center because of the inherently dynamic property of metal-ligand bonds.[16] Transition metals also have the added benefit of being able to predict how they will self-assemble based on their well-defined coordination geometries. For example, a 3D prismatic cage consisting of six $(PEt_3)_2Pt(OTf)_2$ vertices and three bis(pyrrolo)tetrathiafulvalene side walls was constructed under mild conditions (Figure 1.5A).[17] This reaction was shown to go to completion within two hours, forming the cage as the single product and demonstrated host/guest binding abilities with electron-poor guests.

In another report, the synthesis of an anion binding cryptand ($M(Et_2CNS_2)_3$) was achieved using octahedrally coordinating metals (Fe, Co, and Ni) and a dithiocarbamate complex containing secondary diamines (Figure 1.5B).[18] This structure showed an affinity to binding multiple anions, including Cl^-, OBz^-, HSO_4^-, and $H_2PO_4^-$. Other recent impressive supramolecular metal-assisted self-assembled structures include a truncated tetrahedron containing platinum vertices and hexapyridyl walls with a 1 nm inner cavity,[19] a bimetallic molecular ball with a diameter of 3 nm,[20] and a chiral nano-capsule that is formed from 24 carboxylate ligands and 18 lanthanum ions,[21] among numerous other examples.[22]

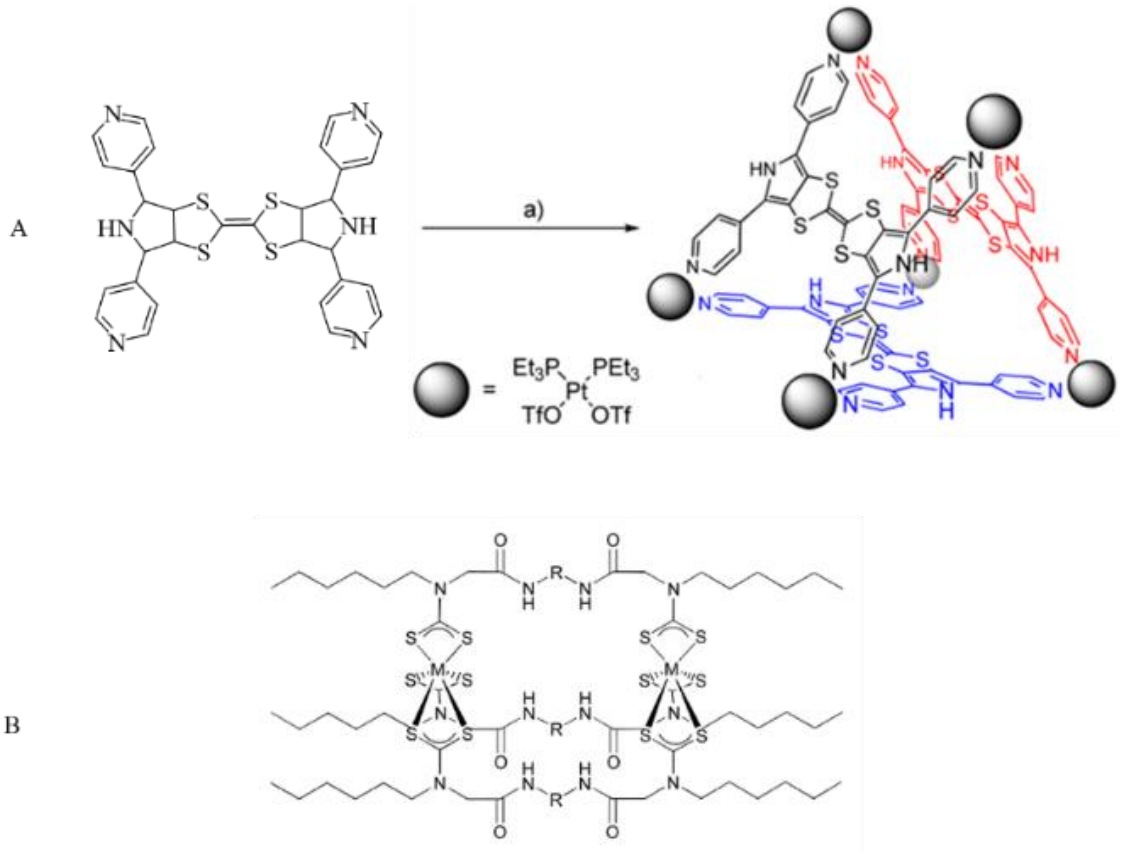

Figure 1.5: Selected studies using metal-assisted self-assembly to form complex structures including A) 3D prismatic cage and B) an anion binding cryptand. A) Reproduced from *J. Am. Chem. Soc.* **2012**, 134, (29), 11968-11970 with permission from the American Chemical Society. B) Reproduced from *Chem. Commun.* **2003**, (19), 2408-2409 with permission from the Royal Society of Chemistry.

Introduction to Pnictogen-Assisted Self-Assembly of Organic Macrocycles, Cages, and Cyclophanes

Although there are many examples of metal-organic motifs that utilize transition metals with common coordination geometries to form 2D and 3D structures, the use of metals and metalloids with more flexible coordination geometries had been far less explored.[23] This difficulty is what first inspired the Darren W. Johnson (DWJ) laboratory to begin exploring synthetic methods of pnictogen (Pn)-containing macrocycles and cages. Our first metalloid-cryptand to be synthesized was the As^{III}-thiolate-containing

As_2L_3 metallacryptand **2**.[24] This metalloid was chosen because of (i) its rather unusual tripodal coordination geometry (featuring a stereochemically active lone pair on As), and (ii) from a desire to make a targeted chelator for the highly toxic As^{III} ion.[25] Using the known affinity of thiolates towards As^{III}, dithiol **1** and $AsCl_3$ were reacted with KOH to form the cryptand **2** (Scheme 1.1).

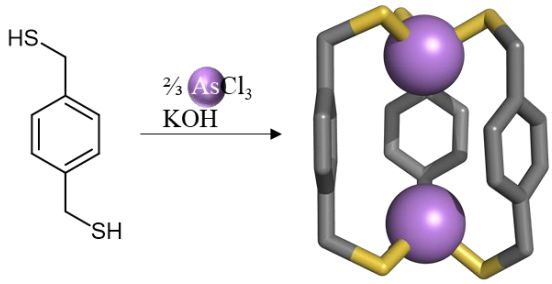

1 **2**

Scheme 1.1: Synthesis of an arsenic(III)-thiolate complex by the reaction of 1 in the presence of AsCl3 and a base to form the cryptand 2 (single crystal XRD)

To probe this chemistry further, arene-extended 1,4-dimercaptomethylnaphthalene **$H_2$3** was treated with a base and $AsCl_3$, $SbCl_3$, or $BiCl_3$ to form the corresponding homomeric-Pn_2L_3 and heteromeric-$Pn_1Pn'L_3$ metallacryptands. Scheme 1.2 showcases our group's approach to pnictogen-directed self-assembly in the context of dithiol **$H_2$3**.[26]

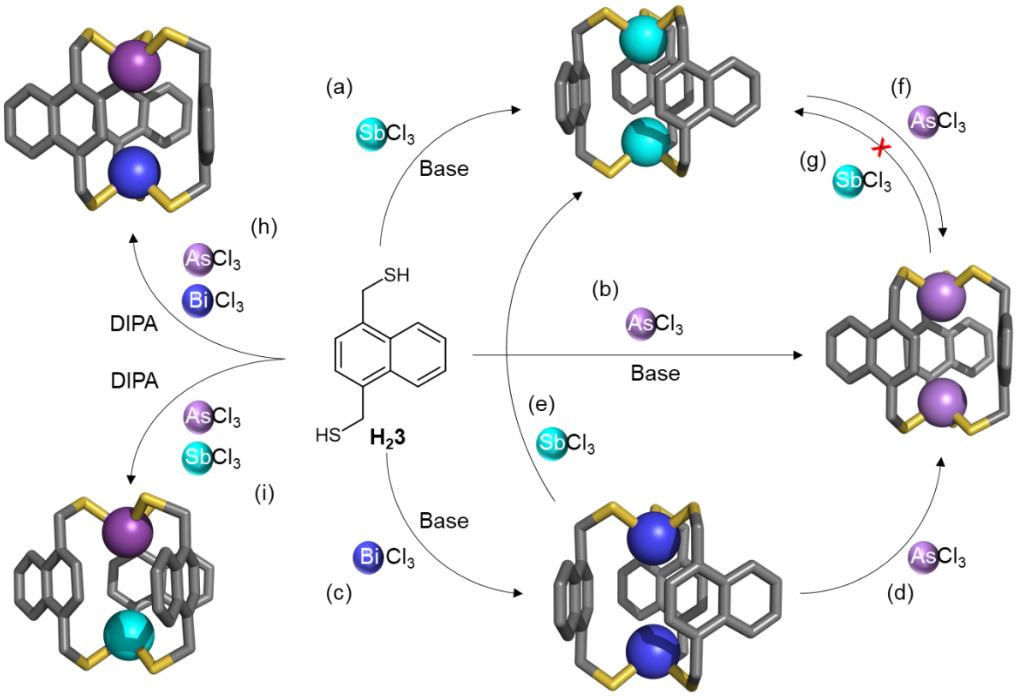

Scheme 1.2: Synthesis of homo- and heterometallacryptands. Treatment of dithiol **3** with $PnCl_3$ (Pn = As, Sb, Bi) and a base provides the homometallacryptands: (a) Sb_2L_3, (b) As_2L_3, and (c) Bi_2L_3. The cryptand Bi_2L_3 (d, e) can then undergo transmetalation to form As_2L_3 and Sb_2L_3, while Sb_2L_3 (f, g) can be converted into As_2L_3, however, the reverse process does not occur. Heterometallacryptands (h, i) are formed by treating **3** with excess $AsCl_3$, diisopropylamine (DIPA) and either $SbCl_3$ or $BiCl_3$. All structures shown were confirmed by single-crystal XRD.

While investigating the reactivity of these Pn-cryptands and their related 1,5- and 2,6-dimercaptomethylnaphthalene isomers, we stumbled upon a vial containing 1,5-dimercaptomethylnaphthalene and $AsCl_3$ that had been open to air for over a year, in which rather nice single crystals had grown fortuitously. Analysis revealed that the compound present was a trimeric tris-disulfide species **4** (Scheme 1.3), which we believe had formed via the slow oxidation of the As_2L_3 type cryptand.[27] This was surprising since previous studies had shown the As_2L_3 cryptands to be fairly stable to a variety of oxidizing conditions, including TFA in refluxing $CHCl_3$ (open to air) and even hydrogen peroxide in $CHCl_3$. This crystal structure encouraged us to reinvestigate the issue of

oxidation in these main group assemblies. Hypothesizing that the poor solubility of the peroxide oxidizing agent could have led to reduced reactivity, *m*-CPBA in $CHCl_3$ was treated with compound **2**, but this led to complex mixtures of many insoluble products. However, with crystals of **4** in hand—from what we assumed to be quite mild oxidizing conditions—we still sought to pursue an understanding around the formation of this disulfide macrocycle from our metallacryptands. Therefore, we began to explore additional oxidizing agents to provide a facile route towards new disulfide macrocycles and cages.

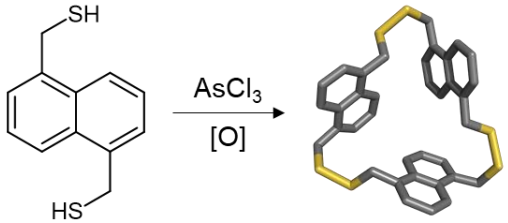

4

Scheme 1.3: Structural confirmation of **4** via single-crystal XRD provided our first evidence that disulfide macrocycles could be formed via oxidative processes using simple dithiols in the presence of a pnictogen trichloride.

Spurred on by this initial discovery, preassembled As^{III} cryptands were synthesized using dithiol **1** and were intentionally oxidized.[28] The cryptand **2** was shown to be very reactive with chemical oxidants such as NBS, DDQ, m-CPBA and peroxide, leading to complex mixtures of insoluble oligomers and polymers. However, when I_2 was used as the oxidizing species, clean conversion into a series of discrete disulfide macrocycles was observed; a dimer, trimer, and tetramer were the dominant products (Scheme 1.4). Surprisingly, we discovered that using preassembled arsenic cryptands was not even required for this reaction to proceed: simply reacting a pnictogen trichloride ($AsCl_3$ or less toxic $SbCl_3$), a dithiol, and I_2 in a single pot led to rapid, discrete disulfide

macrocycle formation in high yields. While the oxidation of thiols using I_2 is well known,[29] oxidation of such dithiols usually leads to predominantly oligomeric and polymeric products with macrocyclic species being a minor side product. Additionally, our method appeared to enable facile synthesis of the macrocyclic disulfide trimer and tetramer, which would be more challenging species to synthesize using traditional stepwise methods.

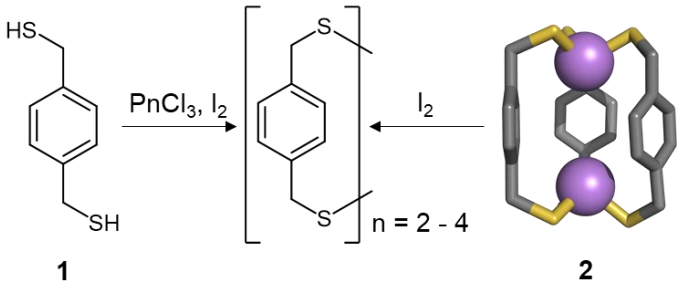

Scheme 1.4: Pnictogen-assisted oxidation of **1** or **2** cleanly form discrete disulfide species. Pn = As or Sb.

The finding that these macrocycles could be easily formed in a one-pot reaction in minutes was a big leap for us in developing our self-assembly strategy for forming disulfide macrocycles. These disulfide structures are also precursors to well-known thiacyclophanes and hydrocarbon cyclophanes, which encouraged us to pursue the scope of these reactions as a route to new and hard-to-make cyclophanes. Previous methods to access cyclophanes often require high dilution and/or extreme temperatures. Usually, statistical homocoupling reactions such as Wurtz or McMurry couplings[30] are used, resulting in a mixture of oligomers and polymers. The Wittig reaction[31] has also been employed to make macrocycles, but still relies on unfavorable thermodynamic ring formation steps. While these reactions have been successful in preparing a variety of

interesting macrocycles, they often provide low yields, limited selectivity, low functional group tolerance and/or require difficult purification.

In contrast, the directing behavior of the metal[32] or metalloid[33] in these disulfide formation reactions enables targeted synthesis of thermodynamically favorable disulfide macrocycles rather than the competing kinetic polymeric products. This self-assembly approach has allowed the facile, one-pot synthesis of several motifs of new discrete disulfide products, ranging from small and strained macrocycles to more complex 3D cages, in high yields under mild reaction conditions.

Using this synthetic method, we have accessed a variety of disulfide assemblies, exemplified by the structures shown in Figure 1.6. Syntheses of these disulfide macrocycles result in varying sized assemblies, depending on the starting reaction conditions, from a single-pot reaction.[33] Separation of each discrete macrocycle is easily and cleanly achieved using size exclusion chromatography (SEC). Traditional silica gel column chromatography can also be used, but due to the very similar polarity of each macrocycle, this method is sometimes more difficult.

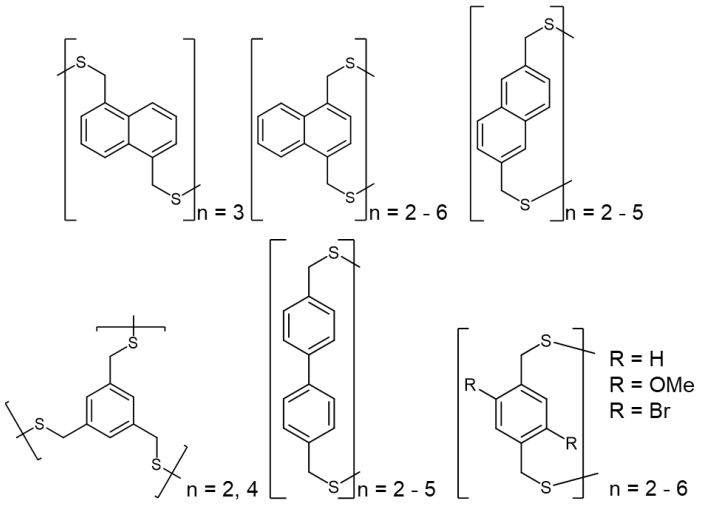

Figure 1.6: Selected cyclophanes synthesized by our lab resulting in 2D, 3D and functionalizable disulfide macrocycles.

More complex, 3D cage-like macrocycles were also found to be easily formed with this new method by using a 3-fold symmetric trithiol such as **5** (Scheme 1.5). Through the self-assembly of **5**, the resulting disulfide dimer **6** and tetrahedron **7** are readily formed in high yield. Fortunately, all disulfide macrocycles synthesized through this method have been shown to undergo sulfur extrusion on treatment with hexamethylphosphoroustriamide (HMPT) at ambient temperature, resulting in the more kinetically stable thioether derivatives. Perhaps surprisingly, even complex hexakis-disulfide cage **7** undergoes this sulfur extrusion reaction, which requires the extrusion of six sulfur atoms, representing 24 bonds broken/formed in a single step at ambient temperature, resulting in the corresponding tetrathioether in 94% yield.[33]

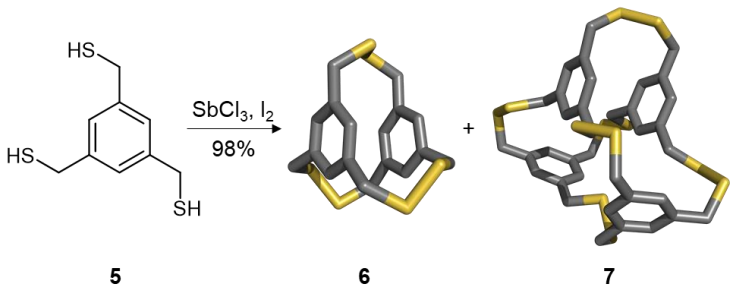

Scheme 1.5: Synthesis of more complex 3D cage-like structures are possible. The trithiol **5** is readily oxidized to form the 3-fold symmetric dimer **6** and the more complex tetrahedron **7**, both confirmed via single crystal XRD.

To further explore the scope of this synthetic method in providing access to difficult to synthesize macrocycles, a biphenyl dithiol and **1** were reacted together (Scheme 1.6).[34] This should lead to a statistical mixture of both symmetrical (narcissistic sorting) and unsymmetrical (social sorting) macrocycles. However, using oxidation with $SbCl_3$ and I_2, we have shown that it was possible to bias the reaction beyond what is statistically expected, readily forming the unsymmetrical macrocycles in good yields

(AAB and BBA in Scheme 1.6). Subsequent sulfur extrusion with HMPT yielded the expected unsymmetrical thioethers. In addition, we have shown that these thioethers can then be converted into new hydrocarbon cyclophanes using photochemical sulfur extrusion to provide two new unsymmetrical macrocyclic congeners of [2,2,2]paracyclophane featuring both a combination of phenyl and biphenyl bridges.

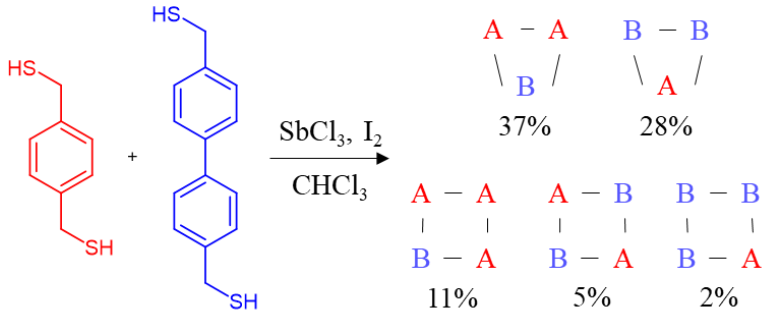

Scheme 1.6: Synthesis of symmetric and unsymmetric macrocycles.

Bridge to Chapter II

Chapter I reviewed the complementary process of dynamic covalent chemistry and self-assembly and their importance within supramolecular chemistry. We reviewed an example of a disulfide connected trefoil knot being constructed under DCC by taking advantage of on the hydrophobic inner NDI units and hydrophilic carboxylate side chains. Chapter I also covered a number of examples of self-assembly, from highly selective formation of the DNA double helix to a chiral nano-capsule containing 24 carboxylate ligands and 18 lanthanum ions. Capitalizing on these principles, we highlighted how the DWJ lab used pnictogen directing agents to form homo- and heterometallacryptands and their subsequent mild oxidation using I_2 to form discrete disulfide macrocycles, including self-sorting systems. In Chapter II, the functionalization

of discrete disulfide macrocycles is shown, including the use of ‘design of experiments’ to dramatically increase the yield of a targeted species that is difficult to synthesize using traditional methods.

CHAPTER II

'DESIGN OF EXPERIMENTS' AS A METHOD TO OPTIMIZE DYNAMIC DISULFIDE ASSEMBLIES, CAGES, AND FUNCTIONALIZABLE MACROCYCLES

Contributions

This chapter presents the synthesis and characterization of functionalizable macrocycles and the use of 'design of experiments' (DOE) in the optimization of specific macrocycles from multiple self-assembling systems. This co-authored work was published in *Angewandte Chemie International Edition*.[1] Dr. Fuding Lin provided editorial assistance in writing the explanation of how DOE works and is used. Dr. Lev N. Zakharov performed X-ray crystallography. Prof. Darren W. Johnson provided intellectual input and editorial feedback. I carried out all experimentation, characterization, and DOE analysis and execution. I also co-authored majority of the manuscript.

Introduction

The use of metalloid-directed self-assembly and dynamic covalent chemistry (DCC) within the field of supramolecular chemistry has facilitated the synthesis of many complex molecular structures from relatively simple starting materials.[2] Typically, these types of reactions use complementary building blocks that utilize structural functionality to assist in their self-assembly. These types of interactions can include hydrogen bonding,[3] π-stacking,[4] and metal-ligand bonds.[5] Ideally, these systems have a strong

enthalpic driving force and low kinetic barriers, resulting in high yields with low side-product formation.

However, synthesis of complex supramolecular structures is not always so straight forward; many self-assembly reactions end up in 'kinetic traps' and result in undesired oligomer and polymer formation. These traps can be avoided by incorporating the inherent 'proofreading' of DCC, enabled through reversable covalent bonding, allowing these types of systems to auto-correct any thermodynamically unfavorable products.[6] This effect can be further improved by the use metalloid-assisted self-assembly which allows for thermodynamic control of product formation, while further avoiding undesired kinetic pathways which often lead to oligomer and polymer formation.[7]

Within our laboratory, we utilize these two synthetic tools by using a pnictogen additive (usually Sb^{3+}) and di/tri-thiols to form strained disulfide cyclophanes species. Initial discovery of this method was obtained during the investigation of arsenic-thiolate self-assembled complexes, specifically 1,5-naphthalenedimethanethiol (**1**) was being used to form the arsenic-thiolate complex.[8] Serendipitously, it was discovered that in the presence of an oxidating agent, the arsenic complex would readily oxidize into discrete disulfide bridged macrocycles (**2**) (Scheme 2.1). Since this discovery, it has been shown that formation of the arsenic complex is not a prerequisite for macrocycle formation and we routinely oxidize thiol building blocks directly to macrocycles during I_2 in the presence of Sb^{3+}.

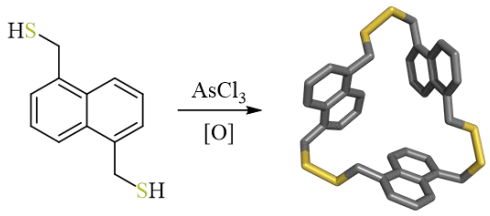

1 2

Scheme 2.1: Structural confirmation of **2** via single-crystal XRD provided first evidence of oxidative macrocyclic disulfide formation in the presence of a pnictogen tri-chloride. Hydrogens have been removed for clarity.

Capitalizing on the principles of self-assembly and DCC, it is possible to influence product distribution of these discrete mixtures by carefully altering the chemical environment by utilizing properties such as host-guest chemistry,[9] external stimuli,[10] and concentration effects.[6b] However, with a multitude of potentially important factors in any chemical reaction, an exhaustive approach of all possible experimental properties would be very difficult, if not impossible. Herein, we report the synthesis of new, functionalizable macrocycles and the optimization of chemical conditions using DOE to greatly increase the yield of an otherwise trace species in half the required experimental runs had a traditional approach been used.

Results and Discussion

Synthesis of new disulfide, thioether, and sulfone macrocycles containing reactive functional groups

Previously, our laboratory has shown that mixtures of discrete disulfide macrocycles of varying sizes are readily formed using a di/tri-thiol in the presence of an oxidizing agent (I_2) and a pnictogen additive (As^{3+} or Sb^{3+}).[11] This is in stark contrast to the typical oligomer and polymer formation that is observed when only an oxidizing

agent and base are used to prepare macrocyclic disulfides, providing a facile route to form the desired disulfides. However, up until now, our method had only been tested on relatively stable starting materials where the risk for side reactivity was low. To probe our approach further and to test its compatibility with more reactive functional groups, 1,4-dibromo-2,5-bis(mercaptomethyl)benzene (**H_2L**) was used to form discrete disulfide macrocycles. This material was chosen due to the reactive bromoarene structure not only allowing for the compatibility testing of our method with reactive functional groups, but this would also give us a handle for more post-synthetic modification via Suzuki-Miyaura and related cross-couplings, if desired.

Satisfyingly, the metalloid-assisted self-assembly was shown to be quite tolerant of the reactive bromoarenes and readily formed a mixture of discrete disulfide macrocycles; dimer (**L_2^1**), trimer (**L_3^1**), tetramer (**L_4^1**), pentamer (**L_5^1**) all formed in combined 83% yield with no oligomer or polymer present (Scheme 2.2). As with many self-assembly systems, these reactions were done under dilute conditions (2 – 5 mM), with **L_2^1** formation dominating (65% relative yield) while **L_3^1**, which is more difficult to synthesize using traditional methods, was obtained in a 15% relative yield.

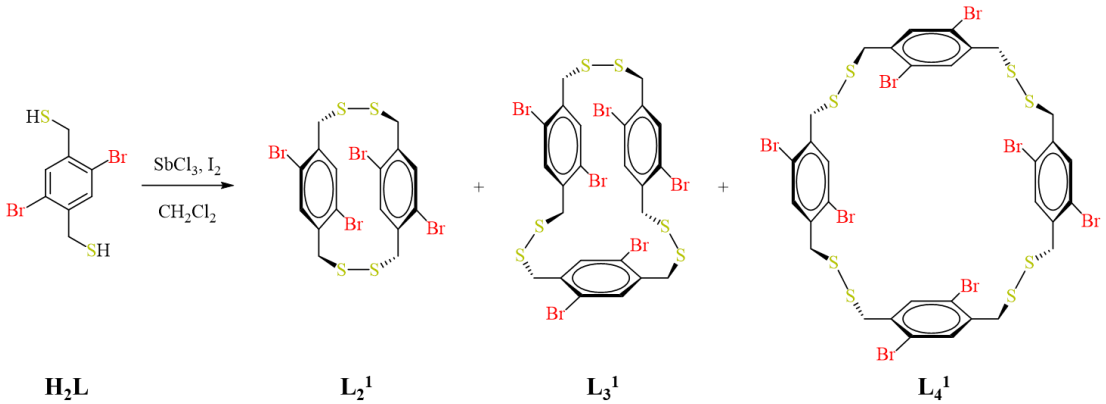

H_2L **L_2^1** **L_3^1** **L_4^1**

Scheme 2.2: Pnictogen-assisted self-assembly of **H_2L** to form functionalizable disulfide macrocycles: dimer (**L_2^1**), trimer (**L_3^1**), tetramer (**L_4^1**) (pentamer **L_5^1** are not shown).

Analysis of $\mathbf{L_2^1}$ with ^{1}H-NMR spectroscopy indicated that the macrocycles formed with two possible conformations: one with an eclipsed arylbromide conformation and one with a staggered conformation. Due to the confined nature of $\mathbf{L_2^1}$, the pendant bromines are unable to freely rotate through the inner cavity at room temperature, giving rise to two different AB quartets for the methylene protons for each conformation. However, variable-temperature ^{1}H-NMR showed that at 25 °C, the relative ratio of staggered to eclipsed is 4:1, which increases to 6:1 at 125 °C (Figure 2.1). Interestingly, the eclipsed conformation is not always present in each experimental run; this leads to the conclusion that this conformation is likely a kinetically trapped product and is a result of the local chemical environment.

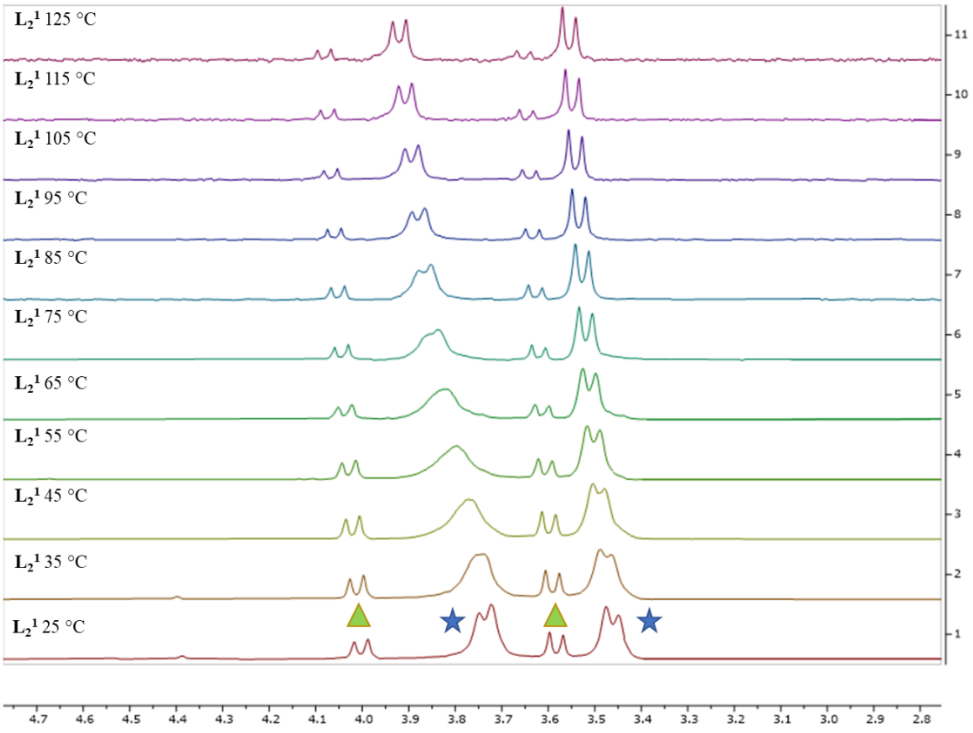

Figure 2.1: Variable-temperature ^{1}H NMR of $\mathbf{L_2^1}$. Staggered conformation (blue stars) and eclipsed conformation (green triangles) increase from 4:1 ratio at 25° C to 6:1 at 125 °C. NMR study was conducted in 1,1,2,2-tetrachloroethane-d_2.

X-ray quality crystals of $\mathbf{L_2^1}$ were grown by slow evaporation in $CHCl_3$ and only showed the staggered conformation present which crystallizes in the *Pbca* space group. The C-S-S-C disulfide dihedral angles diverge considerably from ideality (90°), taking on highly strained disulfide bond angles (C-S-S-C ∡'s: 116°, 117°, Figure 2.2, A).[12] After performing a review of the Cambridge Structural Database (CSD) for similar disulfide dihedral bond angles, only 15 structures were found to have angles ≥ 115°, highlighting the ability of this facile route to provide quite strained disulfide macrocycles in high yield. The interplanar distance between the aryl rings is 3.66 Å, which may provide favorable, stabilizing transannular π-π interactions. Crystals of $\mathbf{L_3^1}$ were also grown from slow evaporation in $CHCl_3$, crystallizing in the *P*-1 space group. Unlike the dimer, only the dihedral C-S-S-C angle that bridges the sandwiched aryl rings deviated from ideality (C-S-S-C ∡'s: 88°, 91°, 114°, Figure 2.2, B).

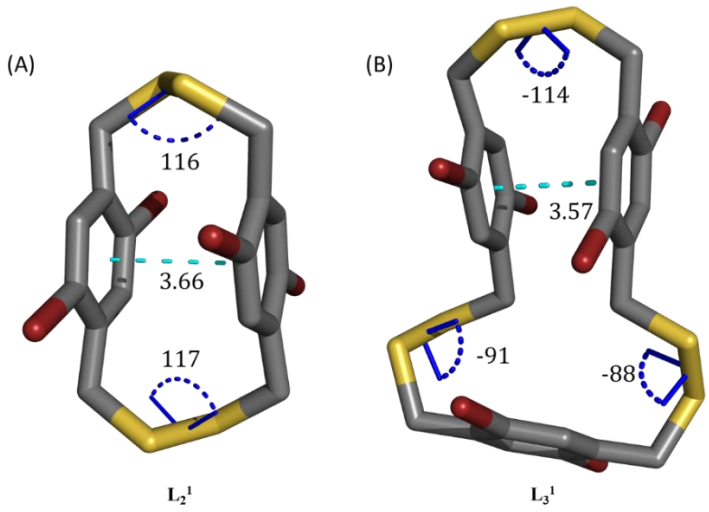

Figure 2.2: (A) Single-crystal XRD reveals the highly strained nature of $\mathbf{L_2^1}$ as can be seen in the associated disulfide dihedral angles (blue). (B) $\mathbf{L_3^1}$ also shows one disulfide dihedral angle that adopts a highly strained conformation. Stabilization via transannular π-π interactions between adjacent C_6-rings may assist in the formation of these compounds. Hydrogens have been removed for clarity.

Sulfur extrusion of $\mathbf{L_2^1}$ and $\mathbf{L_3^1}$ was then performed using hexamethylphosphoroustriamide (HMPT) in chloroform, resulting in thiacyclophanes $\mathbf{L_2^2}$ (dimer) and $\mathbf{L_3^2}$ (trimer) in quantitative yield (Scheme 2.3). Both compounds were purified with SEC to remove any residual phosphine oxide/sulfide present after aqueous workup. Analysis of $\mathbf{L_2^2}$ with ^{1}H-NMR showed no eclipsed conformation present in any experimental run due to reordering into the staggered conformation, which is more thermodynamically favorable, during sulfur extrusion. X-ray quality crystals of $\mathbf{L_2^2}$ and $\mathbf{L_3^2}$ were both grown from slow evaporation in $CHCl_3$. $\mathbf{L_2^2}$ crystallizes in the *C*1*c*1 space group and in the solid state assumes a *cis* C-S-C bond conformation rather than the expected *trans* conformation and aligns with ideal bond angles for this bond connectivity (ideal: 103°, C-S-C ∢'s: 101°, 103°, Figure 2.3, A). Increasing transannular π-π interactions were also observed by a decrease in distance of the two aryl rings to 3.26 Å. $\mathbf{L_3^2}$ crystallizes in the $P2_1/n$ space group and showed all C-S-C bond angles aligned with ideality and the two parallel aryl rings had moved from a sandwiched to a parallel displacement conformation (C-S-C ∢'s: 100°, 100°, 98°, Figure 2.3, B).

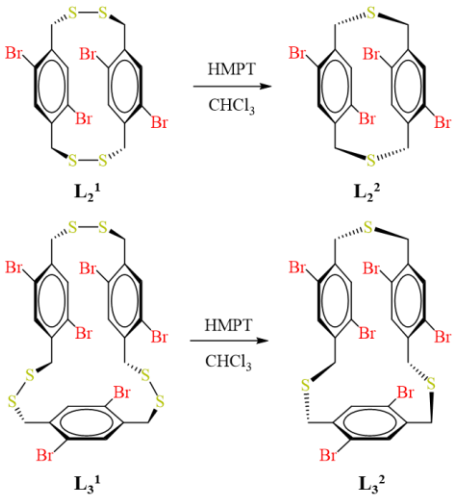

Scheme 2.3: Synthesis of functionalizable thiacyclophanes $\mathbf{L_2^2}$ (dimer) and $\mathbf{L_3^2}$ (trimer) via sulfur extrusion using hexamethylphosphous triamide.

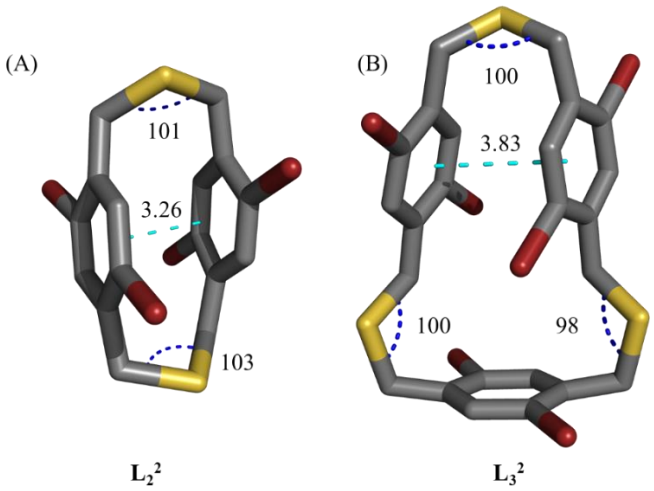

L_2^2 L_3^2

Figure 2.3: (A) Single-crystal XRD of $\mathbf{L_2^2}$ shows the *cis*-conformation of the thioether bonds, which align closely with ideality (blue) and increased transannular π-π interactions shown by a reduction in spacing between the aryl rings (teal). (B) $\mathbf{L_3^2}$ also shows thioether bond angles that align with ideality (blue) with a decrease in transannular π-π interactions due to an increase in spacing between the parallel aryl rings (teal). Hydrogens have been removed for clarity.

The thiacyclophanes were then treated with *meta*-chloroperoxybenzoic acid resulting in the corresponding sulfones $\mathbf{L_2^3}$ (dimer) and $\mathbf{L_3^3}$ (trimer) in quantitative yields (Scheme 2.4).

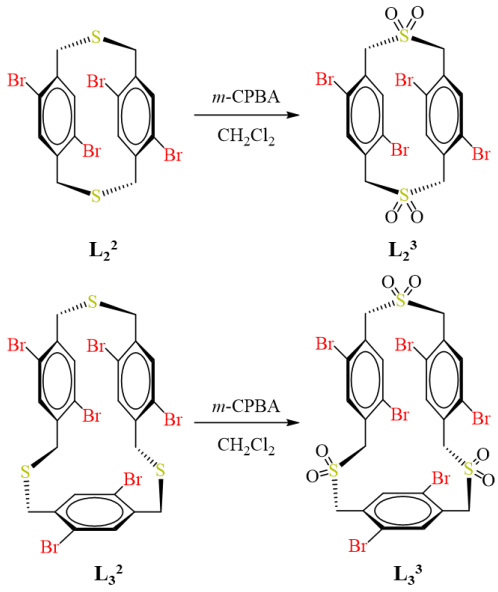

L_2^2 L_2^3 L_3^2 L_3^3

Scheme 2.4: Thiacyclophane oxidation using *meta*- chloroperoxybenzoic acid to form sulfone dimer ($\mathbf{L_2^3}$) and trimer ($\mathbf{L_3^3}$).

Crystals of $\mathbf{L_2^3}$ were grown from slow evaporation in CH_2Cl_2 and it crystallizes in the *C*2/*c* space group with two symmetrically independent molecules. Due to the strained nature of $\mathbf{L_2^3}$, the Br···O distance (3.21 Å ± 0.021 Å) is less than the sum of their van der Waals radii (3.37 Å), resulting in steric repulsion and as a consequence, the C-SO_2-C bond angles (C-SO_2-C ∡'s: $\mathbf{L_2^2{}_1}$: 109°, 109° $\mathbf{L_2^2{}_2}$**:** 109°, 111°, Figure 2.4, A) deviate from ideality (106°). Surveying the CSD for similar C-SO_2-C bond angles of 110° ± 5° revealed that $\mathbf{L_2^3}$ matched and exceeded the largest bond angle of this type yet recorded (109°). The Br···O interaction has two further consequences on the molecule: the repulsion causes the arylbromides, that would normally be 180° from the aryl rings, to lay out of planarity by 175° ± 1.3° and causes the C_6-rings to deviate from planarity as well (9.4° ± 3.7°, Figure 2.4, B). Slow evaporation in $CHCl_3$ provided X-ray crystals of $\mathbf{L_3^3}$ which crystallizes in the *P*1 space group with three symmetrically independent molecules and $CHCl_3$ solvent molecule. These retain the parallel displacement of the aryl rings with an increased distance of 4.18 Å, 4.52 Å, and 4.53 Å, respectively for each independent molecule. The C-SO_2-C bond angles also deviated from ideality, again due to the Br···O repulsion (C-SO_2-C ∡'s: $\mathbf{L_3^3{}_1}$: 102°, 104°, 108° $\mathbf{L_3^3{}_2}$: 103°, 105°, 110° $\mathbf{L_3^3{}_3}$: 103°, 107°, 105°, Figure 2.6).

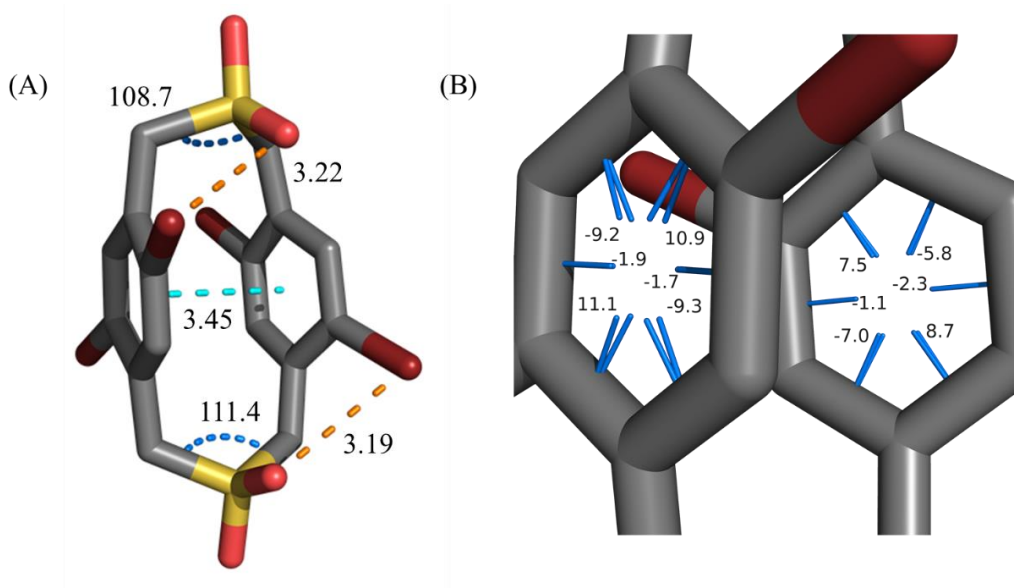

Figure 2.4: (A) Single-crystal XRD structure of $\mathbf{L_2^3}$ reveals its highly strained nature. The Br···O distance is less than the sum of their van de Waals radii (orange), resulting in highly strained C-SO_2-C bond angles (blue). Compared to $\mathbf{L_2^1}$ (the disulfide precursor), the transannular π-π distance has further decreased (teal), likely helping to increase the relative stability of the structure. (B) As a consequence of the Br···O steric repulsion, the C_6-rings have bent out of planarity considerably (blue). Hydrogens have been removed for clarity.

These distinctive structural features serve to underscore the utility of this synthetic method to synthesize highly strained macrocycles quickly, easily, and in high yield. Initially, strained disulfides can be generated through metalloid-assisted self-assembly then more highly strained macrocycles can be kinetically trapped via sulfur extrusion and/or oxidation. Additionally, these new macrocycles containing multiple reactive bromine functional groups proves the ability of this method to generate high overall yields while tolerating such motifs and provides a path toward a wide breadth of possible post-synthetic modifications.

Use of 'Design of Experiments' to optimize the yield of targeted macrocycles from a discrete mixture

It is well understood that DCC occurs under thermodynamic control with the most stable product dominating.[6b] Considering this, it's not surprising that the dimeric species ($\mathbf{L_2^1}$) would be the dominate product under our standard reaction conditions. However, it has been shown that by altering the chemical environment it is possible to bias the reaction to form products in high yields that would otherwise form in trace amounts.[11, 13] With this in mind, we sought to optimize reaction conditions to maximize the yield of $\mathbf{L_3^1}$ selectively and intentionally. This target molecule was chosen due to the difficulty of synthesis using traditional disulfide synthetic strategies. The use of DOE was employed due to the ability to screen multiple factors, including multi-factor interactions, quickly and efficiently on their impact on $\mathbf{L_3^1}$ formation.

DOE is a method of systematically probing how the effects of different factors within a process affect the outcome. Traditionally, scientists would probe how factors affect an outcome by consecutively varying one factor at a time while holding the rest constant which is known as a full factorial approach. This is intrinsically inefficient and makes discovering multi-factor interactions quite difficult. DOE avoids this by using a fractional factorial approach where all possible combinations, or a statistically useful portion, of factors are investigated simultaneously. This approach allows for not only the investigation of each factor by itself but also multi-factor interactions where the effect of one factor is dependent on the effect of another.[14] Inaccurate results can also be highlighted using DOE by revealing any factors that may be aliased, which is when the effect of one factor is affected by other factor(s). While there are numerous factors that

can influence the results of any experiment, we chose to focus our efforts on the impact of five factors that was thought to be the most impactful on thermodynamic product distribution: dithiol concentration, I_2 equivalents, $SbCl_3$ equivalents, solvent, and temperature.[11, 15]

With five factors at two levels (Table 2.1), a ½ factorial DOE with resolution V was used to reduce the number of required runs from 32, had a full factorial been used, down to 16.

Table 2.1: Full-scale DOE for $\mathbf{L_3^1}$ using 5-factors at 2-levels.

Factor	Role	Low Level	High Level
Dithiol conc. [mM]	Continuous	0.2	2
I_2 equiv.	Continuous	0.5	3
$SbCl_3$ equiv.	Continuous	0.5	2
Solvent	Categorical	$CHCl_3$	CH_2Cl_2
Temperature (°C)	Discrete Numeric	0	24

Although it has been shown that when $SbCl_3$ is at 2 equivalents, this reaction is completed in < 5 minutes, since sub-stoichiometric amounts were being used, each of the 16 reactions were allowed to run for 8-hours to fully establish thermodynamic equilibrium.[11, 15a] Full synthetic workup was also included into the DOE to include any random errors into the model and since this reaction is using DCC, this would also help account for any effects that purification or concentration changes (i.e., removing solvent) would have on the thermodynamic equilibria.[6b] Results showed that the most important factor for maximizing $\mathbf{L_3^1}$ yield are I_2 equivalents (p-value = 0.00531), dithiol concentration (p-value = 0.00637), the two factor interaction between I_2 and dithiol

concentration (p-value = 0.0110), and temperature (p-value = 0.0355) at the 95% confidence interval. Specifically, a high loading of I_2 equivalents, high concentration of dithiol and 24 °C resulted in a more than four-fold increase in $\mathbf{L_3^1}$ yield over the standard 15% yield previously obtained (Figure 2.5). Surprisingly, the amount of $SbCl_3$ used was shown by the model to be unimportant to the increased yield. This seemed odd since we know that this reaction does not take place without the addition of $SbCl_3$.

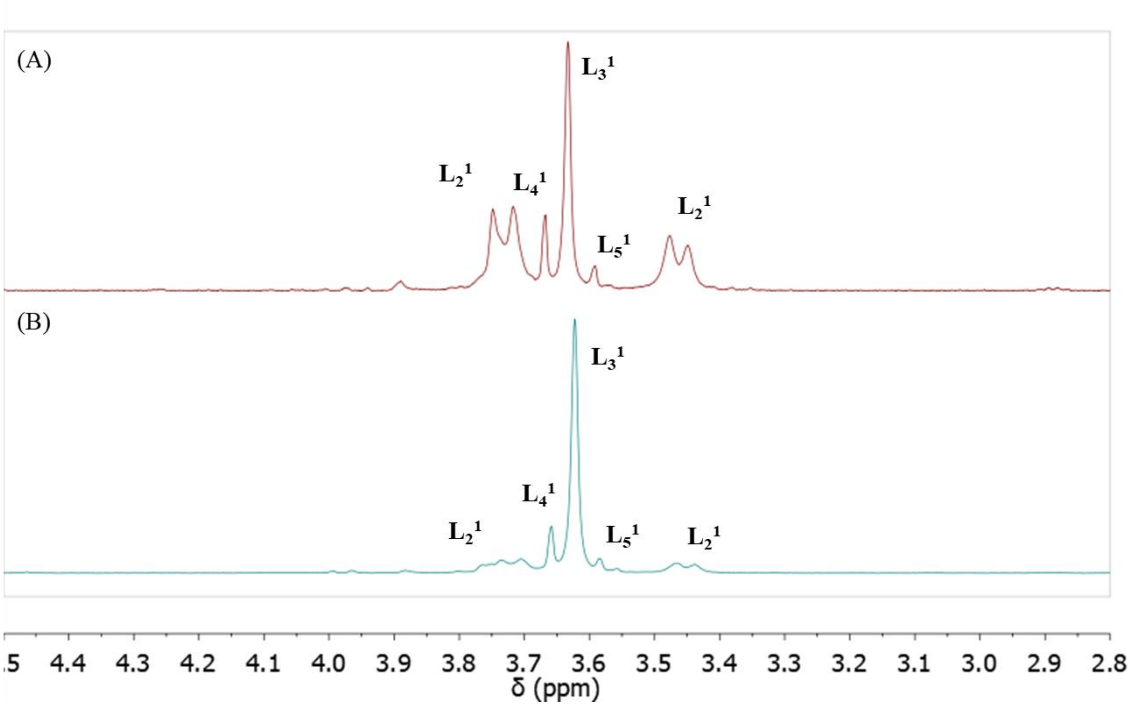

Figure 2.5: (A) ^{1}H NMR spectrum of unoptimized pnictogen-assisted self-assembly of $\mathbf{H_2L}$ forming a mixture of disulfides (reaction conditions: 1mM $\mathbf{H_2L}$, 2 equivalents of I_2, 2 equivalents of $SbCl_3$, solvent: $CHCl_3$, temperature: 24 °C). (B) ^{1}H NMR of optimized reaction conditions for the formation of $\mathbf{L_3^1}$ using parameters provided by DOE analysis (reaction conditions: 4mM $\mathbf{H_2L}$, 4 equivalents of I_2, 2 equivalents of $SbCl_3$, solvent: $CHCl_3$ or CH_2Cl_2, temperature: 24 °C).

To investigate these results further and investigate as to why $SbCl_3$ was seen as unimportant to the model, a second set of DOE experiments were performed. However, to probe any effects that post-synthetic work up and changes in concentration may have, this series of experiments were performed in an NMR tube with an internal standard of trichloroethylene (TCE) to calculate yields *in-situ*. The previous experimental runs showed that no reaction occurred when conducted at 0 °C and the DOE model showed no difference in product distribution between $CHCl_3$ and CH_2Cl_2, so these factors were ignored. Additionally, the upper and lower bounds of all factors were adjusted as can be seen in Table 2.2.

Table 2.2: ^{1}H-NMR DOE for $\mathbf{L_3^1}$ using 3-factors at 2-levels.

Factor	Role	Low Level	High Level
Dithiol conc. [mM]	Continuous	0.2	4
I_2 equiv.	Continuous	0.1	2
$SbCl_3$ equiv.	Continuous	0.5	4

Results of the NMR experiments were consistent with the most important factor remaining I_2 (p-value = 0.0047) in the optimization of $\mathbf{L_3^1}$ yield (>65%). This was followed by $SbCl_3$ equivalents (p-value = 0.0077) and dithiol concentration (p-value = 0.0099). The fact that SbCl3 had now become an important factor in the model was likely due to the reduction in the lower bounds of $SbCl_3$ equivalent. While $SbCl_3$ was not important between 0.5 – 2 equivalents, reducing the equivalents by a factor of 5 allowed for otherwise small changes in the thermodynamic equilibria to become more noticeable in the optimization of $\mathbf{L_3^1}$ yield. This also highlights the fact that $SbCl_3$ can be used as a sub-stoichiometric reagent. The results of both DOEs highlights the fact that it is possible

to control reaction conditions to bias the thermodynamic product distribution in DCC/self-assembled system containing multiple products. Under previous standard conditions, $\mathbf{L_3^1}$ yield was a maximum of 15%. However, after DOE optimization, a maximum yield of >65% was achieved. Both models show that I_2 equivalents is the most important factor, followed by dithiol concentration and that post-synthetic work up or concentration effects have little to no effect on altering product distribution.

To test the scope of using DOE to synthesize a targeted product from an otherwise random mixture, we extended this investigation by exploring three-fold symmetric trithiols, which form cages rather than macrocycles. Specifically, $\mathbf{H_3L}$ was used which has been down to form a dimer ($\mathbf{L_6^1}$) and a complex tetrahedron ($\mathbf{L_7^1}$) species (Scheme 2.5).[11] The DOE was performed on the NMR scale and TCE was used as an internal standard once more. This model included four-factors at two-levels, which were chosen based on the results of the bromoarene DOE (Table 2.3).

Table 2.3: ^{1}H-NMR DOE for $\mathbf{L_6^1}$ and $\mathbf{L_7^1}$ using 4-factors at 2-levels.

Factor	Role	Low Level	High Level
Trithiol conc. [mM]	Continuous	0.5	4
I_2 equiv.	Continuous	2	6
$SbCl_3$ equiv.	Continuous	1	4
Solvent	Categorical	$CDCl_3$	C_6D_6

Results showed that it was possible to bias the maximum yield of either species based on the chemical environment. $\mathbf{L_6^1}$ achieved a maximum yield of 95% where as $\mathbf{L_7^1}$ reached 45%. These yields are amplified substantially over the previous maximum yields of 69% and 29%, respectively, which themselves were previously optimized with far

more synthetic effort.[16] While this increase in yield of either species is not as remarkable as compared to $\mathbf{L_3^1}$, it again underscores which factors and interaction of factors have the most impact on product distribution. Trithiol concentration was the more important factor by a large margin (p-value = <0.0001), then solvent (p-value = 0.0002), I_2 equivalents (p-value = 0.0009), and finally the interaction between solvent and trithiol concentration (p-value = 0.0035) at the 95% confidence interval. The large impact of trithiol concentration on product distribution likely arises from the availability of $\mathbf{H_3L}$ in solution. At low concentrations, it is much more likely that two trithiols will meet and form $\mathbf{L_6^1}$ (6 bonds broken, 3 bonds formed) more often than $\mathbf{L_7^1}$ (12 bonds broken, 6 bonds formed). By increasing $\mathbf{H_3L}$ concentration, this allows for more chances of the more complex $\mathbf{L_7^1}$ to readily form which is consistent with known concentration effects in monomer-dimer equilibria. This is also supported by the DOE model that showed when a lower concentration of $\mathbf{H_3L}$ was used (0.5 mM), a maximum of 17% yield was achieved in contrast of a maximum yield of 45% at higher concentrations (4 mM). Solvent effects also played an important role in product distribution, showing that $CDCl_3$ favors the formation of $\mathbf{L_6^1}$ and C_6D_6 favored $\mathbf{L_7^1}$ formation.

Conclusion

Synthesis of four new dibromo disulfide macrocycles using metalloid-assisted self-assembly was successfully achieved. The dimeric and trimeric disulfides have been shown to cleanly undergo sulfur extrusion, followed by oxidation, to produce the new thiacyclophanes and sulfone derivatives. The bromoarene reactivity of these macrocycles will provide a facile route to synthesis of new and interesting complexes, including

tubular structures and/or polymeric derivatives through cross-coupling reactions. We have also highlighted the utility of DOE in the area of supramolecular self-assembly by optimizing reaction conditions of two different systems, producing traditionally difficult to synthesize species selectively and in high yields.

Bridge to Chapter III

Chapter II presented work on the exploration of the tolerance of the pnictogen-assisted self-assembly method to proceed cleanly with reactive functional groups. Utilizing a dibromo arene motif, the dimer through hexamer were cleanly formed and underwent facile sulfur extrusion and oxidations to give the corresponding thioether and sulfone derivatives. 'Design of experiments' was then used to quickly and efficiently discover reaction conditions to optimize the trimeric species, which is difficult to synthesize using traditional methods, increasing its yield by over 400%. To show the generality of using DOE to optimize reaction conditions, a trithiol was then used to selectively increase the resulting dimer or tetrahedron species. In Chapter III, we discuss the synthesis of a normally trace trithioorthoformate cage species during the trithiol synthesis. The yield of this species under normal conditions was 3%, but after optimization, was increased to 60%.

Experimental

General Procedures

All chemicals were used as received, except N-bromosuccinimide (NBS) which was recrystallized from H_2O prior to use. Purification and separation of disulfide and

thioether products were performed using a Japan Analytical Instruments Inc. LC-9101 recycling preparative high-performance liquid chromatography with size exclusion chromatography columns JAIGEL-1H and JAIGEL-2H in serial. ^{1}H-NMR, ^{13}C-NMR, and 2D-DOSY spectra were recorded on a Bruker AVANCE 600 MHz or Varian INOVA 500 MHz spectrometer using Topspin software in $CDCl_3$, CD_2Cl_2, or C_6D_6. 2D-DOSY experiments were performed with gradient stimulated echo with spinlock and convection compensation pulse sequences. Data were processed in MestReNova. NMR yield experiments were determined by integration of selected peak areas using trichloroethylene or tetrachloroethane as an internal standard. High resolution mass spectrometry was performed on a Xevo G2-XS ToF system from Waters using an atmospheric solids analysis probe. Preparation of 1,4-dibromo-2,5-bis(bromomethyl)benzene[17] and 1,3,5-tris(mercaptomethyl)benzene (**H_3L**)[11] was synthesized using previously reported literature procedures.

Synthetic Procedures

Synthesis of 1,4-dibromo-2,5-bis(mercaptomethyl)benzene (H_2L)

1,4-dibromo-2,5-bis(bromomethyl)benzene (1.75 g, 4.15 mmol) was dissolved in $CHCl_3$ (50 mL) and thiourea (0.693 g, 9.10 mmol) in acetone (50 mL) was added and stirred for 16 hours at 63 °C. The thiouronium salt was filtered, washed with cold $CHCl_3$ and added to a 3-neck 250 mL round bottom flask and purged with N_2. Sparged 3M NaOH was added via cannula into the solution and was stirred for 12 hours at 80 °C. The reaction mixture was removed from heat and sparged 4M HCl was cannulated into the flask in an ice bath. The product was extracted from the aqueous fraction with $CHCl_3$

(3x) and washed with brine. The organic fractions were collected and dried with $MgSO_4$, filtered, and concentrated to give a white solid (97%). ^{1}H NMR (500 MHz, $CDCl_3$) of **H_2L**: δ = 7.57 ppm (s, 2H, C_6H_2), 3.75 ppm (d, J = 8.2 Hz, 4H, CH_2), 1.99 ppm (t, 2H, SH, J = 8.25, 8.25 Hz); ^{13}C NMR (150 MHz, CD_2Cl_2): δ = 141.79, 134.38, 122.93, 29.12 ppm.

Synthesis of 6,9,16,19-tetrabromo-2,3,12,13-tetrathia[4.4]paracyclophane, 6,9,16,19,26,29-hexabromo-2,3,12,13, 22,23-hexathia[4.4.4]paracyclophane, 6,9,16,19,26,29,36,39-octabromo-2,3,12,13, 22,23, 32,33-octathia[4.4.4.4]paracyclophane, 6,9,16,19,26,29,36,39, 46, 49-decabromo-2,3,12,13, 22,23, 32,33, 42,43-decathia[4.4.4.4.4]paracyclophane (L_2^1, L_3^1, L_4^1, and L_5^1)

Under ambient air, **H_2L** (876 mg, 2.67 mmol) was added to CH_2Cl_2 (100 mL). A second flask was charged with $SbCl_3$ (1.22 g, 5.35 mmol) and I_2 (1.99 g, 7.84 mmol) in CH_2Cl_2 (500 mL). The solution of $SbCl_3$ and I_2 was added to the solution of **H_2L** slowly and allowed to stir for 6 hours. The reaction was quenched with Na_2SO_3 until the solution turned from dark purple to clear. The organic layer was washed with deionized water (3x). The solution was dried with $MgSO_4$ and concentrated to give an off-white solid. The powder was then dissolved in 3 mL of $CHCl_3$ and purified by SEC (86% combined yield: 61% dimer, 15% trimer, 6% tetramer, 4% pentamer). ^{1}H NMR (500 MHz, CD_2Cl_2) of **L_2^1** (staggered): δ = 3.50 ppm (d, J = 14.2, 4H, CH_2), 3.77 ppm (d, J = 14.4, 4H, CH_2), 7.26 ppm (s, 4H, C_6H_2); ^{1}H NMR (500 MHz, CD_2Cl_2) of **L_2^1** (eclipsed): δ = 3.62 ppm (d, J = 14.7, 4H, CH_2), 4.03 ppm (d, J = 14.9, 4H, CH_2), 7.29 ppm (s, 4H, C_6H_2); ^{13}C NMR (150 MHz, CD_2Cl_2): δ = 137.45, 135.17, 121.66, 42.34 ppm; HRMS-ASAP [M+H]+

$C_{16}H_{13}Br_4S_4$ predicted: 648.6634, found: 648.6526; ^{1}H NMR (500 MHz, CD_2Cl_2) of $\mathbf{L_3^1}$: δ = 3.64 ppm (s, 6H, C_6H_2), 7.39 ppm (s, 12H, CH_2); ^{13}C NMR (150 MHz, CD_2Cl_2): δ = 138.71, 135.22, 123.23, 44.51 ppm; HRMS-ASAP [M+H]+ $C_{24}H_{19}Br_6S_6$ predicted: 972.4911, found: 972.4769; ^{1}H NMR (500 MHz, CD_2Cl_2) of $\mathbf{L_4^1}$: δ = 3.67 ppm (s, 8H, C_6H_2), 7.44 ppm (s, 16H, CH_2); ^{13}C NMR (150 MHz, CD_2Cl_2): δ = 138.07, 135.71, 123.27, 43.28 ppm; HRMS-ASAP [M+H]+ $C_{32}H_{24}Br_8S_8$ predicted: 1296.3189, found: 1296.3096; ^{1}H NMR (500 MHz, CD_2Cl_2) of $\mathbf{L_5^1}$: δ = 3.59 ppm (s, 10H, C_6H_2), 7.35 ppm (s, 20H, CH_2); HRMS-ASAP [M+H]+ $C_{40}H_{30}Br_{10}S_{10}$ predicted: 1631.3641, found: 1631.3837.

Synthesis of 5,8,14,17-dithia[3.3]paracyclophane ($\mathbf{L_2^2}$)

$\mathbf{L_2^1}$ (95mg, 0.146 mmol) was added to dry CH_2Cl_2 (20 mL) and sparged with N_2 for 30 minutes. HMPT (66 µL, 0.365 mmol) was added slowly while stirring and allowed to react for 24 hours. The desired product was obtained by washing with deionized water (5x) until the organic fraction turned clear. The solution was dried with $MgSO_4$ and concentrated under reduced pressure. The white solid product was dissolved in 3 mL of $CHCl_3$ and separated from residual HMPT with SEC to afford 71 mg of product (83% yield). ^{1}H NMR (500 MHz, CD_2Cl_2) of $\mathbf{L_2^2}$: δ = 3.70 ppm (d, J = 15.2, 4H, CH_2), 3.95 ppm (d, J = 15.2, 4H, CH_2), 7.47 ppm (s, 4H, C_6H_2); ^{13}C NMR (150 MHz, CD_2Cl_2): δ = 37.31, 123.92, 134.52, 136.85 ppm. HRMS-ASAP $[M+H]^+$ $C_{16}H_{13}Br_4S_2$ predicted: 584.7192, found: 584.7094.

Synthesis of 5,8,14,17-dithiaoxide[3.3]paracyclophane ($\mathbf{L_2^3}$)

L_2^2 (70 mg, 0.119 mmol) was added to dry CH_2Cl_2 (20 mL) and sparged with N_2 for 30 minutes. In a separate round bottom flask, *m*-CPBA (93 mg, 0.536 mmol) was added to dry CH_2Cl_2 (5 mL), sparged for 15 minutes, and cannulated into the reaction flask on an ice bath with stirring. The solution was allowed to slowly reach room temperature and continue stirring for 12 hours. The solution was washed with $NaHCO_3$ (4x), brine (1x) dried with $MgSO_4$ and concentrated under reduced pressure to afford 71 mg of product (92% yield). ^{1}H NMR (500 MHz, CD_2Cl_2) of **L_2^3**: δ = 4.22 ppm (d, J = 15.2, 4H, CH_2), 4.83 ppm (d, J = 15.2, 4H, CH_2), 7.92 ppm (s, 4H, C_6H_2); ^{13}C NMR (150 MHz, CD_2Cl_2): δ = 61.50, 124.83, 131.87, 135.39 ppm. HRMS-ASAP $[M+H]^+$ $C_{16}H_{13}Br_4O_4S_2$ predicted: 648.6989, found: 648.7027.

Synthesis of 5,8,14,17,23,26-hexabromo-2,11,20-trithia[3.3.3]paracyclophane (L_3^2)

L_3^1 (34mg, 0.035 mmol) was added to dry CH_2Cl_2 (20 mL) and sparged with N_2 for 30 minutes. HMPT (38 µL, 0.210 mmol) was added slowly while stirring and allowed to react for 24 hours. The desired product was obtained by washing with deionized water (5x) until the organic fraction turned clear. The solution was dried with $MgSO_4$ and concentrated under reduced pressure. The white solid product was dissolved in 3 mL of $CHCl_3$ and separated from residual HMPT with SEC to afford 23 mg of product (75% yield). ^{1}H NMR (500 MHz, CD_2Cl_2) of **L_3^2**: δ = 3.72 ppm (s, 6H, C_6H_2), 7.29 ppm (s, 12H, CH_2); ^{13}C NMR (150 MHz, CD_2Cl_2): δ = 36.45, 123.42, 134.71, 138.16 ppm. HRMS-ASAP $[M+H]^+$ $C_{24}H_{19}Br_6S_6$ predicted: 876.5749, found: 876.5574.

Synthesis of 5,8,14,17,23,26-hexabromo-2,11,20-trithiaoxide[3.3.3]paracyclophane (L_3^3)

L_3^2 (23 mg, 0.026 mmol) was added to dry CH_2Cl_2 (20 mL) and sparged with N_2 for 30 minutes. To a separate round bottom flask, *m*-CPBA (43 mg, 0.186 mmol) was added to dry CH_2Cl_2 (5 mL), sparged for 15 minutes, and cannulated into the reaction flask on an ice bath with stirring. The solution was allowed to slowly reach room temperature and continue stirring for 12 hours. The solution was washed with $NaHCO_3$ (4x), brine (1x) dried with $MgSO_4$ and concentrated under reduced pressure to afford 23 mg of product (90% yield). ^{1}H NMR (500 MHz, CD_2Cl_2) of L_3^3: δ = 4.48 ppm (s, 6H, C_6H_2), 7.58 ppm (s, 12H, CH_2); ^{13}C NMR (150 MHz, CD_2Cl_2): δ = 59.64, 125.14, 131.30, 136.07 ppm. HRMS-ASAP $[M+H]^+$ $C_{24}H_{18}Br_6O_6S_6$ predicted: 972.5444, found: 972.5481.

Supplemental Characterization Data

For NMR and mass spectrometry data relating to synthesis and DOE experiments, please see Supplemental Information of article *"Design of Experiments" as a Method to Optimize Dynamic Disulfide Assemblies Cages and Functionalizable Macrocycles.*[1]

Design of Experiments

Terminology

Resolution: Term which describes the extent to which main effects are alised with higher order interactions. For example, if some main effects are aliased with some 2-level interactions, this is resolution III. If some main effects are aliased with some 4-level

interactions, this is resolution V. Resolution V is excellent, resolution IV is good, and resolution III is good for screening designs.

Alias: When the estimate of an effect includes the estimate of another effect, the two effects are considered aliased.

Factors: Inputs that can be manipulated by an experimenter to change the output. For example, solvent, time, and heat are all potential factors in an experiment.

Levels: The different values allowed for each factor. For example, if heat (factor) had two levels, these could be 0° C and 24° C, or any temperature the experimenter decided to use.

Software: JMP 13.0 Pro statistical software from SAS Institute Inc.

^{1}H NMR spectra were recorded with a Bruker AVANCE 500 or Bruker AVANCE 600 in CD_2Cl_2 or C_6D_6. Spectra were referenced using the residual solvent resonances and reported in ppm. A known amount of trichloroethylene or 1,1,2,2-tetrachloroethane was added to the dithiol and trithiol NMR scale DOE, after the reaction was complete, to calculate yield. The following formula was used to calculate ^{1}H NMR yields: $n \cdot [\int(\text{product}) / \int(\text{standard})] \cdot 100\%$, where n is the ratio of standard to starting material (in mol) and $\int(\text{product}) / \int(\text{standard})$ is the integral ratio of the corresponding ^{1}H NMR peaks.

Design of Experiments Model Analysis

Full scale dithiol DOE analysis

H_2L (20mg) was added to a round bottom flask with a stir bar and dissolved in 300 mL (0.2 mM) or 30 mL (2 mM) of $CHCl_3$ or CH_2Cl_2. In a separate round bottom flask, $SbCl_3$ (7 mg or 28 mg) and I_2 (8 mg or 46 mg) was added and dissolved in the appropriate solvent with sonication. For room temperature experiments, the $SbCl_3/I_2$ mixture was added slowly to the reaction flask and allowed to stir for 8 hours. For the 0 °C experiments, the $SbCl_3/I_2$ mixture was allowed to cool prior to adding into the reaction flask. The randomized experimental matrix can be seen in Table 2.4. The reaction was then quenched with Na_2SO_3 until the solution turned clear. The organic layer was washed with $NaHCO_3$ (2x), brine (1x), and dried with $MgSO_4$ and condensed under reduced pressure.

Table 2.4: Full scale DOE experimental matrix

Exp. Run	Dithiol Conc. (mM)	$SbCl_3$ Equiv.	I_2 Equiv.
1	0.2	0.5	3
2	2	2	3
3	0.2	2	3
4	2	0.5	3
5	0.2	0.5	0.5
6	0.2	0.5	3
7	2	0.5	0.5
8	0.2	2	3

9	2	0.5	3
10	2	2	0.5
11	0.2	2	0.5
12	2	2	0.5
13	2	2	3
14	0.2	0.5	0.5
15	2	0.5	0.5
16	0.2	2	0.5

Effects test of full-scale DOE results

Effect Tests

Source	Nparm	DF	Sum of Squares	F Ratio	Prob > F
Iodine Equivalence(0.5,3)	1	1	3128.8966	53.2467	0.0053*
SM Concentration (mM)(0.2,2)	1	1	2755.8628	46.8985	0.0064*
SM Concentration (mM)*Iodine Equivalence	1	1	1868.9479	31.8053	0.0110*
Temp (C)(0,24)	1	1	782.2241	13.3117	0.0355*
Iodine Equivalence*Solvent	1	1	475.2179	8.0871	0.0654
SM Concentration (mM)*Temp (C)	1	1	470.0796	7.9997	0.0663
Iodine Equivalence*Temp (C)	1	1	357.7159	6.0875	0.0903
SbCl3 Equivalence*Temp (C)	1	1	295.9697	5.0367	0.1105
Temp (C)*Solvent	1	1	203.8688	3.4694	0.1594
SbCl3 Equivalence*Iodine Equivalence	1	1	192.1920	3.2707	0.1682
Solvent	1	1	157.9050	2.6872	0.1997
SbCl3 Equivalence*Solvent	1	1	148.9924	2.5355	0.2096
SM Concentration (mM)*Solvent	1	1	81.3740	1.3848	0.3242
SM Concentration (mM)*SbCl3 Equivalence	1	1	26.7377	0.4550	0.5483
SbCl3 Equivalence(0.5,2)	1	1	16.8481	0.2867	0.6295

NMR scale dithiol DOE analysis

Stock solutions (SS) of **H_2L**, $SbCl_3$, and I_2 were made in CD_2Cl_2 according to Table 2.5. Each NMR tube used was prefilled with the required amount of CD_2Cl_2 to provide the final volume of 1 mL.

Table 2.5: Stock solutions for dithiol NMR scale DOE

Stock solution	**H_2L**	$SbCl_3$	I_2
Stock solution conc. (mM)	20	20	40
Stock solution vol. (mL)	3	3	3
Stock solution mass (mg)	19.7	13.7	30.5

H_2L SS was added to a pre-filled (CD_2Cl_2) NMR tube (10 µL, 105 µL, or 200 µL) followed by I_2 SS (2.5 µL, 20 µL, 50 µL, 118.125 µL, or 400 µL) and $SbCl_3$ SS (1 µL, 20 µL, 110.25 µL, or 400 µL). The tube was then sealed with parafilm and shook vigorously to thoroughly mix and let stand for 8 hours. Prior to NMR analysis, 10 µL of trichloroethylene was added as an internal standard. The randomized experimental matrix can be seen in Table 2.6.

Table 2.6: Dithiol NMR scale experimental matrix

Exp. Run	Dithiol Conc. (mM)	$SbCl_3$ Equiv.	I_2 Equiv.
1	0.2	0.1	0.5
2	4	0.1	0.5
3	4	2	0.5
4	2.1	1.05	2.25
5	0.2	0.1	4
6	4	2	0.5

7	0.2	2	0.5
8	0.2	2	0.5
9	4	2	4
10	4	0.1	4
11	4	2	4
12	0.2	2	4
13	4	0.1	4
14	0.2	0.1	0.5
15	0.2	0.1	4
16	2.1	1.05	2.25

Effects summary of dithiol NMR-scale DOE results

Effect Tests

Source	Nparm	DF	Sum of Squares	F Ratio	Prob > F
I2 Equivalence(0.1,4)	1	1	1388.9686	13.8620	0.0047*
SbCl3 Equivalence(0.1,2)	1	1	1298.8631	12.9627	0.0057*
SM Concentration (mM)*SbCl3 Equivalence	1	1	1063.6407	10.6152	0.0099*
SM Concentration (mM)*I2 Equivalence	1	1	913.4532	9.1163	0.0145*
SbCl3 Equivalence*I2 Equivalence	1	1	863.8030	8.6208	0.0166*
SM Concentration (mM)(0.2,4)	1	1	742.8333	7.4135	0.0235*

NMR scale trithiol DOE analysis

Stock solutions (SS) of **H_3L**, $SbCl_3$, and I_2 were made in $CDCl_3$ or C_6D_6 according to Table 2.7. Each NMR tube used was prefilled with the required amount of deuterated solvent to provide the final volume of 1 mL.

Table 2.7: Stock solutions for trithiol NMR-scale DOE

Stock solution	**H_3L**	$SbCl_3$	I_2
Stock solution conc. (mM)	50	50	100
Stock solution vol. (mL)	1.5	2	2
Stock solution mass (mg)	16.2	50.8	22.8

H_3L SS was added to a pre-filled (CD_2Cl_2 or C_6D_6) NMR tube (10 µL, 45 µL, or 80 µL) followed by I_2 SS (10 µL, 30 µL, 80 µL, 90 µL, or 240 µL) and $SbCl_3$ SS (10 µL, 40 µL, 80 µL, 112.5 µL, or 320 µL). The tube was then sealed with parafilm and shook vigorously to thoroughly mix and let stand for 8 hours. Prior to NMR analysis, 10 µL of 1,1,2,2-tetrachloroethane was added as an internal standard. The randomized experimental matrix can be seen in Table 2.8.

Table 2.8: Trithiol NMR-scale experimental matrix

Exp. Run	Trithiol Conc. (mM)	SbCl3 equiv.	I2 equiv.	Solvent
1	0.5	4	2	Benzene
2	4	1	2	Benzene
3	0.5	4	2	Chloroform
4	4	1	6	Chloroform
5	4	4	6	Chloroform
6	4	4	6	Chloroform
7	4	4	6	Benzene
8	0.5	1	2	Chloroform
9	0.5	1	2	Chloroform

10	0.5	1	6	Benzene
11	4	1	2	Chloroform
12	0.5	4	6	Chloroform
13	4	4	2	Chloroform
14	2.25	2.5	4	Benzene
15	4	1	6	Benzene
16	0.5	4	6	Benzene
17	0.5	1	2	Benzene
18	2.25	2.5	4	Benzene
19	0.5	1	6	Chloroform
20	4	4	2	Benzene

Effects summary of trithiol NMR-scale DOE results

Effect Tests

Source	Nparm	DF	Sum of Squares	F Ratio	Prob > F
SM Conc. (mM)(0.5,4)	1	1	3052.6997	146.7983	<.0001*
Solvent	1	1	338.3172	16.2690	0.0030*
I2 equiv.(2,6)	1	1	156.2792	7.5152	0.0228*
SM Conc. (mM)*Solvent	1	1	101.2978	4.8712	0.0547
SM Conc. (mM)*I2 equiv.	1	1	37.3430	1.7957	0.2131
I2 equiv.*Solvent	1	1	36.6483	1.7623	0.2170
SbCl3 equiv.*Solvent	1	1	20.9780	1.0088	0.3414
SbCl3 equiv.*I2 equiv.	1	1	13.8546	0.6662	0.4354
SbCl3 equiv.(1,4)	1	1	10.0416	0.4829	0.5047
SM Conc. (mM)*SbCl3 equiv.	1	1	5.0490	0.2428	0.6340

X-ray Crystallography

Diffraction intensities for $\mathbf{L_2^1}$, $\mathbf{L_3^1}$, $\mathbf{L_2^2}$, $\mathbf{L_2^3}$ and $\mathbf{L_3^3}$ were collected at 173 K and 293 K ($\mathbf{L_2^2}$) on a Bruker Apex2 CCD and a Rigaku XtaLAB Synergy S, HyPix ($\mathbf{L_2^2}$ and

L_3^2) diffractometers using CuKα radiation, λ= 1.54178 Å. Space groups were determined based on systematic absences (**L_2^1**, **L_2^3**, and **L_3^2**) and intensity statistics (**L_3^1** and **L_3^3**). Absorption corrections were applied by SADABS.[3] Structures were solved by direct methods and Fourier techniques and refined on F^2 using full matrix least-squares procedures. All non-H atoms were refined with anisotropic thermal parameters. H atoms in all structures were refined in calculated positions in a rigid group model. The structure of **L_3^3** has three symmetrically independent molecules and five solvent $CHCl_3$ molecules. Some of these solvent molecules are disordered. On the residual density map for **L_3^3** there are three relatively high peaks; 3.76, 2.23 and 1.89 eÅ^{-3}. The first peak is close to one of the Br atoms (at 1.18 Å) and indicates that this Br atom could be slightly disordered over two positions similar to the disorder of the solvent molecule $CHCl_3$. Two other peaks are close to two other possible positions of the Br atoms in one of the $C_6H_2Br_2$ groups corresponding two different orientations of this group in the crystal structure. However, contribution of the second possible orientation of this group is small and was not taken into consideration in the final structure refinement. It was found that the crystal structure of **L_3^2** also has molecules with two different orientations for one of $C_6H_2Br_2$ groups. In this case the disorder of the Br atoms was resolved and refinement shown that ratio of these two types of molecules is 0.915/0.085. All calculations were performed by the Bruker SHELXL-2014 package. Deposition Numbers 1906244-1906247 and 194318 contain the supplementary crystallographic data for this paper. These data can be obtained free of charge from The Cambridge Crystallographic Data Center via www.ccdc.cam.ac.uk/data_request/cif.

Crystallographic data for L_2[1]

$C_{16}H_{12}Br_4S_4$, M = 652.14, 0.12 x 0.07 x 0.03 mm, T = 173(2) K, Orthorhombic, space group *Pbca*, *a* = 13.9638(6) Å, *b* = 14.40 Å, *c* = 19.5201(9) Å, *V* = 3925.6(3) Å^3, *Z* = 8, D_c = 2.207 Mg/m^3, μ(Cu) = 13.965 mm^{-1}, *F*(000) = 2496, $2\theta_{max}$ = 133.28°, 19718 reflections, 3473 independent reflections [R_{int} = 0.0739], R1 = 0.0452, wR2 = 0.1075 and GOF = 1.030 for 3473 reflections (217 parameters) with I>2σ(I), R1 = 0.0657, wR2 = 0.1167 and GOF = 1.030 for all reflections, max/min residual electron density +0.616/-0.959 eÅ^{-3}.

Crystallographic data for L_3[1]

$C_{25}H_{19}Br_6Cl_3S_6$, M = 1097.57, 0.16 x 0.08 x 0.01 mm, T = 173(2) K, Triclinic, space group *P*-1, *a* = 9.2484(2) Å, *b* = 9.7411(2) Å, *c* = 19.6762(5) Å, α = 80.725(2)°, β = 82.234(2)°, γ = 85.214(2)°, *V* = 1729.95(7) Å^3, *Z* = 2, D_c = 2.107 Mg/m^3, μ(Cu) = 14.058 mm^{-1}, *F*(000) = 1052, $2\theta_{max}$ = 133.15°, 22350 reflections, 6065 independent reflections [R_{int} = 0.0482], R1 = 0.0458, wR2 = 0.1204 and GOF = 1.039 for 6065 reflections (374 parameters) with I>2σ(I), R1 = 0.0550, wR2 = 0.1281 and GOF = 1.039 for all reflections, max/min residual electron density +1.384/-1.000 eÅ^{-3}.

Crystallographic data for L_2[2]

This structure was previously reported[5] under CCDC deposition number 189356 and the collected crystallographic data agreed with previously submitted data.

Crystallographic data for L_2^3

$C_{16}H_{12}Br_4O_4S_2$, M = 652.02, 0.12 x 0.07 x 0.06 mm, T = 293 K, Monoclinic, space group *C*2/*c*, *a* = 27.2583(4) Å, *b* = 9.18350(10) Å, *c* = 24.6937(3) Å, β = 111.312(2)°, *V* = 5758.77(15) Å^3, *Z* = 12, Z' = 1.5, D_c = 2.256 Mg/m^3, μ(Cu) = 12.461 mm^{-1}, *F*(000) = 3744, $2\theta_{max}$ = 135.37°, 20040 reflections, 5700 independent reflections [R_{int} = 0.0204], R1 = 0.0319, wR2 = 0.0846 and GOF = 1.041 for 5700 reflections (352 parameters) with I>2σ(I), R1 = 0.0344, wR2 = 0.0864 and GOF = 1.041 for all reflections, max/min residual electron density +1.303/-1.248 eÅ^{-3}.

Crystallographic data for L_3^2

$C_{24}H_{18}Br_6S_3$, M = 882.02, 0.12 x 0.06 x 0.01 mm, T = 173 K, Monoclinic, space group *P*2$_1$/*n*, *a* = 11.1593(1) Å, *b* = 7.6034(1) Å, *c* = 31.1347(3) Å, β = 90.932(1)°, *V* = 2641.39(5) Å^3, *Z* = 4, Z' = 1, D_c = 2.218 Mg/m^3, μ(Cu) = 13.308 mm^{-1}, *F*(000) = 1680, $2\theta_{max}$ = 148.70°, 16008 reflections, 5180 independent reflections [R_{int} = 0.0256], R1 = 0.0420, wR2 = 0.1032 and GOF = 1.032 for 5180 reflections (317 parameters) with I>2σ(I), R1 = 0.0447, wR2 = 0.1073 and GOF = 1.134 for all reflections, max/min residual electron density +2.306/-0.826 eÅ^{-3}.

Crystallographic data for L_3^3

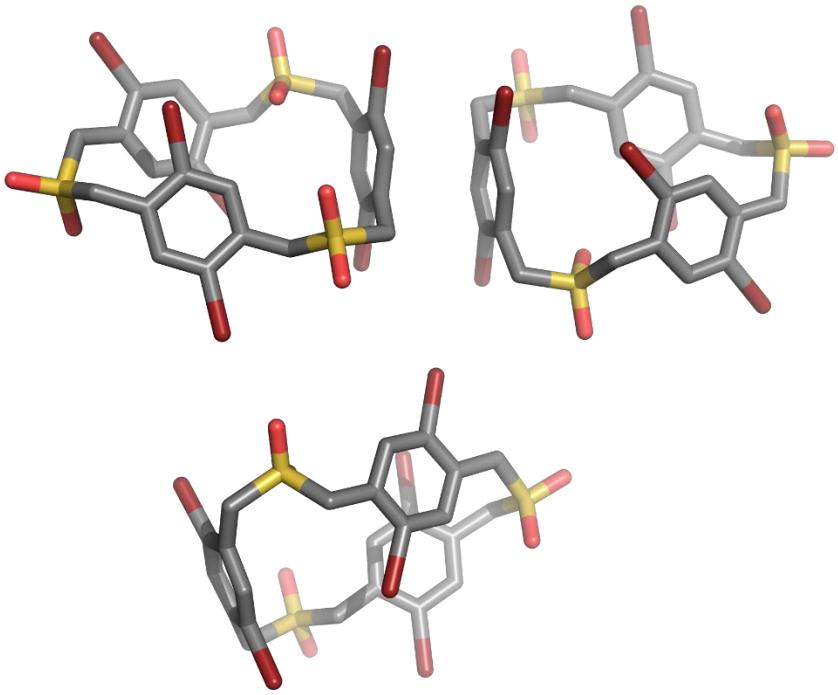

Figure 2.6: Single crystal XRD of $\mathbf{L_3^3}$ showing three symmetrically independent molecules. Hydrogens and solvents of crystallization have been removed for clarity.

$C_{25.67}H_{19.67}Br_6Cl_5O_6S_3$, $C_{24}H_{18}Br_6O_6S_3 \cdot 1.67(CHCl_3)$, M = 1176.97, 0.10 x 0.06 x 0.02 mm, T = 173(2) K, Triclinic, space group *P*-1, *a* = 16.1790(4) Å, *b* = 17.5216(4) Å, *c* = 19.7966(5) Å, α = 82.669(1)°, β = 81.107(1)°, γ = 88.163(1)°, *V* = 5498.8(2) Å^3, *Z* = 6, Z'=3, D_c = 2.133 Mg/m^3, μ(Cu) = 13.209 mm^{-1}, *F*(000) = 3388, $2\theta_{max}$ = 133.75°, 68117 reflections, 19385 independent reflections [R_{int} = 0.0615], R1 = 0.0678, wR2 = 0.1818 and GOF = 1.033 for 19385 reflections (1227 parameters) with I>2σ(I), R1 = 0.0898, wR2 = 0.1988 and GOF = 1.033 for all reflections, max/min residual electron density +3.757/-2.316 eÅ^{-3}.

CHAPTER III

SELF-ASSEMBLY OF A TRITHIOORTHOFORMATE-CAPPED CYCLOPHANE

Contributions

This co-authored work was published in *Chemistry – A European Journal*.[1] Dr. Mary Collins wrote the bulk of the manuscript and experimentation. Prof. Darren W. Johnson provided intellectual input and editorial feedback. Dr. Lev N. Zakharov resolved all X-ray crystallography experiments. Dr. S. Michael Strain assisted in deconvolution and 2D NMR experiments. I performed experiments related to the optimization of the yield for the target compound, contributed to the manuscript, and performed supplemental experimentation related to journal peer-reviewed questions with the assistance of Elizabeth K. Smith.

Introduction

Orthoesters and orthothioesters are functionalities seldom used in self-assembling supramolecular systems despite their relevance as acylating, alkylating, and formylating agents and as protecting groups in synthetic organic chemistry. Recent work from von Delius and co-workers features the templated synthesis of dynamic orthoester cryptates, in which kinetic stabilization is induced via metal encapsulation.[2] Unique to this family is the addition of a single orthoformate group adjoining dissimilar ligands to generate a supramolecular heteroleptic self-assembly. Our present work focuses on metal-mediated dynamic covalent chemistry of disulfides and their capture via

sulfur-extrusion.[3] In this study, we show the surprising integration of a trithioorthoformate moiety using iodine oxidation of thiols to self-assemble an unexpected cyclophane cage featuring both a trithioorthoformate-cap and a tris-disulfide base (Scheme 1). The labile trithioorthoester appears to be stabilized by endohedral encapsulation of its methine group, allowing for selective sulfur extrusion of the disulfides to trap the corresponding tris-thioether and leaving the trithioorthoformate unchanged.

Previous accounts of alkyl thioorthoformates appear in the literature as components in Seebach's research on umpolung reactions using lithiated dithianes.[4] However, the incorporation of a trithioorthoformate moiety as part of an in-cyclophane – where a methine hydrogen is projected directly into the ring system – has not been observed as a product of supramolecular self-assembly.[5] We previously described an unusual pnictogen-enhanced iodine oxidation method for the self-assembly of disulfide-based cyclophanes.[6] The directing behavior of the pnictogen leads to remarkable resistance to the formation of insoluble, kinetic polymers, enabling rapid and selective syntheses of many discrete disulfide macrocycles and cages for an assortment of different ligand systems. The use of a three-fold symmetric trithiol **H_3L** were hypothesized to form only a dimeric and tetrahedral product, however, an unexpected secondary cage species was also isolated (Scheme 3.1, top). The synthesis of this caged structure may provide insight into how solvent can be used to influence intermolecular interactions during self-assembly processes. Herein we describe the optimized synthesis and characterization of a thioorthformate-capped thiacyclophane synthesized by supramolecular self-assembly.

Results and Discussion

Previously, our lab has showcased an unusual pnictogen-assisted iodine-oxidation method for the self-assembly of discrete disulfide cyclophanes.[6] While this technique exhibits impressive yields for the aforementioned discrete disulfides over polymeric species, other unanticipated side-products can be isolated in appreciable yields under the proper conditions. The oxidation of 1,3,5-tris-(mercaptomethyl)benzene (**H_3L**) was executed by treating the free trithiol with iodine and antimony trichloride in a solution of chloroform, resulting in the self-assembly of these primary products: tetrahedron (**L_1^1**) and dimer (**L_3^1**) (Scheme 3.1, top).[6a] However, we did not expect to isolate a third species of intermediate size, cage **L_2^1**, upon purification by size exclusion chromatography. The formation of **L_2^1** appears to result from reaction of the thiols of **H_3L** with the chloroform solvent, as no evidence of this product is observed in other non-haloform solvents.

Initial synthesis using chloroform as the solvent and apparent methine source resulted in a limited 3% yield for **L_2^1** (Scheme 3.1, top). We sought to optimize this yield and believing that the formation of the trithioorthoformate cap to be the limiting step, exchanged the solvent to bromoform which provided a dramatic increase in yield to 58% (Scheme 3.1, bottom). The remarkable increase in yield is due to the better leaving ability of bromide, allowing the trithioorthoformate cap to be easily formed.[7] Subsequent sulfur extrusion to produce **L_2^2** resulted in a 62% yield after purification using size exclusion chromatography.

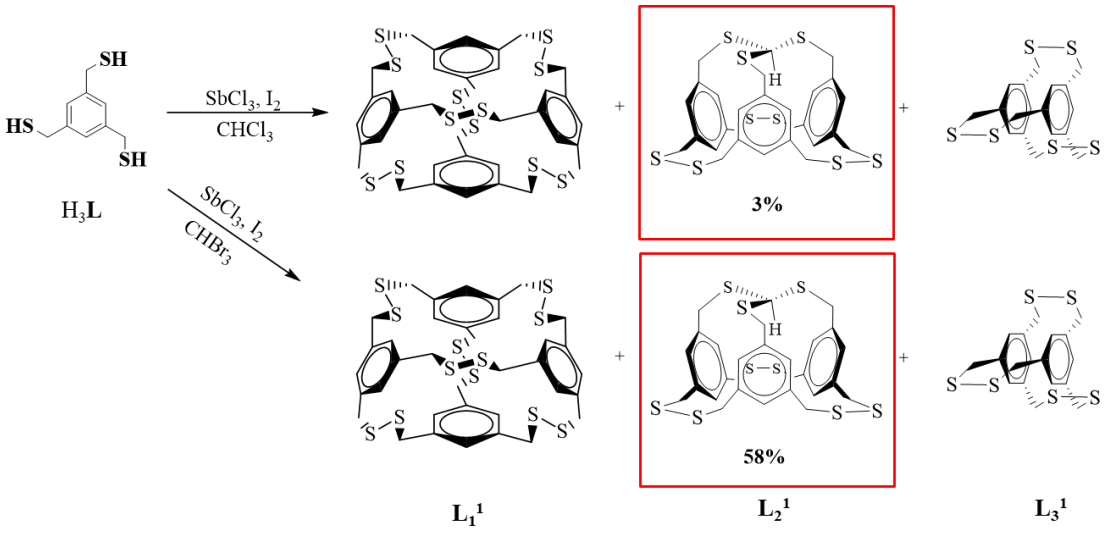

Scheme 3.1: The self-assembly of trithioorthoformate cyclophane cage $\mathbf{L_2^1}$. Unoptimized yield with $CHCl_3$ (top) and optimized yield with $CHBr_3$ (bottom).

X-ray quality single crystals of $\mathbf{L_2^1}$ were grown by solvent evaporation of chloroform (Figure 3.1). The cage crystallizes in the *P*2$_1$/*c* space group and does not co-crystallize with the solvent or any encapsulated guest. $\mathbf{L_2^1}$ exhibits some mild distortion from ideal 90° C-S-S-C dihedral bond angles (∡'s: 99.0°, 94.1°, 92.8°), falling in line with the possibility that self-assembly is likely driven by formation of complexes which yield the least amount of strain in the disulfide bond. The methine hydrogen is positioned directly into the small cavity. The cage has a slight twist along the three-fold axis, with the -S_3CH group twisted counter-clockwise along the C_3 axis with an average torsional twist angle of 55.1°. Centroid-to-centroid distances between the three benzene rings are 5.31 Å, 5.29 Å, and 6.42 Å, suggesting a wide enough pocket for a potential guest. In solution, the cage displays overlapping ^{1}H NMR resonances in both the aromatic and methylene regions causing the assignment of peaks to be unclear in $CDCl_3$ (Figure 3.2). In addition to the overlapping singlets, three signals at 6.98 ppm, 3.86 ppm, and 3.84 ppm were significantly broadened, suggesting dynamic behavior on the NMR timescale.

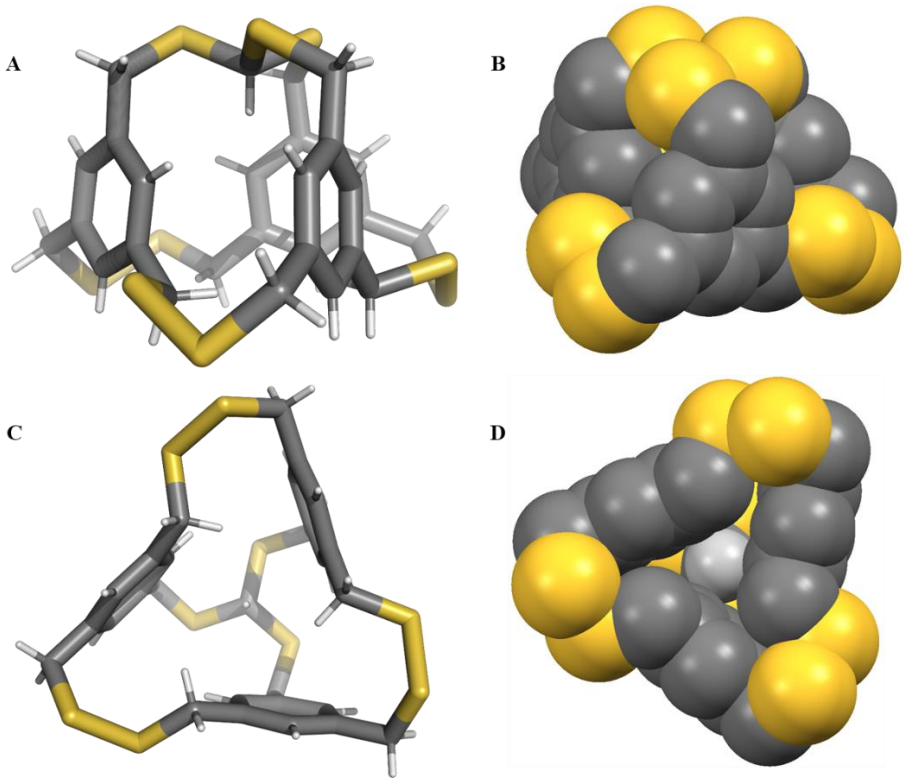

Figure 3.1: Representation of X-ray crystal structure of $\mathbf{L_2^1}$ as stick figure, side view (A), with space-filling (B), and stick figure, bottom view (C), with space-filling (D). Sulfur atoms are shown in yellow.

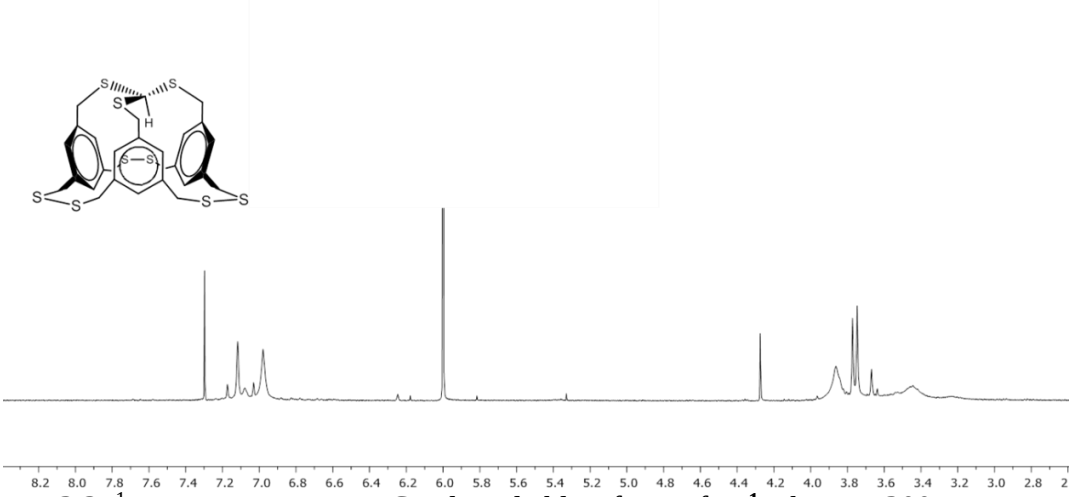

Figure 3.2: ^{1}H NMR spectra in TCE-d_2 and chloroform of $\mathbf{L_2^1}$ taken on 300 MHz spectrometer.

As an approach to bring clarity to the dynamic solution behavior due to the disulfide bonding, sulfur extrusion of $\mathbf{L_2^1}$ with stoichiometric hexamethylphosphorous triamide (HMPT) in dichloromethane produced the more stable hexathioethercyclophane cage $\mathbf{L_2^2}$ within two hours at ambient temperature. The ^{1}H NMR spectrum (CD_2Cl_2) of $\mathbf{L_2^2}$ revealed two singlet peaks at δ=7.17 ppm (broad singlet) and 6.67 ppm in a 6:3 ratio (Scheme 3.2), which were assigned to the aromatic protons.

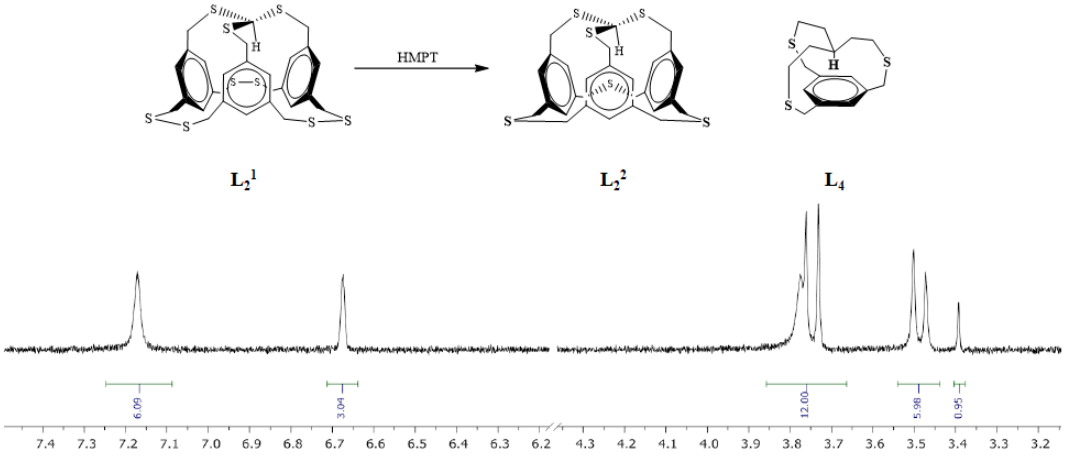

Scheme 3.2: The desulfurization of $\mathbf{L_2^1}$ to form $\mathbf{L_2^2}$ (top left); 2,3,17-trithia[45,12][9]metacyclophane42 $\mathbf{L_4}$ (top right) and ^{1}H NMR (CD_2Cl_2) spectrum of $\mathbf{L_2^2}$ (bottom).

To elucidate the methylene region of $\mathbf{L_2^2}$, a deconvolution of the ^{1}H NMR resonances was performed. Calculated integrals show the broad singlet at 3.77 ppm overlapping the *ABq* (δ=3.74–3.48 ppm) integrates to six protons with each individual *ABq* signal integrating to three. The solution structure of $\mathbf{L_2^2}$ was confirmed by a NOESY NMR experiment and was found to complement the integration of protons provided by deconvolution (Figure 3.3). As summarized in Figure 3.3, the signals assigned to the methine proton singlet (3.39 ppm) correlated with broad signal attributed to the six aromatic protons ortho (δ=7.17 ppm), but not para, to the trithioorthoformate. The twelve methylene protons meta to the trithioorthoformate strongly correlate to the three aromatic

protons at 6.67 ppm, while the trithioorthoformate methylene protons do not. Furthermore, we believe the *ABq* splitting for the methylene protons in $\mathbf{L_2^2}$ suggest the thioether bridges adopt a "locked" conformation in space. In contrast, the broadness observed in the singlets designated to the trithioorthoformate methylenes and their nearby aromatic protons (δ=7.17 ppm and 3.77 ppm) indicate evidence of dynamic helical twisting in solution. The chemical shift of the methine proton at 3.39 ppm exhibited a 1–2 ppm shift up field relative to the few examples of free alkyl trithioorthoformate molecules that are not incorporated in a cage. These signals typically range between 5.3–4.1 ppm.[8] Such a shift is reminiscent of that observed in $\mathbf{L_4}$, synthesized by Pascal, Jr. and Grossman, in which the methine proton resonance is at -1.68 ppm ($CDCl_3$; a standard -CH proton is δ 1–2 ppm) and shielded by the benzene ring current.[5b] In relation to ^{13}C NMR, uncaged trithioorthoformate carbons are typically found around 50 ppm, whereas the carbon in $\mathbf{L_2^2}$ is seen at 44.1 ppm, confirmed by ^{13}C HSQC 2D NMR.

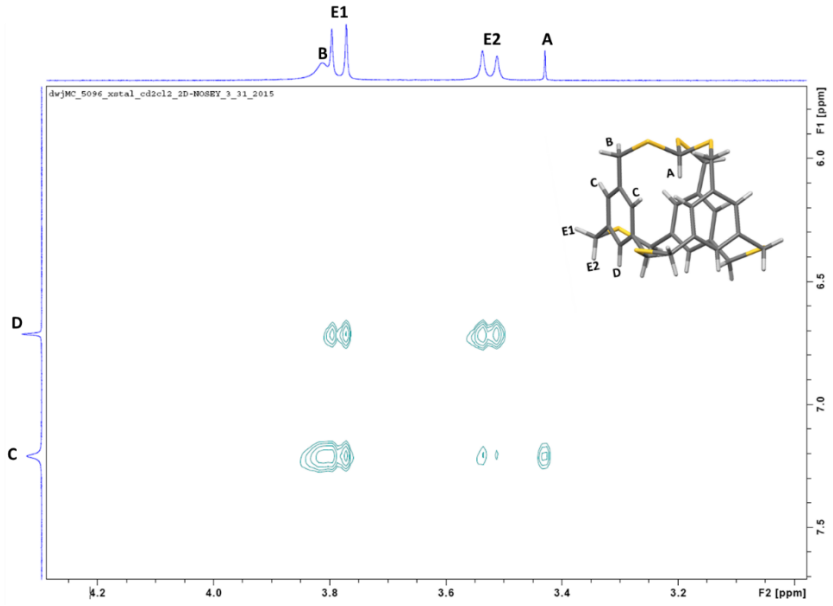

Figure 3.3: NOESY spectra in CD_2Cl_2 for $\mathbf{L_2^2}$ taken on 600 MHz spectrometer.

In support of the solution-state structural assignments, X-ray quality crystals of $\mathbf{L_2^2}$ were obtained by layering hexanes over dichloromethane in 48% crystalline yield (Figure 3.4). The hexathiacyclophane $\mathbf{L_2^2}$ crystallizes in a *Pna2₁* space group; similarly to $\mathbf{L_2^1}$, yet due to the removal of three sulfur atoms, the size of the cavity diminishes, although the methane proton is still found within this small cavity. The C-S-C bond angles are less acute than the disulfide dihedral angles in congener $\mathbf{L_2^1}$ ((∡'s: 102.8°, 101.7°, and 102.0°). Again, consistent with the proposed trithioorthoformate helical twisting in solution, the -S_3CH group is disordered over two positions in a 1:1 ratio such that the torsional twist of the trithioorthoformate is clockwise or counter-clockwise. The clockwise torsional twist displays an averaged angle of 51.8°, whereas the counter-clockwise twist is 54.3°. We recognize this could be of interest to the synthesis and discovery of molecular machinery components as this type of motion is applicable to molecular gears, rotors, and gyroscopes[9] and would be a rare example prepared via dynamic covalent chemistry.

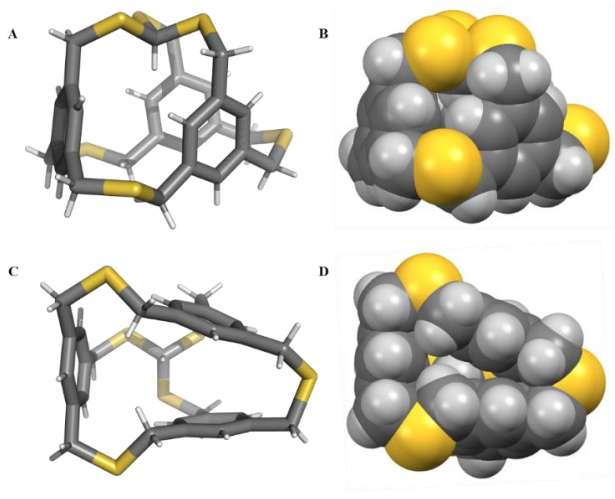

Figure 3.4: Representation of X-ray crystal structure of $\mathbf{L_2^2}$ as stick figure, side view (A), with space-filling (B), and stick figure, bottom view (C), with space-filling (D). Sulfur atoms are shown in yellow.

Conclusion

In conclusion, this is the first report of a self-assembled trithioorthoformate-capped cyclophane, and it surprisingly features a methine proton pointing into the small cavity of the cage. The synthesis of the cage was accomplished via pnictogen-directed iodine oxidation and self-assembly of a trithiol. This formation provides an unexpected effect where solvent directly participates during thiol oxidation intended to form discrete disulfides in the presence of a pnictogen additive. The disulfide bridges undergo facile desulfurization to give the fully captured, stable thioether/trithioorthoformate cyclophane cage, the synthesis of which was optimized using bromoform as an intentional reagent (and solvent). The assignment of peaks in ^{1}H NMR solution state studies were facilitated by 2D NOESY experiments and further supported by X-ray crystallography, and these structures suggest that disulfide exchange and thioorthoester formation might both be suitable, complementary tools in the dynamic covalent chemistry toolkit.

Bridge to Chapter IV

Chapter III reported the self-assembly of an unusual disulfide trithioorthoformate cage. The disulfide bridges are sulfur extruded using HMPT, resulting in the trithioether cage capped by a trithioorthoformate. These cages possess a single methine proton that points into the inner cavity. Initial investigation hypothesized that the methine source was a result of the $CHCl_3$ solvent during oxidation. This was confirmed using $CHBr_3$, and due to the increased leaving ability of the substituent bromines, increased the yield from 3% to 58%. In Chapter IV, the previous assumption that Pn-π interaction is required for the

pnictogen-assisted self-assembly is tested and its generalized ability to form disulfide macrocycles is examined.

Experimental

General Procedures

^{1}H NMR and ^{13}C spectra were measured using Varian INOVA-300 and 500 spectrometers in CD_2Cl_2 and TCE-d_2. 2D NMR spectra were measured using Bruker AVANCE 600 MHz NMR spectrometer with Prodigy BBO multinuclear cryoprobe in CD_2Cl_2. Spectra were referenced using the residual solvent resonances as internal standards and reported in ppm. Single crystal X-ray diffraction studies were performed on a Bruker Apex2 CCD diffractometer using MoKα radiation. Commercially available reagents were used as received. The reported yields are for isolated sample. Caution: Antimony compounds are toxic and should be handled with care! (This accounts for the small scale of the reactions reported herein.) The preparation of 1,3,5-benzenetrimethanethiol (**H_3L**) was previously reported.[6a]

Synthetic Procedures

Synthesis of L_2[1]

H_3L (95 mg, 0.439 mmol) was dissolved in 100 mL $CHCl_3$ in a 250 mL flask with a stir bar. In a separate flask, $SbCl_3$ (200 mg, 0.878 mmol) and I_2 (446 mg, 1.756 mmol) were dissolved in 100 mL $CHCl_3$. The solution of iodine and $SbCl_3$ was slowly poured into **H_3L** while stirring. The solution turns dark purple. The reaction was stirred at 25° C for 12 hours. The reaction was quenched with saturated aqueous Na_2SO_3 and

stirred vigorously until the solution was no longer purple. The mixture was then washed with H_2O (2x), dried with Na_2SO_4, and then filtered. The filtrate was concentrated and purified via size exclusion chromatography (2.53 mg, 2.72% isolated yield). ^{1}H NMR (TCE-d_2): δ 7.17-6.98 ppm (m, 9H, CH), 3.86-3.44 ppm (m, 19H, CH_2).

Synthesis of L_2^2

L_2^1 (0.86 mg, 0.001 mmol) was dissolved in 1.5 mL dry CD_2Cl_2 then transferred to an acid washed, oven-dried NMR tube. HMPT (0.766 µL, 0.004 mmol) was quickly added to the NMR tube under a cone of N_2 and the tube was shaken vigorously. Reaction is observed to be complete in 2 hours at ambient temperature by ^{1}H NMR giving the desired hexathiacyclophane. The solution was pulled through a short silica plug and then layered with hexanes for crystallization. After 2.5 weeks, the solvent was decanted and rinsed with pentanes yielding small colorless needles suitable for X-ray diffraction. (0.35 mg; 48% crystalline yield). ^{1}H NMR (CD_2Cl_2): δ7.17 ppm (bs, 6H, CH), 6.67 ppm (s, 3H, CH), 3.77 ppm (bs, 6H, CH_2), 3.74 ppm (d, 6H, CH_2, J = 15.0 Hz), 3.48 ppm (d, 6H, CH_2, J = 15.0 Hz), 3.39 ppm (s, 1H, CH). ^{13}C NMR (150 MHz, $CDCl_3$): δ = 138.7, 137.5,128.9, 127.8, 44.1, 36.4, 35.8 ppm.

Yield optimization of L_2^1 and L_2^2

L_2^1: **H_3L** (120 mg, 0.555 mmol) was dissolved in 15 mL $CHBr_3$ in a 100 mL flask with a stir bar. In a separate flask, $SbCl_3$ (253mg, 1.11 mmol) and I_2 (563mg, 2.22 mmol) were dissolved in 30 mL $CHBr_3$. The solution of I_2 and $SbCl_3$ was slowly poured into **H_3L** while stirring. The reaction was stirred at 25° C for 16 hours. The

reaction was quenched with saturated sodium sulfite and stirred vigorously until the solution was no longer purple. The mixture was then washed with H_2O (4x), brine (1x), dried with $MgSO_4$, and filtered. Removal of the crude mixture from bromoform was achieve by crash out using hexanes followed by purification via size exclusion chromatography (72.9 mg, 58% isolated yield).

L_2^2: **L_2^1** (25 mg, 0.038 mmol) was dissolved in dry 15 mL $CHCl_3$ in a 50 mL flask with a stir bar. The solution was purged with N_2 for 1 hour. HMPT (34 µL, 0.188 mmol) was removed under a cone of N_2 and added to the reaction flask. The reaction was stirred at 25° C under N_2 for 12 hours. The reaction was washed with H_2O (5x), brine (1x), dried with $MgSO_4$, and filtered. The filtrate was concentrated and purified via size exclusion chromatography (13.1 mg, 62% yield).

Supplemental Characterization Data

For additional information pertaining to NMR experimental data, please see Supplemental Information of article "*Self-Assembly of a Trithioorthoformate-Capped Cyclophane and Its Endohedral Inclusion of a Methine Group"*.[1]

X-ray Crystallography

Diffraction intensities were collected at 173(2) on a Bruker Apex2 CCD diffractometer using MoKα radiation, l=0.71073 Å, (**L_2^1**) and CuKα radiation, l=1.54178 Å, (**L_2^2**). Space groups were determined based on systematic absences. Absorption corrections were applied by SADABS. Structures were solved by direct methods and

Fourier techniques and refined on F2 using full matrix least-squares procedures. All non-H atoms were refined with anisotropic thermal parameters. H atoms in all structures were refined in calculated positions in a rigid group model. H atoms were refined in calculated positions in a rigid group model. The -S_3CH group in $\mathbf{L_2^2}$ is disordered over two positions in a 1:1 ratio. The structure of $\mathbf{L_2^2}$ was determined in non-centrosymmetric space group *Pna2₁* and refined as a racemic twin consisting of two domains in the ratio 0.37/0.63. All calculations were performed by the Bruker SHELXTL (v. 6.10) package. CCDC 1058643 and 1058644 contain the supplementary crystallographic data for this paper.

Crystallographic data for $\mathbf{L_2^1}$

$C_{28}H_{28}S_9$, M=653.04, 0.07x0.04x0.02 mm, T = 173(2) K, Monoclinic, space group $P2_1/c$, a=8.6892(7) Å, b=15.4784(13) Å, c=22.5056(18) Å, β=97.096(2)°, V= 3003.7(4) Å^3, Z=4, ρ_{cald}=1.444 Mg m^{-3}, μ(Mo)=0.683 mm^{-1}, F(000)=1360, $2\theta_{max}$=56.0°, 42386 reflections, 7547 independent reflections [R_{int}=0.0705], $R1$=0.0473, $wR2$=0.1004 and GOF=1.018 for 7547 reflections (334 parameters) with I > 2σ(I), $R1$=0.0913, $wR2$=0.1169 and GOF=1.018 for all reflections, maxmin^{-1} residual electron density +1.215/@0.355 eÅ^3.

Crystallographic data for $\mathbf{L_2^2}$

$C_{28}H_{28}S_6$, M=556.86, 0.17x0.04x0.03 mm, T = 173(2) K, Orthorhombic, space group *Pna2₁*, a=19.1437(12) Å, b=9.2921(6) Å, c=14.6648(9) Å, V=2608.7(3) Å^3, Z=4, ρ_{cald}=1.418 Mg m^{-3}, μ(Cu)=4.961 mm^{-1}, F(000)=1168, $2\theta_{max}$=137.72°, 16134 reflections, 4265 independent reflections [R_{int}=0.0712], $R1$=0.0718, $wR2$=0.1779 and

GOF=1.013 for 4265reflections (335 parameters) with I > 2σ(I), *R*1=0.0934, *wR*2=0.1928 and GOF=1.013 for all reflections, the Flack=0.37(5), maxmin^{-1} residual electron density +0.249/@0.396 eÅ^{3}.

CHAPTER IV

A GENERALIZED METHOD FOR DISULFIDE AND THIOETHER CYCLOPHANES

Contributions

This chapter discusses the synthesis and characterization of 20 new disulfide and thioether macrocycles using a generalized method of our labs pnictogen-assisted self-assembly. The manuscript for these data is currently in preparation. Jacob Mayhugh, Isabella Demachkie, Luca Zocchi, Henery Trubenstrin and I performed experimentation on various thiols. Dr. Lev N. Zakharov performed all X-ray crystal analysis. Prof. Darren W. Johnson provided intellectual support. Jacob Mayhugh and I co-authored the manuscript.

Introduction

Cyclophanes are a fundamentally interesting class of compounds that host a wide range of unique and emergent properties. However, synthesis of complex and/or functionalized cyclophanes can often suffer from harsh reaction conditions, long reaction times, and sometimes low yields using stepwise methods. We have previously reported an efficient, high-yielding, metalloid-directed self-assembly method to prepare disulfide, thioether, and hydrocarbon cyclophanes and cages that feature mercaptomethyl-arene as starting materials. Herein, we report the synthesis of 20 new disulfide and thioether macrocycles that expand this high yielding self-assembly method to a wide breadth of macrocycles. Remarkably, the high-yielding, efficient syntheses still proceeded (under

dynamic covalent chemistry control) with electron-deficient, heteroaryl, cycloalkyl, spiro, and even short alkenyl/alkynyl substrates.

Results and Discussion

By exploiting weak noncovalent interactions, supramolecular chemistry has transformed the bottom-up preparation of discrete macrocycles and cages with efficient synthetic measures.[1] Specifically, self-assembly yields thermodynamic control over reaction pathways in the synthesis of discrete structures while deterring the formation of undesirable side products that result from kinetic pathways.[2] By using reversible covalent reactions, dynamic covalent chemistry (DCC) combines the error-correction and directionality of self-assembly with the robustness of a covalent bond.[2-3] DCC is shown to be applicable in tailor-made molecules for use in various applications, including plastics,[4] host-guest chemistry,[5] and organic electronics,[6] among others .

Recently, we have shown that this strategy can be applied to the formation of cyclophanes from benzylic di- and trithiol precursors (Figure 4.1) by manipulating dynamic disulfide exchange with the inclusion of a pnictogen (Pn) directing agent coupled with a mild oxidant.[7] This approach enables quick (as fast as 5 minutes) and quantitative formation of discrete disulfide-bridged macrocycles and cages from these simple di- and/or trithiols.[7a, 8] Moreover, using design of experiments (DOE),[9] we have shown we can easily bias the self-assembly reaction mixture to optimize specific multimeric products[8b] and, using self-sorting methods, readily form asymmetric disulfide macrocycles[10]; however, thus far, our methods have been limited to utilizing benzylic

thiol precursors as we believed the Pn-π interaction to be of paramount importance in the pnictogen's directing ability,[11] greatly limiting the scope of suitable precursors.

In this work, we show this Pn-directing self-assembly method is, in fact, capable of forming a wider array of discrete disulfide macrocycles with a variety of starting multi-thiol substrates (Figure 4.2, **$H_2$1-$H_2$7**). Specifically, we vary the spacer size, shape, and electronics in a series of di- and trithiols to showcase the scope and utility of this reaction in the formation of a of disulfide-linked macrocycles before kinetically trapping them as thioether-linked macrocycles, utilizing sulfur extrusion methods.

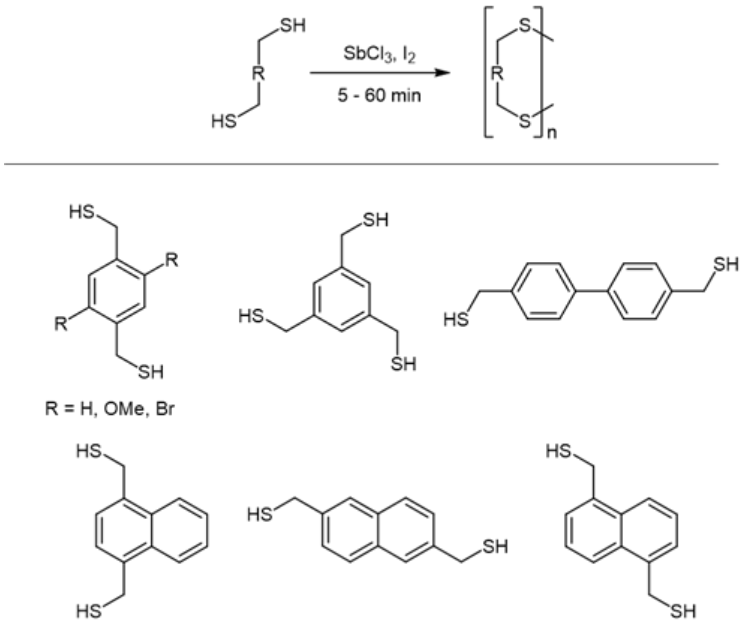

Figure 4.1: Top: General reaction scheme for the pnictogen-assisted self-assembly. Bottom: Previously reported starting thiols used to generate disulfide macrocycles.

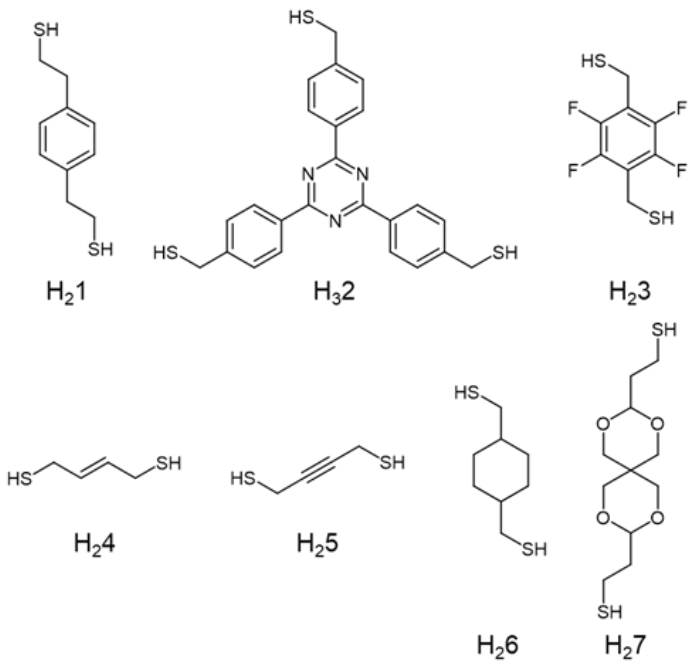

Figure 4.2: New di- and trithiols tested in this report for formation of disulfide macrocycles, including sulfur extrusion to the corresponding thioether.

To probe the extent of this method, we began to assess the necessity of the Pn-π interaction, which was previously thought to be required for proper alignment of the Pn-directing agent ($AsCl_3$, $SbCl_3$, or $BiCl_3$) via metalloid-π secondary bonding interactions.[19]

Our investigation began with testing extended benzylic linking arms, such as those seen in 1,4-bis(2-mercaptoethyl)benzene (**$H_2$1**) and the extended triazine system 2,4,6-tris(4-mercaptomethyl)-1,3,5-triazine (**$H_3$2**) and reducing the electron density of the arene system using 2,3,5,6-tetrafluoro-1,4-bis(mercaptomethyl)benzene (**$H_2$3**). The extended arm systems were chosen primarily because of their added flexibility, and also to investigate if having a heterocyclic substrate would affect the synthetic method. Substrate **$H_2$3** was chosen due to previous experimentation showing limited ability of extremely electron deficient systems (such as 2,3,5,6-tetranitro-1,4-

bis(mercaptomethyl)benzene showing limited or no reactivity with this method to form disulfide macrocycles. All substrates easily underwent Pn-directed self-assembly to form discrete disulfides, including the dimer through tetramer (79% combined yield) for $\mathbf{H_2 1}$ and dimer and trimer (72% combined yield) for $\mathbf{H_2 3}$. Approximately 20% of the lost yield in the formation of $\mathbf{H_2 3}$ can be accounted for by the formation of an easily isolatable S_NAr side product that also underwent cyclization. Substrate $\mathbf{H_3 2}$ only forms the dimer (93% yield), although a more complex tetrahedron should be theoretically possible and has been seen in simpler trithiols.[7a] It is likely this tetrahedron species is only formed in trace amounts, as the inner cavity would be expected to collapse unless a suitable guest were introduced to provide further stabilization.[13]

X-ray quality crystals of the mercaptomethyl dimer ($\mathbf{1_{D2}}$) were grown from vapor diffusion of hexanes into $CHCl_3$ and crystallized in the $P2_1/n$ space group (Figure 4.3, A). The C-S-S-C dihedral angles (∢: 84.1°, 84.1°) are close to ideality (90°) and the arene rings adopt a parallel displacement conformation with an interplanar distance of 4.81 Å.[23] The triazine dimer ($\mathbf{2_{D2}}$) crystallized in the $P2/n$ space group upon layering benzene on a solution of the cage in $CHCl_3$ (Figure 4.3, B). The C-S-S-C dihedral bond angle of all three disulfide bridges deviate considerably from ideality (∢: 104.2°, 111.1°, 112.7°). The distance between the three benzene ring pairs (3.58 Å, 3.64 Å, 3.71 Å) , and the two triazine cores (3.58 Å), suggest that there may be slightly favorable transannular π-π stabilization which allows such strained disulfide bonds to readily form. All adjacent ring systems within $\mathbf{2_{D2}}$ adopt a parallel-displacement conformation. Sulfur extrusion using hexamethylphosphorous triamide (HMPT) with $\mathbf{2_{D2}}$ (95% yield) resulted in the respective thiacyclophane and was purified via recirculating gel permeation chromatography (GPC).

Crystals of the triazine thioether (**2$_{T2}$**) were grown from slow evaporation in $CHCl_3$ and crystallized in the *P*-1 space group (Figure 4.3, C). The associated C-S-C bond angles (∢: 99.0°, 102.7°, and 104.2°) all align closely with ideality (103°). The interplanar distance between the three benzene rings decreased (3.51 Å, 3.53 Å, 3.59 Å), while the C_3N_3-C_3N_3 distance increased (3.85 Å) and the overall π-π stacking adopted more of a sandwich stacking conformation.

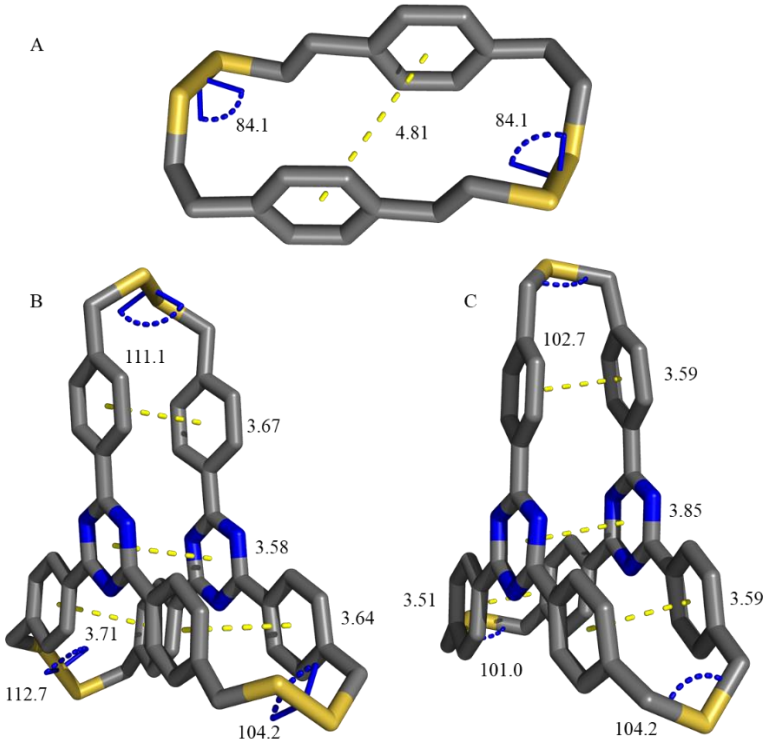

Figure 4.3: Single-crystal X-ray structures of **1$_{D2}$** (A), **2$_{D2}$** (B) and **2$_{T2}$** (C). Disulfide dihedral angles are shown in blue, arene-arene distances are shown in yellow. Hydrogens have been omitted for clarity.

Continuing our investigation, we began to deviate from the standard substrate motif of di- or trithiols that featured an arene ring spacer. Instead, the aromatic interactions believed to be required for this method to function were tested in the context of two dithiols with a π-system but lacking aromaticity: *trans*-2-butene-1,4-dithiol (**$H_2$4**)

and 2-butyne-1,4-dithiol (**$H_2$5**).[11b] These substrates readily undergo discrete disulfide macrocycle formation using our self-assembly methods, with **$H_2$4** generating the dimer through tetramer (95% combined yield). The dimer has been previously reported, although in very low yields in comparison to using our method (5.6% vs 32%).[24] Substrate **$H_2$5** underwent an unexpected transformation and actually formed the thioether directly (36% yield) and a smaller amount of disulfide (13% yield). This was quite surprising since this was the first time our pnictogen-assisted self-assembly method had not produced exclusively disulfides. Rather, the thioether forms in decent yield, which generally requires sulfur extrusion of the disulfides using HMPT. This is hypothesized to occur because of the alkyne's heightened nucleophilicity towards the polarized disulfide bond. Following the alkynes nucleophilic displacement of the disulfide bond, the generated sulfide can readily attack the other sulfur's α-carbon to yield a neutral thioether species. Further evidence in support of this transformation is the combined 51% loss of alkyne disulfide and thioether products following work-up, suggesting that half of the alkyne is consumed in this transformation to facilitate sulfur extrusion to the thioether. This reactivity has been previously shown utilizing trisulfide antimonate salts to form thiirenium ions selectively from alkyne substrates.[16]

X-ray quality crystals of the alkene disulfide trimer (**4_{D3}**) and alkyne thioether dimer (**5_{T2}**) were both grown from vapor diffusion of hexanes into $CHCl_3$ (Figure 4.4). **4_{D3}** crystallized in the $P2_1/c$ space group with two of the three disulfide dihedral angles diverging from ideality substantially (C-S-S-C ∢: 80.9°, 96.4°, 109.6°). **5_{T2}** has been reported in the literature previously,[17] however, we have crystallized a new polymorph of this structure which crystallized in the $P2_1$ space group with thioether bond angles close

to ideality (C-S-C ∢: 99.7°, 101.4°). The alkyne cores are slightly bent out of linearity, varying between 5-8° with parallel alkyne units lying 3.10 Å from each other. Sulfur extrusion on $\mathbf{4_{D3}}$ was attempted using HMPT and hexaethylphosphorous triamide (HEPT) but proved to be unsuccessful due to the reactivity of the alkene core, resulting in polymer and/or oligomer formation. These two examples showed that this method of forming disulfide and thioether macrocycles is not limited to substrates that possess a benzylic π-system as previously thought and can be extended into linear π-systems. It also suggests that alkynyl substrates might be useful sulfur-extrusion reagents in these systems, which we are currently exploring and may enable formation of the so far elusive thioether $\mathbf{4_{T3}}$.

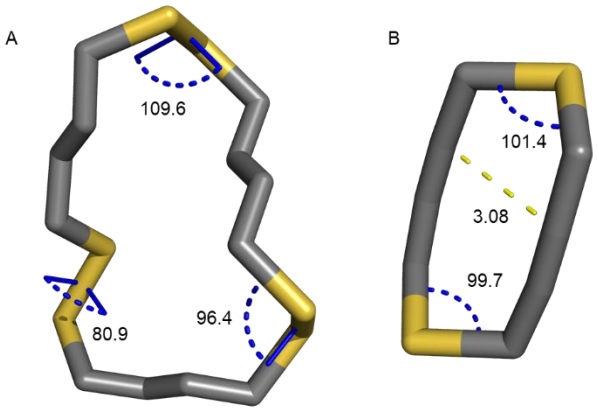

Figure 4.4: Single-crystal X-ray crystal structure of $\mathbf{4_{D3}}$ (A) and $\mathbf{5_{T2}}$ (B). Disulfide dihedral and thioether bond angles are shown in blue, alkyne-alkyne distances are shown in yellow. Hydrogens have been omitted for clarity.

Next, we sought to assess if any π-system is even necessary for this method to function properly. For this, we chose to use *trans*-1,4-bis(mercaptomethyl)cyclohexane (**$\mathbf{H_2}$6**). To our surprise, this method produced discrete disulfide macrocycles, including the dimer through heptamer (89% combined yield), with the tetramer and pentamer being

the dominate products (31% and 23% respectively). The trimer (**6$_{D3}$**) crystallized from vapor diffusion of hexanes into $CHCl_3$, the tetramer (**6$_{D4}$**) crystallized from slow evaporation in $CHCl_3$, and the pentamer (**6$_{D5}$**) crystallized from slow evaporation in DCM (Figure 4.5). **6$_{D3}$** crystallized in the $P2_1/c$ space group with the disulfide bridges showing slight strain (C-S-S-C ∡: 80.0°, 85.3°, 100.5°). **6$_{D4}$** crystallized in the $P2/c$ space group with disulfide bridges adopting a slightly more strained conformation (C-S-S-C ∡: 79.8°, 79.8°, 81.49°, 81.49°). **6$_{D5}$** crystallized in the *Iba*2 space group with three of the five disulfide bridges deviating from ideality by a considerable amount (C-S-S-C ∡: 78.1°, 79.6°, 84.7°, 92.9°, 133.3°). All crystals showed only the chair conformation of the cyclohexane core to be present with no considerable deviation from ideal cyclohexane bond angles (Figure 4.5). **6$_{D4}$** was then treated with HMPT, generating the thioether (**6$_{T4}$**) in quantitative yield.

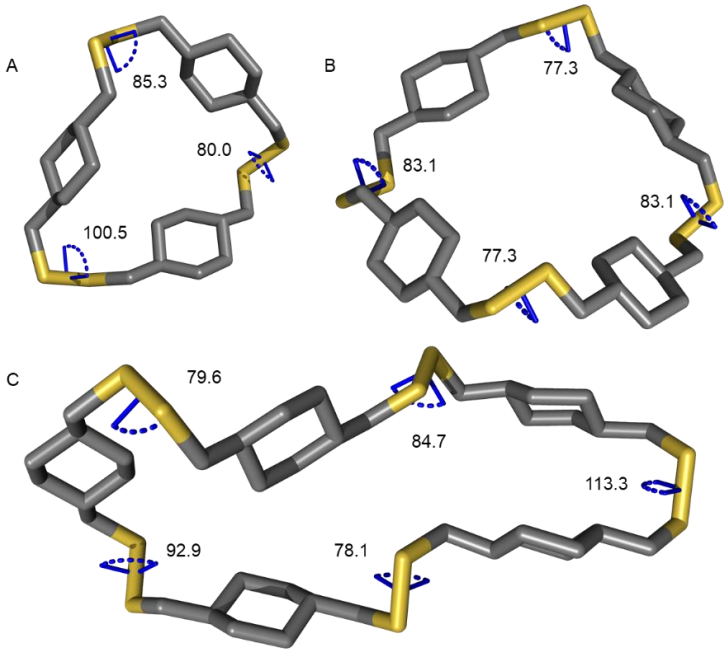

Figure 4.5: Single-crystal X-ray crystal structure of **6$_{D3}$** (A) **6$_{D4}$** (B), and **6$_{D5}$** (C). Disulfide dihedral angles are shown in blue. Hydrogens have been omitted for clarity.

In an attempt to fully explore the viability of this method to make truly unique disulfide macrocycles, a substrate that lacks a π-system, contains heteroatoms, and possesses an inherently unique spatial arrangement was synthesized. To accomplish this, we chose to use 3,9-ethanedithiol-2,4,8,10-tetraoxaspiro[5.5]undecane (**$H_2$7**) which to our amazement formed the disulfide dimer (**7_{D2}**) with relative ease in 50% yield, with higher ordered species forming only in trace yields. Crystals of **7_{D2}** were grown from vapor diffusion of hexanes into $CHCl_3$ and crystallized in the $P2_1/c$ space group (Figure 4.6). The disulfide bridges adopt a rather strained conformation, likely due to the unique structural twist of the spiro center (C-S-S-C ∢: 73.7°, 73.7°). This also leads the ^{1}H and ^{13}C NMR spectra to be quite complicated. Assignment of all associated peaks were confirmed using ^{1}H COSY and ^{13}C HSQC 2D NMR experiments and further validated with ^{13}C DEPT45, 90, and 135 NMR experiments, which confirms that the crystallized dimeric structure also persists in solution (see Appendix A). Facile generation of this dimer highlights the ability of this method to form disulfide macrocycles, even with substrates containing unique heterocyclic geometries and without any π-system coordination.

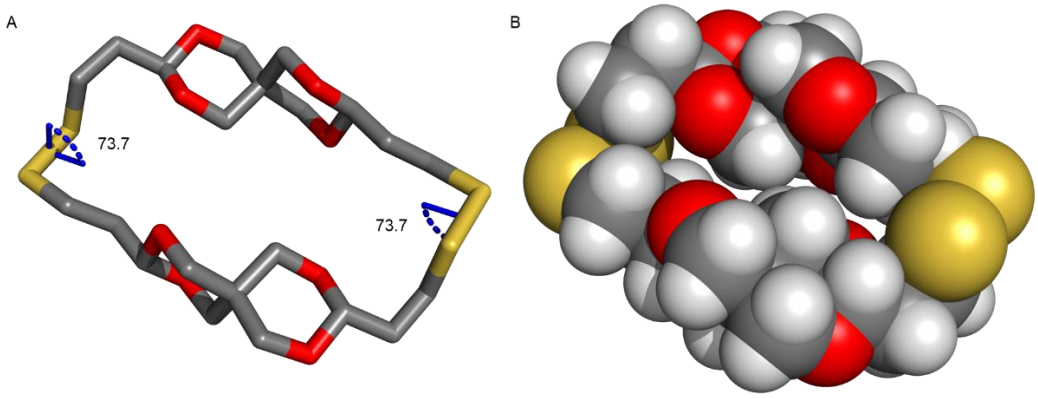

Figure 4.6: (A) Stick and (B) space-filling representation of single-crystal X-ray crystal structure of **7_{D2}**. Disulfide dihedral angles are shown in blue. Hydrogens have been omitted from stick representation for clarity.

Conclusion

In conclusion, we have successfully synthesized 21 new disulfide and thioether macrocycles containing a wide breadth of structural and electronic properties, including extended linker arms (**$H_2$1**), expanded π-systems (**$H_3$2**), electron deficient arene rings (**$H_2$3**), alkene (**$H_2$4**), alkyne (**$H_2$5**), cyclohexane (**$H_2$6**), and twisted heterocyclic spiro motifs (**$H_2$7**). Of these 21 total structures, 9 crystal structures have been obtained, elucidating many interesting and unique fundamental characteristics. We have shown that an aromatic system is not required for this metalloid-assisted self-assembly method to proceed, which makes this reaction amenable to a wide range of di- and trithiol substrates (and perhaps even more complex thiols). This discovery allows for a generalized method for the facile formation of discrete disulfide and thioether macrocycles in high yields with excellent efficiency. This new insight will undoubtedly lead to several new and exciting disulfide, thioether, and hydrocarbon macrocycles which have not been previously discovered.

Bridge to Chapter V

In Chapter IV we explore the ability of our pnictogen-assisted self-assembly method to form disulfide macrocycles on a wide variety of substrates. These include extended triazine-arene systems to linear alkene/alkyne to twisted heterocyclic spiro structures. All thiols tested showed the ability to form discrete disulfide macrocycles, resulting in 20 new structures and 9 crystal structures. These examples proved the ability for this method to be used as a general method for disulfide macrocycle formation, which can be sulfur extruded with HMPT. Chapter V discusses the current work toward forming

highly conjugated disulfide and thioether cyclophanes using perylene-3,4,9,10-tetracarboxylic acid diimide dithiols.

Experimental

General Procedures

Unless otherwise stated, reactions were conducted under atmospheric conditions. All commercially obtained reagents were used as received unless otherwise stated. Purification and separation of disulfide and thioether products were performed by using Japan Analytical Instruments Inc. LC-9101 recycling preparative high-performance liquid chromatography with gel permeation chromatography columns JAIGEL-1H and JAIGEL-2H. ^{1}H, ^{13}C NMR and 2D-COSY and HSQC spectra were recorded with a Bruker AVANCE 500 MHz, Bruker AVANCE 600 MHz or Varian INOVA 500 MHz spectrometer in $CDCl_3$. Spectra were referenced using the residual solvent resonances as internal standards and reported in ppm. High resolution mass spectrometry was obtained with a Xevo G2-XS TOF system from Waters using an atmospheric solids analysis probe.

Synthetic Procedures

Synthesis of thiols

The preparation of 1,4-bis(2-mercaptoethyl)benzene (**$H_2$1**), 2,3,5,6-tetrafluoro-1,4-bis(mercaptomethyl)benzene (**$H_2$3**), *trans*-2-butene-1,4-dithiol (**$H_2$4**), 2-butyne-1,4-dithiol (**$H_2$5**), and *trans*-1,4-bis(mercaptomethyl)cyclohexane (**$H_2$6**) were previously reported and characterized. Synthesis of precursors to trans-1,4-bis(mercaptomethyl)cyclohexane (**$H_2$6**) and 2,4,6-tris(4-bromomethyl)-1,3,5-triazine

(**$H_3$2**) were previously reported. Synthesis of 3-9,ethanedithiol-2,4,8,10-tetaoxaspiro[5.5]undecane (**$H_2$7**) was accomplished using a slightly modified literature procedure. ^{1}H-NMR spectral data and mass spectrometry data matched those reported in the literature.

Synthesis of 2,4,6-tris[4-(mercaptomethyl)phenyl]-1,3,5-triazine ($H_3$2)

To a 250 mL round bottom flask, 2,4,6-tris[4-(bromomethyl)phenyl]-1,3,5-triazine (0.988 g, 1.68 mmol) was dissolved in 60 mL $CHCl_3$. In a flask, thiourea (0.766 g, 10.1 mmol) was added to 50 mL acetone and sonicated. The thiourea solution was added to the RBF and left to stir for 16 hours at reflux. The resulting thiouronium salt was then vacuum filtered and washed with acetone. The solid was collected and used without further purification. The thiouronium triazine salt was added to a 500 mL RBF and 150 mL of NaOH (3M) and heated to 80 °C for 16 hours. The reaction was then cooled and put on ice then 9M HCl was added until the solution turned acidic, and a white precipitate formed. The solid was vacuum filtered, washed with water, and used without further purification (95% yield). ^{1}H-NMR (500 MHz, CD_2Cl_2) δ: 8.73 – 8.72 ppm (d, 6H), 7.56 – 7.55 ppm (d, 6H), 3.87 – 3.86 ppm (d, 6H), 1.93 ppm (t, 3H).

Modified synthesis of 3-9,ethanedithiol-2,4,8,10-tetaoxaspiro[5.5]undecane ($H_2$7)

To a 100 mL round bottom flask, 3,9-divinyl-2,4,8,10-tetraoxaspiro[5.5]undecane (1 g, 47 mmol), thioacetic acid (7.4 mL, 104 mmol) and DMPA (0.24 g, 0.90 mmol) were added in 25 mL THF. The reaction was sparged with N_2 and irradiated with LED-UV (λ = 370 nm) for 3 hours. The solvent was then evaporated and product was

recrystallized from hexane/ethyl acetate (9:1). The product was filtered and washed with hexane to yield the dithioacetate as white crystals (76% yield). Deprotection of the thioacetate followed literature procedures and matched previously reported characterization data (50% yield).

Synthesis of disulfide macrocycles

General synthetic procedure

To a dilute solution of a di- or trithiol, a separate solution of I_2 (2-4 equivalents) and $SbCl_3$ (2-4 equivalents) are added slowly under ambient conditions with stirring. The reaction is then allowed to stir briefly (15-60 minutes), then quenched with saturated Na_2SO_3 solution until the reaction is no longer purple. The reaction is then washed with H_2O, dried with $MgSO_4$ and condensed. The discrete disulfide macrocycle species are then separated using a prep-HPLC. Equivalents of I_2 and $SbCl_3$ to be used is substrate dependent. Solvents are generally $CHCl_3$, CH_2Cl_2, or C_6H_6 (others could be used).

Synthesis of 1,4-bis(2-mercaptoethyl)benzene ($\mathbf{1}_{D2\text{-}4}$) associated disulfide macrocycles

To a 50 mL solution of $\mathbf{H_2 1}$ (164 mg, 0.83 mmol) in $CHCl_3$, a 50 mL solution of $SbCl_3$ (340 mg, 1.5 mmol) and I_2 (380 mg, 2 mmol) was added slowly through a cotton-stuffed funnel. The reaction was allowed to stir for 15 minutes under ambient conditions. The reaction was then quenched with Na_2SO_3 until the reaction mixture turns from purple to white. The organic layer was collected and washed with 100 mL of H_2O (3x), dried with $MgSO_4$, and condensed to yield 159 mg of a white powder (79% combined yield:

57% dimer, 14% trimer, 13% tetramer). Dimer: ^{1}H-NMR (500 MHz, $CDCl_3$) δ: 7.07 ppm (s, 8H), 2.66 ppm (t, 8H), 2.50 ppm (t, 8H); ^{13}C-NMR (125 MHz, $CDCl_3$) δ: 138.19, 129.12, 43.18, 35.79 ppm; HRMS-ASAP [M+H]+ $C_{20}H_{25}S_4$ predicted: 393.0839, found: 393.0814. Trimer: ^{1}H-NMR (500 MHz, $CDCl_3$) δ: 7.15 ppm (q, 2H), 3.84 ppm (t, 6H), 2.99 – 2.86 ppm (m, 12H), 2.84 ppm (t, 6H); ^{13}C-NMR (125 MHz, $CDCl_3$) δ: 138.34, 136.74, 129.35, 129.01, 63.79, 40.44, 38.93, 35.45 ppm; HRMS-ASAP [M+H]+ $C_{30}H_{37}S_6$ predicted: 589.1220, found:589.1200. Tetramer: ^{1}H-NMR (500 MHz, $CDCl_3$) δ: 7.10 ppm (s, 16H), 2.90 ppm (m, 32H); ^{13}C-NMR (125 MHz, $CDCl_3$) δ: 138.30, 128.90, 40.60, 35.51 ppm; HRMS-ASAP [M+H]+ $C_{40}H_{49}S_8$ predicted 785.1600, found: 785.4924.

Synthesis of 12,4,6-tris(4-mercaptomethyl)-1,3,5-triazine (2_{D2}) associated disulfide macrocycles

To a 200 mL solution of **$H_3$2** (297 mg, 0.66 mmol) in benzene, a 100 mL solution of I_2 (1.02 g, 4.01 mmol) and $SbCl_3$ (611 mg, 2.68 mmol) was added slowly. The reaction was allowed to stir for 30 minutes under ambient conditions. The reaction was then quenched with Na_2SO_3 until the reaction mixture turns from purple to clear. The organic layer was collected and washed with 100 mL of H_2O (3x), dried with $MgSO_4$, and condensed to yield an off-white powder (92% yield). ^{1}H-NMR (500 MHz, $CDCl_3$) δ: 8.31 – 8.29 ppm (d, 6H), 7.12 – 7.11 ppm (d, 6H), 3.78 (s, 6H); ^{13}C-NMR (125 MHz, $CDCl_3$) δ: 170.65, 143.47, 134.86, 129.05, 128.91 ppm; HRMS-ASAP [M+H]+ $C_{48}H_{37}N_6S_6$ predicted: 888.1326, found: 888.1453.

Synthesis of trans-2-butene-1,4-dithiol (4_{D2-4}) associated disulfide macrocycles

To a 50 mL solution of **$H_2$4** (60 mg, 0.5 mmol) in $CHCl_3$, a 50 mL solution of I_2 (254 mg, 1 mmol) and $SbCl_3$ (228 mg, 1 mmol) was added slowly through a cotton-stuffed funnel. The reaction was allowed to stir for 15 minutes under ambient conditions. The reaction was then quenched with Na_2SO_3 until the reaction mixture turns from purple to white. The organic layer was collected and washed with 100 mL of H_2O (3x), dried with $MgSO_4$, and condensed to yield an orange oil (94% combined yield: 32% dimer, 29% trimer, 25% tetramer, 8% pentamer). Dimer: ^{1}H-NMR (500 MHz, $CDCl_3$) δ: 5.67 ppm (m, 4H), 3.36 – 3.35 ppm (m, 8H) ppm; ^{13}C-NMR (125 MHz, $CDCl_3$) δ: 129.52, 42.15 ppm; HRMS-ASAP [M+H]+ $C_8H_{13}S_4$ predicted: 236.9900, found: 236.9937. Trimer: ^{1}H-NMR (500 MHz, $CDCl_3$) δ: δ 5.70 ppm (m, 6H), 3.41 – 3.40 ppm (m, 12H); ^{13}C-NMR (125 MHz, $CDCl_3$) δ: 129.69, 41.68 ppm; HRMS-ASAP [M+H]+ $C_{12}H_{19}S_6$ predicted: 354.9811, found: 354.9891. Tetramer: ^{1}H-NMR (500 MHz, $CDCl_3$) δ: 5.72 – 5.64 ppm (m, 8H), 3.43 – 3.33 ppm (m, 16H); ^{13}C-NMR (125 MHz, $CDCl_3$) δ: 129.59, 41.76 ppm; HRMS-ASAP [M+H]+ $C_{16}H_{25}S_8$ predicted: 472.9722, found: 472.9787. Pentamer: ^{1}H-NMR (500 MHz, $CDCl_3$) δ: 5.72 – 5.68 ppm (m, 10H), 3.40 – 3.36 ppm (m, 20H); ^{13}C-NMR (125 MHz, $CDCl_3$) δ: 129.56, 41.59 ppm; HRMS-ASAP [M+H]+ $C_{20}H_{31}S_{10}$ predicted: 590.9633, found: 590.9696.

Synthesis of 2-butyne-1,4-dithiol associated disulfide (5_{D2}) and thioether (5_{T2}) macrocycles

To a 100 mL solution of **$H_2$5** (230 mg, 1.9 mmol) in $CHCl_3$, a 150 mL solution of I2 (533 mg, 2.1 mmol) and $SbCl_3$ (866 mg, 3.8 mmol) in $CHCl_3$ was added slowly through a cotton-stuffed funnel. The reaction was allowed to stir for 15 minutes under ambient conditions. The reaction was then quenched with Na_2SO_3 until the reaction mixture turns from purple to white. The organic layer was collected and washed with 100 mL of H_2O (3x), dried with $MgSO_4$, and condensed to yield a dark orange oil (49% combined yield: 36% thioether dimer, 13% disulfide dimer). Thioether dimer: ^{1}H-NMR (500 MHz, $CDCl_3$) δ: 3.48 ppm (s, 8H); ^{13}C-NMR (125 MHz, $CDCl_3$) δ: 80.7, 22.19 ppm. Disulfide dimer: ^{1}H-NMR (500 MHz, $CDCl_3$) δ: 3.47 ppm (s, 8H); ^{13}C-NMR (125 MHz, $CDCl_3$) δ: 81.65, 80.17, 29.17, 22.22 ppm; HRMS-ASAP [M+H]+ $C_8H_9S_4$ predicted: 232.9587, found: 233.0991.

Synthesis of trans-1,4-bis(mercaptomethyl)cyclohexane (6_{D2-7}) associated disulfide macrocycles

To a 100 mL solution of **$H_2$6** (385 mg, 2.18 mmol) in $CHCl_3$, a 150 mL solution of I_2 (2.2 g, 8.67 mmol) and $SbCl_3$ (1.07 g, 4.41 mmol) in $CHCl_3$ was added slowly. The reaction is allowed to stir for 30 minutes under ambient conditions. The reaction was then quenched with Na_2SO_3 until the reaction mixture turns from purple to clear. The organic layer was collected and washed with 100 mL of H_2O (3x), dried with $MgSO_4$, and condensed to yield a brown powder (76% combined yield: 3% dimer, 17% trimer, 24% tetramer, 17% pentamer, 10% hexamer, 5% heptamer). Dimer: ^{1}H-NMR (500 MHz,

$CDCl_3$) δ: 2.61 – 2.60 ppm (d, 4H), 2.00 – 1.80 ppm (m, 4H), 1.63 – 1.41 ppm (m, 2H), 1.03 – 0.94 ppm (m, 4H); ^{13}C-NMR (125 MHz, $CDCl_3$) δ: 46.90, 37.74, 32.01 ppm; HRMS-ASAP [M+H]+ $C_{16}H_{29}S_4$ predicted: 349.1152, found: 349.1146. Trimer: ^{1}H-NMR (500 MHz, $CDCl_3$) δ: 2.66 – 2.65 ppm (d, 4H), 2.05 – 1.98 ppm (m, 4H), 1.63 – 1.50 ppm (m, 2H), 1.04 – 0.95 ppm (m, 4H); ^{13}C-NMR (125 MHz, $CDCl_3$) δ: 48.06, 37.57, 32.45 ppm; HRMS-ASAP [M+H]+ $C_{24}H_{43}S_6$ predicted: 523.1689, found: 523.1693. Tetramer: ^{1}H-NMR (500 MHz, $CDCl_3$) δ: 2.64 – 2.63 ppm (d, 4H), 2.03 – 1.87 ppm (m, 4H), 1.67 – 1.50 ppm (m, 2H), 1.05 – 0.96 ppm (m, 4H); ^{13}C-NMR (125 MHz, $CDCl_3$) δ: 47.35, 37.71, 32.31 ppm; HRMS-ASAP [M+H]+ $C_{32}H_{57}S_8$ predicted: 697.2226, found: 697.4011. Pentamer: ^{1}H-NMR (500 MHz, $CDCl_3$) δ: 2.63 – 2.62 ppm (d, 4H), 1.98 – 1.92 ppm (m, 4H), 1.63 – 1.51 ppm (m, 2H), 1.04 – 0.95 ppm (m, 4H); ^{13}C-NMR (125 MHz, $CDCl_3$) δ: 47.34, 37.69, 32.28 ppm; HRMS-ASAP [M+H]+ $C_{40}H_{71}S_{10}$ predicted: 871.2763, found:871.6844. Hexamer: ^{1}H-NMR (500 MHz, $CDCl_3$) δ: 2.62 – 2.61 ppm (d, 4H), 1.98 – 1.92 ppm (m, 4H), 1.65 – 1.51 ppm (m, 2H), 1.03 – 0.95 ppm (m, 4H); ^{13}C-NMR (125 MHz, $CDCl_3$) δ: 47.08, 37.63, 32.27 ppm; HRMS-ASAP [M+H]+ $C_{48}H_{85}S_{12}$ predicted: 1045.3300, found: 1045.5718. Heptamer: ^{1}H-NMR (500 MHz, $CDCl_3$) δ: 2.62 – 2.60 ppm (d, 4H), 1.98 – 1.91 ppm (m, 4H), 1.63 – 1.51 ppm (m, 2H), 1.03 – 0.95 ppm (m, 4H); ^{13}C-NMR (125 MHz, $CDCl_3$) δ: 46.99, 37.60, 32.26 ppm; HRMS-ASAP [M+H]+ $C_{56}H_{99}S_{14}$ predicted: 1219.3837, found: 1219.2675.

Synthesis of 3-9,ethanedithiol-2,4,8,10-tetaoxaspiro[5.5]undecane (7_{D2}) associated disulfide macrocycles

To a 250 mL solution of **$H_2$7** (200 mg, 12 mmol) in CH_2Cl_2, a 100 mL solution of I_2 (0.536 g, 23 mmol) and $SbCl_3$ (0.594 g, 23 mmol) in CH_2Cl_2 was added slowly. The reaction was allowed to stir for 30 minutes under ambient conditions. The reaction was then quenched with Na_2SO_3 until the reaction mixture turns from purple to clear. The organic layer was collected and washed with 100 mL of H_2O (3x), dried with $MgSO_4$, and condensed to yield an off-white powder (50% dimer). ^{1}H-NMR (500 MHz, $CDCl_3$) δ: 4.66 ppm (q, 2H), 4.56 ppm (t, 2H), 3.56 – 3.61 ppm (m, 4H), 3.36 - 3.40 ppm (dd, 2H), 2.81 – 2.86 ppm (dm, 2H), 1.94- 2.08 ppm (m, 4H); ^{13}C-NMR (125 MHz, $CDCl_3$) δ: 100.98, 100.93, 70.58, 70.56, 70.20, 70.16, 33.77, 32.65, 32.50, 32.42, 32.00 ppm; HRMS-ASAP [M+H]+ $C_{22}H_{37}O_8S_4$ predicted: 557.1293, found: 557.2857.

Synthesis of thioether macrocycles

Synthesis of triazine thioether (2_{T2})

To a 40 mL solution of **2_{D2}** (50 mg, 0.06 mmol) in N_2 sparged $CHCl_3$, hexamethylphosphorous triamide (50 µL, 0.28 mmol) was added via glass syringe and allowed to react for 16 hours. The reaction was then opened to atmosphere, condensed to dryness, and purified using a prep-HPLC (91% yield). ^{1}H-NMR (500 MHz, $CDCl_3$) δ: 8.21 – 8.20 ppm (d, 6H), 7.19 – 7.18 ppm (d, 6H), 3.97 ppm (s, 6H); ^{13}C-NMR (125 MHz, $CDCl_3$) δ: 170.78, 143.28, 134.37, 129.30, 128.74 ppm; HRMS-ASAP [M+Na]+ $C_{48}H_{37}N_6S_3Na$ predicted: 815.2061, found: 815.2087.

Synthesis of 5,8,14,17,23,24,30,31-tetrathia[3.3.3.3]paracyclohexane (6_{T4})

To a 15 mL solution of **6_{T4}** (46 mg, 0.066 mmol) in N_2 sparged $CHCl_3$, hexamethylphosphorous triamide (70 µL, 0.39 mmol) was added via glass syringe and allowed to react for 16 hours. The reaction was then opened to atmosphere, condensed to dryness, and purified using a prep-HPLC (87% yield). ^{1}H-NMR (500 MHz, $CDCl_3$) δ: 2.66 – 2.65 ppm (d, 4H), 2.04 – 1.98 ppm (m, 4H), 1.67 – 1.51 ppm (m, 2H), 1.04 – 0.95 ppm (m, 4H) ^{13}C-NMR (125 MHz, $CDCl_3$) δ: 48.07, 37.57, 32.46 ppm; HRMS-ASAP [M+Na]+ $C_{32}H_{56}S_4Na$ predicted: 591.3163, found: 591.7262.

CHAPTER V

SYNTHESIS OF PERYLENE DIIMIDE MACROCYCLES

Contributions

This chapter discusses a current, unpublished project utilizing perylene diimide cores to synthesis new disulfide, thioether, and hydrocarbon cyclophanes. Dr. Lev N. Zakharov performed all X-ray crystallography and Prof. Darren W. Johnson provided intellectual support. I performed all experimentation, crystal growth, and characterization.

Introduction

Since the early 20th century, derivatives of perylene-3,4,9,10-tetracarboxylic acid diimide (PDI) have been explored thoroughly, with their initial use being found in the dye industry.[1] However, recent developments have shown that this substructure can be easily modified at the *bay*,[2] *ortho*,[3] and *peri*[4] positions (Figure 5.1) while also containing a large polycyclic aromatic core and strong electron-withdrawing carbonyl groups. These unique structural characteristics allow PDIs to have a host of desirable properties, such as low cost, large optical absorption range, chemical, thermal, and photochemical stability, and high fluorescence quantum yields.[5] This has led to a wide array of academic and industrial uses, including single molecule spectroscopy,[6] artificial photosynthesis,[7] singlet fusion,[8] dye lasers,[9] and fluorescent solar light harvesters[10] to name a few.

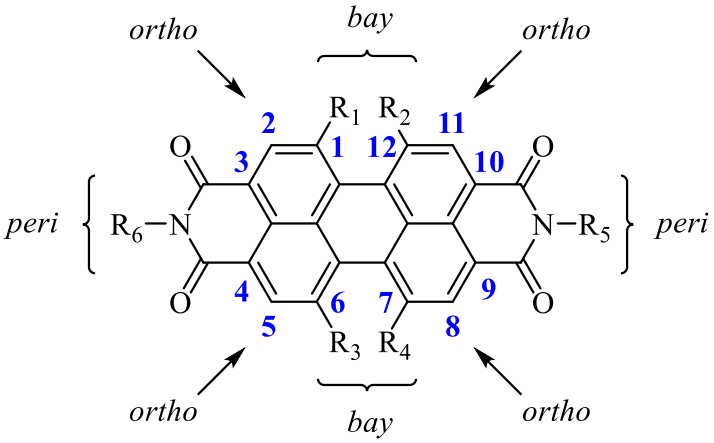

Figure 5.1: General structure of PDIs. The numbering of PDIs is based on the carbons that make up the outer boundary of the molecule. The overall molecule is generally separated by three categories: Positions 1, 6, 7, and 12 are known as *bay*, positions 2, 5, 8, and 11 are known as *ortho*, and positions 3, 4, 9, 10 are known as *peri*.

Interestingly, the optoelectronic properties of PDI derivatives can be easily altered by substituting different imide nitrogen motifs at the *peri* position and modifying the "core" region. Imidization of the perylene dianhydrides is accomplished by condensation with a primary amine using three common approaches (Scheme 5.1). The nature of the imide substituent primarily affects crystal morphology and solubility but rarely affects the optoelectronic properties due to the nitrogen atoms of the imide being located in a nodal plane for the HOMO and LUMO. This also limits inductive effects of *peri* substituents on the PDI aromatic core[5b] (Figure 5.2). The use of imidization to increase solubility was first described by Langhals and co-workers[11] by adding "swallowtail" substituents[12] – long alkyl chains attached to the imide nitrogen and branching at a central point, such as 5-aminononane. The increased solubility arises from the steric interaction of the carbonyl groups and the bulky "swallowtails", forcing them out of the plane of the PDI chromophore resulting in limited ability of the PDI molecules to stack via face-to-face π-π stacking.[12-13] Additionally, water solubilizing properties have been added to the

otherwise hydrophobic PDIs by modification of the *peri* position with *L*-β-amino-alanine,[14] cyclodextrin,[15] and polyglycerol dendrons.[16]

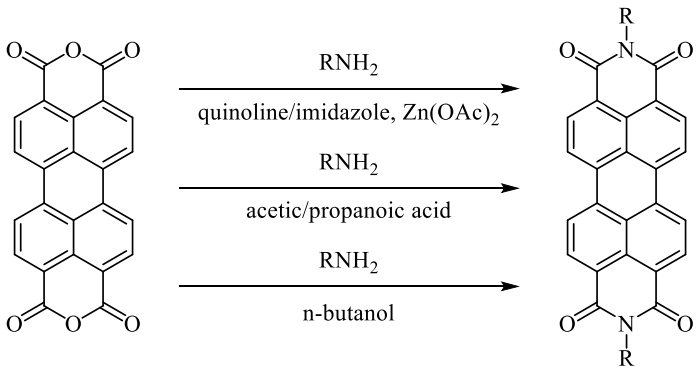

Scheme 5.1: General method for imidization of perylenetetracarboxylic dianhydride via condensation with primary amines.

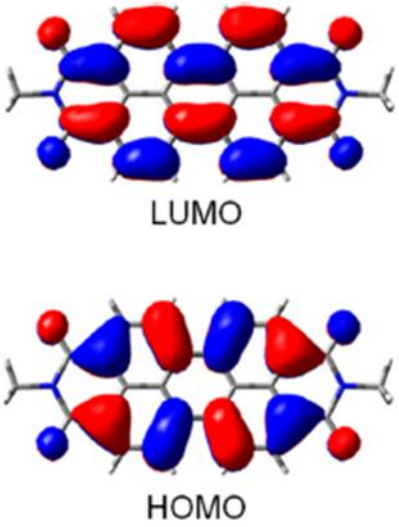

Figure 5.2: B3LYP/6-31++G** Calculated HOMO and LUMO energy levels of N,N'-bis(methyl)perylene-3,4,9,10-tetracarboxylic diimide. Adapted with permission from *Chemical Reviews* **2016**, *116*, (3), 962-1052. Copyright 2016 American Chemical Society.

Conversely, substituents at the core positions have considerable effect on all properties of the PDI, including morphological and solubilizing as well as optical and electrochemical. As shown in Scheme 5.2, tetrachloro and dibromo derivatives are important synthetic intermediates for high yielding synthesis of a wide range of PDIs.

The 1,6,7,12-tetrachloro version, which is synthesized using sulfuric acid and chlorine,[17] is not as widely used due to the harsh reaction conditions required compared to the milder synthesis of the dibromo variant, accomplished using Br_2 at room temperature in dichloromethane.[2] Some consideration has to be taken into account for the dibromo synthesis, as it also gives mono- and tribrominated side products in addition to the 1,6- and 1,7-regioisomers. While the mono- and tribrominated products are easily separated using column chromatography, the regioisomers can be very challenging to separate and can only be differentiated using high-field ^{1}H-NMR spectroscopy (Appendix C, Figure 1).[18]

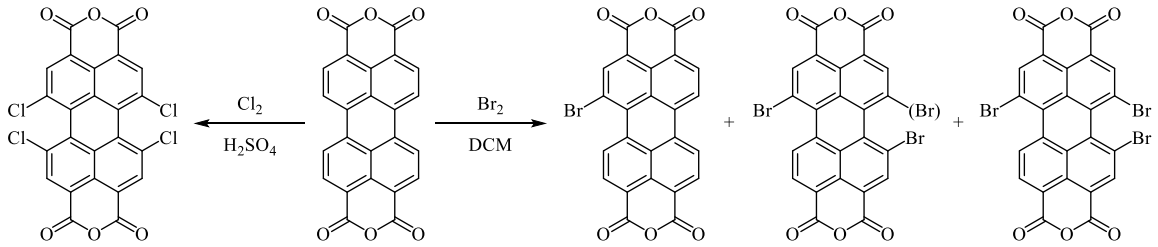

Scheme 5.2: Most common methods of halogenations of the *bay* region to give tetrachlorinated (left) and mono-, di-, and tribrominated (right) dianhydrides. The dibrominated product (left center) provides a mixture of 1,6- and 1,7-regioisomers.

Facile nucleophilic substitution of the dibromo PDI is generally straightforward and high yielding (Scheme 5.3). For example, cyano, aryl, alkyl, and amine nucleophiles have been synthesized resulting in a wide variety of optoelectronic and redox properties due to the electronic coupling between the aromatic core and the substituents.[19] Additionally, C-C coupling reactions such as Suzuki,[20] Stille,[21], Negishi,[22] and Sonogashira[23] reactions have been used to obtain further functionality in the *bay* region.

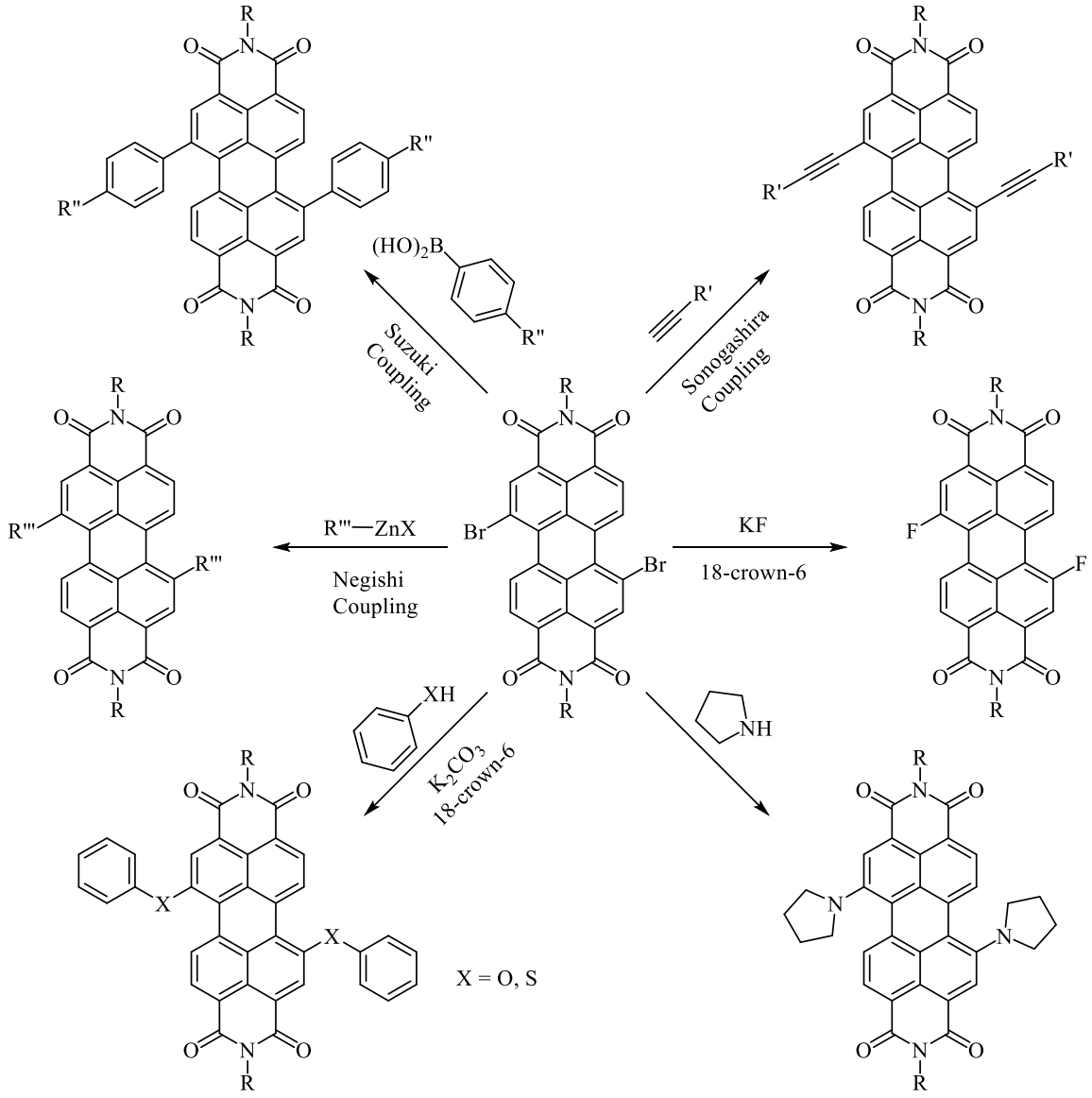

Scheme 5.3: Selected examples of *bay* region functionalization of 1,6- and 1,7-regioisomers of PDIs. The 1,6-regioisomer is excluded for clarity, however, these reactions often occur with both regioisomers present due to the extreme difficulty in separation.

The type of functional group that is used at the *bay* position can have a large impact on the electronic properties of the resulting PDI. Groups that withdraw electron density from the aromatic core, such as halogens, lowers both the HOMO and LUMO energy levels similarly via inductive effects through the σ bond. This has only a small

impact on the absorption and emission properties compared to unsubstituted PDIs.[24] Functional groups that are π-donors, such as pyrrolidinyl and phenoxy groups, tend to raise the HOMO more than the LUMO, resulting in a large shift in absorption.[4] Using these principles allows for intentional tuning of the HOMO and LUMO and can have a large impact on their use in organic electronic devices.

While PDIs have been studied for decades, macrocyclization of these molecules has remained relatively unexplored. Some recent examples include phenyl-bithiophene-phenyl linked PDI units developed by the Nuckolls group.[21, 25] These reports showcased the ability of these macrocycles to be *n*-type electronic materials and that the conformations of the cyclic PDIs provide a marked difference on the electron transporting properties. They also showed that in comparison to the linear version of the PDI, the macrocyclic versions were superior in organic photovoltaics. The Beer group has also shown that PDI macrocycles can be used to encapsulate a guest molecule, such as C_{60}.[26] While there are many impressive examples of macrocyclic PDI motifs, most of them suffer from difficult and harsh reaction conditions and are almost universally low yielding. Considering our previous success in making libraries of discrete disulfide macrocycles in near quantitative yields,[27] we sought to use our metalloid-assisted self-assembly method to generate new disulfide, thioether, and hydrocarbon PDI macrocycles and explore their properties.

Results and Discussion

While there has been much work in making various derivatives of PDIs, there are only a few examples of PDI motifs containing thiols at the *peri* position, while there are even less examples of thiols at the *bay* position.[28] These *peri* position thiols, while interesting, either lack a flexible arm to form disulfide bonds (thiophenol) or contain large, extended arms (PEG chains) which would likely homocouple, reducing the overall effectiveness of our method, which is generally very fast (< 30min) and results in high yields. For these reasons, we decided to attempt to synthesize a *bay* position benzylic thiol PDI since benzylic thiols have previously shown to be highly effective in our metalloid-assisted self-assembly method. Imidization of perylenetetracarboxlic dianhydride was accomplished using 3-aminopentane (**PDI-3AP**, 97% yield) followed by bromination of the *bay* region (**PDI-Br**) using Br_2, resulting in a 1:4 ratio of 1,6- and 1,7-regionisomers following literature procedures (Scheme 5.4).[2] Successful imidization is quite apparent, as the starting material perylenetetracarboxlic dianhydride (PTCDA) is completely insoluble, while the resulting PDI is very soluble. There is also a color change from purple-red (PTCDA) to crimson-red (**PDI-3AP**) to bright-red (**PDI-Br**) (Figure 5.3). Separation of the 1,6- and 1,7-regioisomers was attempted using silica gel column chromatography and recycling prep-HPLC with no success; however, mono- and tribrominated PDI side products were easily separated from the regioisomers with silica gel column chromatography using 100% $CHCl_3$ as eluent (first spot = regioisomers, second spot = monobrominated, third spot = tribrominated).

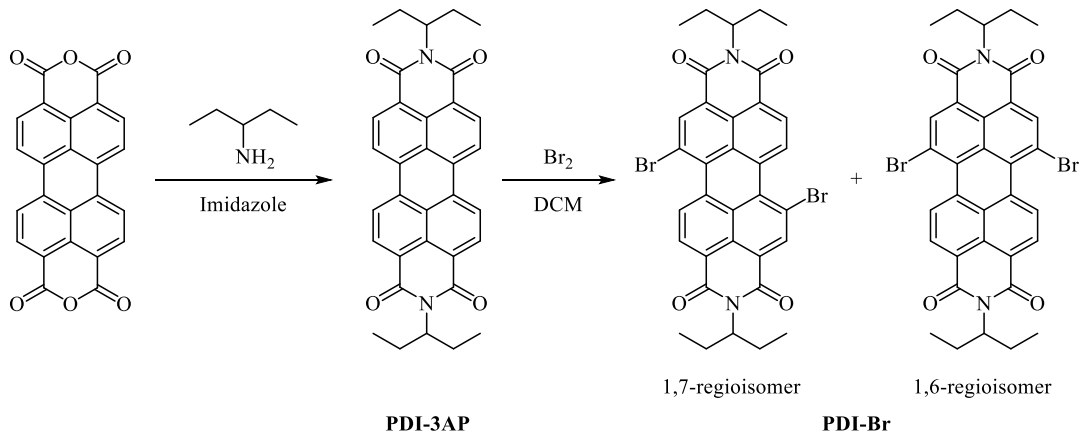

Scheme 5.4: Synthetic procedure for generating the required perylene dibromo diimide (**PDI-Br**). The regioisomers ratio were found to be in a ~1:4 ratio of 1,7- to 1,6-regioisomer as seen with 600 MHz ^{1}H-NMR.

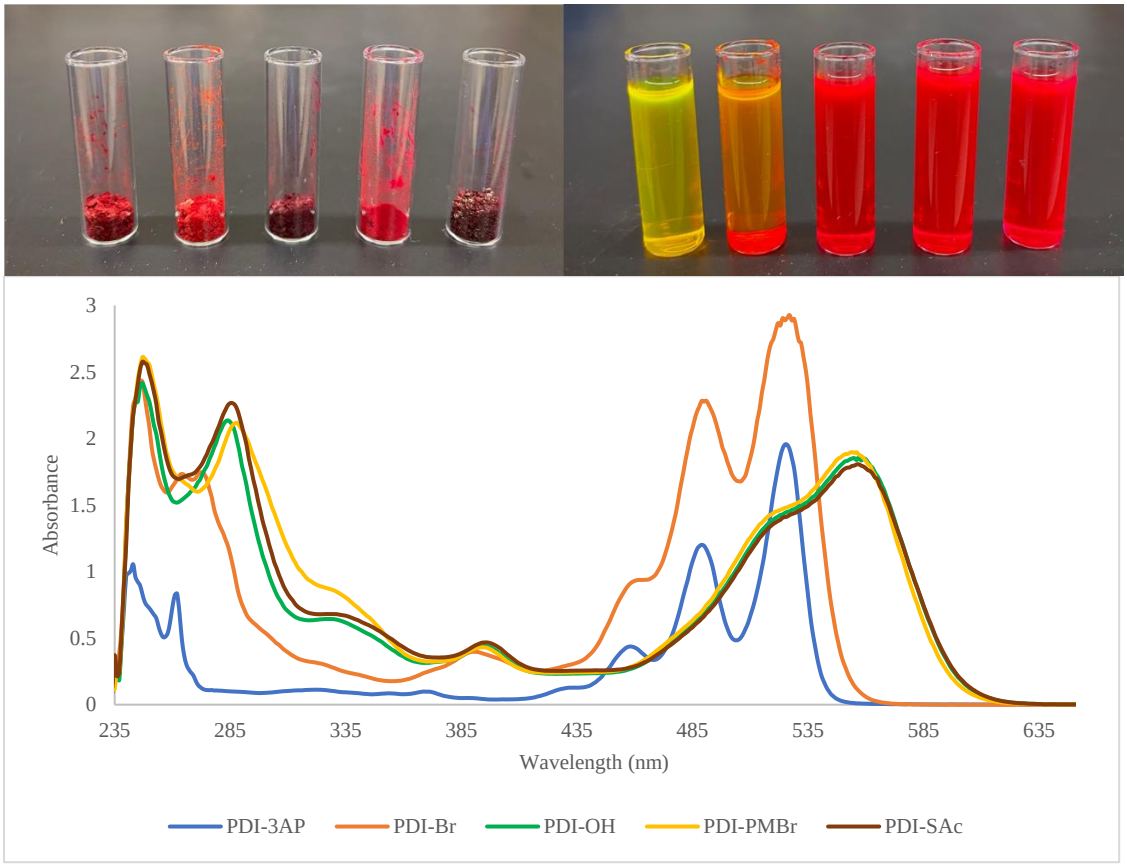

Figure 5.3: Solid phase (top-left) and solution phase (top-right, DCM) color shifts during the synthetic process (left to right: **PDI-3AP, PDI-Br, PDI-OH, PDI-PMBr, PDI-SAc**). Bottom: UV/Vis spectroscopy of all intermediates.

Next, synthesis of a benzylic structure at the *bay* position was attempted, initially via Suzuki coupling 4-(bromomethyl)phenylboronic acid as this had shown to be successful in previous reports.[25] However, only homocoupled product was formed and lots of unknown side reactions occurred. Next, we tried 4-toylboronic acid which did prove to be successful. Unfortunately, subsequent radical bromination using N-bromosuccinimide and 2,2'-azobis(2-methylpropionitrile) proved to give a combination of mono- through tetrabrominated species that proved extremely difficult to separate. Finally, 4-(hydroxymethyl)phenylboronic acid (**PDI-OH**, Scheme 5.5) was attempted and was successful resulting in a deep purple solid in 60% yield (Figure 5.3).

Converting the pendent hydroxyl groups into a reactive handle that would provide a path towards the desired thiol was next. Initially, tosylation of these groups was tried, however, this proved to be difficult as no conditions could be found to provide anything but unreacted starting material. Instead, bromination of the hydroxyl group was easily achieved using refluxing 48% HBr, resulting in quantitative yields (**PDI-PMBr**, Scheme 5.5) of a bright red solid (Figure 5.3). Initially column chromatography was used to attempt purification of the desired product using a gradient of 0 – 100% Hexanes/$CHCl_3$. Unexpectedly, this solvent system showed separation of the 1,6- and 1,7-regioisomers with the first fractions being enriched in the 1,6-isomer and the latter fractions being enriched in the 1,7-isomer. This was an important discovery because most reports show that purification of these two isomers required either very long recrystallizations (months) or expensive chiral columns for specialized HPLCs. Purification of both isomers was shown to be most effective using a "long" plug in 100% DCM.

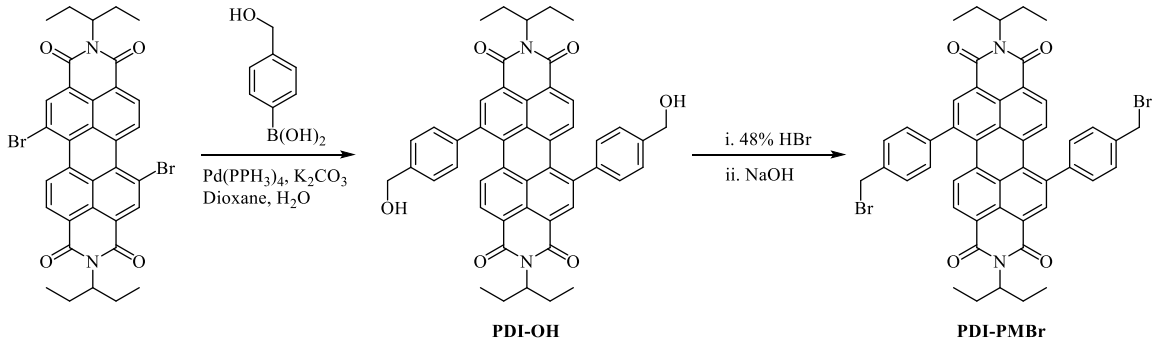

Scheme 5.5: Synthetic procedure utilizing Suzuki coupling to generate **PDI-OH** followed by bromination (**PDI-PMBr)** in refluxing 48% HBr.

X-ray quality crystals were grown of **PDI-PMBr** from slow evaporation in $CHCl_3$ and crystallized in the *P*-1 space group. Interestingly, due to the large steric bulk of the pendent 4-(bromomethyl)phenyl "arms" at the *bay* position, there is a large helical twist through the PDI aromatic core of 21.7° as measured from imide to imide (Figure 5.4). This helical twist is a known phenomenon and when constrained in a macrocycle, induces chirality which will have to be accounted for during macrocyclic characterization.[29] This steric hindrance also causes the arms to rotate considerably from planarity in relation to the PDI core (PDI-core – phenyl-arm ∢'s: 54.6°, 56.6°).

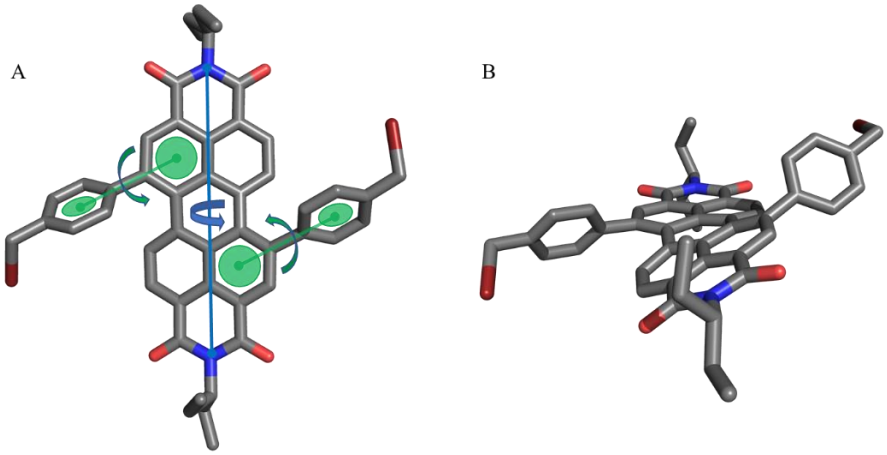

Figure 5.4: X-ray crystal structure of **PDI-PMBr**. (A) The structure contains a helical twist along the long axis (blue line, 21.7°) and the pendent "arms" are twisted out of planarity with the PDI core by 54.6° and 56.6° (green circles/lines). Hydrogens have been omitted for clarity. (B) *Peri* position view highlights these twisting characteristics.

The final step of synthesizing the desired thiol has proven to be difficult. Many synthetic pathways have been attempted, including thiourea, TBASH, and thioacetate. The latter method has shown the most promise using potassium thioacetate in THF at room temperature, resulting in the desired dithioacetate (**PDI-SAc**) in 80% yield (Scheme 5.6) and a deep metallic purple solid (Figure 5.3). Of note, this reaction works best in THF, however, the common stabilizer 2,6-dimethyl-4-tert-butylphenol (BHT) has shown to be difficult to remove during the post-synthetic purification steps for unknown reasons; ideally, unstabilized THF is used to avoid this difficult to remove impurity.

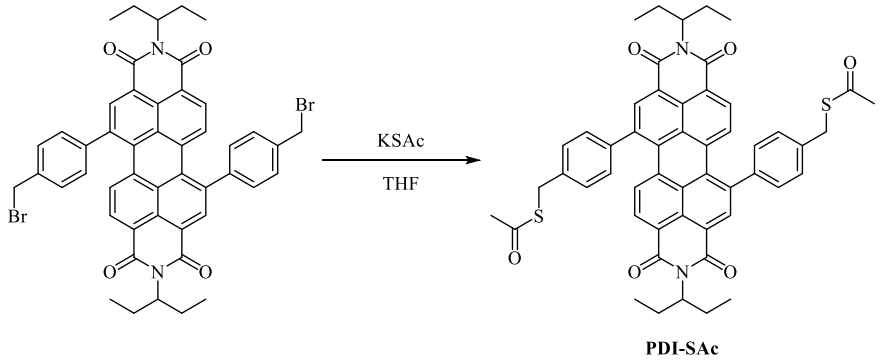

Scheme 5.6: Synthetic procedure to the final intermediate (**PDI-SAc**) before the desired PDI thiol.

Subsequent deprotection of the thioacetate into the thiol has not been successful as of yet. Several ways, including base hydrolysis (K_2CO_3/MeOH/THF and NaOH/THF/H_2O/HCl)[30] and using acetyl chloride[28a] have been attempted but only complex mixtures of products and a trace amount of the desired dithiol was present (confirmed with HRMS). While frustrating, there are many ways to convert the thioacetates to thiols, such as treatment with LiOH,[31] NH_4HCO_3,[32] NaSMe/MeOH,[33] and $LiAlH_4$/THF[34] to name a few. It is possible that the unique electronic structure of the PDI is causing the thiols to polymerize as they are formed. If this is true, possible solutions

include using high dilution principles or forming a pre-organized cage structure that can be converted to the thiol *in-situ* during the macrocyclization process.[27b]

Conclusions

In summary, we have attempted to synthesize the starting PDI-thiol required for cyclization using our metalloid-assisted self-assembly method. This process has been difficult, but we have laid the groundwork for future synthetic strategies to achieve this starting material which will be used for disulfide, thioether, and hydrocarbon cyclization. These PDI macrocycles will provide a new structural connectivity within the limited literature of macrocyclic PDIs and will likely provide new and interesting optoelectronic, redox, and host/guest properties.

Bridge to Chapter VI

Chapter V presented the current synthetic progress and challenges toward forming a *bay* position dithiol PDI. Once formed, pnictogen-assisted self-assembly should be straightforward, forming discrete disulfide cyclophanes. Optical and electronic properties of these cyclophanes would then be tested for their use in pigments, dyes, and photovoltaics. These properties would then also be tested against their linear oligomeric counterparts. Chapter VI provides conclusions to this dissertation and provides future directions for the project.

Experimental

General Procedures

All chemicals were used as received. Purification and separation of products were performed using a Japan Analytical Instruments Inc. LC-9101 recycling preparative high-performance liquid chromatography with size exclusion chromatography columns JAIGEL-1H and JAIGEL-2H in serial or silica gel column chromatography. ^{1}H-NMR and ^{13}C-NMR spectra were recorded on a Bruker AVANCE 600 MHz or Varian INOVA 500 MHz spectrometer using Topspin software in $CDCl_3$, CD_2Cl_2. Data were processed in MestReNova. High resolution mass spectrometry was performed on a Xevo G2-XS ToF system from Waters using an atmospheric solids analysis probe. N,N'-bis(ethylpropyl)perylene-3,4,9,10-tetracarboxylic diimide (**PDI-3AP**) and 1,6- and 1,7-dibromo-N,N'-bis(ethylpropyl)perylene-3,4,9,10-tetracarboxylic diimide (**PDI-Br**) was synthesized using previously reported literature procedures.[2]

Synthetic Procedures

Synthesis of 1,6- and 1,7-di(4-(hydroxymethyl)phenyl)-N,N'-bis(ethylpropyl)perylene-3,4,9,10-tetracarboxylic diimide (PDI-OH)

To a 1 L RBF was added **PDI-Br** (4.1g, 5.96 mmol), 4-(hydroxymethyl)phenyl (3.62g, 23.8 mmol), K_2CO_3 in 80 ml H_2O (22g, 2M), and dioxane (340 ml) and sparged with N_2 for 3 hours. Tetrakis(triphenylphosphine)palladium(0) was then added under positive N_2 flow and sparged another 10 minutes before left to react for 16 hours at 90 °C. The reaction was then cooled to room temperature and added to separatory funnel. The layers were allowed to settle, then collected the organic layer and condensed.

Redissolved the product in $CHCl_3$ and washed with water (3x), dried with $MgSO_4$, and condensed to give a deep purple solid (60% yield). ^{1}H NMR (500 MHz, $CDCl_3$): δ = 8.61 – 8.59 ppm (d, 2H), 8.12 ppm (t, 2H), 7.84 – 7.83 ppm (d, 1H), 7.79 – 7.78 ppm (d, 1H), 7.58 – 7.44 ppm (m, 8H), 5.11 – 4.97 ppm (m, 2H), 4.85 – 4.83 ppm (d, 4H), 2.32 – 2.16 ppm (m, 4H), 1.97 – 1.85 ppm (m, 4H), 1.85 – 1.81 ppm (bs, 2H), 0.97 – 0.84 ppm (m, 12H); ^{13}C NMR (150 MHz, $CHCl_3$): δ = 141.97, 141.92, 141.64, 141.57, 141.49, 140.93, 134.95, 134.30, 132.93, 132.68, 130.34, 129.85, 129.62, 129.43, 129.19, 128.67, 128.64, 128.07, 64.67, 57.75, 25.14, 11.43 ppm; HRMS-ASAP [M+H]+ $C_{48}H_{43}N_2O_6$ predicted: 743.3121, found: 743.2923.

Synthesis of 1,6- and 1,7-di(4-(bromomethyl)phenyl)-N,N'-bis(ethylpropyl)perylene-3,4,9,10-tetracarboxylic diimide (PDI-PMBr)

To a 500 ml RBF was added **PDI-OH** (2.4g, 3.23 mmol) and 48% HBr (200 ml) and allowed to reflux for 16 hours. The reaction was then cooled to room temperature then placed in an ice bath. 12M NaOH was added until the solution became basic. Added to separatory funnel and washed with $CHCl_3$ until aqueous layer became clear (emulsions easily formed), dried with $MgSO_4$, and condensed to give a red solid (95% yield). ^{1}H NMR (500 MHz, $CDCl_3$): δ = 8.65 – 8.53 ppm (m, 2H), 8.19 – 8.06 ppm (m, 2H), 7.82 – 7.81 ppm (d, 1H), 7.78 – 7.77 ppm (d, 1H), 7.58 – 7.39 ppm (m, 8H), 5.10 – 4.98 ppm (m, 2H), 4.59 – 4.58 ppm (d, 4H), 2.31 – 2.17 ppm (m, 4H), 1.96 – 1.85 ppm (m, 4H), 0.97 – 0.84 ppm (m, 12H); ^{13}C NMR (150 MHz, $CHCl_3$): δ = 142.79, 142.38, 141.43, 140.46, 138.63, 138.51, 134.75, 134.07, 132.95, 132.66, 131.00, 130.46, 129.98, 129.69,

129.46, 129.35, 128.15, 57.78, 32.79, 25.14, 11.44 ppm; HRMS-ASAP [M+H]+ $C_{48}H_{41}N_2O_4Br_2$ predicted: 867.1433, found: 867.1293.

Synthesis of 1,6- and 1,7-di(4-(thioacetatemethyl)phenyl)-N,N'-bis(ethylpropyl)perylene-3,4,9,10-tetracarboxylic diimide (PDI-SAc)

To a 250 ml RBF was added **PDI-PMBr** (402 mg, 0.464 mmol), unstabilized THF (60 ml), and potassium thioacetate (162 mg, 1.42 mmol) and allowed to react for 16 hours at room temperature. The reaction was then condensed, redissolved in DCM, washed with water (3x), dried with $MgSO_4$, and condensed to give a deep metallic purple solid (80% yield). ^{1}H NMR (500 MHz, $CDCl_3$): δ = 8.63 – 8.51 ppm (m, 2H), 8.18 – 8.06 ppm (m, 2H), 7.83 – 7.81 ppm (d, 1H), 7.78 – 7.77 ppm (d, 1H), 7.52 – 7.33 ppm (m, 8H), 5.08 – 4.96 ppm (m, 2H), 4.22 – 4.21 ppm (d, 4H), 2.29 – 2.17 ppm (m, 4H), 1.94 – 1.84 ppm (m, 4H), 0.93 – 0.86 ppm (m, 12H); ^{13}C NMR (150 MHz, $CHCl_3$): δ = 195.13, 141.28, 140.71, 138.64, 134.88, 132.61, 130.76, 130.32, 129.47, 129.35, 129.23, 128.07, 125.66, 57.72, 33.23, 25.13, 11.49 ppm; HRMS-ASAP [M+H]+ $C_{52}H_{47}N_2O_6S_2$ predicted: 859.2876, found: 859.2903.

X-ray Crystallography

Diffraction intensities for **PDI-PMBr** were collected at 173 K on a Bruker Apex2 CCD diffractometer using MoKα radiation, l= 0.71073 Å. Space group was determined based on intensity statistics. Absorption correction was applied by SADABS. Structure was solved by direct methods and Fourier techniques and refined on F^2 using full matrix least-squares procedures. All non-H atoms were refined with anisotropic thermal

parameters. H atoms were refined in calculated positions in a rigid group model. Crystal structure of **PDI-PMBr** includes also solvent molecule $CDCl_3$. All calculations were performed by the Bruker SHELXL-2014 package.

Crystallographic data for PDI-PMBr

$C_{49}H_{41}Br_2Cl_3N2O4$, M = 988.01, 0.16 x 0.11 x 0.04 mm, T = 173(2) K, Triclinic, space group *P*-1, a = 12.3875(7) Å, b = 13.4419(8) Å, c = 14.6722(9) Å, α = 68.954(3) β = 73.906(3)°, γ = 74.550(3)°, V = 2152.5(2) $Å^3$, Z = 2, D_c = 1.524 Mg/m^3, μ(Cu) = 4.489 mm^{-1}, *F*(000) = 1004, $2\theta_{max}$ = 133.37°, 22639 reflections, 7555 independent reflections [R_{int} = 0.0375], R1 = 0.0581, wR2 = 0.1581 and GOF = 1.044 for 7555 reflections (541 parameters) with I>2σ(I), R1 = 0.0627, wR2 = 0.1622 and GOF = 1.044 for all reflections, max/min residual electron density +2.011/-1.033 $eÅ^{-3}$.

CHAPTER VI

CONCLUSIONS AND FUTURE OUTLOOK

CONTRIBUTIONS

This final chapter discusses current and future work for expanding our knowledge and applicability of metalloid-assisted self-assembled cyclophanes. This chapter includes unpublished work performed by Jacob Mayhugh, Henry Trubenstein, Isabella Demachkie, Luca Zocchi, and myself who collected a variety of experimentation and characterization data. Professor Darren W. Johnson provided intellectual support.

INTRODUCTION

By expanding on our understanding of how metalloid-assisted self-assembly functions, we have begun to dive deeply into its full capabilities to form cyclophanes. In Chapter II we discussed our investigation into the ability of this method to tolerate the presence of functional groups that could later be further modified. To our delight, we found this method to be very tolerant, allowing for the facile synthesis of discrete disulfide, thioether, and sulfone dibromo arene cyclophanes in high yields. ‘Design of experiments’ was then used to selectively and intentionally increase the yield of a traditionally difficult to synthesize trimeric species by 400%.

In Chapter III, we reviewed our unexpected discovery of a novel trithioorthoformate cage which was synthesized in high yields using the solvent as a reagent. Chapter IV introduced the broad applicability of this method towards a variety of

di- and trithiols, ranging from large aromatic systems to linear and highly twisted spiro systems. This research highlighted the ability of this technique to form a wide breadth of disulfide and thioether macrocycles, regardless of the structural or electronic makeup, in high yields. In Chapter V, the current synthetic methods and challenges toward forming the first *bay* position disulfide and thioether macrocycles were discussed. In this final chapter, several potential future paths forward will be described.

FUTURE DIRECTIONS

Expansion of functionalized cyclophanes

In Chapter II we examined the synthesis of discrete disulfide, thioether, and sulfone cyclophanes containing a dibromo arene motif. While the dimeric structure is usually the dominant product, 'design of experiments' was used to greatly increase the yield of a synthetically more difficult target, the trimer. While the disulfide variant is rather labile due to the disulfide bridge, the thioether and sulfone are significantly more stable and would likely be easily further modified via the dibromo functional groups. It is well known that bromobenzene structures readily undergo a variety of cross-coupling reactions, such as Suzuki, Sonogashira, and Negishi coupling, opening up a wide array of possible post-synthetic modifications (Scheme 6.1). With this synthetic path, it would be possible to start to develop tube like structures and possibly develop complex cyclophane bridged [*n*]cycloparaphenylenes (Figure 6.1).

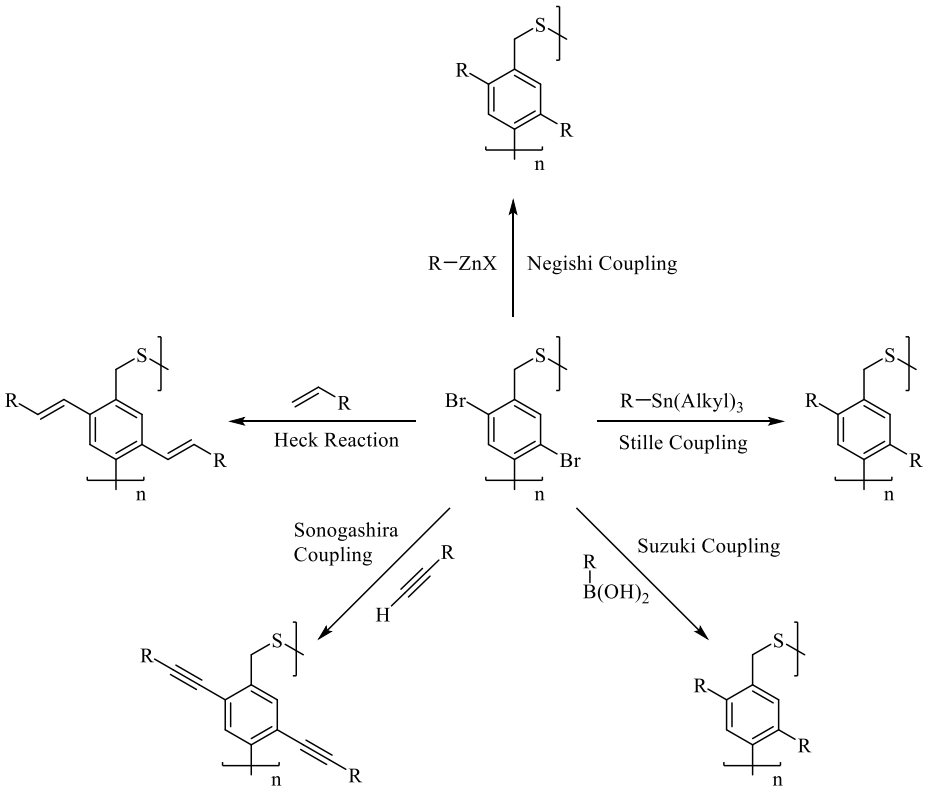

Scheme 6.1: Post-synthetic modification reactions for further functionalization of dibromo arene cyclophanes.

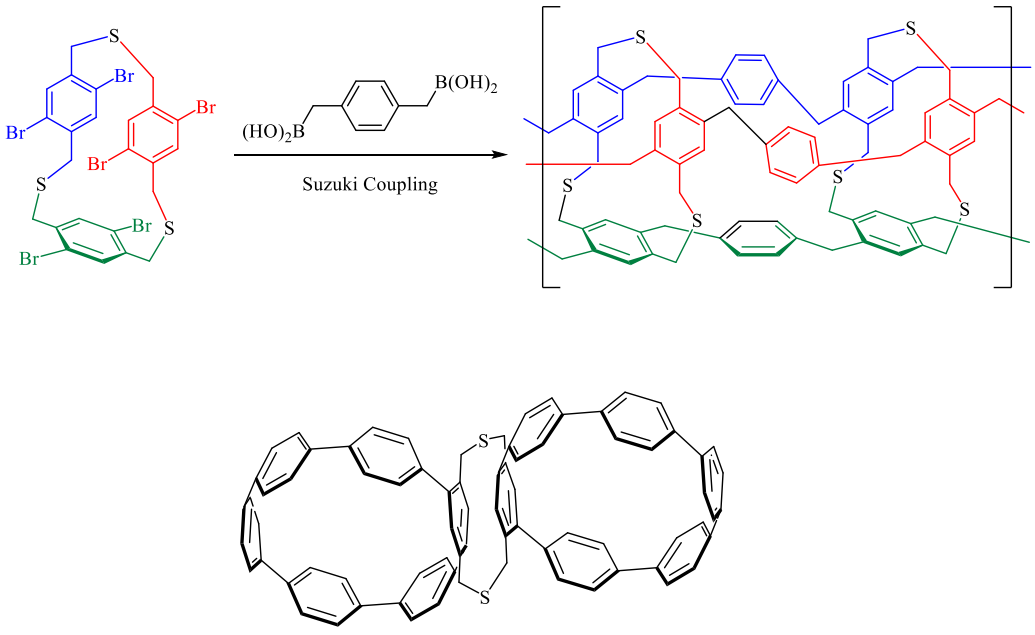

Figure 6.1: Top: Possible synthetic routes to form tube like structures using dibromo arene trimer (coloration is for clarity). Bottom: Cyclophane bridged [*n*]cycloparaphenylenes.

Trithioorthoformate thiol metathesis for unusual thiols

In Chapter III, the discovery of a trace species, a trithioorthoformate cage, was discussed. Under normal conditions, this cage formed in a mere 3%; however, after optimization of reaction conditions, the yield was increased to a respectable 60%. Due to this considerable increase in yield, this structure now has the capability of acting as an unusual thiol, providing access to otherwise inaccessible cyclophanes.

Generation of these new thiols would require the reduction of the disulfide bonds using 2-mercaptoethanol or dithiothreitol[1] which would result in a trithioorthoformate centered hexathiol (Scheme 6.2, A). Additionally, a new trithiol could be formed via thiol metathesis using stoichiometric amounts of strong Brønsted acids (TFA, MsOH, H_2SO_4, etc.) or catalytic amounts of Lewis acids ($FeCl_3$, $AlCl_3$, etc.) (Scheme 6.2, B).[2] Identifying the ideal reaction conditions to form these unique thiols may be time consuming, so the use of 'design of experiments' should be employed to facilitate these discoveries.

Treatment of the resulting thiols would result in highly atypical dimers and tetrahedral species (Figure 6.2). Subsequent partial hydrolysis of these new macrocycles could then be performed to generate new, extremely unusual thiols that could be used to form new ligands.

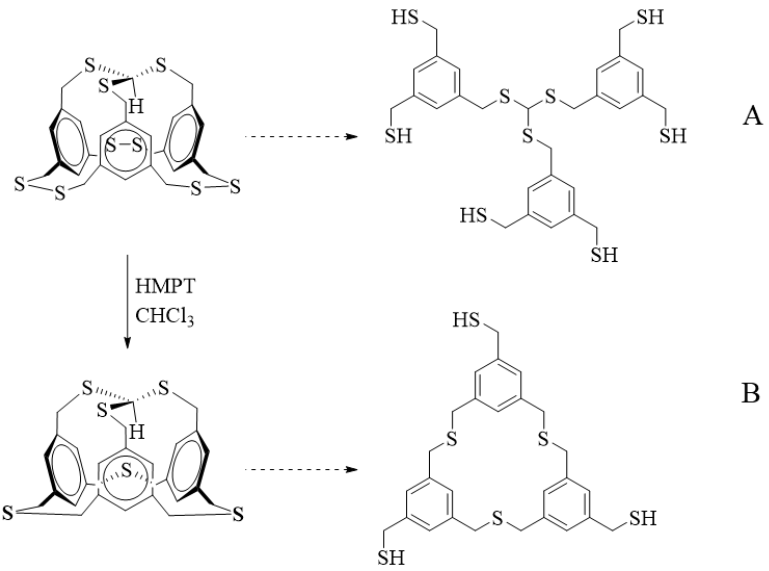

Scheme 6.2: (A) Disulfide bond reduction to produce a trithioorthoformate centered hexathiol. (B) thiol metathesis resulting in a large trithiol structure.

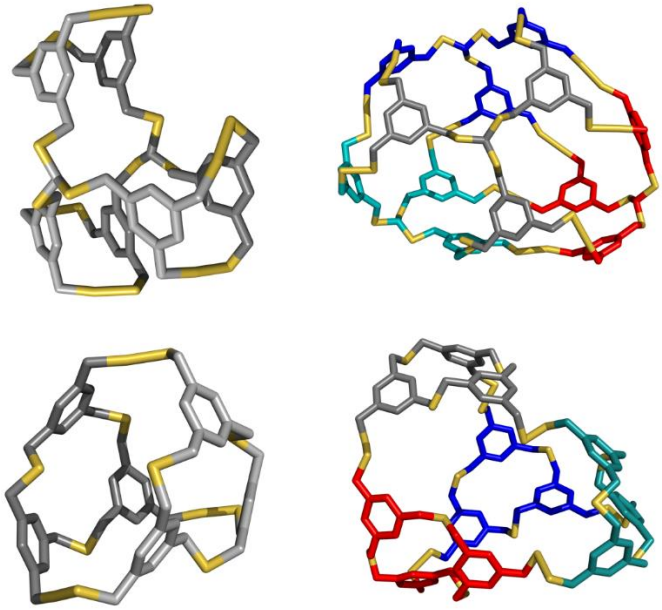

Figure 6.2: Stick representations of DFT models of disulfide dimers (left) and tetrahedra (right) using the resulting hexathiol (top) and trithiol (bottom). Coloration of tetrahedra by individual ligands from Scheme 6.2 is shown for clarity.

Expansion of metalloid-assisted self-assembly cyclophanes

Chapter IV covered our investigation into the full scope of our metalloid-assisted self-assembly method. It was found to be extremely robust, forming disulfide macrocycles that ranged from large aromatic systems to highly twisted spiro motifs containing heteroatoms. Research into further substrates should be readily explored. Possible targets could include biological type substrates, such as short peptides containing cysteine at both terminal ends, thiols that contain other binding motifs, such as hydrogen bonding for guest inclusion, and fluorescent molecules which could be used for medical imaging.

PDI catenanes and host/guest properties

The current synthetic steps towards a PDI dithiol were discussed in Chapter V, including possible synthetic routes to forming the desired product. Once these dithiols are synthesized, macrocyclization should proceed cleanly, providing discrete disulfide macrocycles. Previous studies have shown that due to the parallel arrangement, rigidity, and highly aromatic cores of PDI dimers, planar aromatic guests easily intercalate into the cavity via π-π interactions.[3] These guests can have a large impact on the fluorescent nature of PDIs with electron-poor guests causing an increase in fluorescence and electron-rich guests quenching fluorescence due to charge transfer complexes. While tuning the optoelectronic properties after synthesis of the cyclophanes with guests will be interesting, it may be possible to tune product distribution using these guests during synthesis. For example, would larger guests like $C_{60/70}$ or adamantane force the larger

cyclophanes to form more readily? Would inclusion of non-planar and/or heterocyclic guests affect the cyclization process and in what way?

Using these host/guest principles will allow for even more interesting complexes to form. Due to the strong π-π stacking nature within the PDI cavity, this property could be used to form catenanes under thermodynamic control. Intelligent ligand design will allow the synthesis of dimeric species with a targeted pore size, allowing for the intercalation of dithiol guests. For example, a *peri* substituted dithiol PDI could be used to form the disulfide dimer then converted to the more stable thioether via sulfur extrusion using HMPT. A planar aromatic thiol functionalized guest (i.e., anthracenyl dithiol) would then be introduced and allowed to bind within the PDI dimer cavity (Figure 6.3, A). This complex would then be treated with our metalloid-assisted self-assembly method, resulting in the formation of a [2]catenane (Figure 6.3, B).

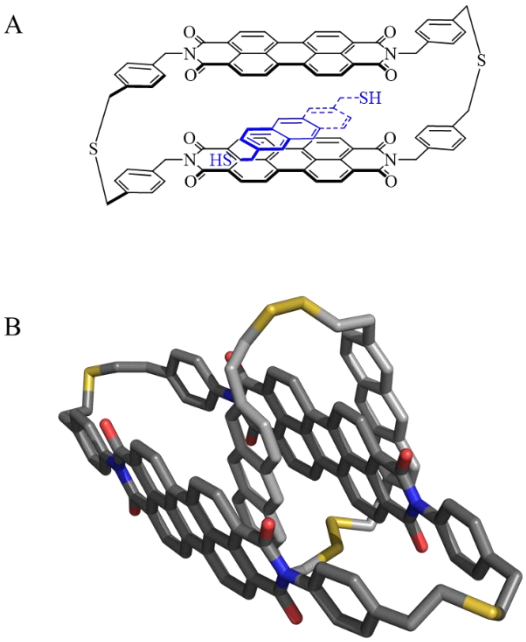

Figure 6.3: (A) Perylene thioether dimer with an anthracenyl dithiol guest (blue). (B) DFT model of potential [2]catenane PDI. Subsequent metalloid-assisted self-assembly of the host/guest complex would lead to disulfide formation of the guest, resulting in a [2]catenane.

Taking this idea to its pinnacle, the use of self-assembly, host/guest chemistry, and self-sorting could be applied. Here, two independent dimeric PDI thiacyclophanes would be linked via an unsymmetrical tetrameric disulfide containing anthracenyl guests which are bridged by phenyl spacers (Figure 6.4). This would be an extremely ambitious project but could be taken a step further to form poly-[*n*]-catenanes as well.

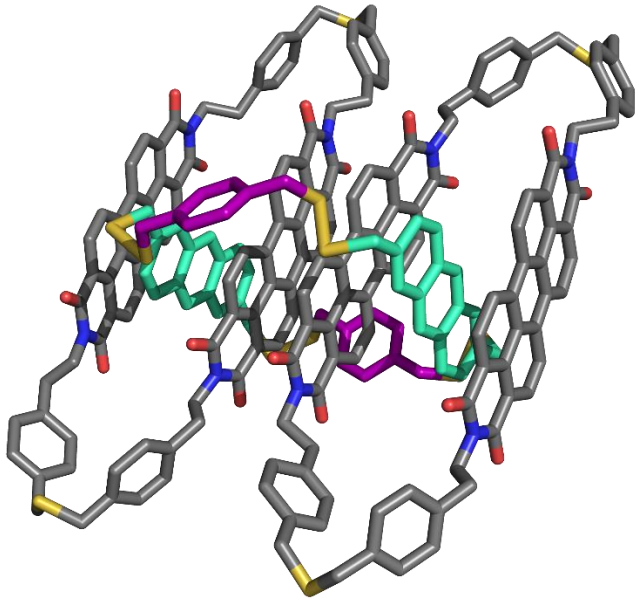

Figure 6.4: DFT model of a [3]catenane utilizing self-assembly, host/guest chemistry, and self-sorting. Anthracenyl dithiol guests (teal) intercalated into dimeric PDI hosts (grey). The guests would then be bridged with phenyl spacers (purple), forming an unsymmetric tetrameric disulfide species, resulting in a [3]catenane.

APPENDIX A

NMR SPECTROSCOPY FOR A GENERALIZED METHOD FOR DISULFIDE AND THIOETHER CYCLOPHANES

1.6 NMR spectra

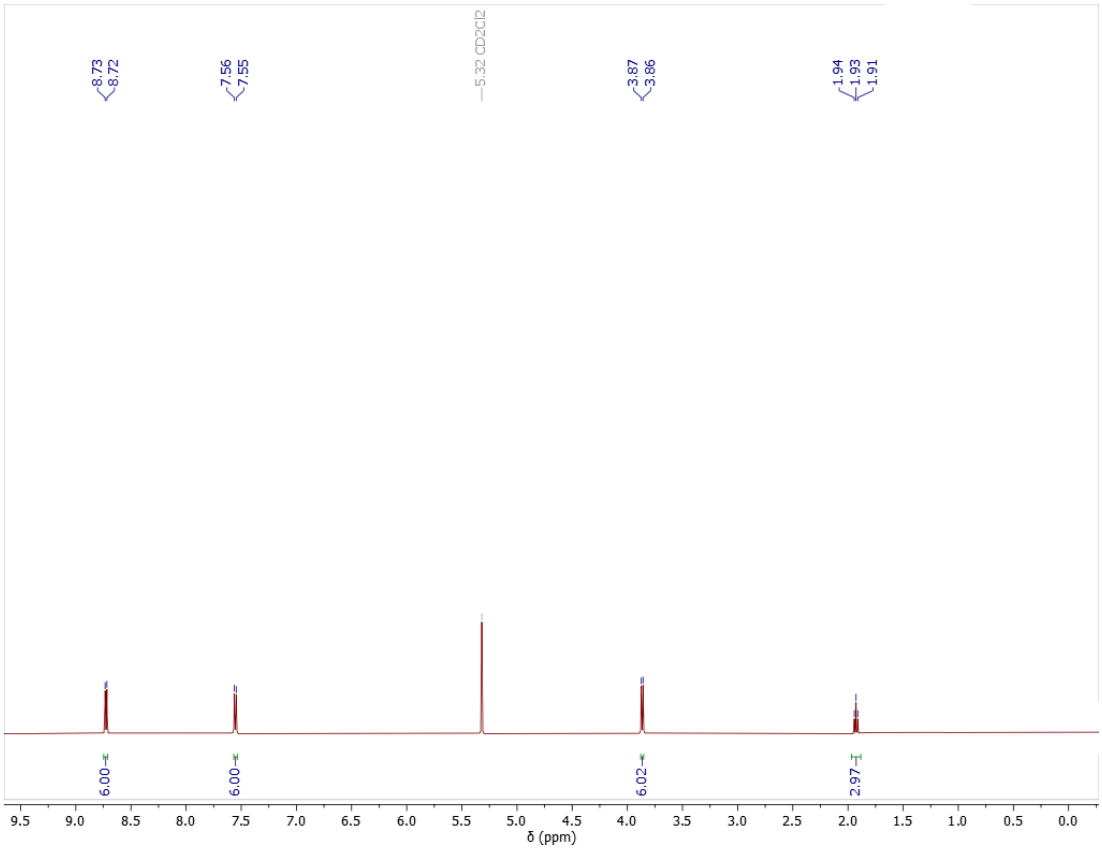

Figure A1: ^{1}H-NMR spectrum of **H$_3$2** in CD_2Cl_2

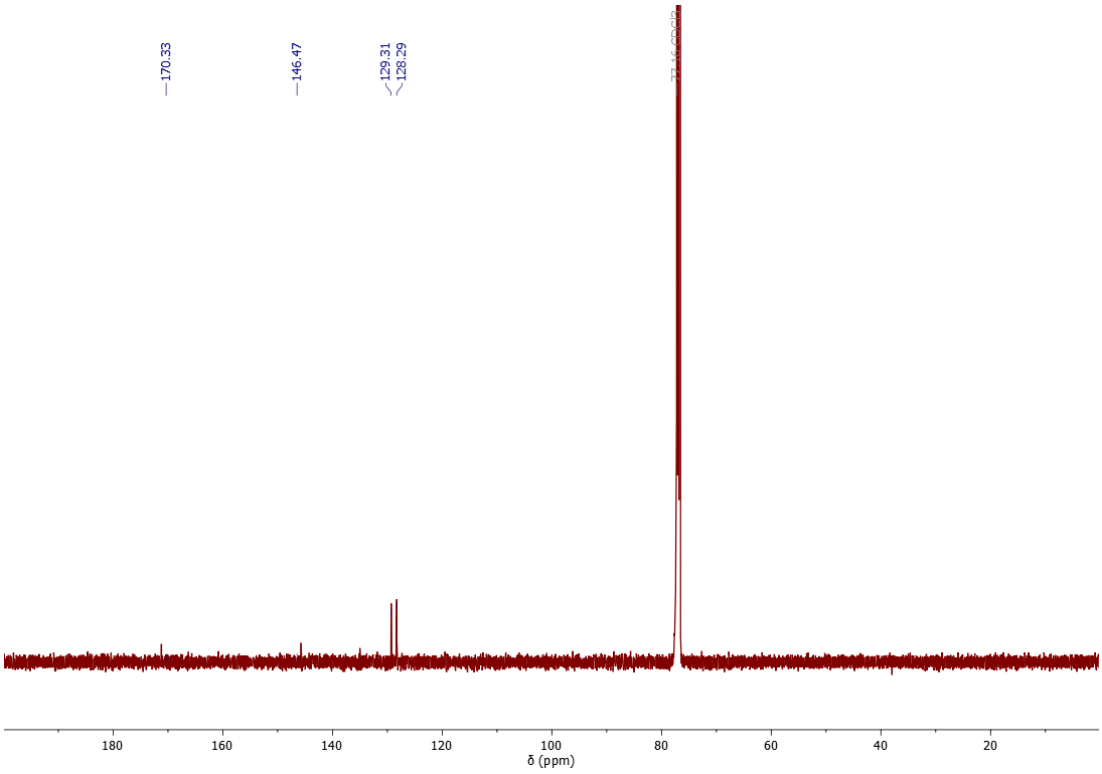

Figure A2: ^{13}C-NMR spectrum of $\mathbf{H_32}$ in $CDCl_3$

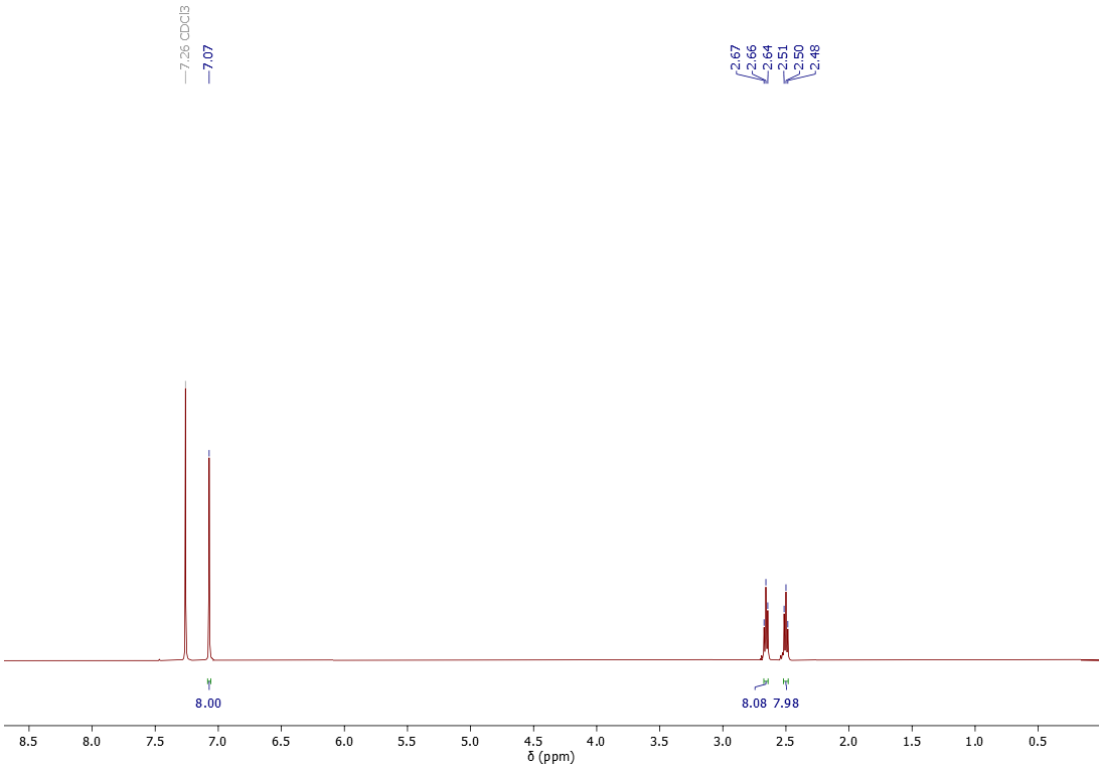

Figure A3: ^{1}H-NMR spectrum of dimer $\mathbf{1_{D2}}$ in $CDCl_3$

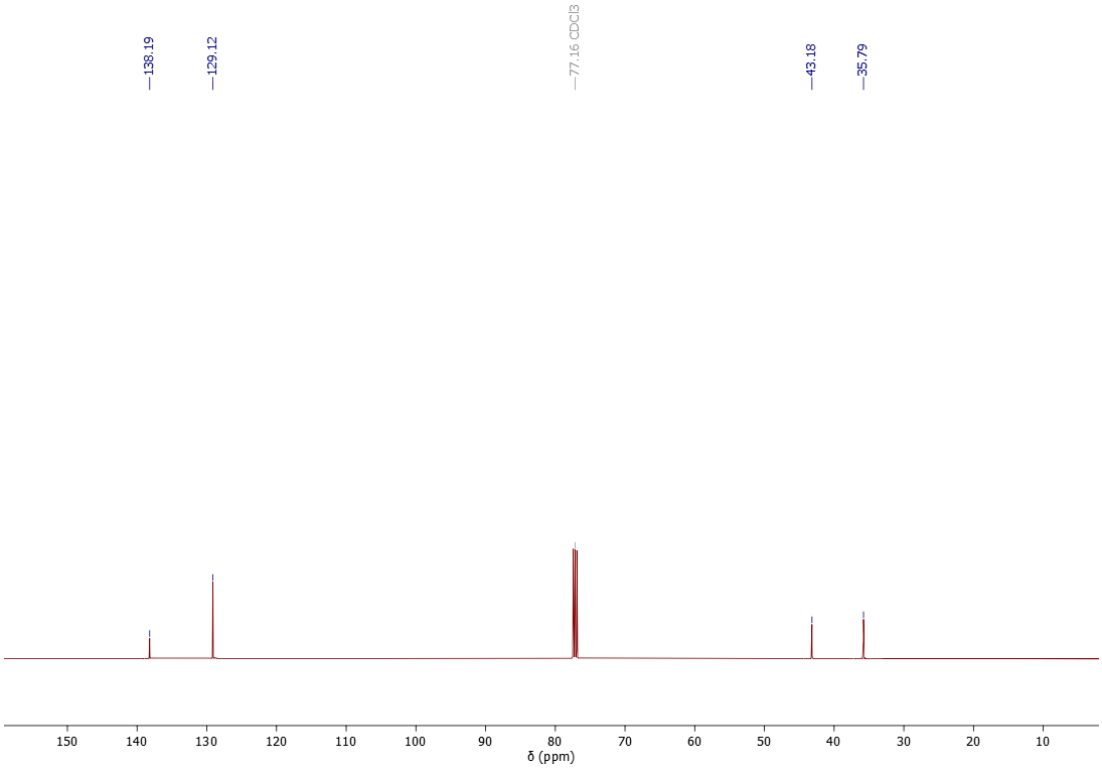

Figure A4: ^{13}C-NMR spectrum of dimer $\mathbf{1_{D2}}$ in $CDCl_3$

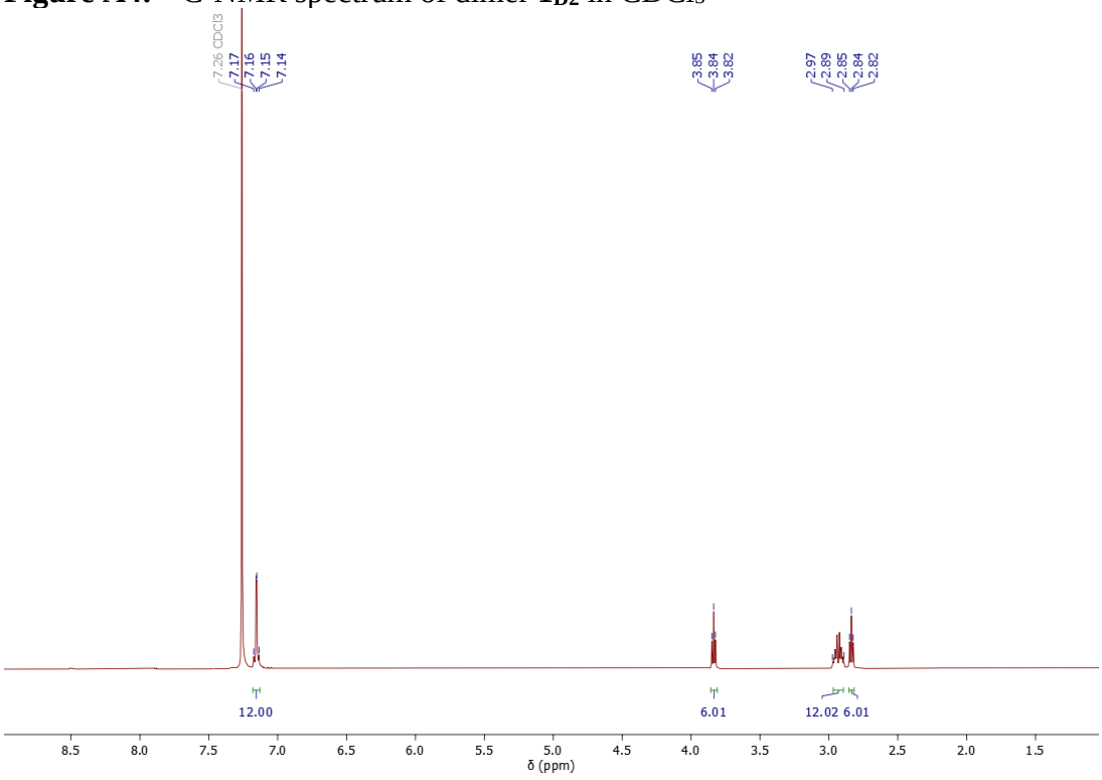

Figure A5: ^{1}H-NMR spectrum of trimer $\mathbf{1_{D3}}$ in $CDCl_3$

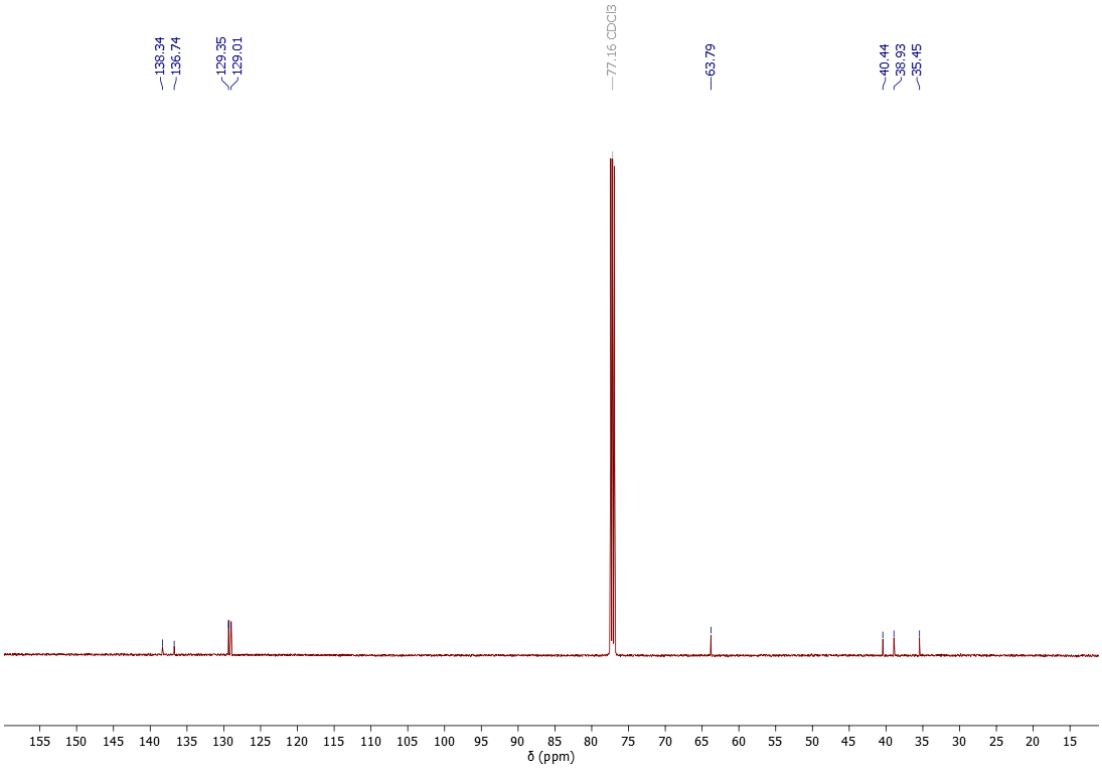

Figure A6: ^{13}C-NMR spectrum of trimer $\mathbf{1_{D3}}$ in $CDCl_3$

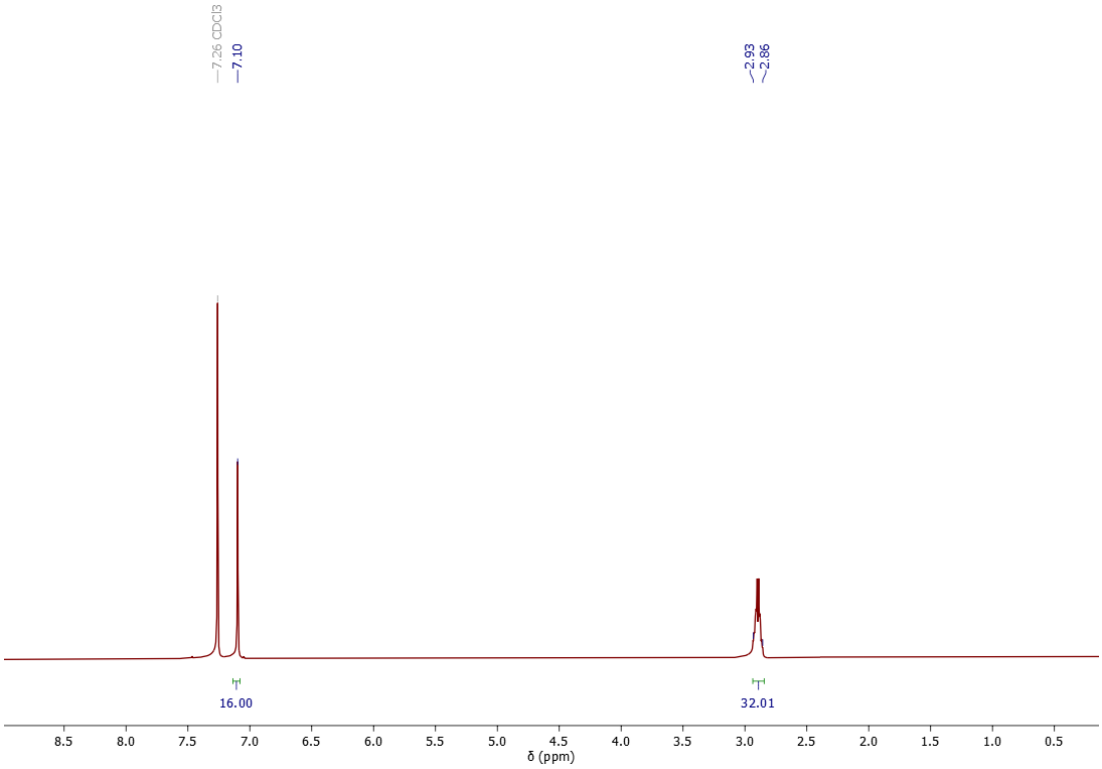

Figure A7: ^{1}H-NMR spectrum of tetramer $\mathbf{1_{D4}}$ in $CDCl_3$

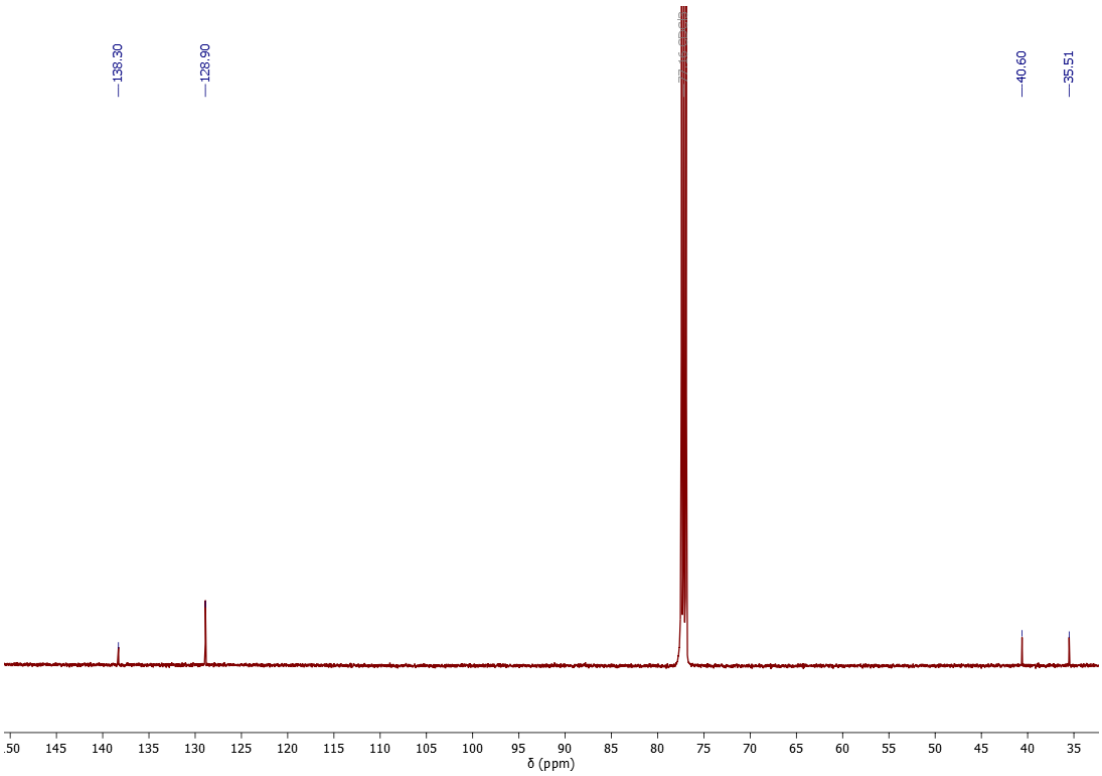

Figure A8: ^{13}C-NMR spectrum of tetramer $\mathbf{1_{D4}}$ in $CDCl_3$

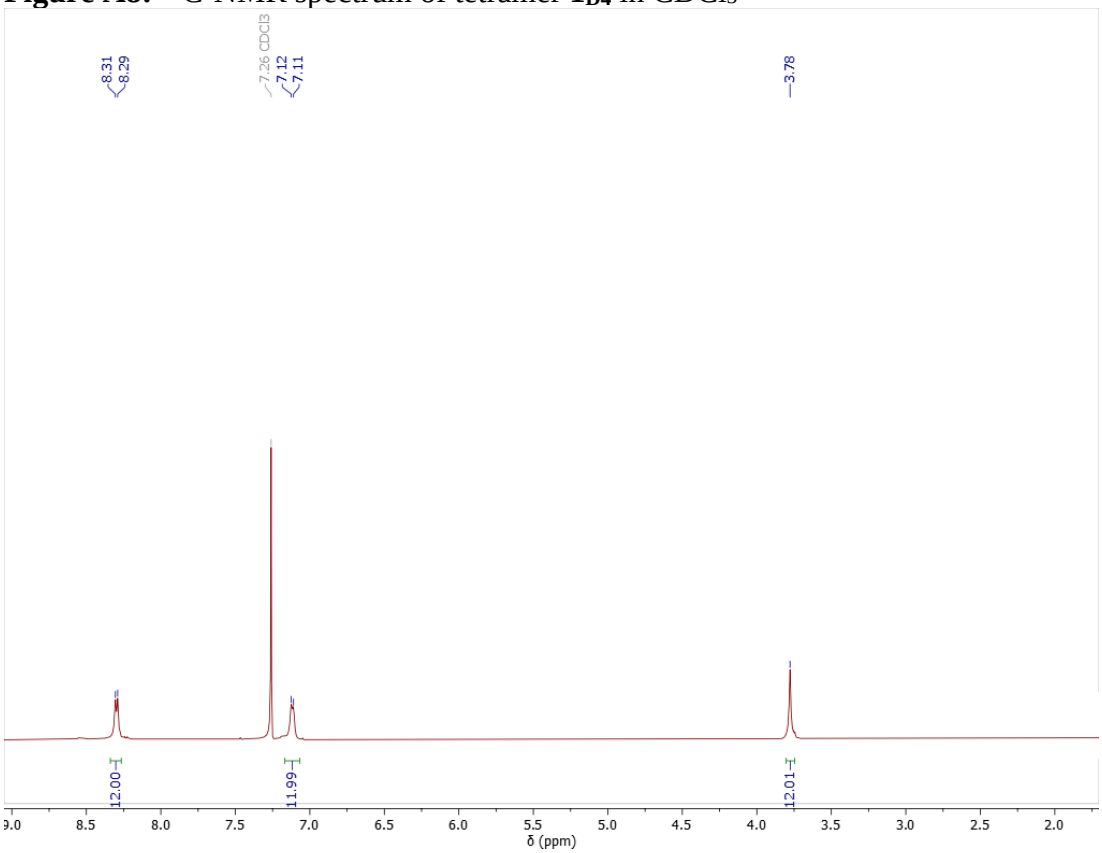

Figure A9: ^{1}H-NMR spectrum of dimer $\mathbf{2_{D2}}$ in $CDCl_3$

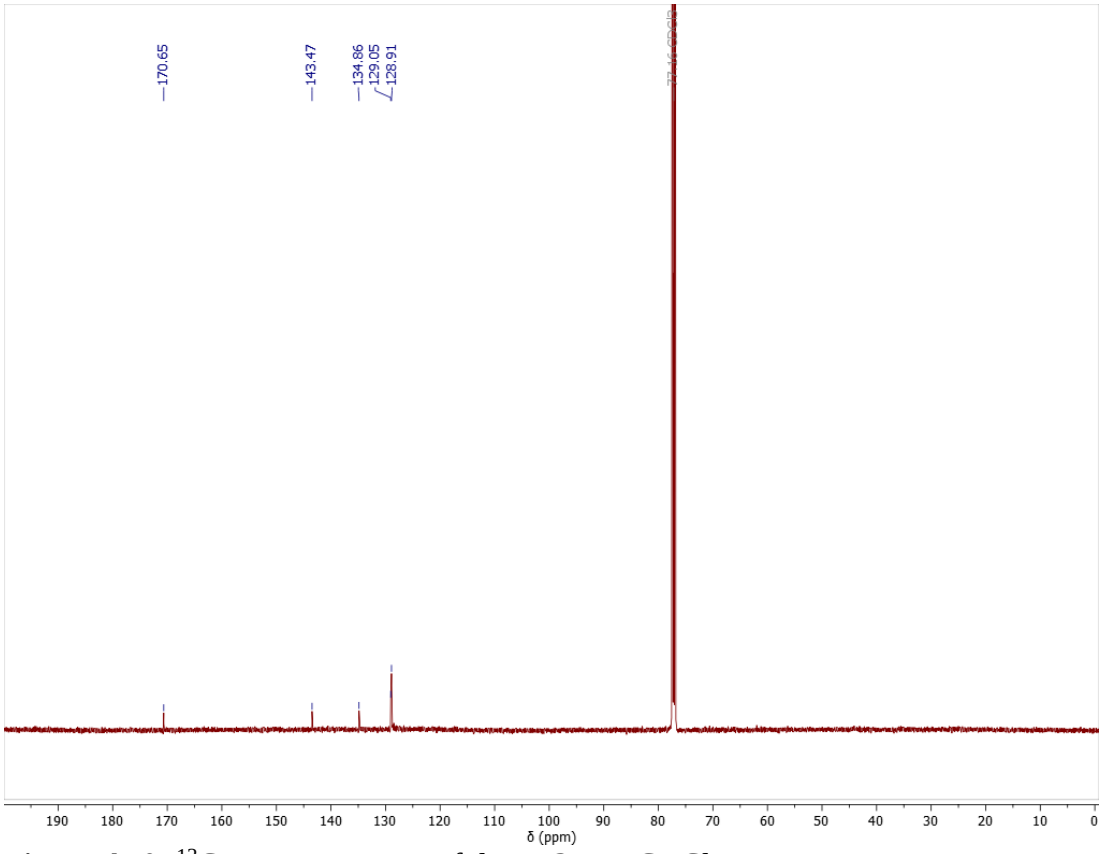

Figure A10: ^{13}C-NMR spectrum of dimer $\mathbf{2_{D2}}$ in $CDCl_3$

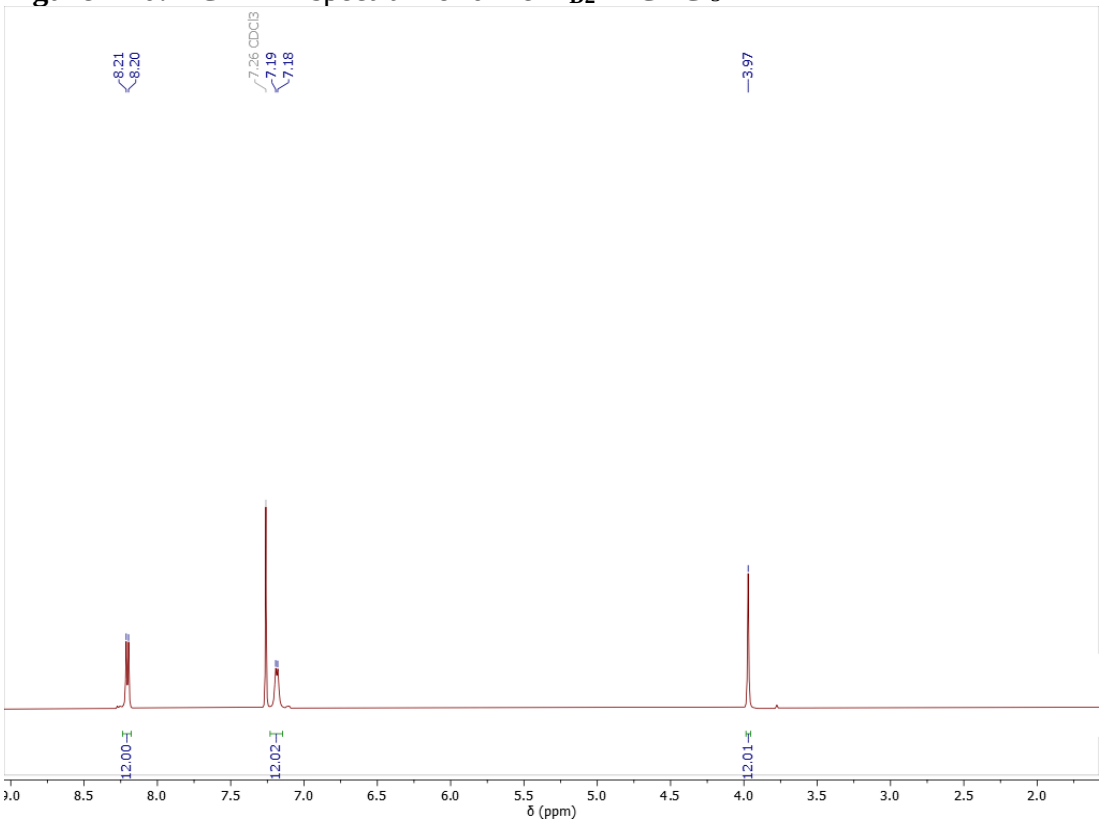

Figure A11: ^{1}H-NMR spectrum of dimer $\mathbf{2_{T2}}$ in $CDCl_3$

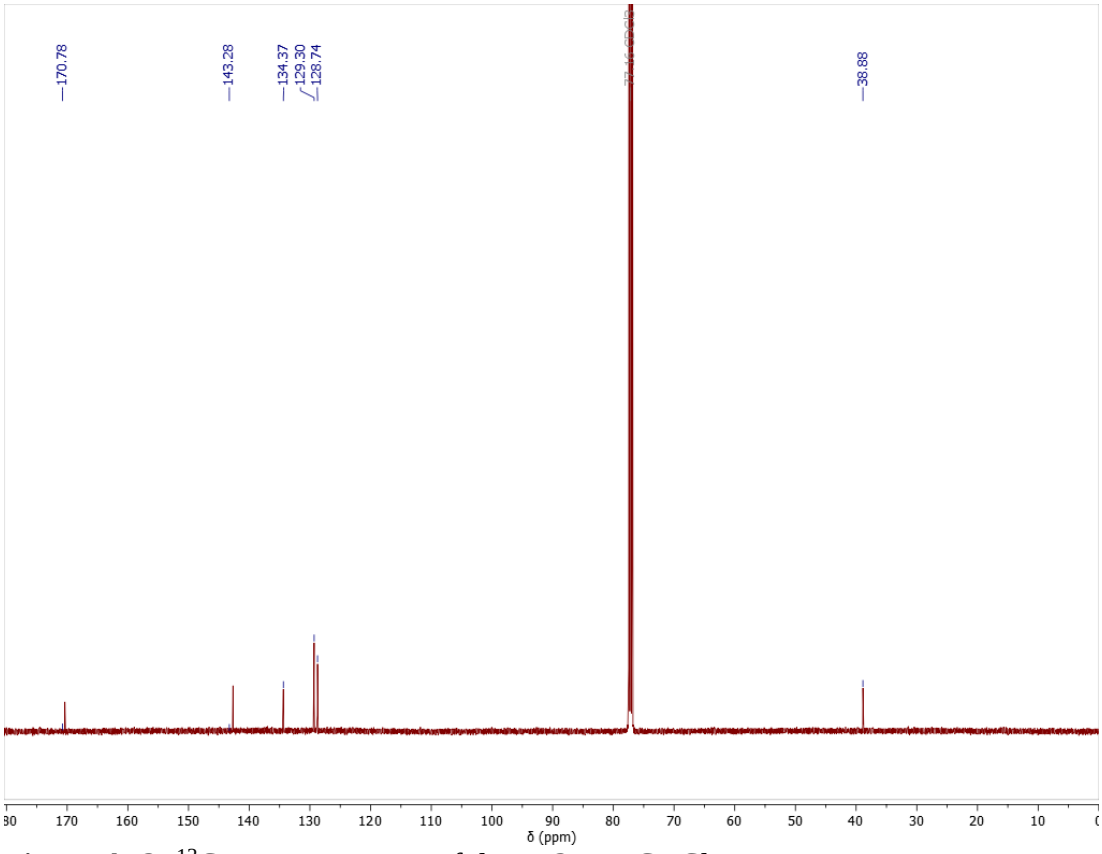

Figure A12: ^{13}C-NMR spectrum of dimer $\mathbf{2_{T2}}$ in $CDCl_3$

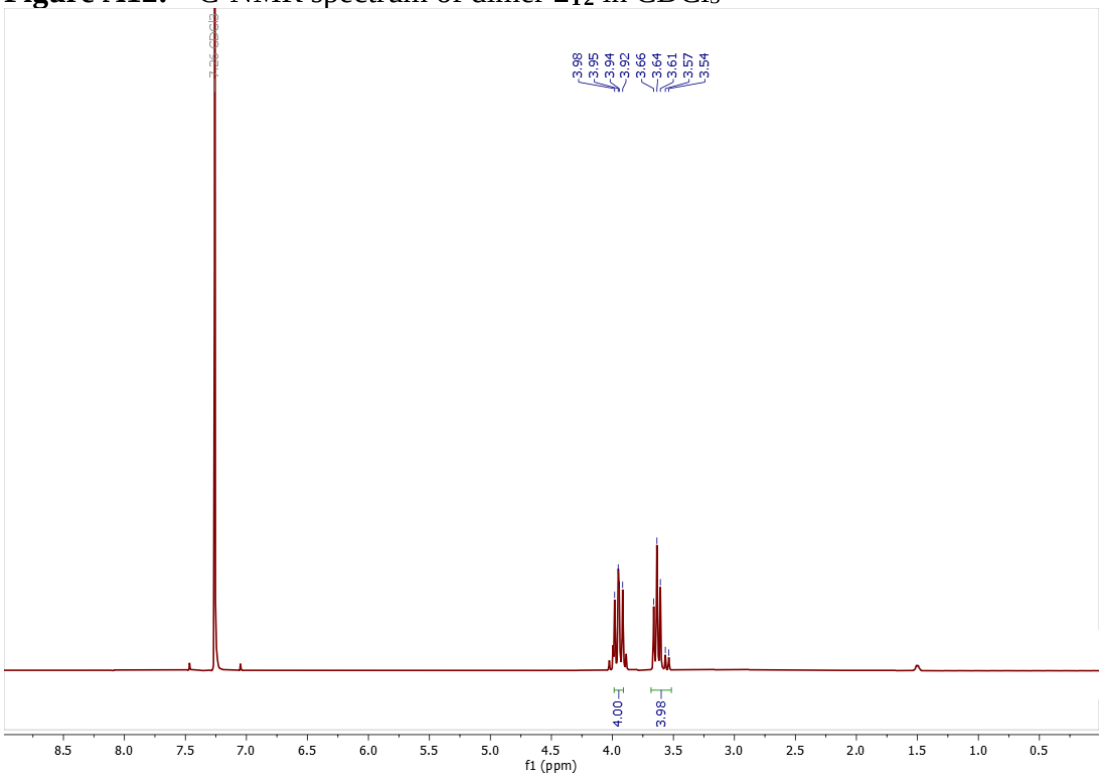

Figure A13: ^{1}H-NMR spectrum of dimer $\mathbf{3_{D2}}$ in $CDCl_3$

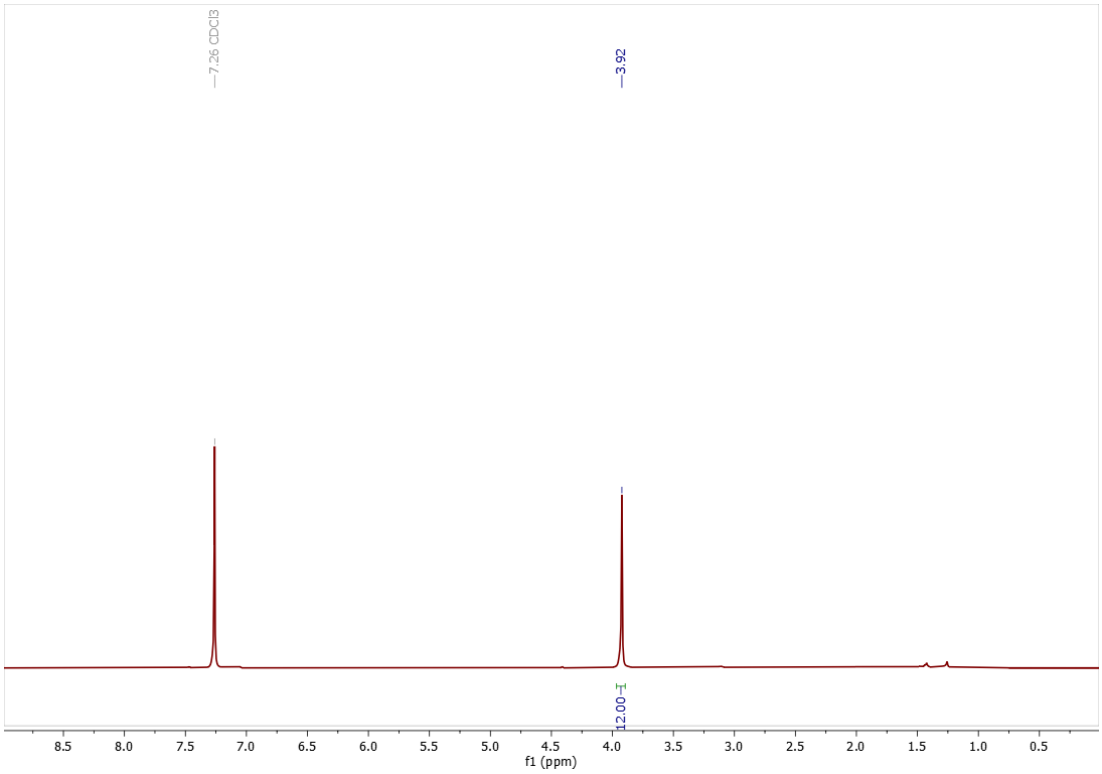

Figure A14: ^{1}H-NMR spectrum of trimer $\mathbf{3_{D3}}$ in $CDCl_3$

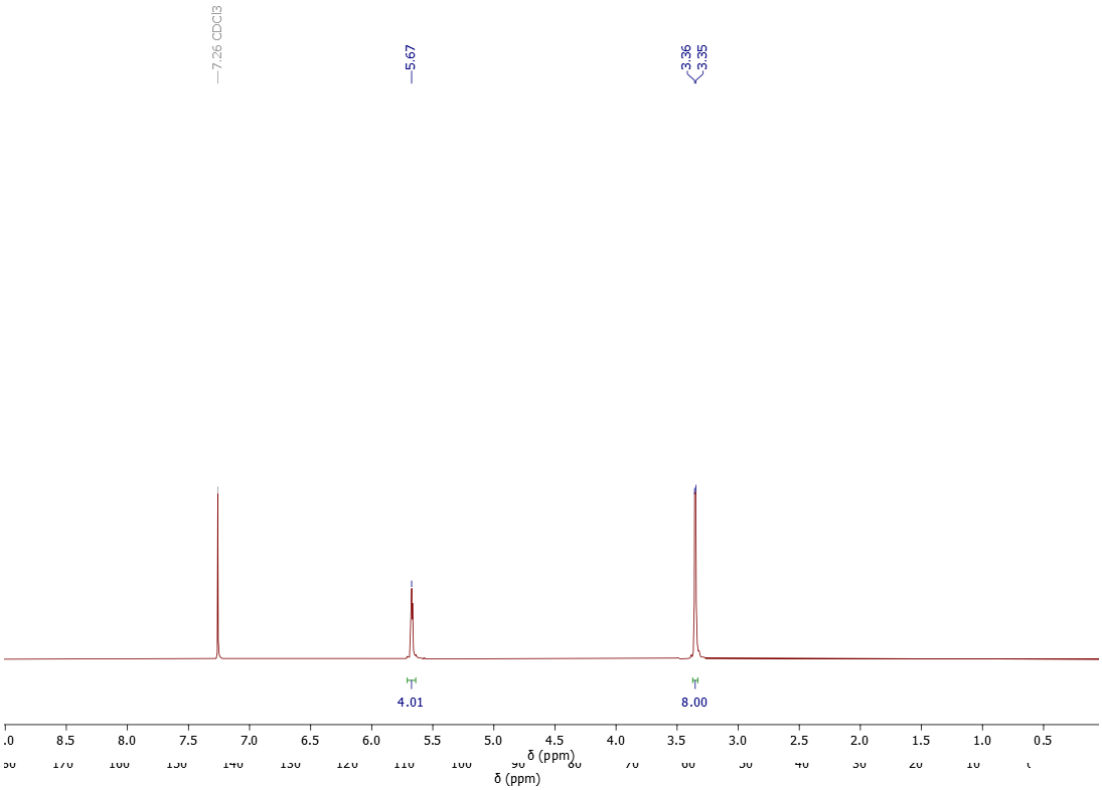

Figure A15: ^{1}H-NMR spectrum of dimer $\mathbf{4_{D2}}$ in $CDCl_3$

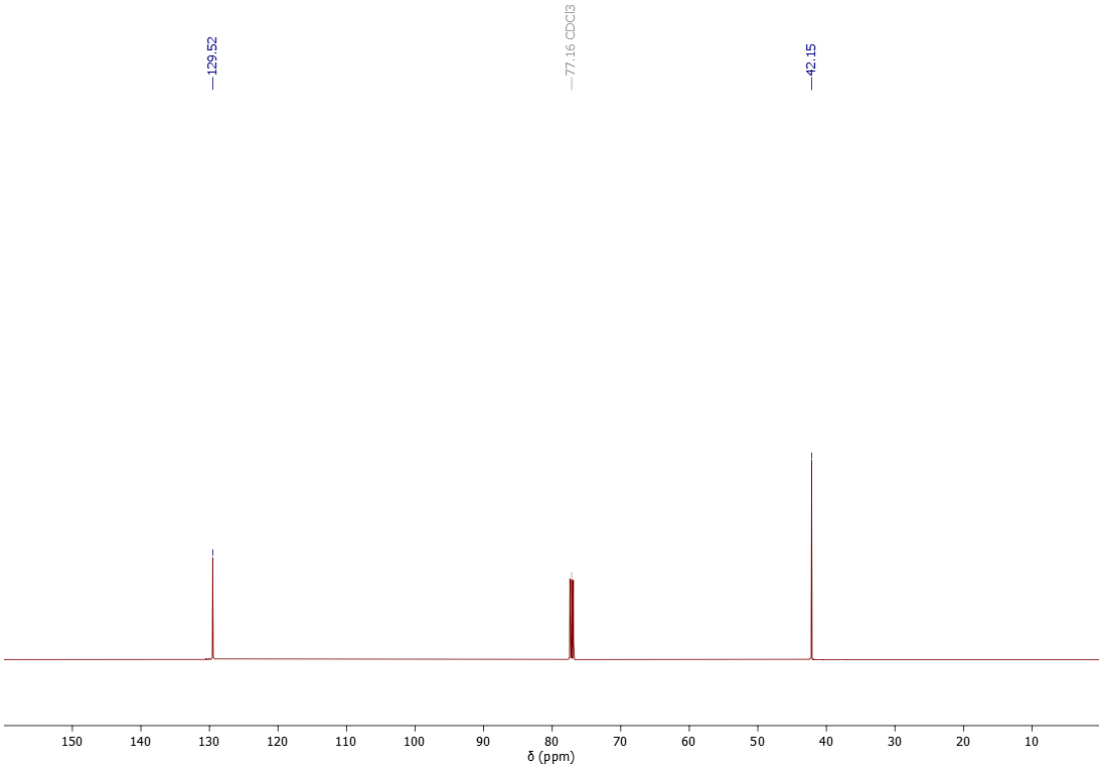

Figure A16: ^{13}C-NMR spectrum of dimer **4$_{D2}$** in $CDCl_3$

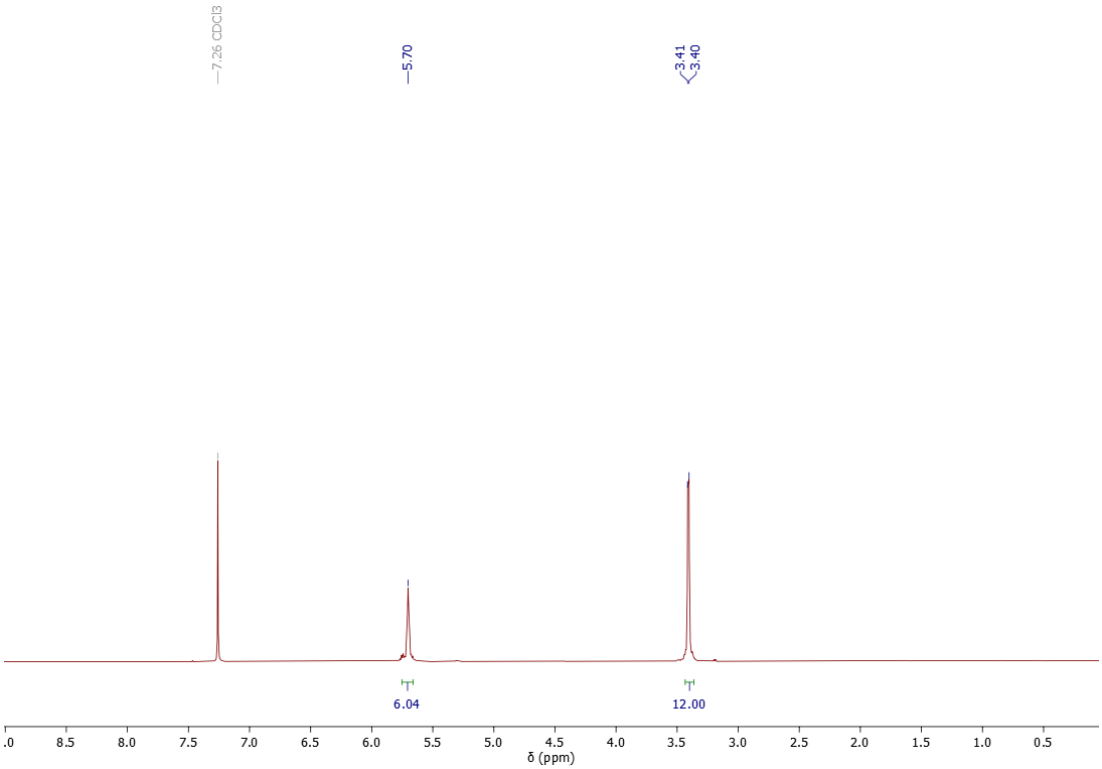

Figure A17: ^{1}H-NMR spectrum of trimer **4$_{D3}$** in $CDCl_3$

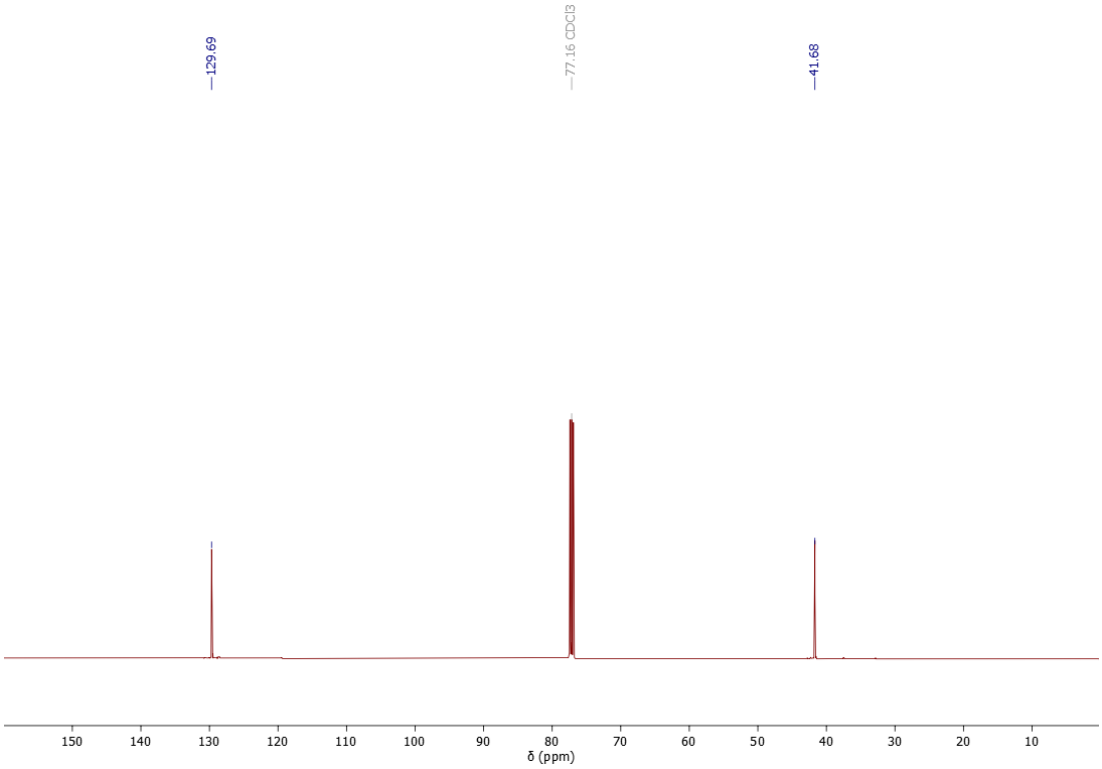

Figure A18: ^{13}C-NMR spectrum of trimer $\mathbf{4_{D3}}$ in $CDCl_3$

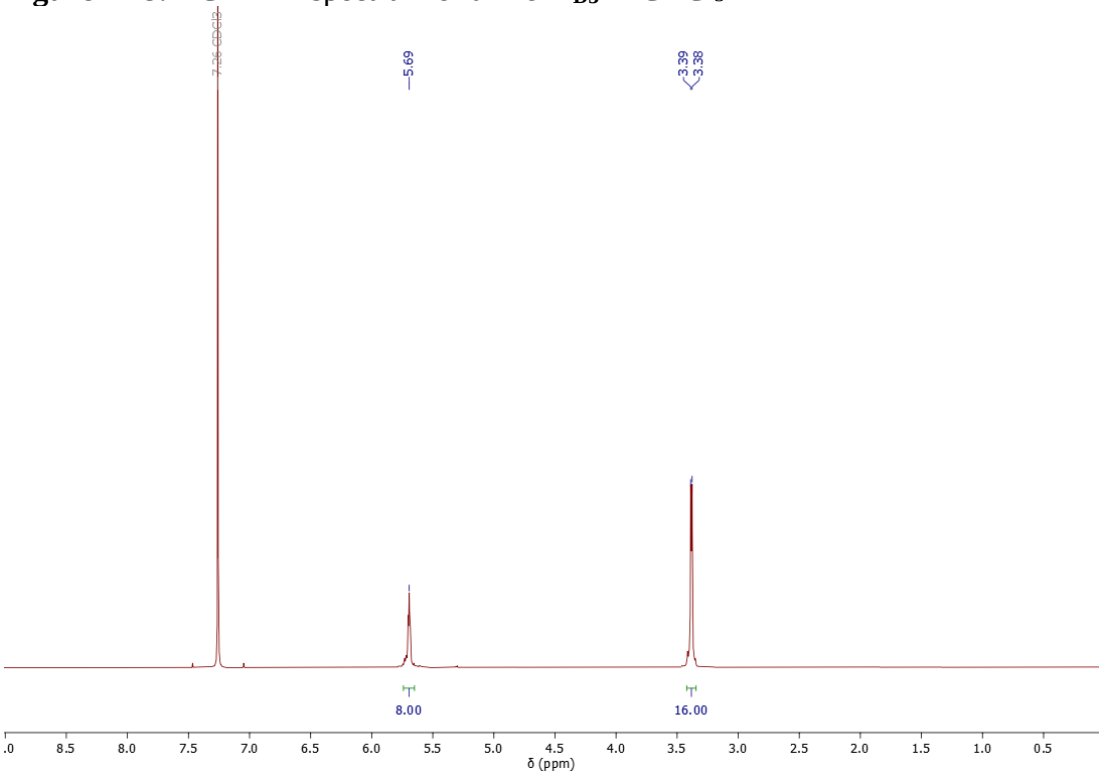

Figure A19: ^{1}H-NMR spectrum of tetramer $\mathbf{4_{D4}}$ in $CDCl_3$

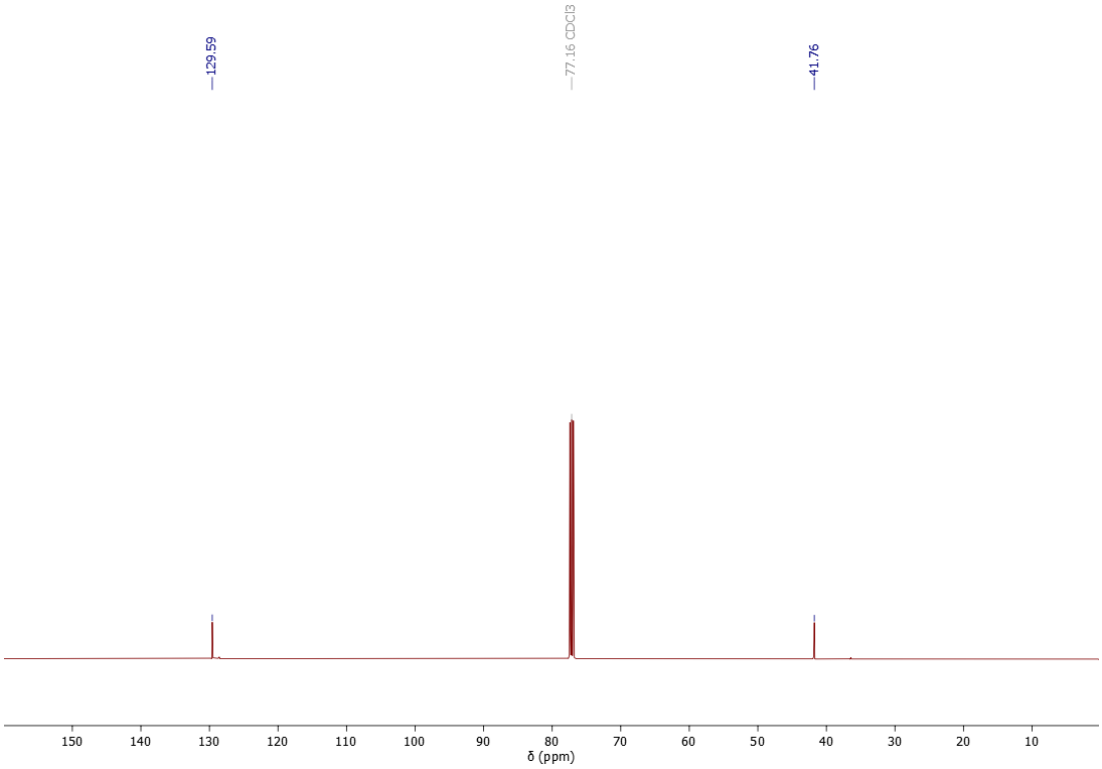

Figure A20: ^{13}C-NMR spectrum of tetramer $\mathbf{4_{D4}}$ in $CDCl_3$

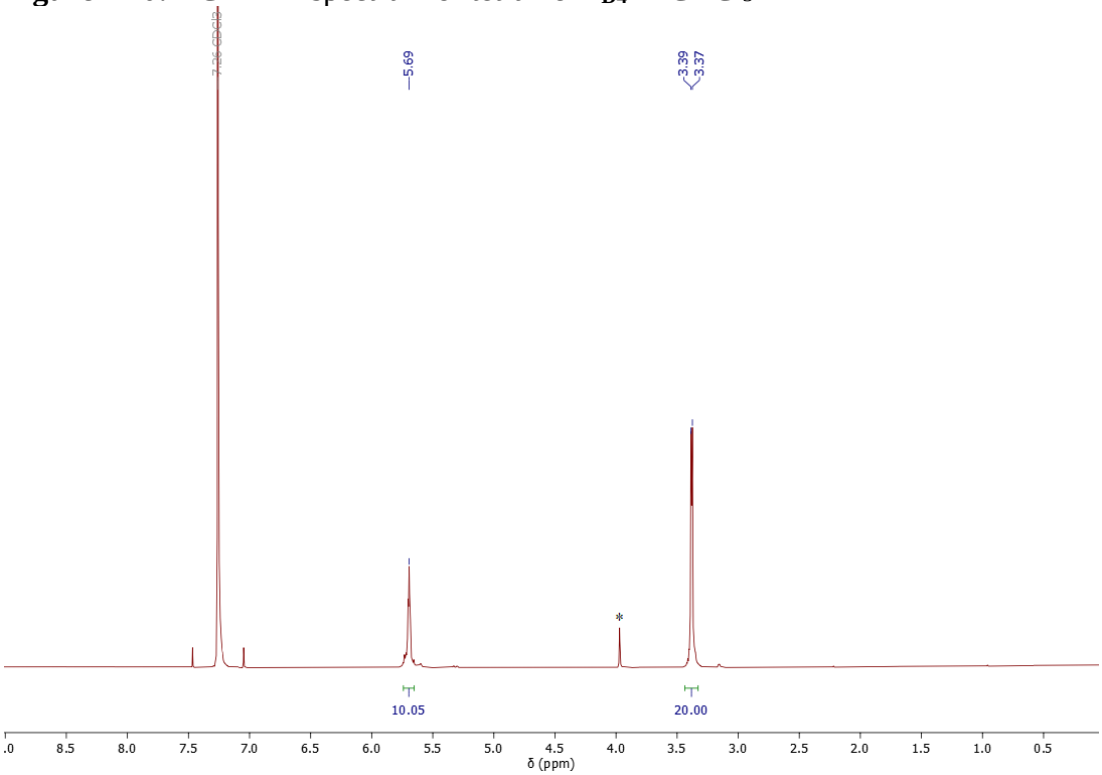

Figure A21: ^{1}H-NMR spectrum of pentamer $\mathbf{4_{D5}}$ in $CDCl_3$. Inseparable impurity denoted with *.

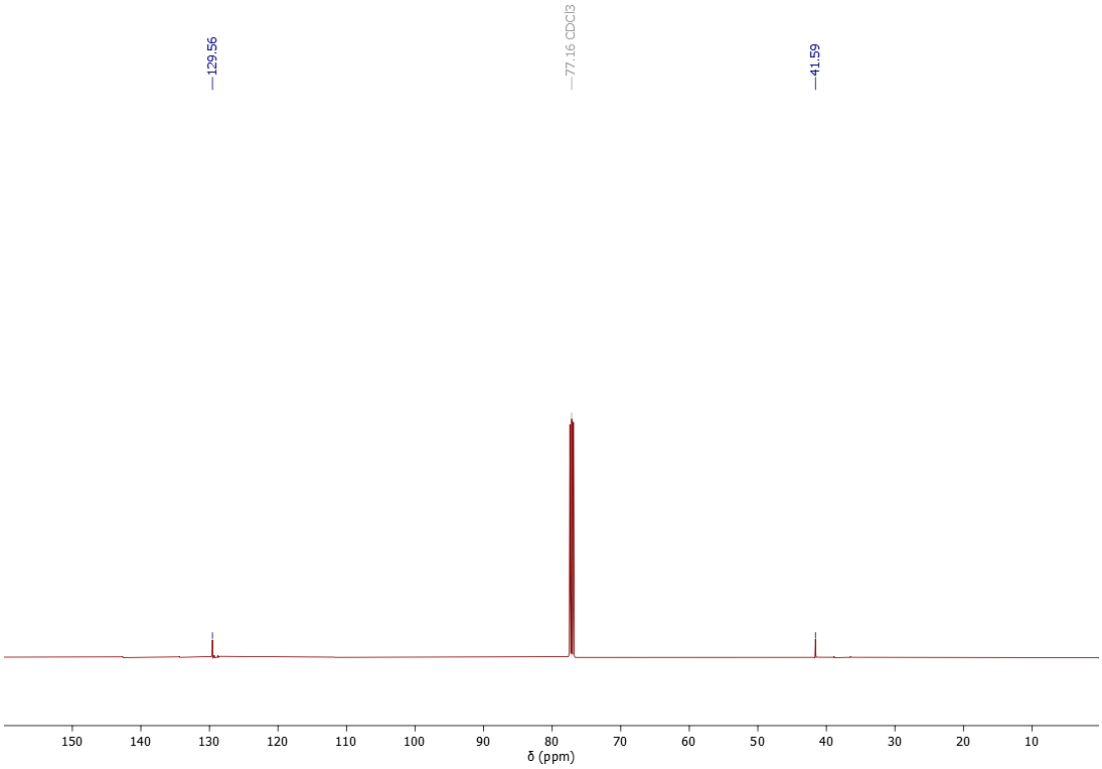

Figure A22: ^{13}C-NMR spectrum of pentamer $\mathbf{4_{D5}}$ in $CDCl_3$

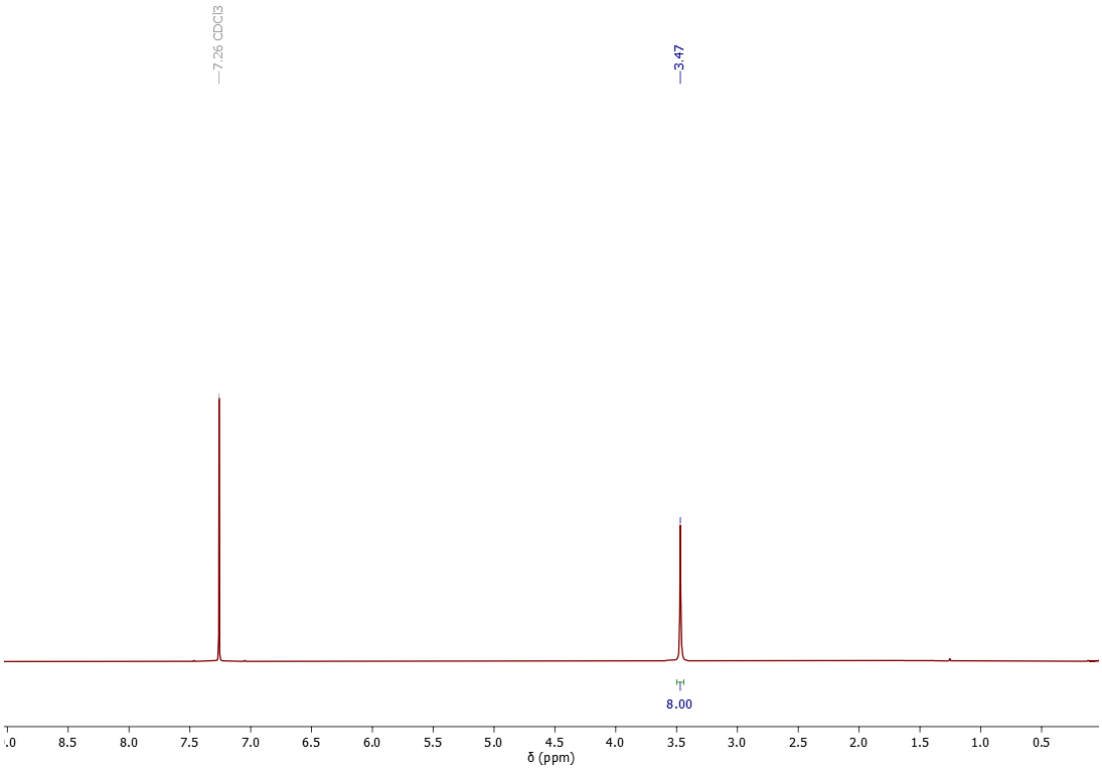

Figure A23: ^{1}H-NMR spectrum of dimer $\mathbf{5_{D2}}$ in $CDCl_3$

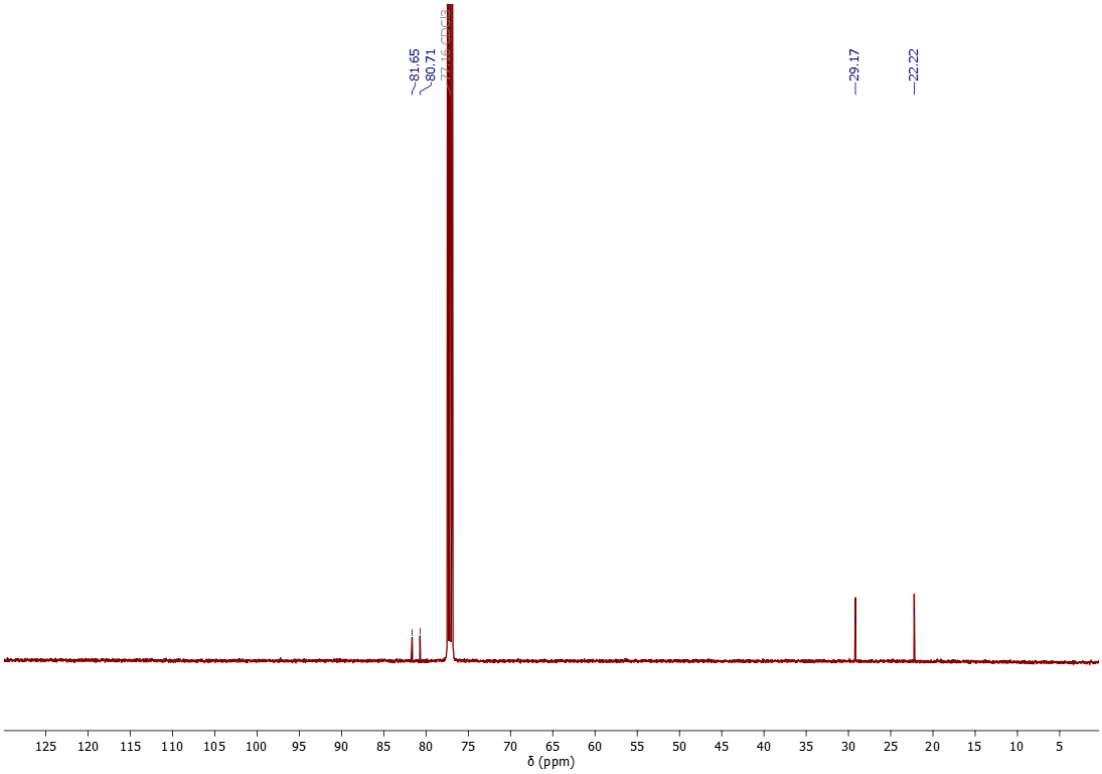

Figure A24: ^{13}C-NMR spectrum of dimer $\mathbf{5_{D2}}$ in $CDCl_3$

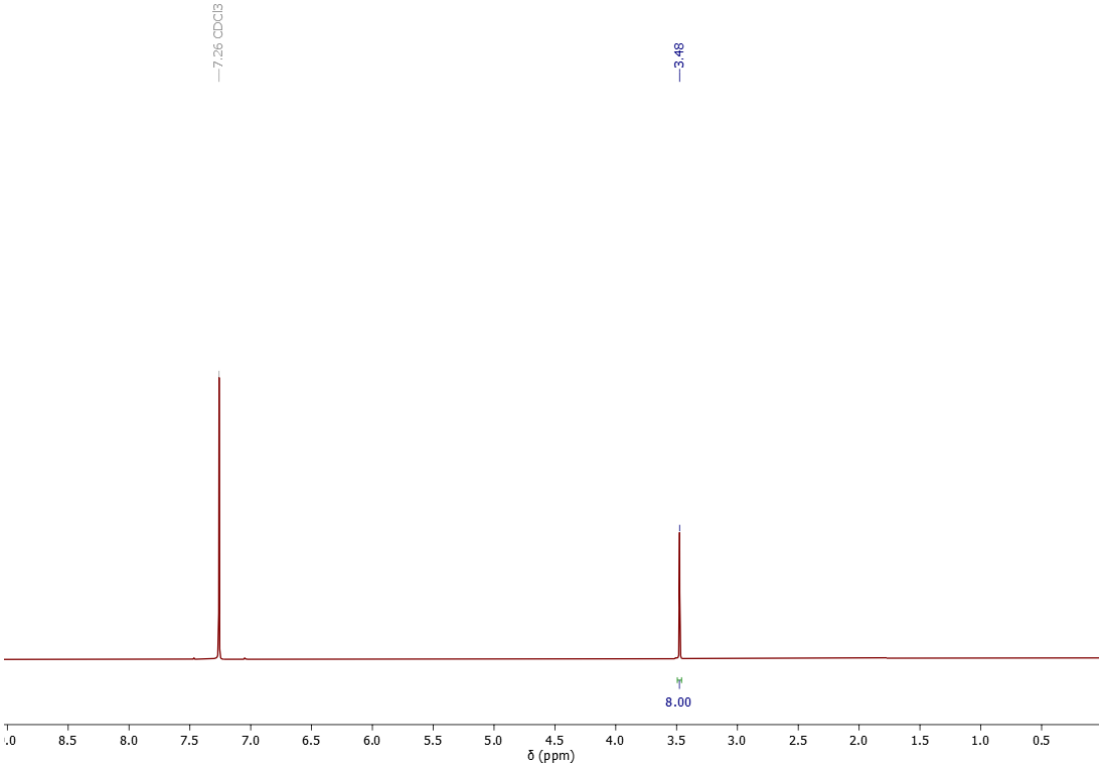

Figure A25: ^{1}H-NMR spectrum of dimer $\mathbf{5_{T2}}$ in $CDCl_3$

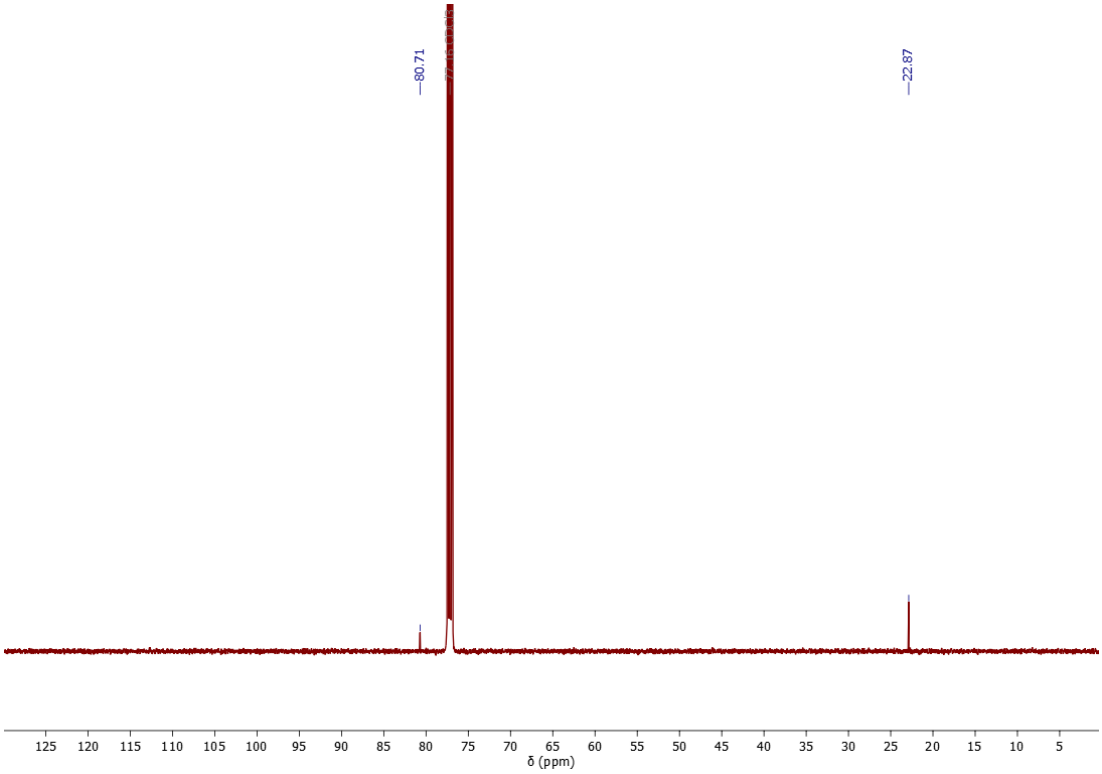

Figure A26: ^{13}C-NMR spectrum of dimer $\mathbf{5_{T2}}$ in $CDCl_3$

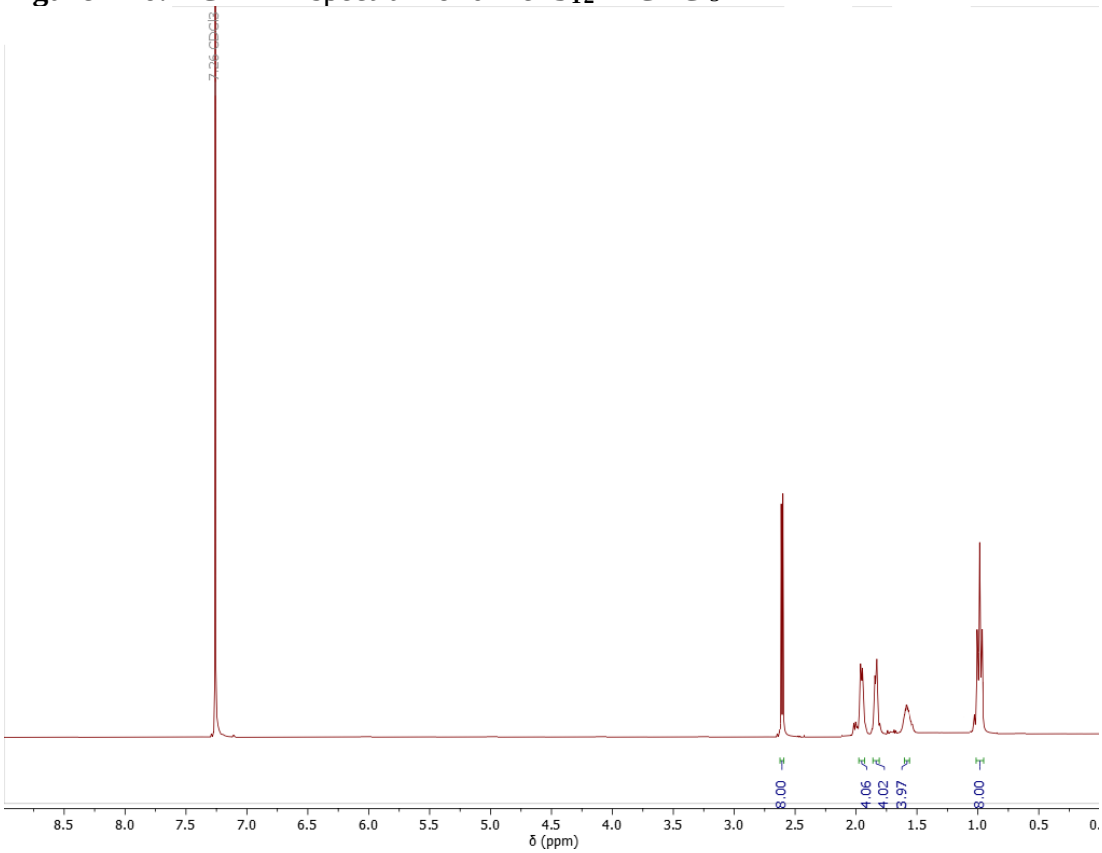

Figure A27: ^{1}H-NMR spectrum of dimer $\mathbf{6_{D2}}$ in $CDCl_3$

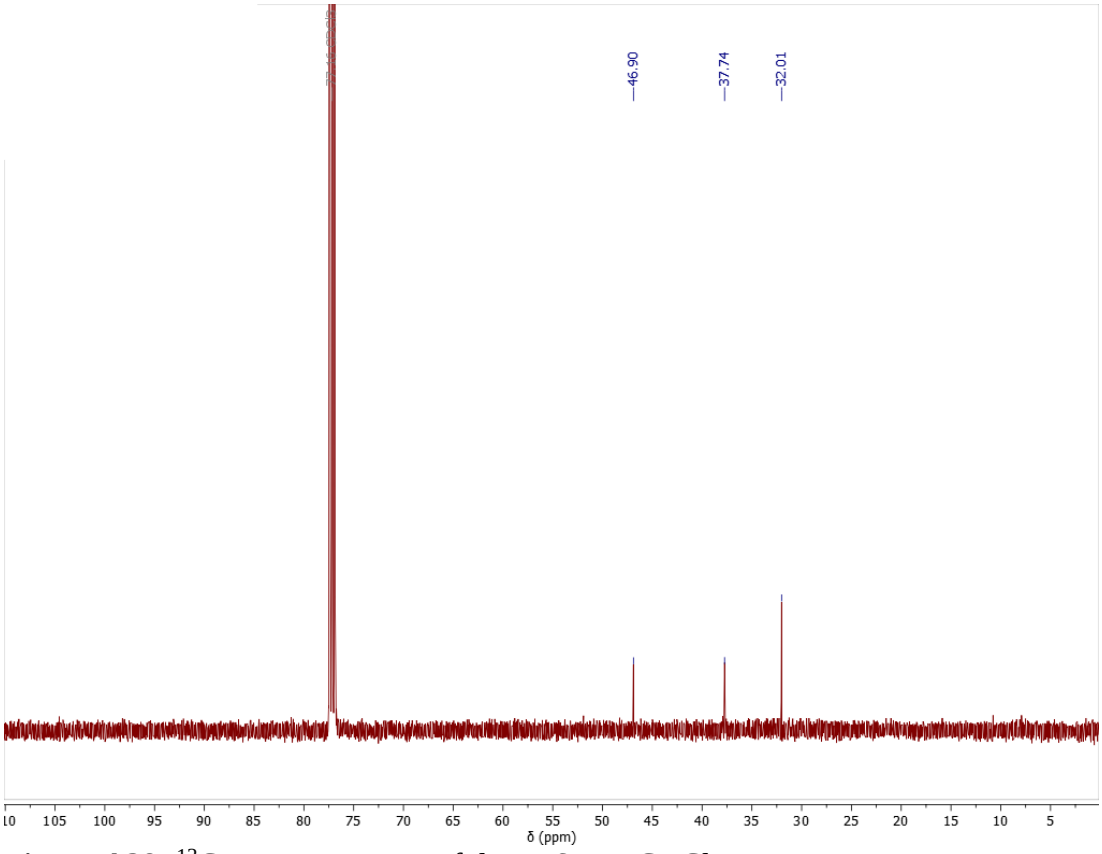

Figure A28: ^{13}C-NMR spectrum of dimer $\mathbf{6_{D2}}$ in $CDCl_3$

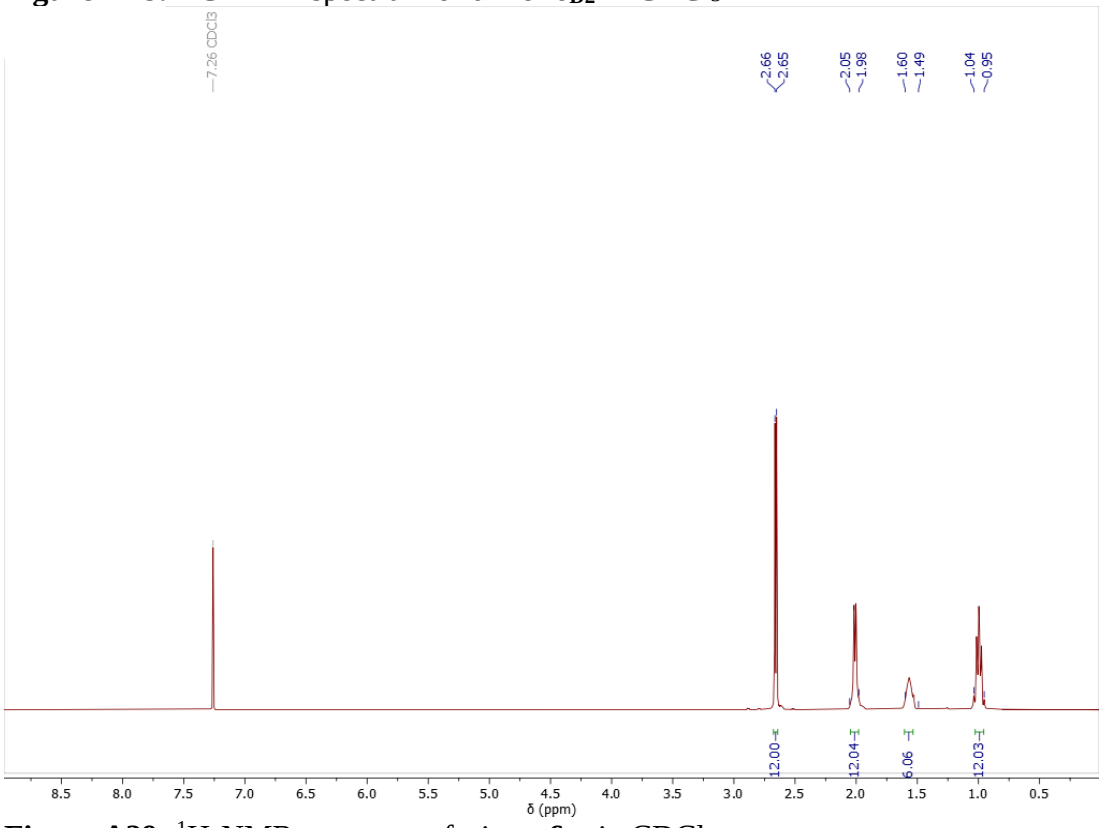

Figure A29: ^{1}H-NMR spectrum of trimer $\mathbf{6_{D3}}$ in $CDCl_3$

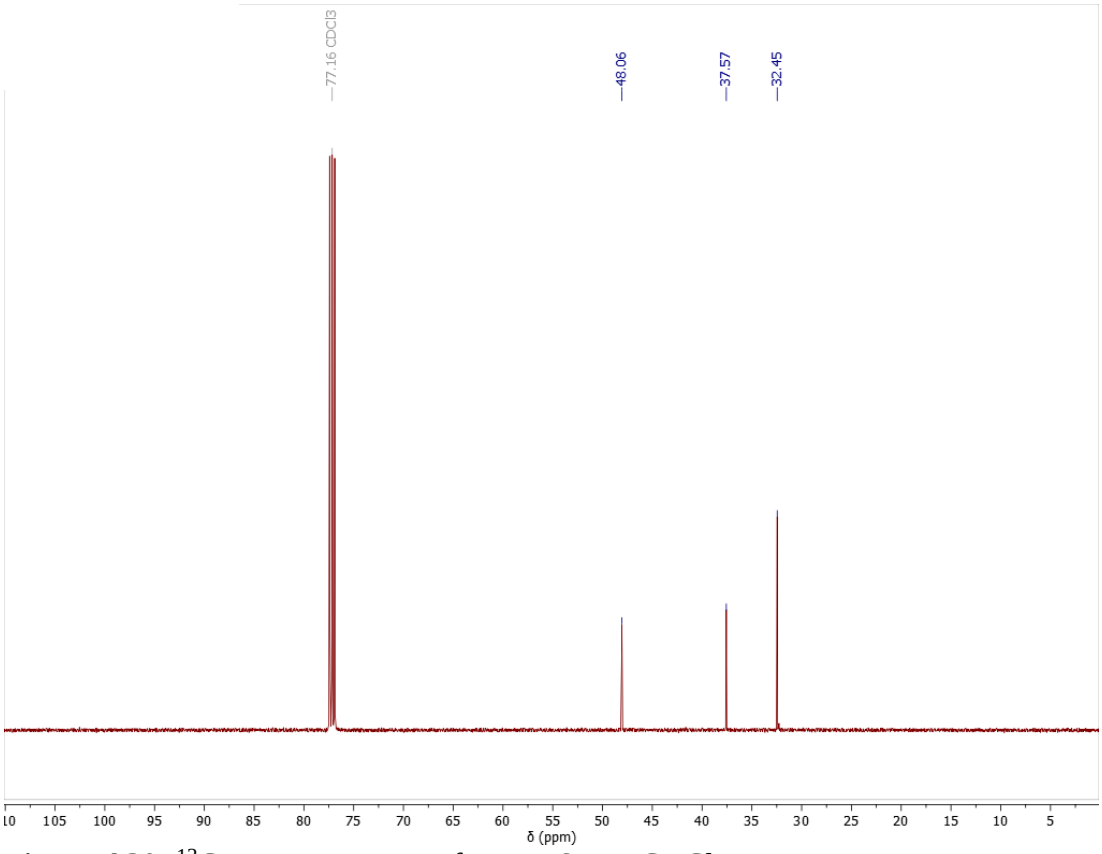

Figure A30: ^{13}C-NMR spectrum of trimer $\mathbf{6_{D3}}$ in $CDCl_3$

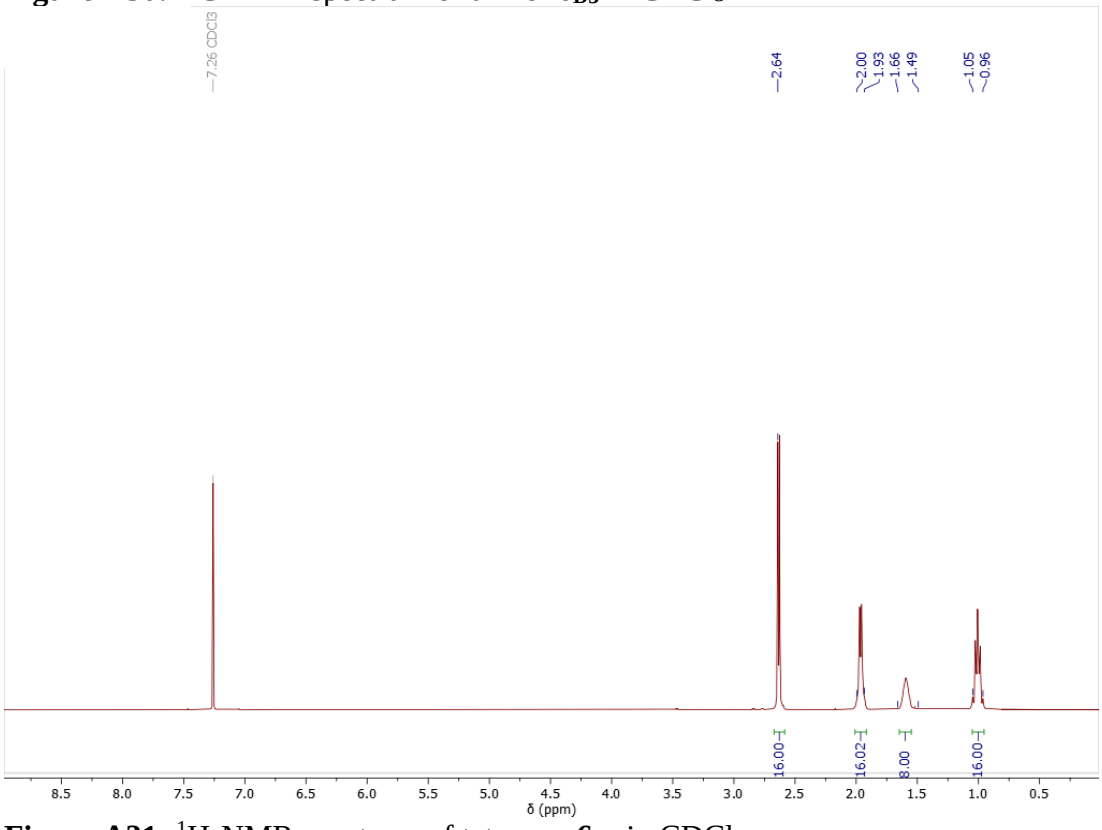

Figure A31: ^{1}H-NMR spectrum of tetramer $\mathbf{6_{D4}}$ in $CDCl_3$

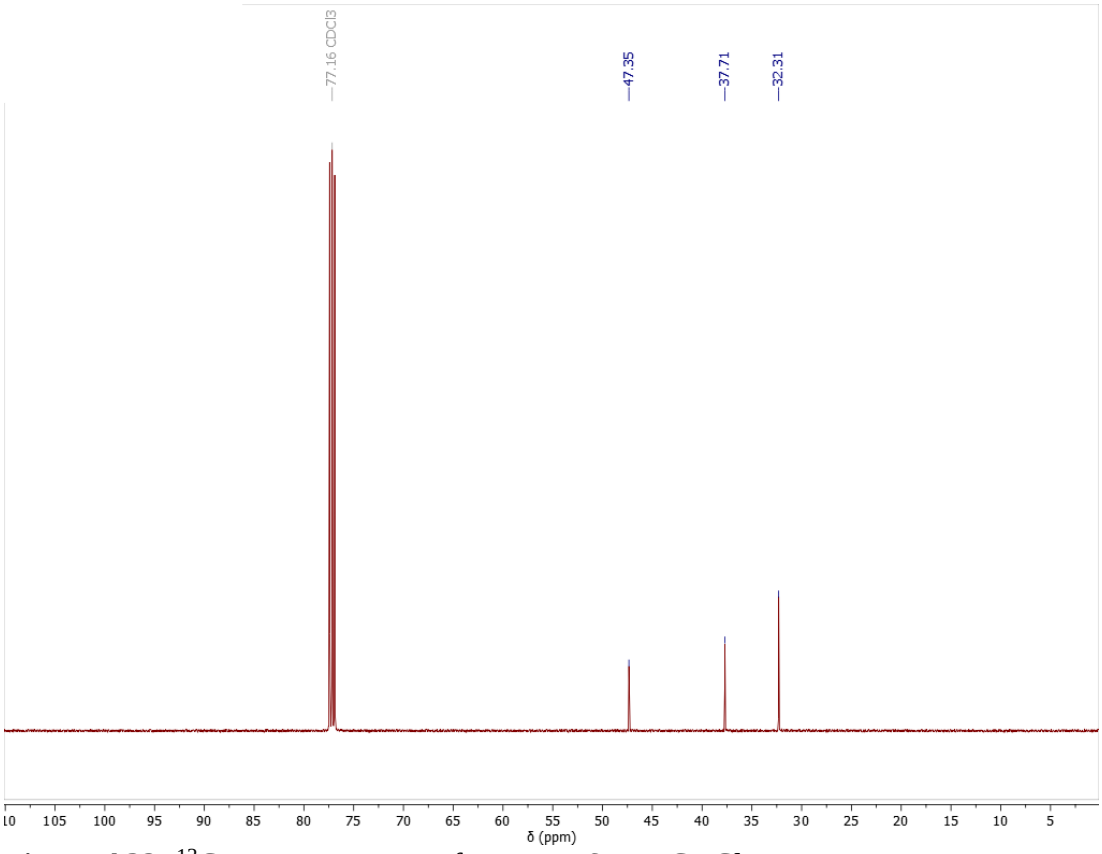

Figure A32: ^{13}C-NMR spectrum of tetramer $\mathbf{6_{D4}}$ in $CDCl_3$

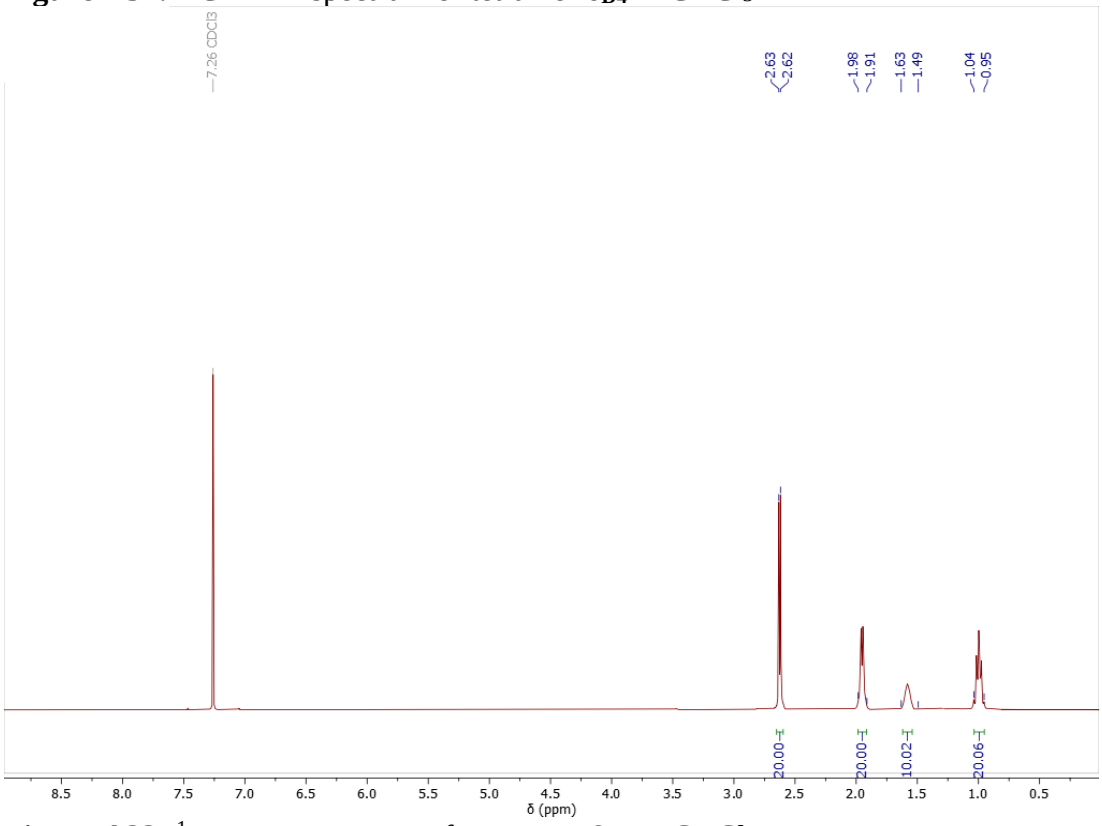

Figure A33: ^{1}H-NMR spectrum of pentamer $\mathbf{6_{D5}}$ in $CDCl_3$

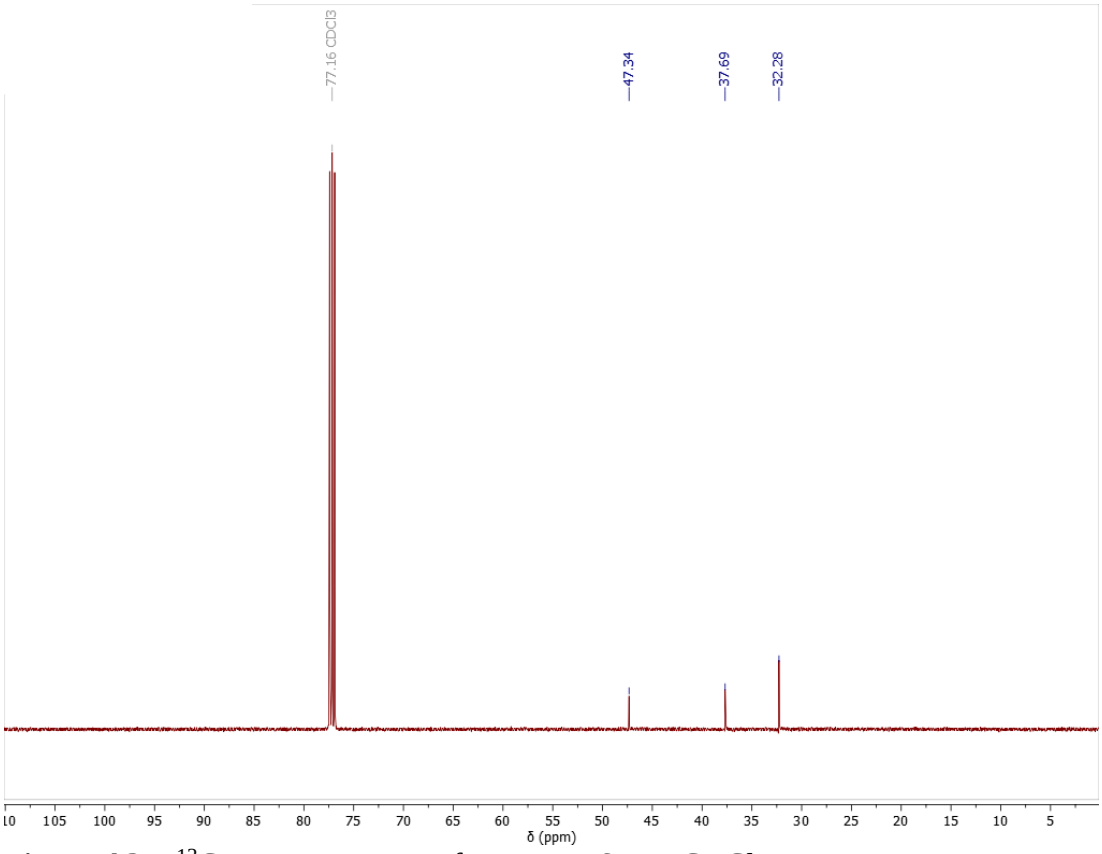

Figure A34: ^{13}C-NMR spectrum of pentamer $\mathbf{6_{D5}}$ in $CDCl_3$

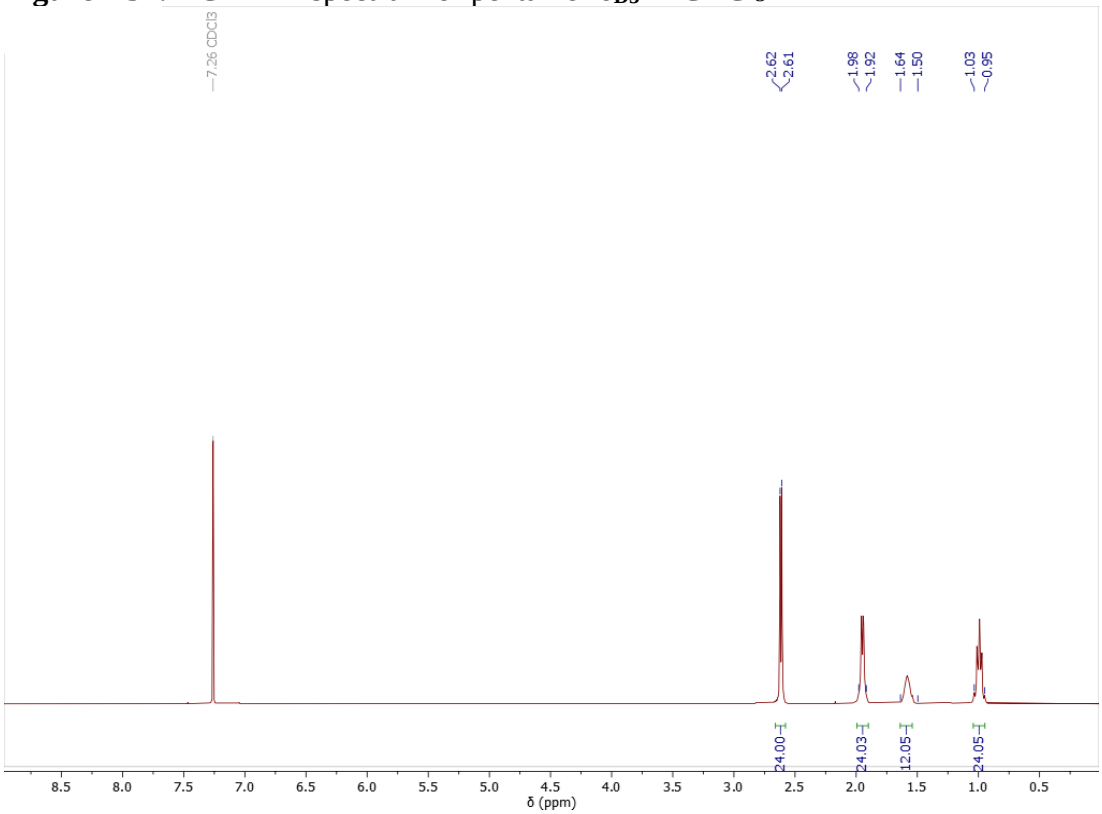

Figure A35: ^{1}H-NMR spectrum of hexamer $\mathbf{6_{D6}}$ in $CDCl_3$

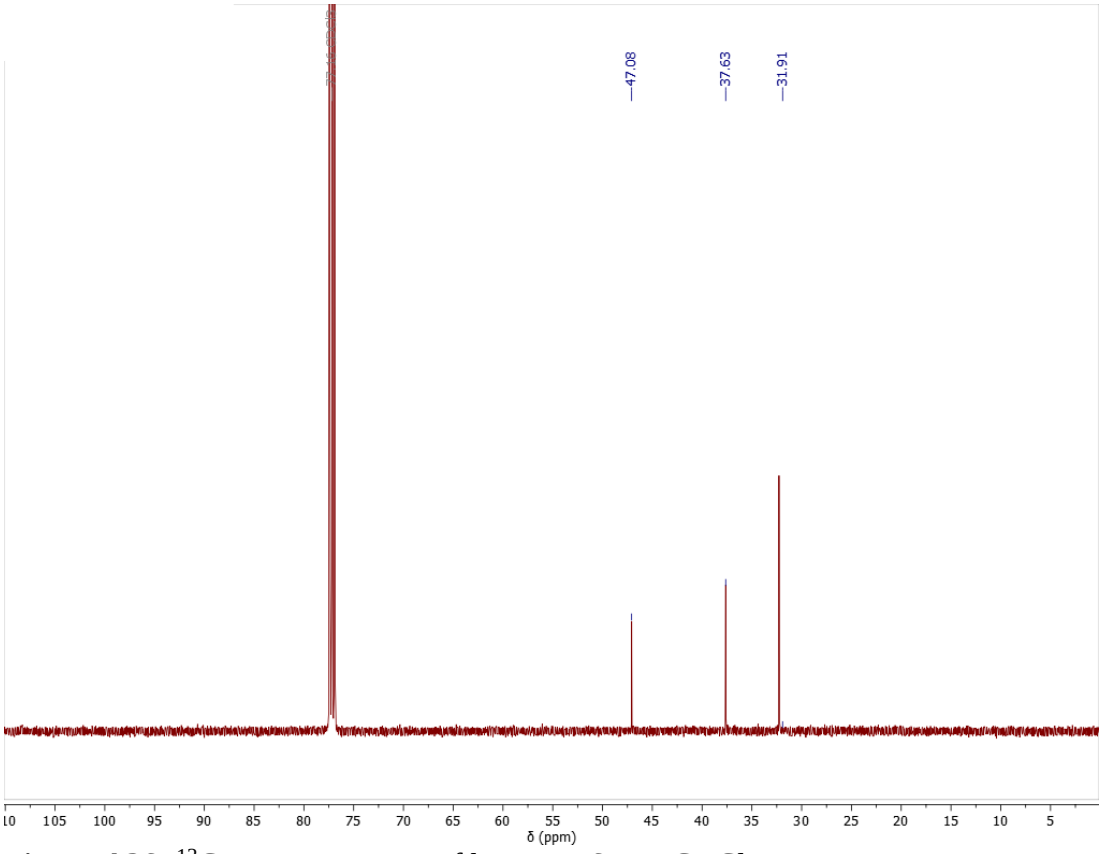

Figure A36: ^{13}C-NMR spectrum of hexamer $\mathbf{6_{D6}}$ in $CDCl_3$

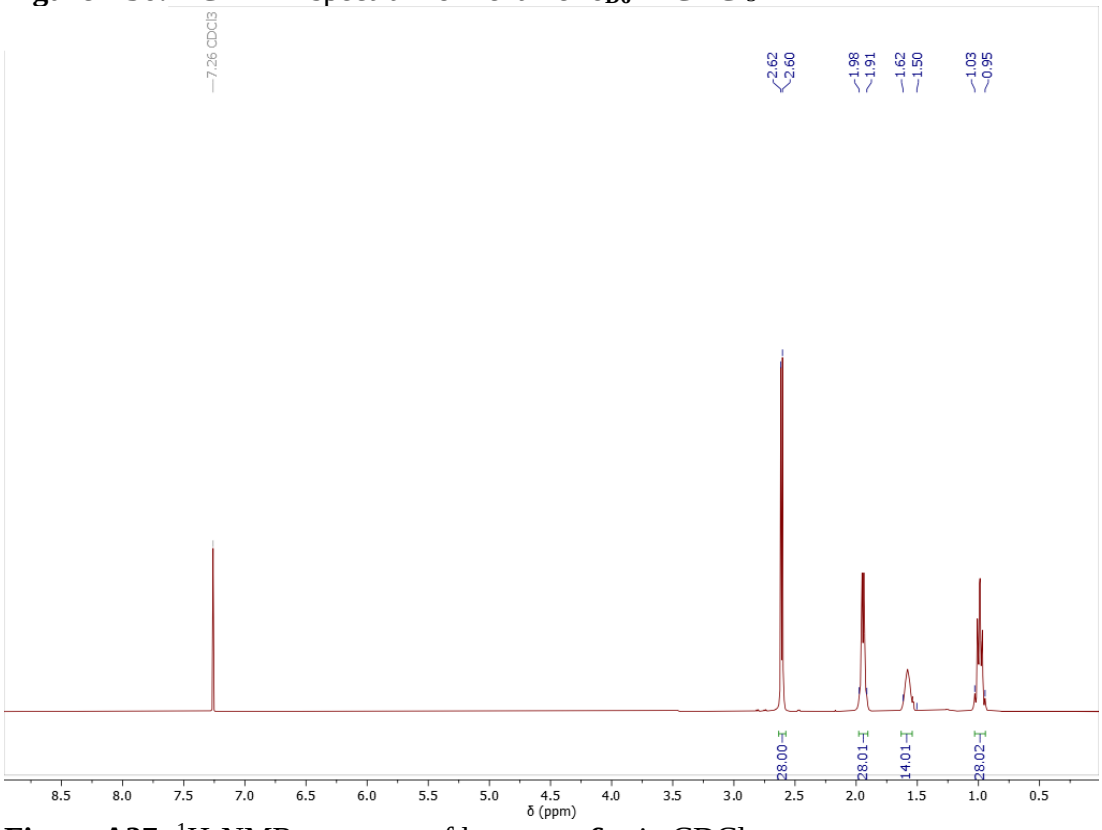

Figure A37: ^{1}H-NMR spectrum of heptamer $\mathbf{6_{D7}}$ in $CDCl_3$

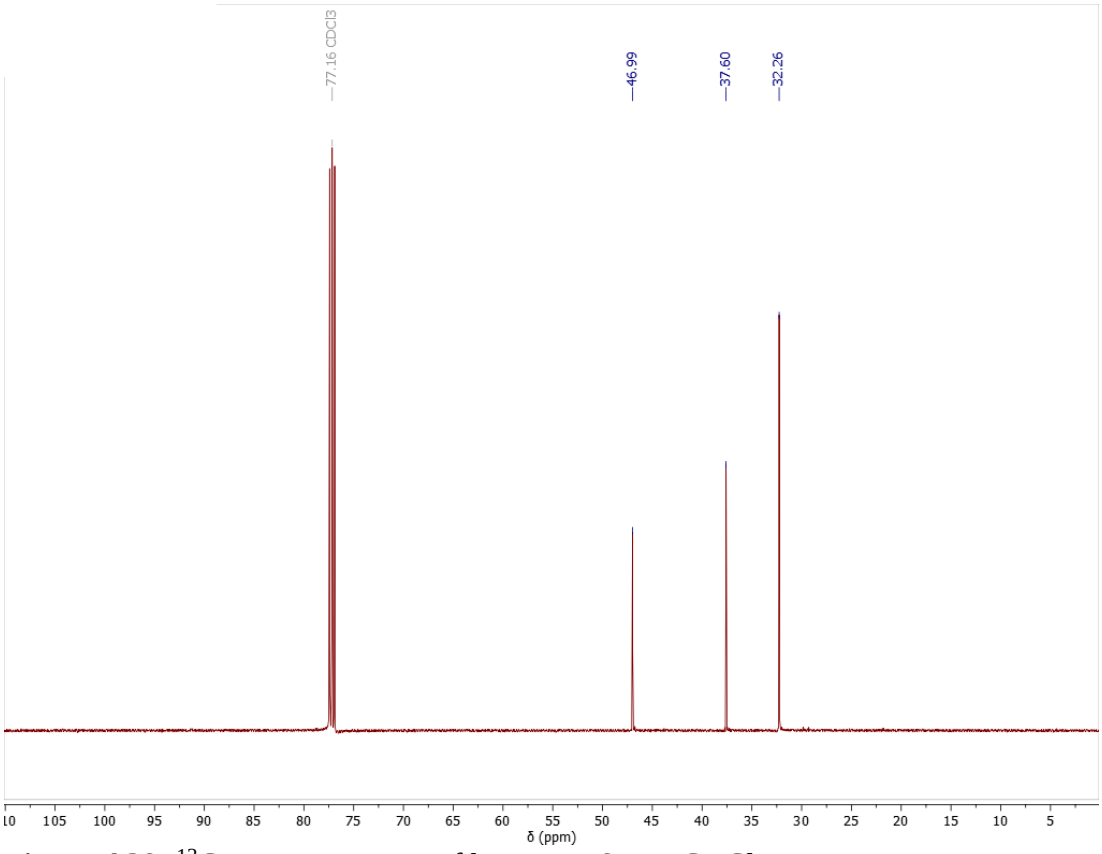

Figure A38: ^{13}C-NMR spectrum of heptamer $\mathbf{6_{D7}}$ in $CDCl_3$

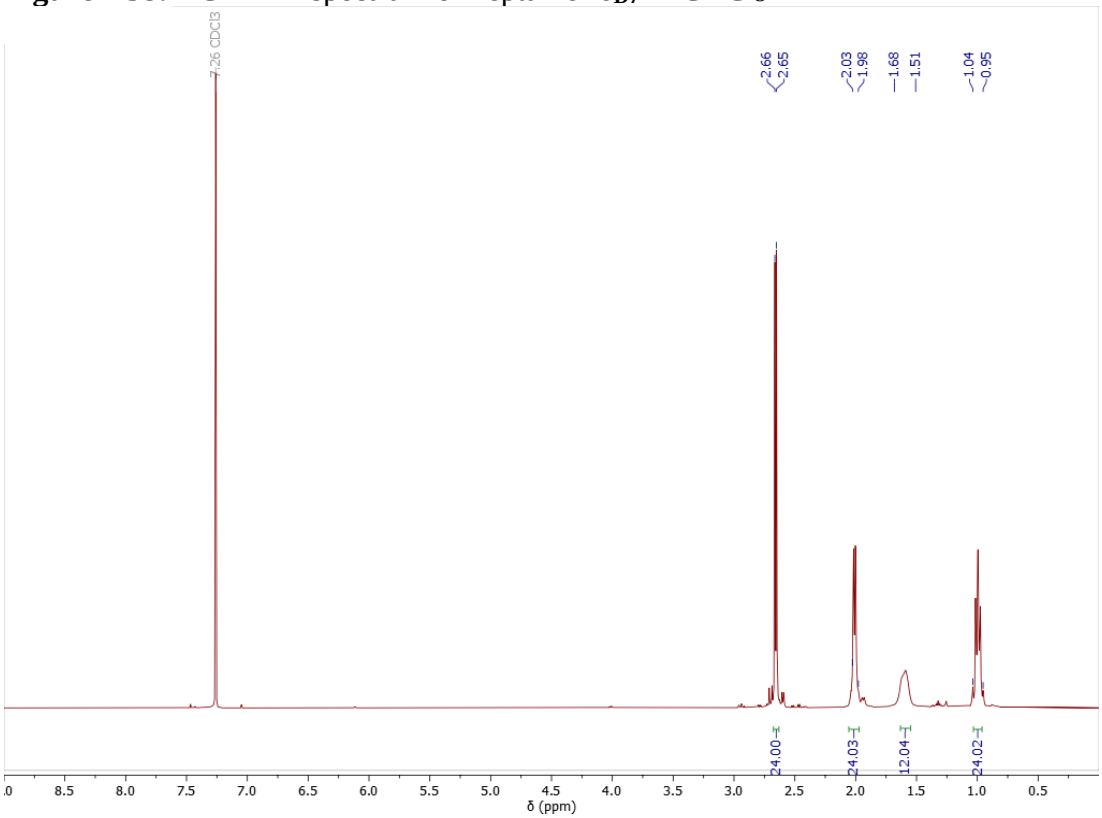

Figure A39: ^{1}H-NMR spectrum of tetramer $\mathbf{6_{T4}}$ in $CDCl_3$

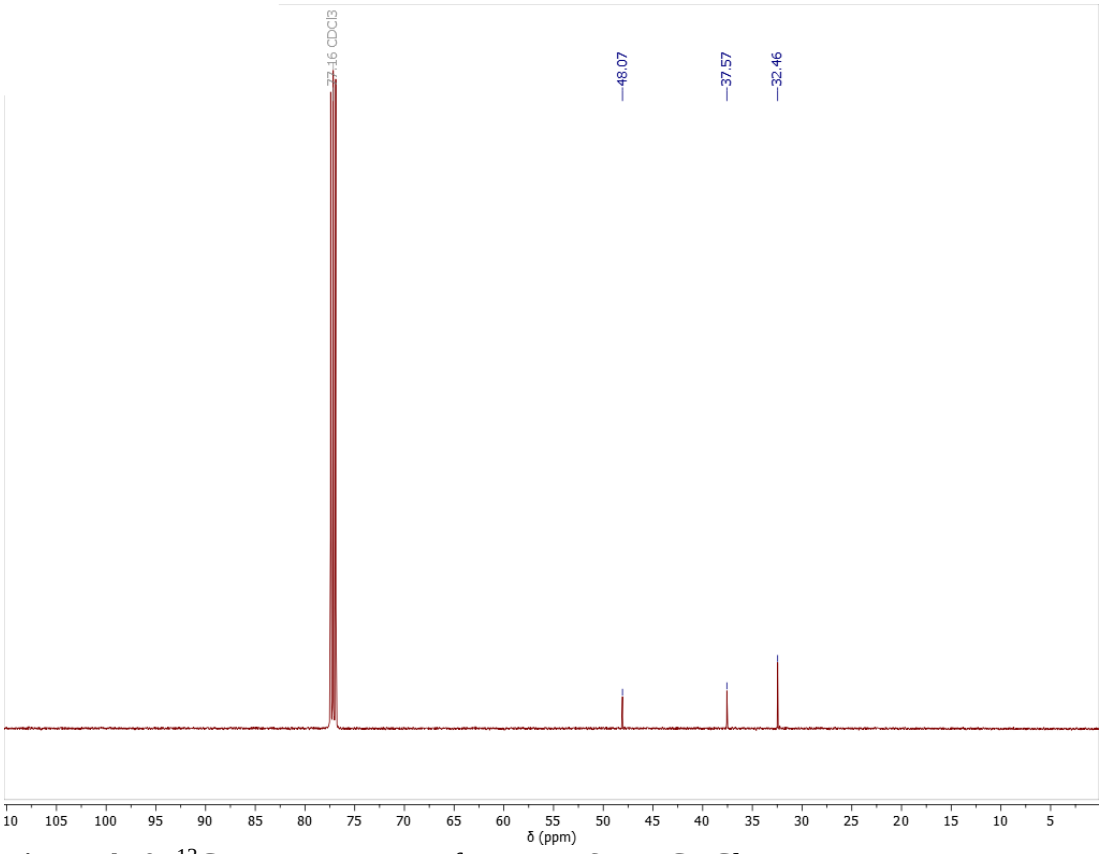

Figure A40: ^{13}C-NMR spectrum of tetramer $\mathbf{6_{T4}}$ in $CDCl_3$

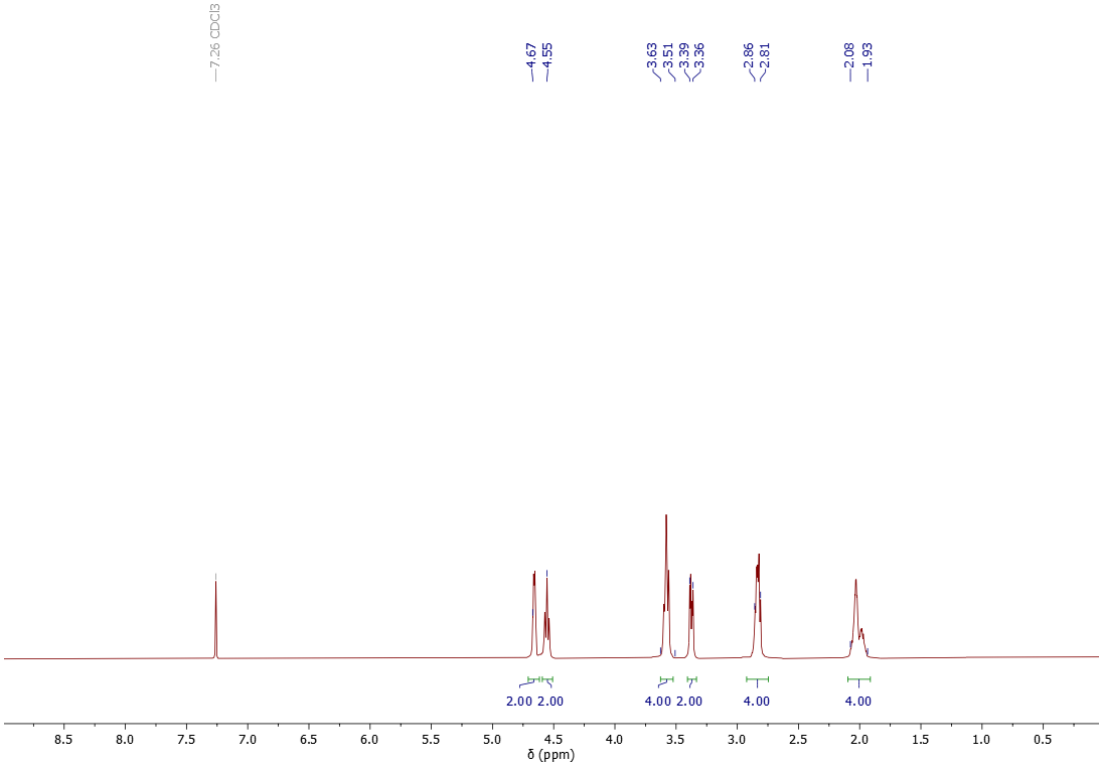

Figure A41: ^{1}H-NMR spectrum of dimer $\mathbf{7_{D2}}$ in $CDCl_3$

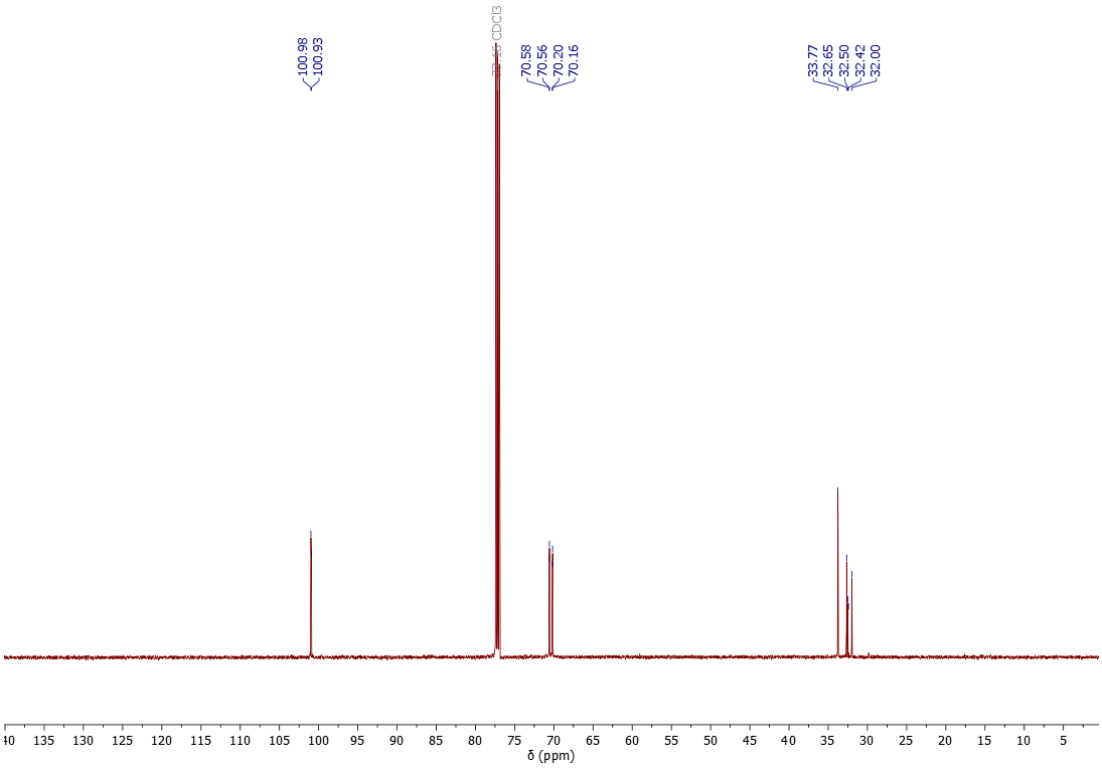

Figure A42: ^{13}C-NMR spectrum of dimer **7_{D2}** in $CDCl_3$

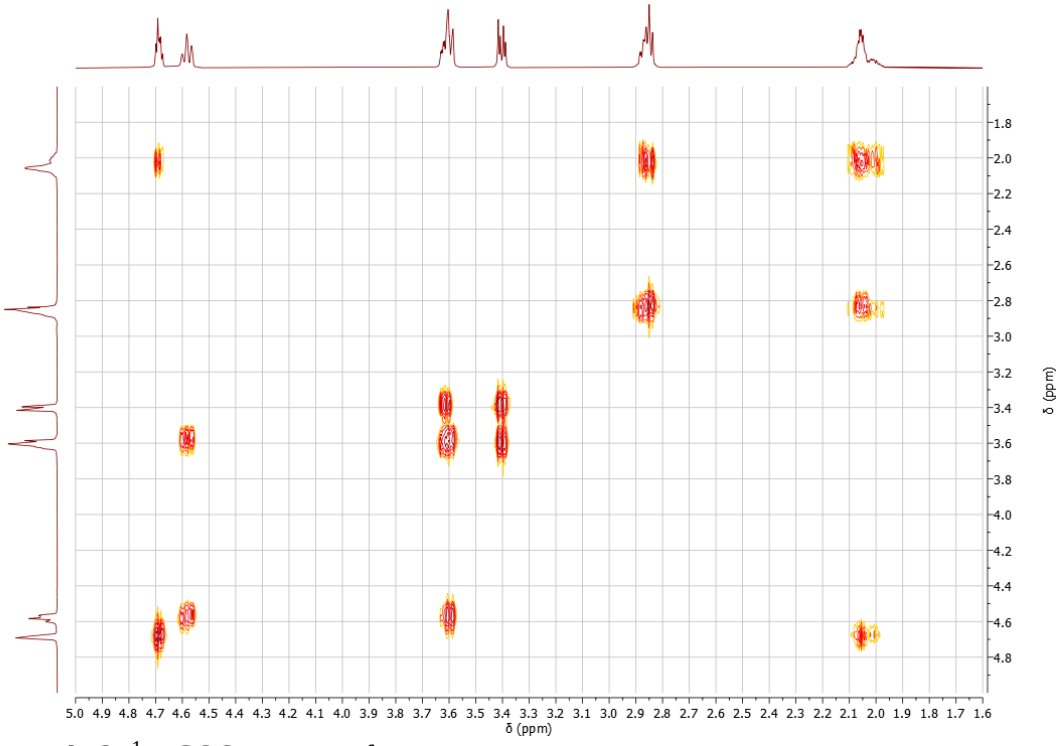

Figure A43: ^{1}H COSY NMR of **7_{D2}**

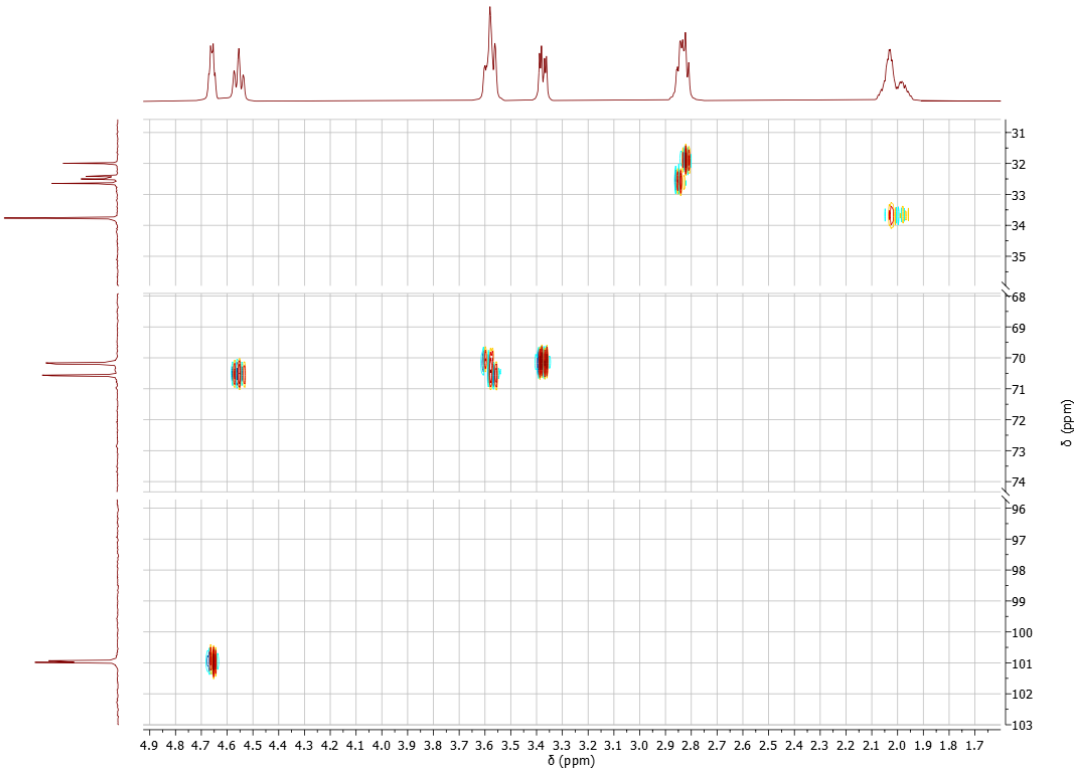

Figure A44: ^{1}H – ^{13}C HSQC NMR of $\mathbf{7_{D2}}$

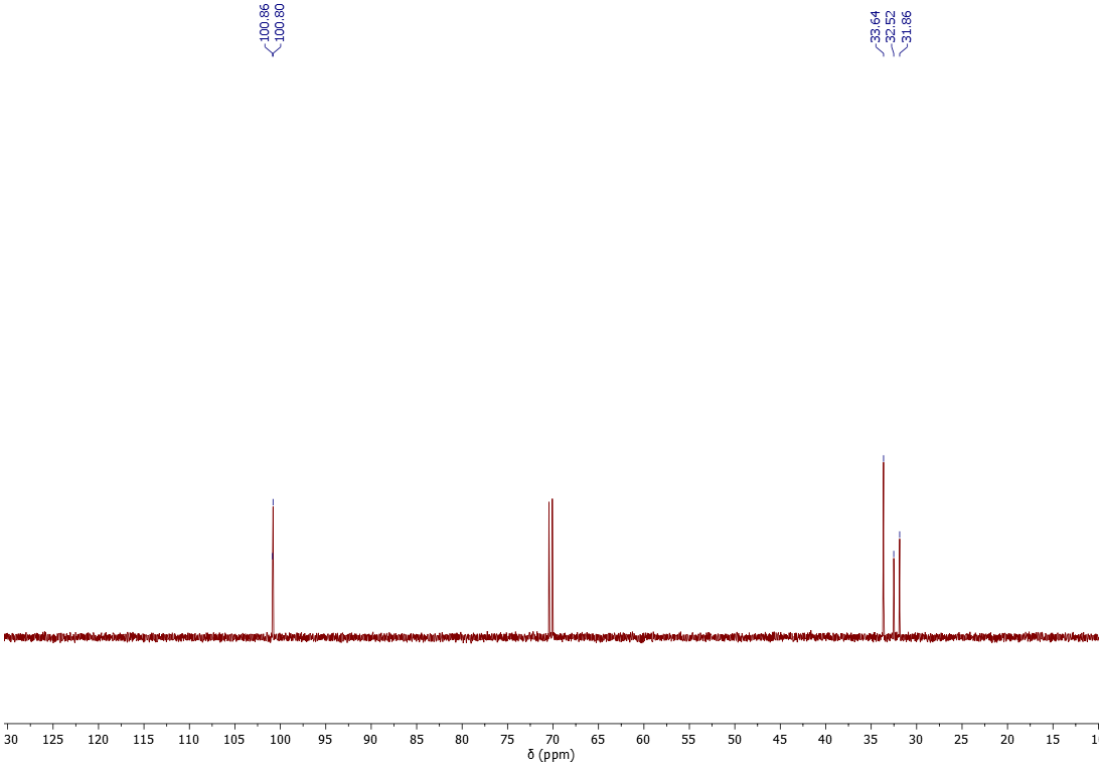

Figure A44: ^{13}C DEPT45 NMR of $\mathbf{7_{D2}}$

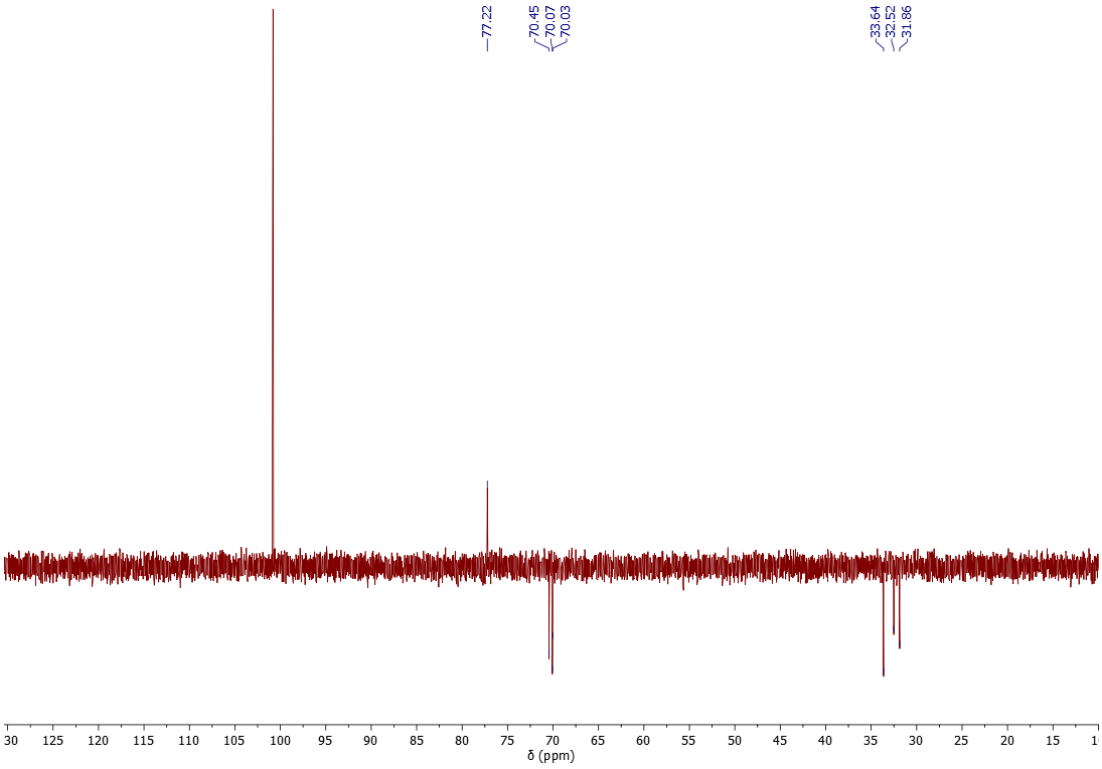

Figure A45: ^{13}C DEPT90 NMR of $\mathbf{7_{D2}}$

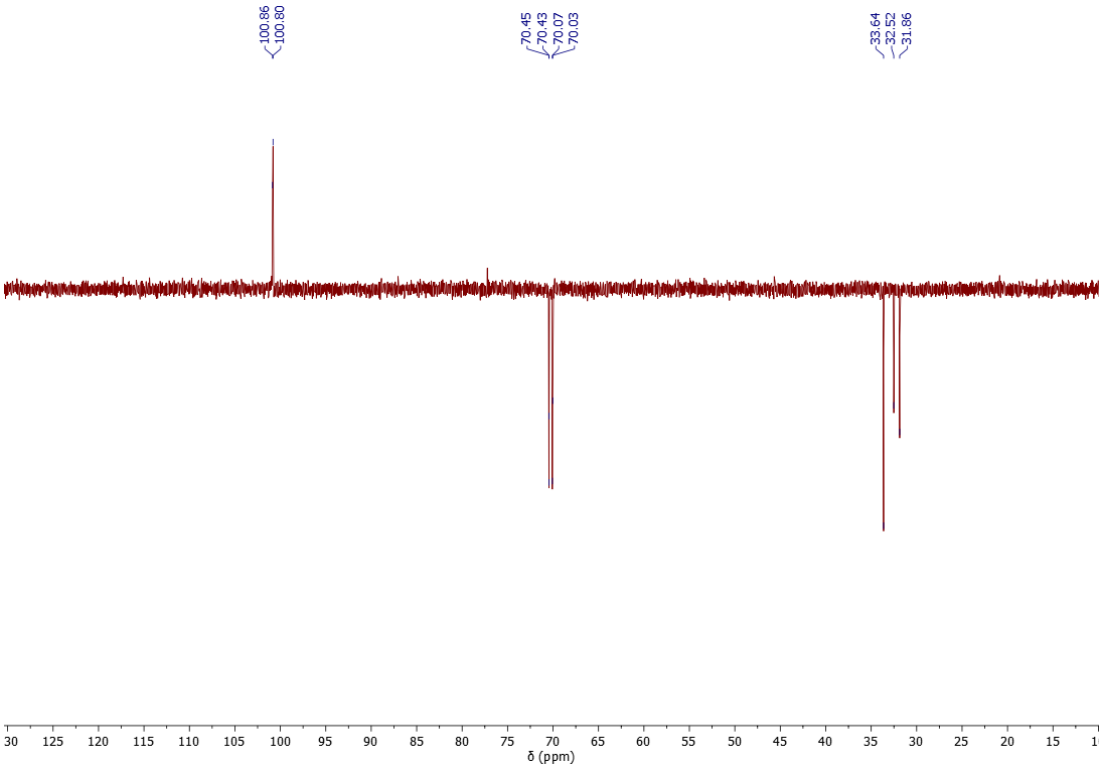

Figure A46: ^{13}C DEPT135 NMR of $\mathbf{7_{D2}}$

APPENDIX B

CRYSTALLOGRAPHIC DATA FOR A GENERALIZED METHOD FOR DISULFIDE AND THIOETHER CYCLOPHANES

X-ray Crystallography

Diffraction intensities for **1**$_{D2}$, **2**$_{D2}$, **2**$_{T2}$, **4**$_{D3}$, **5**$_{T2}$, **6**$_{D3}$, **6**$_{D4}$, **6**$_{D5}$, and **7**$_{D2}$ were collected at 100 K (**2**$_{D2}$), 200 K (**4**$_{D3}$), 223 K (**5**$_{T2}$) and 173 K on a Bruker Apex2 CCD diffractometer using CuKα and MoKα (**2**$_{D2}$ and **1**$_{D2}$) radiation, l = 1.54178 and 0.71073 Å, respectively. Space groups were determined based on systematic absences and intensity statistics (**2**$_{T2}$). Absorption corrections were applied by SADABS. Structures were solved by direct methods and Fourier techniques and refined on F^2 using full matrix least-squares procedures. All non-H atoms were refined with anisotropic thermal parameters. H atoms in all structures were refined in calculated positions in a rigid group model. One S atom in **7**$_{D2}$, two S atoms in **2**$_{T2}$ and one S atom in **2**$_{D2}$ are disordered over two positions in ratio 1:1. Crystals of **2**$_{D2}$ were very thin strips and it was possible collect diffraction data only up to 2θmax = 46.65° using a Mo-radiation source. However, it provides appropriate number of reflections per number of refined parameters, 6271/588. The structure of **6**$_{D5}$ was solved as a racemic twin consisting of two domains, the Flack is 0.15(3). The structure of **5**$_{T2}$ was solved having two symmetrically independent molecules in chiral space group of symmetry $P2_1$. The found Flack parameter, 0.47(4), indicates on a possible centro-symmetrical space group, but all our efforts to get the structure in centro-symmetrical space groups were failed. The structure

of $\mathbf{5_{T2}}$ seems having a pseudo-symmetry. It also should be mentioned that we could not get convergence in the refinement of the structure of $\mathbf{5_{T2}}$ even with applying some geometrical restrictions. The structure of this compound was determined in several possible space groups and it was found that in all of them refinement of the structure can't get converged. We think it could be related to the flat minimum of energy for the molecule of $\mathbf{5_{T2}}$ or them packing in the crystal structure. Crystal structures of $\mathbf{2_{D2}}$ and $\mathbf{2_{T2}}$, $\mathbf{6_{D4}}$ include solvent molecules C_6H_6 and $CHCl_3$, respectively. Three solvent molecules $CHCl_3$, 58 electrons, in the full unit cell of $\mathbf{2_{T2}}$, and four solvent molecules $CHCl_3$ in $\mathbf{6_{D4}}$ are highly disordered and have been treated by SQUEEZE. The corrections of the X-ray data by SQUEEZE are 170 and 240 electron/cell, respectively for $\mathbf{2_{T2}}$ and $\mathbf{6_{D4}}$. All calculations were performed by the Bruker SHELXL-2014 package. Deposition Numbers 2080702 - 2080710 contain the supplementary crystallographic data for this paper. These data can be obtained free of charge from The Cambridge Crystallographic Data Center via www.ccdc.cam.ac.uk/data_request/cif.

Crystallographic Data for $\mathbf{1_{D2}}$

$C_{20}H_{24}S_4$, M = 392.63, 0.18 x 0.16 x 0.14 mm, T = 173(2) K, Monoclinic, space group $P2_1/n$, a = 8.2013(9) Å, b = 6.5677(7) Å, c = 18.298(2) Å, β = 101.160(2)°, V = 966.93(18) Å^3, Z = 2, D_c = 1.349 Mg/m^3, μ(Mo) = 0.491 mm^{-1}, F(000) = 416, $2\theta_{max}$ = 58.17°, 11469 reflections, 2707 independent reflections [R_{int} = 0.0442], R1 = 0.0479, wR2 = 0.1380 and GOF = 1.033 for 2707 reflections (110 parameters) with I>2σ(I), R1 = 0.0540, wR2 = 0.1434 and GOF = 1.033 for all reflections, max/min residual electron density +1.574/-0.371 eÅ^{-3}.

Crystallographic Data for 2_{D2}

$C_{51}H_{45}N_6S_6$, M = 934.29, 0.330 x 0.03 x 0.02 mm, T = 100(2) K, Monoclinic, space group *P*2/*n*, *a* = 18.647(3) Å, *b* = 8.0678(14) Å, *c* = 30.375(5) Å, β = 107.510(3)°, *V* = 4357.8(13) Å^3, *Z* = 4, D_c = 1.424 Mg/m^3, μ(Mo) = 0.360 mm^{-1}, *F*(000) = 1956, $2\theta_{max}$ = 46.65°, 24289 reflections, 6271 independent reflections [R_{int} = 0.1125], R1 = 0.0629, wR2 = 0.1380 and GOF = 1.038 for 6271 reflections (588 parameters) with I>2σ(I), R1 = 0.1409, wR2 = 0.1738 and GOF = 1.038 for all reflections, max/min residual electron density +0.447/-0.447 eÅ^{-3}.

Crystallographic Data for 2_{T2}

$C_{49}H_{37}Cl_3N_6S_3$, M = 912.37, 0.07 x 0.04 x 0.02 mm, T = 173(2) K, Triclinic, space group *P*-1, *a* = 8.7460(2) Å, *b* = 13.2094(2) Å, *c* = 20.2583(3) Å, α = 107.517(2)°, β = 93.520(1)°, γ = 90.456(1)°, *V* = 2226.84(7) Å^3, *Z* = 2, D_c = 1.361 Mg/m^3, μ(Cu) = 3.511 mm^{-1}, *F*(000) = 944, $2\theta_{max}$ = 152.14°, 28159 reflections, 8900 independent reflections [R_{int} = 0.0251], R1 = 0.0536, wR2 = 0.1618 and GOF = 1.069 for 8900 reflections (534 parameters) with I>2σ(I), R1 = 0.0604, wR2 = 0.1682 and GOF = 1.093 for all reflections, max/min residual electron density +0.473/-0.230 eÅ^{-3}.

Crystallographic Data for 4_{D3}

$C_{12}H_{18}S_6$, M = 354.62, 0.21 x 0.08 x 0.07 mm, T = 200(2) K, Monoclinic, space group $P2_1/c$, *a* = 5.3348(1) Å, *b* = 30.1158(9) Å, *c* = 10.7618(3) Å, β = 101.617(1)°, *V* = 1693.59(8) Å^3, Z = 4, D_c = 1.391 Mg/m^3, μ(Cu) = 7.301 mm^{-1}, *F*(000) = 744, $2\theta_{max}$ =

136.53°, 15587 reflections, 3097 independent reflections [R_{int} = 0.0717], R1 = 0.0687, wR2 = 0.1804 and GOF = 1.049 for 3097 reflections (163 parameters) with I>2σ(I), R1 = 0.0708, wR2 = 0.1823 and GOF = 1.049 for all reflections, max/min residual electron density +0.909/-0.526 eÅ^{-3}.

Crystallographic Data for $\mathbf{5_{T2}}$

$C_8H_8S_2$, M = 168.26, 0.16 x 0.14 x 0.09 mm, T = 223(2) K, Monoclinic, space group $P2_1$, a = 4.3260(8) Å, b = 11.792(2) Å, c = 15.762(3) Å, β = 95.731(9)°, V = 800.1(3) Å^3, Z = 4, D_c = 1.397 Mg/m^3, μ(Cu) = 5.332 mm^{-1}, F(000) = 352, $2\theta_{max}$ = 136.70°, 6094 reflections, 2779 independent reflections [R_{int} = 0.0446], R1 = 0.0472, wR2 = 0.1495 and GOF = 1.005 for 2779 reflections (182 parameters) with I>2σ(I), R1 = 0.0561, wR2 = 0.1697 and GOF = 1.005 for all reflections, the Flack = 0.47(4), max/min residual electron density +0.374/-0.250 eÅ^{-3}.

Crystallographic Data for $\mathbf{6_{D3}}$

$C_{24}H_{42}S_6$, M = 522.93, 0.23 x 0.09 x 0.02 mm, T = 173(2) K, Monoclinic, space group $P2_1/c$, a = 5.6958(2) Å, b = 22.7213(6) Å, c = 21.1880(5) Å, β = 91.957(2)°, V = 2740.47(14) Å^3, Z = 4, D_c = 1.267 Mg/m^3, μ(Cu) = 4.671 mm^{-1}, F(000) = 1128, $2\theta_{max}$ = 132.95°, 14297 reflections, 4787 independent reflections [R_{int} = 0.0394], R1 = 0.0386, wR2 = 0.0990 and GOF = 1.041 for 4787 reflections (271 parameters) with I>2σ(I), R1 = 0.0457, wR2 = 0.1034 and GOF = 1.041 for all reflections, max/min residual electron density +0.408/-0.237 eÅ^{-3}.

Crystallographic Data for 6_{D4}

$C_{33}H_{57}Cl_3S_8$, M = 816.61, 0.16 x 0.14 x 0.09 mm, T = 173(2) K, Monoclinic, space group *P*2/*c*, *a* = 30.3668(17) Å, *b* = 5.2860(4) Å, *c* = 29.9122(16) Å, β = 119.248(4)°, *V* = 4189.3(5) Å^3, *Z* = 4, D_c = 1.295 Mg/m^3, μ(Cu) = 5.871 mm^{-1}, *F*(000) = 1736, $2\theta_{max}$ = 133.80°, 26763 reflections, 7348 independent reflections [R_{int} = 0.0926], R1 = 0.0866, wR2 = 0.2107 and GOF = 1.098 for 7348 reflections (361 parameters) with I>2σ(I), R1 = 0.0994, wR2 = 0.2178 and GOF = 1.098 for all reflections, max/min residual electron density +1.036/-0.697 eÅ^{-3}.

Crystallographic Data for 6_{D5}

$C_{40}H_{70}S_{10}$, M = 871.56, 0.14 x 0.06 x 0.01 mm, T = 173(2) K, Orthorhombic, space group *Iba*2, *a* = 10.9400(8) Å, *b* = 78.496(7) Å, *c* = 10.7608(9) Å, *V* = 9240.7(13) Å^3, *Z* = 8, D_c = 1.253 Mg/m^3, μ(Cu) = 4.618 mm^{-1}, *F*(000) = 3760, $2\theta_{max}$ = 134.37°, 18659 reflections, 6953 independent reflections [R_{int} = 0.0974], R1 = 0.0686, wR2 = 0.1702 and GOF = 1.005 for 6953 reflections (451 parameters) with I>2σ(I), R1 = 0.1038, wR2 = 0.1906 and GOF = 1.005 for all reflections, the Flack = 0.15(3), max/min residual electron density +0.550/-0.437 eÅ^{-3}.

Crystallographic Data for 7_{D2}

$C_{22}H_{36}O_8S_4$, M = 556.75, 0.18 x 0.11 x 0.02 mm, T = 173(2) K, Monoclinic, space group *P*2$_1$/*c*, *a* = 11.6003(5) Å, *b* = 5.5764(2) Å, *c* = 20.1918(8) Å, β = 97.537(3)°, *V* = 1294.88(9) Å^3, *Z* = 2, Z' = 0.5, D_c = 1.428 Mg/m^3, μ(Cu) = 3.755 mm^{-1}, *F*(000) = 592, $2\theta_{max}$ = 133.11°, 8561 reflections, 2287 independent reflections [R_{int} = 0.0452], R1 =

0.0793, wR2 = 0.2018 and GOF = 1.088 for 2287 reflections (158 parameters) with I>2σ(I), R1 = 0.0875, wR2 = 0.2078 and GOF = 1.088 for all reflections, max/min residual electron density +1.135/-0.403 $eÅ^{-3}$.

APPENDIX C

NMR SPECTROSCOPY AND MASS SPECTROMETRY FOR PDI PRECURSORS

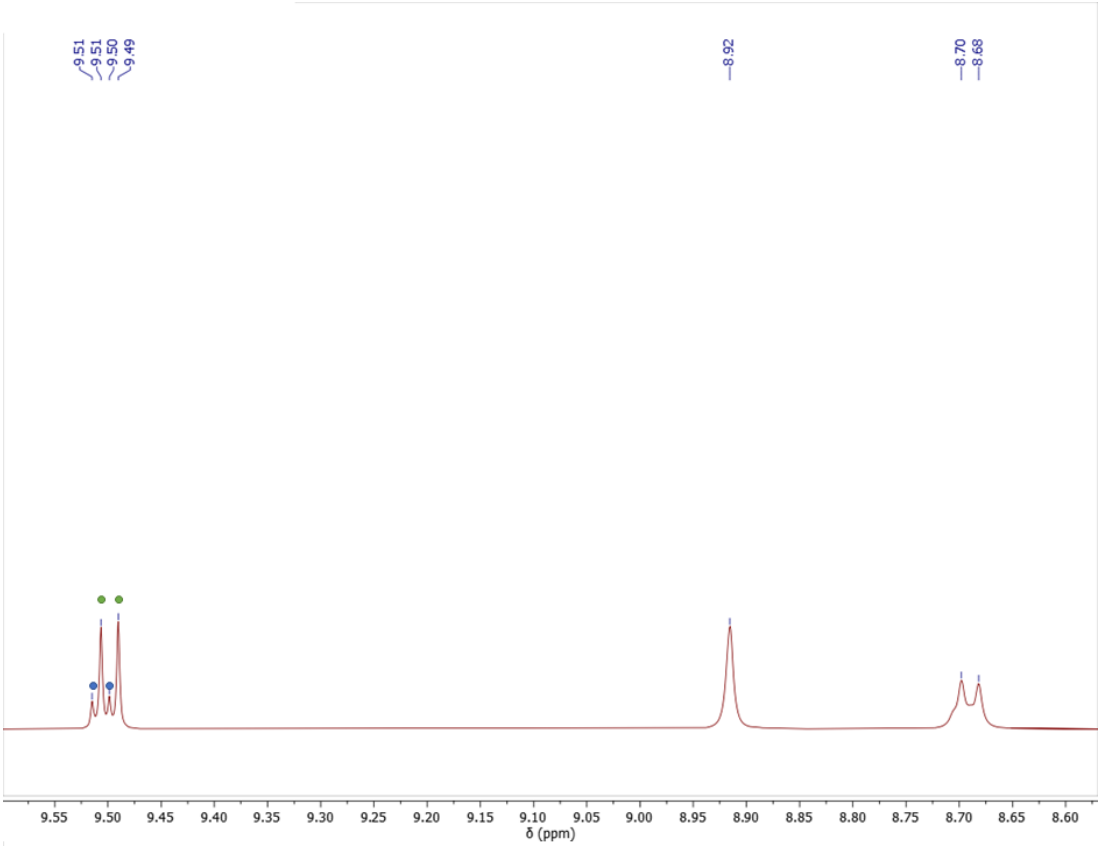

Figure B1: ^{1}H-NMR spectrum of **PDI-Br** in $CDCl_3$. ~1:4 ratio of 1,6- (blue circles):1,7-regioisomer (green circles) on 500 MHz spectrometer.

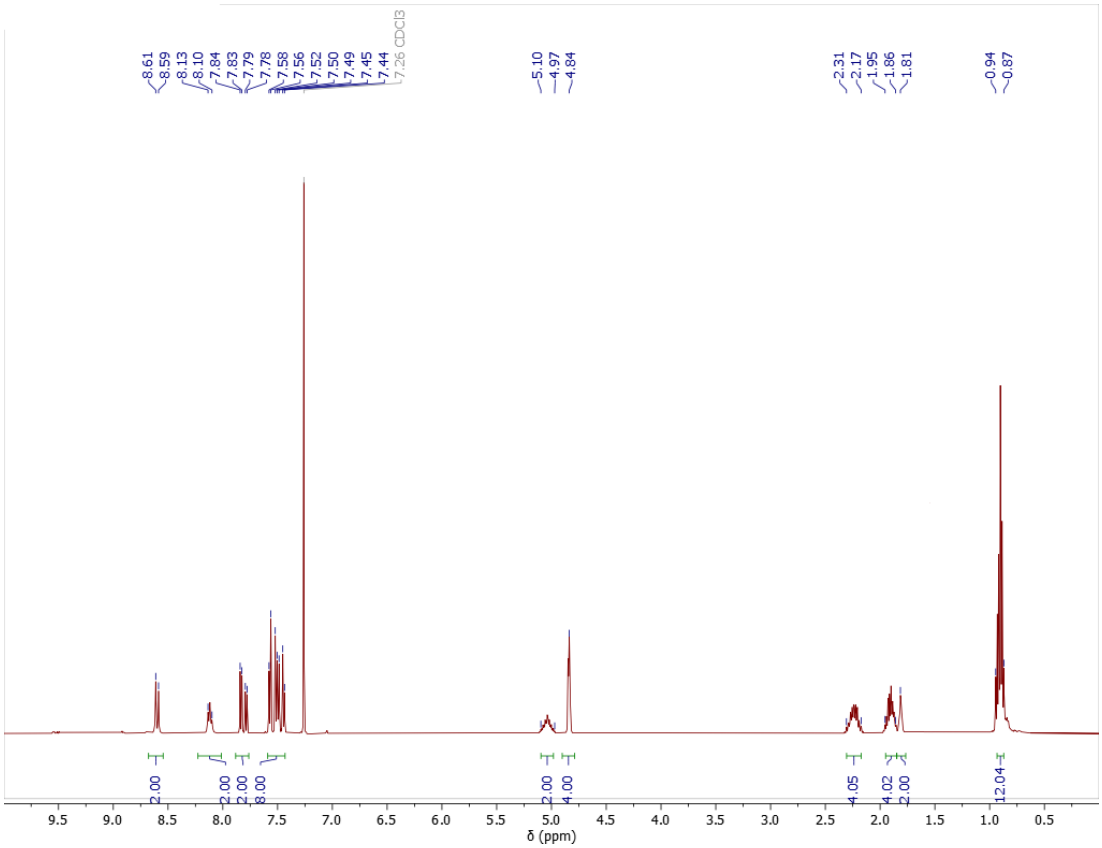

Figure B2: ^{1}H-NMR spectrum of **PDI-OH** in $CDCl_3$

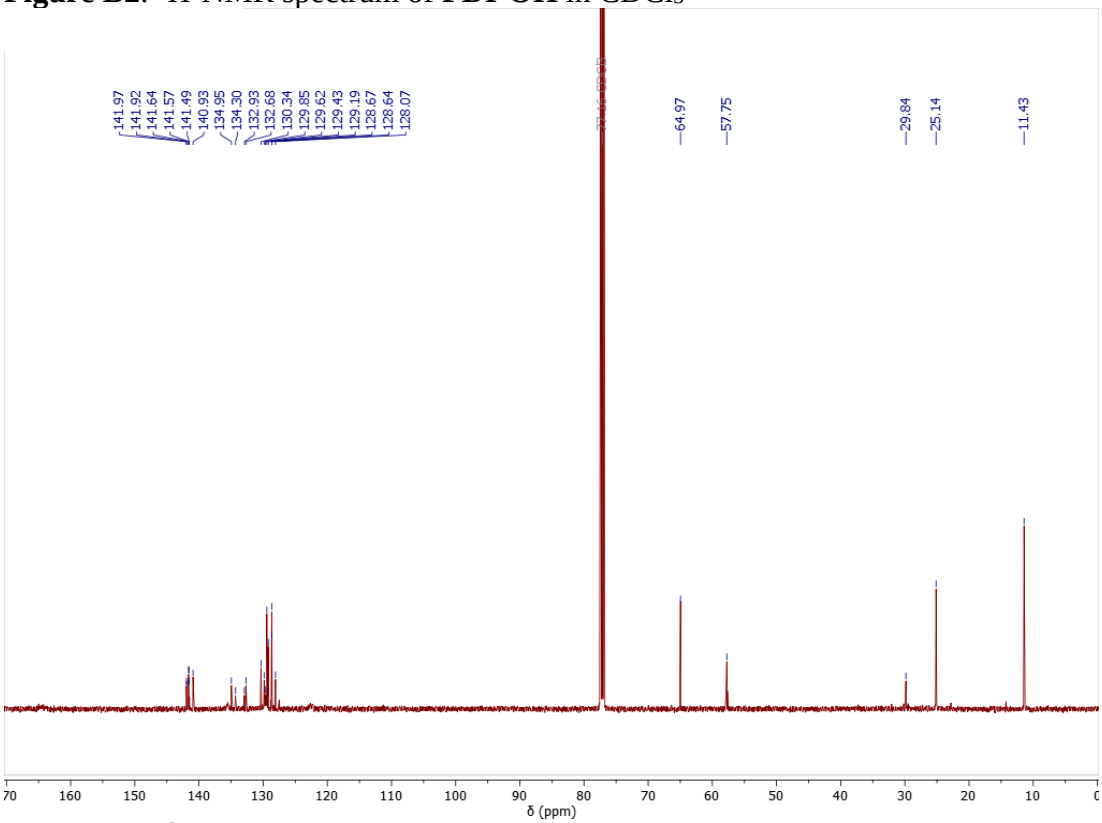

Figure B3: ^{13}C-NMR spectrum of **PDI-OH** in $CDCl_3$

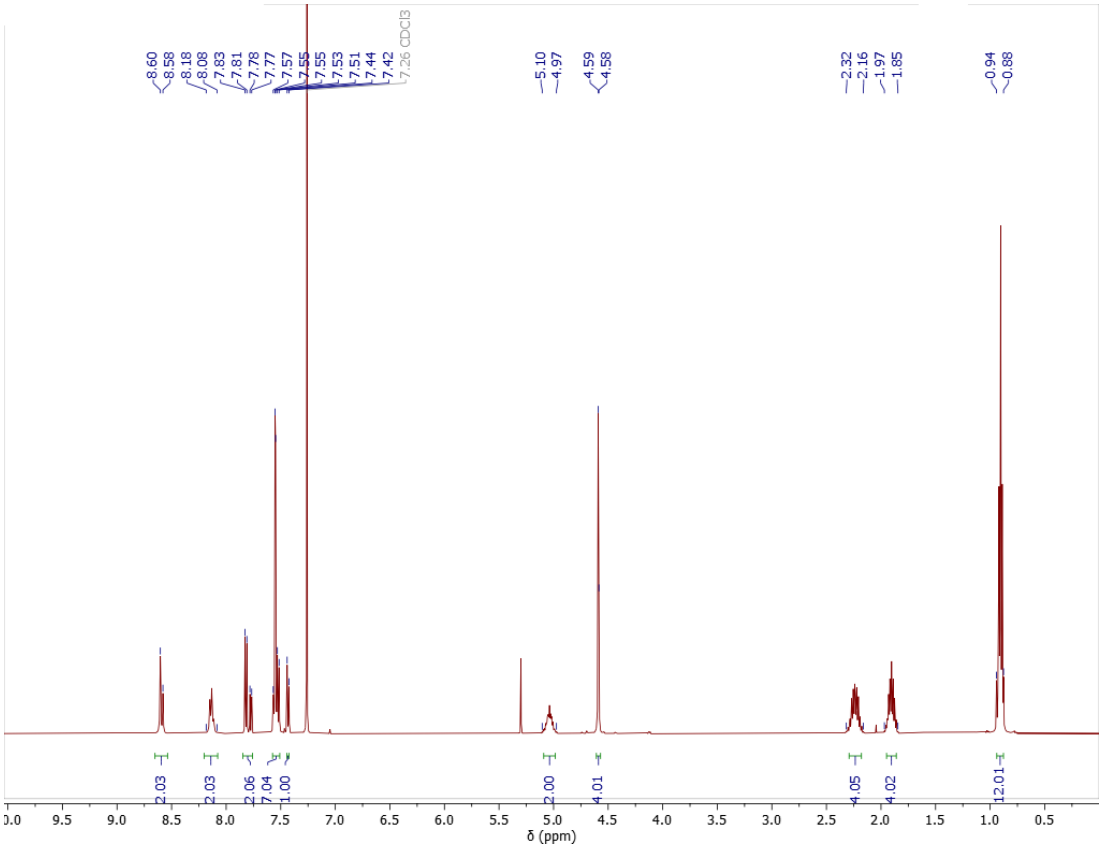

Figure B4: ^{1}H-NMR spectrum of **PDI-PMBr** in $CDCl_3$

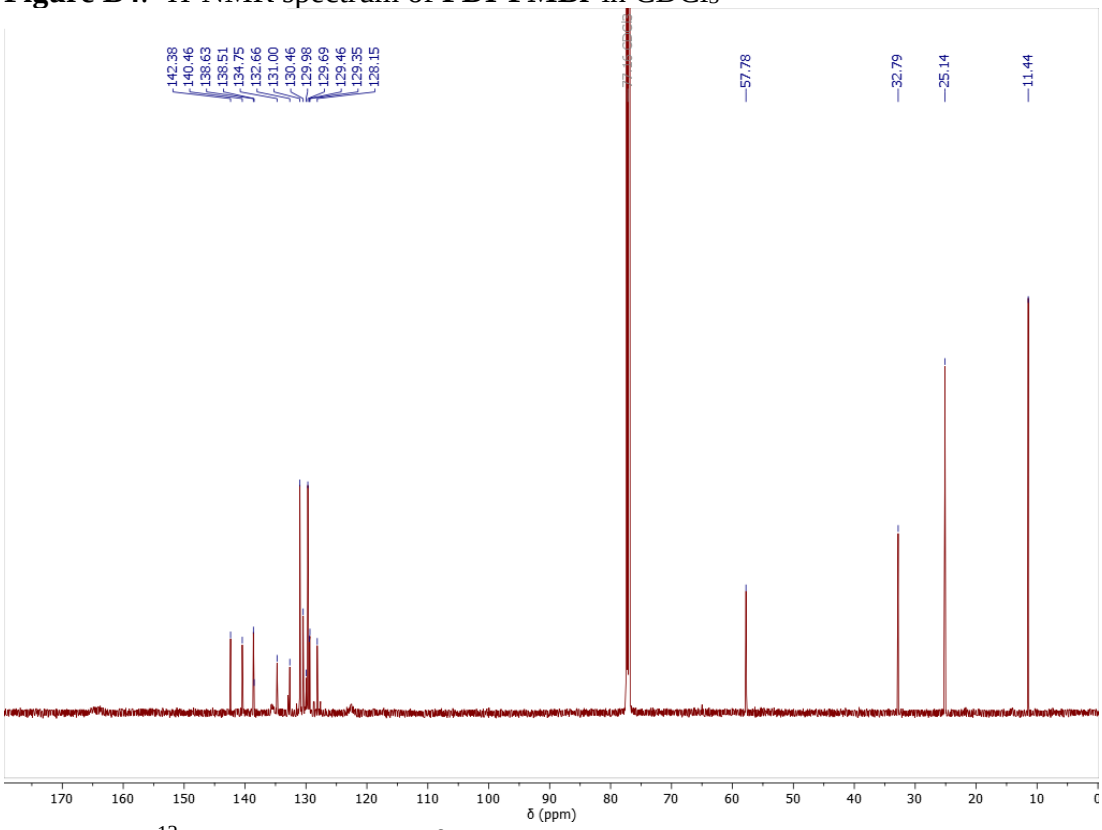

Figure B5: ^{13}C-NMR spectrum of **PDI-PMBr** in $CDCl_3$

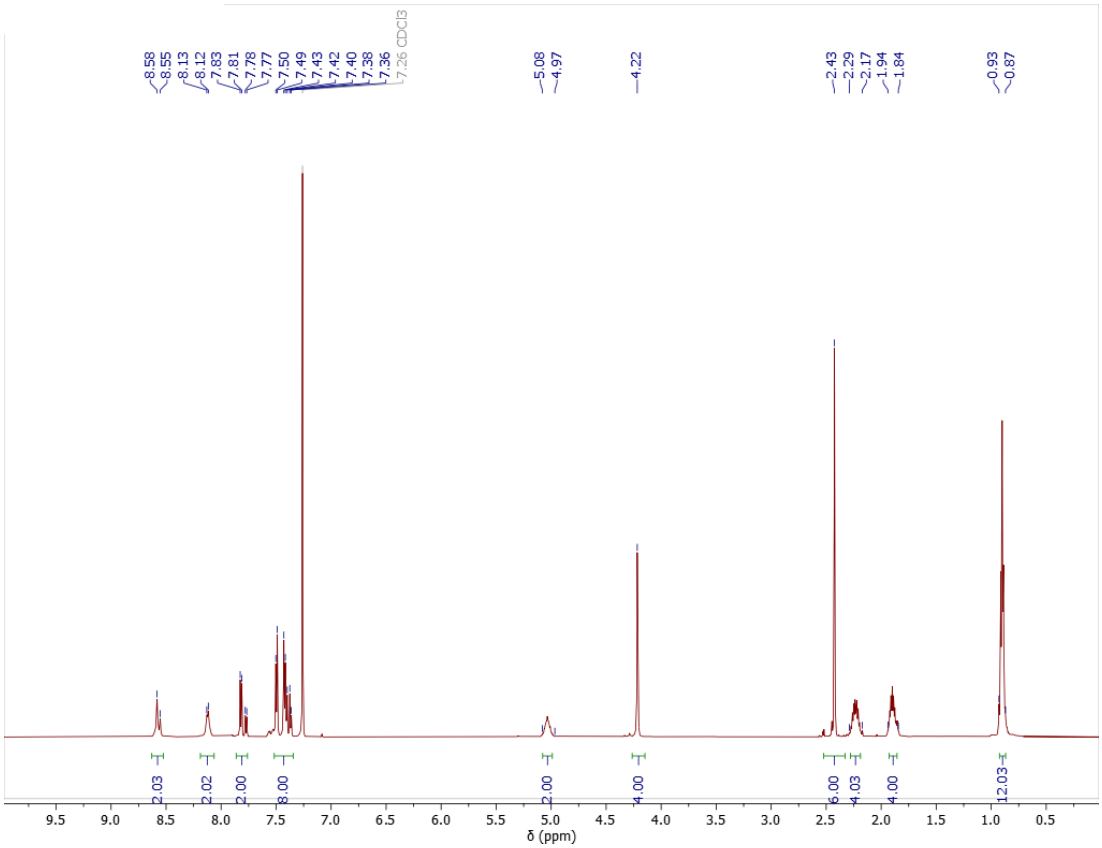

Figure B6: ^{1}H-NMR spectrum of **PDI-SAc** in $CDCl_3$

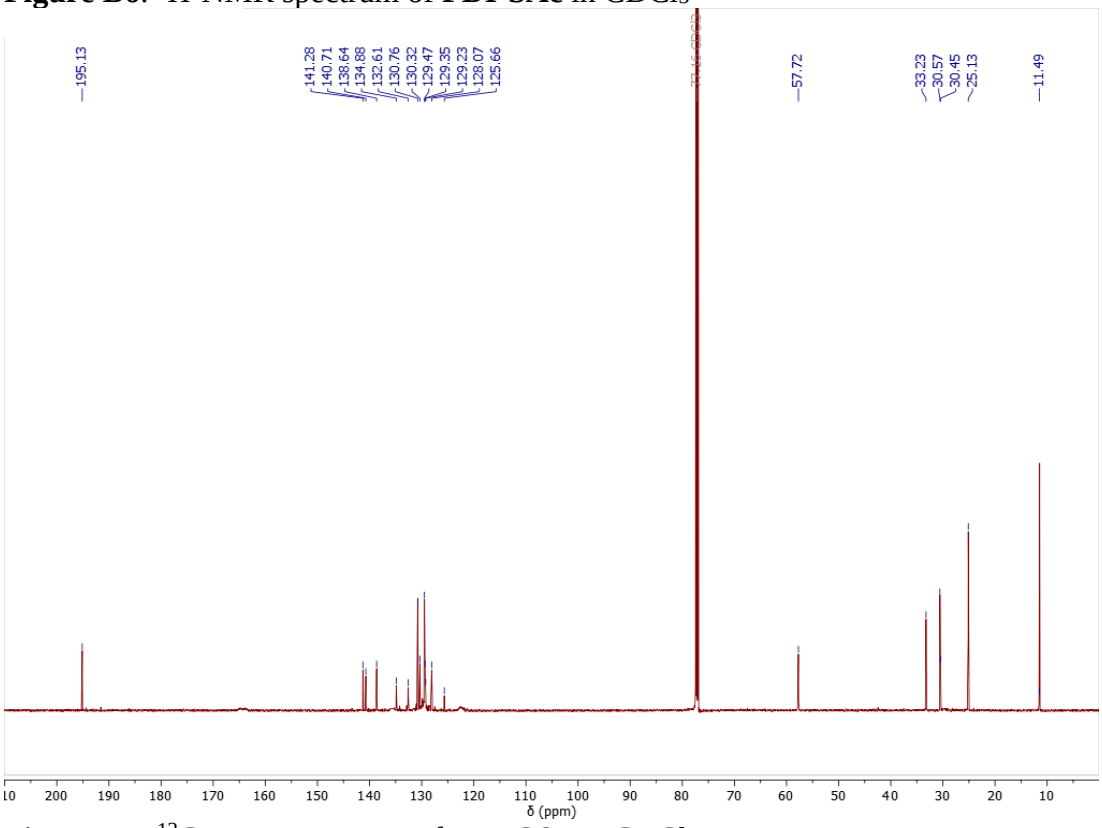

Figure B7: ^{13}C-NMR spectrum of **PDI-SAc** in $CDCl_3$

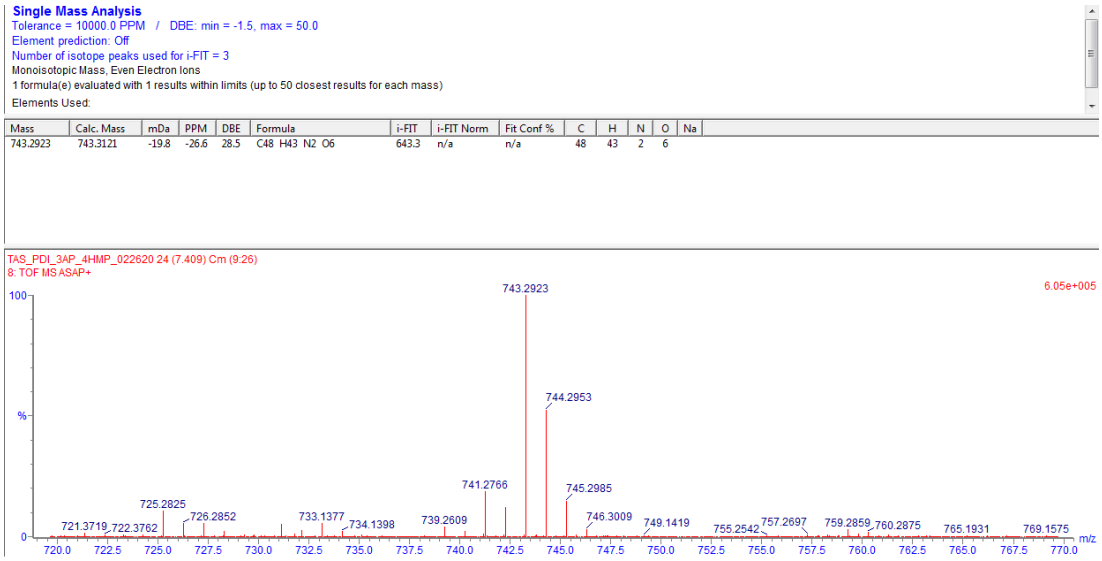

Figure B8: HRMS of **PDI-OH**

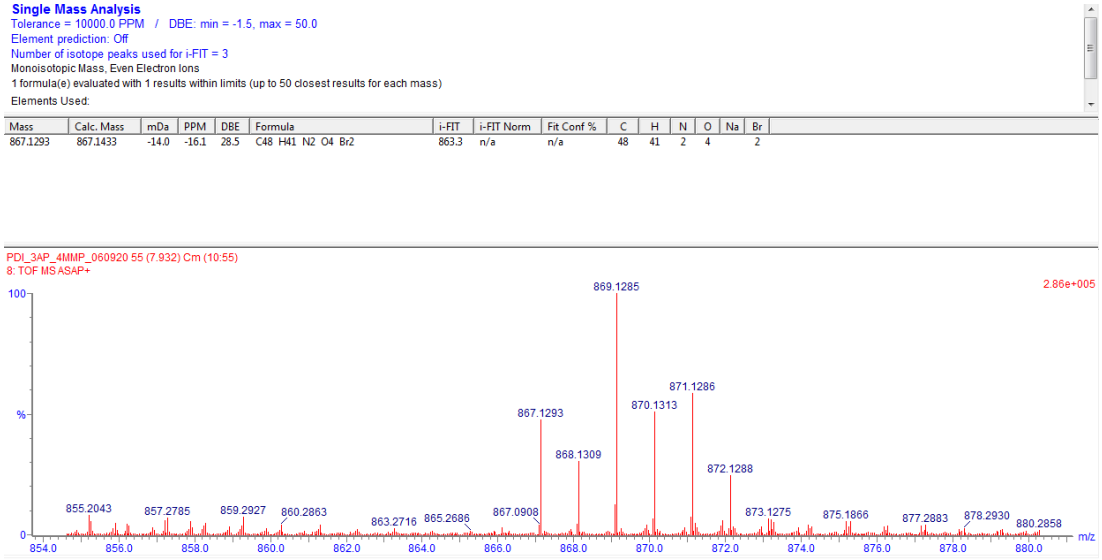

Figure B9: HRMS of **PDI-PMBr**

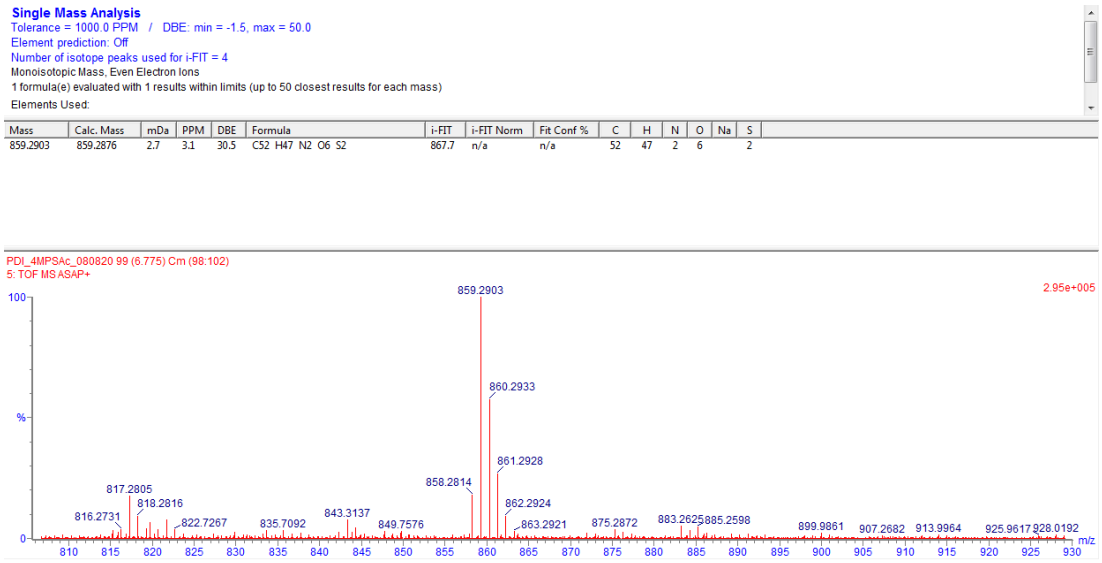

Figure B10: HRMS of **PDI-SAc**

References Cited

Chapter I

1. Shear, T. A.; Johnson, D. W. *Synlett*, (EFirst).

2. Corbett, P. T.; Leclaire, J.; Vial, L.; West, K. R.; Wietor, J.-L.; Sanders, J. K. M.; Otto, S. *Chemical Reviews* **2006,** 106, (9), 3652-3711.

3. Hu, L.; Schaufelberger, F.; Timmer, B. J. J.; Flos, M. A.; Ramström, O., Constitutional Dynamic Chemistry. In *Kirk-Othmer Encyclopedia of Chemical Technology*, ed.; pp 1-25.

4. Anslyn, E. V. D., D. A., , *Modern Physical Organic Chemistry*. ed.; 2006.

5. (a) Thornton, J. M. *Journal of Molecular Biology* **1981,** 151, (2), 261-287; (b) Betz, S. F. *Protein Science* **1993,** 2, (10), 1551-1558.

6. (a) Ahamed, J.; Burg, N.; Yoshinaga, K.; Janczak, C. A.; Rifkin, D. B.; Coller, B. S. *Blood* **2008,** 112, (9), 3650-3660; (b) Patel, S.; Chaffotte, A. F.; Amana, B.; Goubard, F.; Pauthe, E. *The International Journal of Biochemistry & Cell Biology* **2006,** 38, (9), 1547-1560.

7. Ponnuswamy, N.; Cougnon, F. B. L.; Clough, J. M.; Pantoş, G. D.; Sanders, J. K. M. *Science* **2012,** 338, (6108), 783-785.

8. Cougnon, F. B. L.; Ponnuswamy, N.; Jenkins, N. A.; Pantoş, G. D.; Sanders, J. K. M. *Journal of the American Chemical Society* **2012,** 134, (46), 19129-19135.

9. Ji, Q.; Le, H. T. M.; Wang, X.; Chen, Y.-S.; Makarenko, T.; Jacobson, A. J.; Miljanić, O. Š. *Chemistry – A European Journal* **2015,** 21, (48), 17205-17209.

10. Brachvogel, R.-C.; Hampel, F.; von Delius, M. *Nature Communications* **2015,** 6, (1), 7129.

11. (a) Chavez, A. D.; Evans, A. M.; Flanders, N. C.; Bisbey, R. P.; Vitaku, E.; Chen, L. X.; Dichtel, W. R. *Chemistry – A European Journal* **2018,** 24, (16), 3989-3993; (b) Chen, P.; Zhou, Y.; Yang, J. *Chemical Communications* **2017,** 53, (6), 1144-1147.

12. Wang, Q.; Yu, C.; Zhang, C.; Long, H.; Azarnoush, S.; Jin, Y.; Zhang, W. *Chemical Science* **2016,** 7, (5), 3370-3376.

13. Whitesides, G. M.; Grzybowski, B. *Science* **2002,** 295, (5564), 2418-2421.

14. (a) Bancroft, J. B.; Hills, G. J.; Markham, R. *Virology* **1967,** 31, (2), 354-379; (b) Jones, M. R.; Seeman, N. C.; Mirkin, C. A. *Science* **2015,** 347, (6224), 1260901; (c) Seeman, N. C.; Sleiman, H. F. *Nature Reviews Materials* **2017,** 3, (1), 17068.

15. (a) Green, D. E.; Hechter, O. *Proceedings of the National Academy of Sciences of the United States of America* **1965,** 53, (2), 318-325; (b) Israelachvili, J. N.; Mitchell, D. J.; Ninham, B. W. *Journal of the Chemical Society, Faraday Transactions 2: Molecular and Chemical Physics* **1976,** 72, (0), 1525-1568.

16. (a) Cangelosi, V. M.; Carter, T. G.; Zakharov, L. N.; Johnson, D. W. *Chemical Communications* **2009**, (37), 5606-5608; (b) Fujita, M. *Chemical Society Reviews* **1998,** 27, (6), 417-425; (c) Fujita, M. *Molecular Self-Assembly Organic Versus Inorganic Approaches* **2000**, 177-201; (d) Fujita, M.; Nagao, S.; Ogura, K. *Journal of the American Chemical Society* **1995,** 117, (5), 1649-1650; (e) Noveron, J. C.; Lah, M. S.; Del Sesto, R. E.; Arif, A. M.; Miller, J. S.; Stang, P. J. *Journal of the American Chemical Society* **2002,** 124, (23), 6613-6625.

17. Bivaud, S.; Balandier, J.-Y.; Chas, M.; Allain, M.; Goeb, S.; Sallé, M. *Journal of the American Chemical Society* **2012,** 134, (29), 11968-11970.

18. Beer, P. D.; Berry, N. G.; Cowley, A. R.; Hayes, E. J.; Oates, E. C.; Wong, W. W. H. *Chemical Communications* **2003**, (19), 2408-2409.

19. Zheng, Y.-R.; Zhao, Z.; Kim, H.; Wang, M.; Ghosh, K.; Pollock, J. B.; Chi, K.-W.; Stang, P. J. *Inorganic Chemistry* **2010,** 49, (22), 10238-10240.

20. Duriska, M. B.; Neville, S. M.; Moubaraki, B.; Cashion, J. D.; Halder, G. J.; Chapman, K. W.; Balde, C.; Létard, J.-F.; Murray, K. S.; Kepert, C. J.; Batten, S. R. *Angewandte Chemie International Edition* **2009,** 48, (14), 2549-2552.

21. Jeong, K. S.; Kim, Y. S.; Kim, Y. J.; Lee, E.; Yoon, J. H.; Park, W. H.; Park, Y. W.; Jeon, S.-J.; Kim, Z. H.; Kim, J.; Jeong, N. *Angewandte Chemie International Edition* **2006,** 45, (48), 8134-8138.

22. Chakrabarty, R.; Mukherjee, P. S.; Stang, P. J. *Chemical Reviews* **2011,** 111, (11), 6810-6918.

23. (a) Chakrabarty, R.; Mukherjee, P. S.; Stang, P. J. *Chemical reviews* **2011,** 111, (11), 6810-6918; (b) Cook, T. R.; Stang, P. J. *Chemical reviews* **2015,** 115, (15), 7001-7045.

24. Vickaryous, W. J.; Herges, R.; Johnson, D. W. *Angewandte Chemie* **2004,** 116, (43), 5955-5957.

25. Bhattacharya, P.; Frisbie, S.; Smith, E.; Naidu, R.; Jacks, G.; Sarkar, B. *Handbook of Heavy Metals in the Environment, Marcell Dekker Inc., New York* **2002**, 147-215.

26. Cangelosi, V. M.; Carter, T. G.; Crossland, J. L.; Zakharov, L. N.; Johnson, D. W. *Inorganic chemistry* **2010,** 49, (21), 9985-9992.

27. Collins, M. S.; Carnes, M. E.; Sather, A. C.; Berryman, O. B.; Zakharov, L. N.; Teat, S. J.; Johnson, D. W. *Chemical Communications* **2013,** 49, (59), 6599-6601.

28. Cangelosi, V. M.; Zakharov, L. N.; Johnson, D. W. *Angewandte Chemie International Edition* **2010,** 49, (7), 1248-1251.

29. Danehy, J. P.; Doherty, B. T.; Egan, C. P. *The Journal of Organic Chemistry* **1971,** 36, (17), 2525-2530.

30. (a) Baker, W.; Banks, R.; Lyon, D. R.; Mann, F. G. *Journal of the Chemical Society (Resumed)* **1945**, (0), 27-30; (b) Merner, B. L.; Dawe, L. N.; Bodwell, G. J. *Angewandte Chemie* **2009,** 121, (30), 5595-5599; (c) Vögtle, F. *Justus Liebigs Annalen der Chemie* **1970,** 735, (1), 193-195.

31. (a) Vögtle, F. *Angewandte Chemie International Edition in English* **1969,** 8, (4), 274-274; (b) Vögtle, F.; Effler, A. H. *Chemische Berichte* **1969,** 102, (9), 3071-3076.

32. Phan, N.-M.; Zakharov, L. N.; Johnson, D. W. *Chemical Communications* **2018,** 54, (95), 13419-13422.

33. Collins, M. S.; Carnes, M. E.; Nell, B. P.; Zakharov, L. N.; Johnson, D. W. *Nature communications* **2016,** 7, (1), 1-7.

34. Phan, N. M.; Shear, T. A.; Zakharov, L. N.; Johnson, D. W. *European Journal of Organic Chemistry* **2020,** 2020, (43), 6795-6800.

Chapter II

1. Shear, T. A.; Lin, F.; Zakharov, L. N.; Johnson, D. W. *Angewandte Chemie International Edition* **2020,** 59, (4), 1496-1500.

2. (a) Granzhan, A.; Riis-Johannessen, T.; Scopelliti, R.; Severin, K. *Angewandte Chemie International Edition* **2010,** 49, (32), 5515-5518; (b) Jin, Y.; Wang, Q.; Taynton, P.; Zhang, W. *Accounts of Chemical Research* **2014,** 47, (5), 1575-1586; (c) Krishnan-Ghosh, Y.; Balasubramanian, S. *Angewandte Chemie International Edition* **2003,** 42, (19), 2171-2173.

3. Gokel, G. W. *Chemical Communications* **2003**, (23), 2847-2852.

4. Hay, B. P.; Bryantsev, V. S. *Chemical Communications* **2008**, (21), 2417-2428.

5. Cangelosi, V. M.; Carter, T. G.; Crossland, J. L.; Zakharov, L. N.; Johnson, D. W. *Inorganic Chemistry* **2010,** 49, (21), 9985-9992.

6. (a) Jin, Y.; Yu, C.; Denman, R. J.; Zhang, W. *Chemical Society Reviews* **2013,** 42, (16), 6634-6654; (b) Rowan, S. J.; Cantrill, S. J.; Cousins, G. R. L.; Sanders, J. K. M.; Stoddart, J. F. *Angewandte Chemie International Edition* **2002,** 41, (6), 898-952.

7. (a) Liu, L.; Lyu, G.; Liu, C.; Jiang, F.; Yuan, D.; Sun, Q.; Zhou, K.; Chen, Q.; Hong, M. *Chemistry – A European Journal* **2017,** 23, (2), 456-461; (b) Tashiro, S.; Tominaga, M.; Kusukawa, T.; Kawano, M.; Sakamoto, S.; Yamaguchi, K.; Fujita, M. *Angewandte Chemie International Edition* **2003,** 42, (28), 3267-3270; (c) Yoneya, M.; Tsuzuki, S.; Yamaguchi, T.; Sato, S.; Fujita, M. *ACS Nano* **2014,** 8, (2), 1290-1296.

8. Collins, M. S.; Carnes, M. E.; Sather, A. C.; Berryman, O. B.; Zakharov, L. N.; Teat, S. J.; Johnson, D. W. *Chemical Communications* **2013,** 49, (59), 6599-6601.

9. Chen, P.; Zhou, Y.; Yang, J. *Chemical Communications* **2017,** 53, (6), 1144-1147.

10. Tauk, L.; Schröder, A. P.; Decher, G.; Giuseppone, N. *Nature Chemistry* **2009,** 1, 649.

11. Collins, M. S.; Carnes, M. E.; Nell, B. P.; Zakharov, L. N.; Johnson, D. W. *Nature Communications* **2016,** 7, 11052.

12. Bailey, T. S.; Henthorn, H. A.; Pluth, M. D. *Inorganic Chemistry* **2016,** 55, (24), 12618-12625.

13. Tabushi, I.; Yamamura, K. In Water soluble cyclophanes as hosts and catalysts, Cyclophanes I, Berlin, Heidelberg, 1983//, 1983; Vögtle, F., Ed. Springer Berlin Heidelberg: Berlin, Heidelberg, 1983; pp 145-182.

14. Montgomery, D. C., Design and Analysis of Experiments. ed.; John Wiley & Sons, Inc.: 2017.

15. (a) Collins, M. S.; Phan, N.-M.; Zakharov, L. N.; Johnson, D. W. *Inorganic Chemistry* **2018,** 57, (7), 3486-3496; (b) Li, J.; Carnall, J. M. A.; Stuart, M. C. A.; Otto, S. *Angewandte Chemie International Edition* **2011,** 50, (36), 8384-8386; (c) Phan, N.-M.; Zakharov, L. N.; Johnson, D. W. *Chemical Communications* **2018,** 54, (95), 13419-13422.

16. Bertrand, P.; Bayle, F.; Combe, C.; Goeuriot, P.; Smurov, I. *Applied Surface Science* **2007,** 254, (4), 989-992.

17. Evoniuk, C. J.; Gomes, G. d. P.; Hill, S. P.; Fujita, S.; Hanson, K.; Alabugin, I. V. *Journal of the American Chemical Society* **2017,** 139, (45), 16210-16221.

Chapter III

1. Collins, M. S.; Shear, T. A.; Smith, E. K.; Strain, S. M.; Zakharov, L. N.; Johnson, D. W. *Chemistry – A European Journal* **2019,** 25, (58), 13290-13293.

2. (a) Brachvogel, R.-C.; Hampel, F.; von Delius, M. *Nature Communications* **2015,** 6, (1), 7129; (b) Brachvogel, R.-C.; von Delius, M. *Chemical Science* **2015,** 6, (2), 1399-1403; (c) Löw, H.; Mena-Osteritz, E.; von Delius, M. *Chemical Science* **2018,** 9, (21), 4785-4793; (d) Shyshov, O.; Brachvogel, R.-C.; Bachmann, T.; Srikantharajah, R.; Segets, D.; Hampel, F.; Puchta, R.; von Delius, M. *Angewandte Chemie International Edition* **2017,** 56, (3), 776-781.

3. (a) Black, S. P.; Sanders, J. K. M.; Stefankiewicz, A. R. *Chemical Society Reviews* **2014,** 43, (6), 1861-1872; (b) Carnes, M. E.; Collins, M. S.; Lindquist, N. R.; Guzmán-Percástegui, E.; Pluth, M. D.; Johnson, D. W. *Chemical Communications* **2014,** 50, (1), 73-75; (c) Kieran, A. L.; Bond, A. D.; Belenguer, A. M.; Sanders, J. K. M. *Chemical Communications* **2003**, (21), 2674-2675; (d) Otto, S.; Furlan, R. L. E.; Sanders, J. K. M. *Science* **2002,** 297, (5581), 590-593; (e) Rowan, S. J.; Cantrill, S. J.; Cousins, G. R. L.; Sanders, J. K. M.; Stoddart, J. F. *Angewandte Chemie International Edition* **2002,** 41, (6), 898-952; (f) West, K. R.; Bake, K. D.; Otto, S. *Organic Letters* **2005,** 7, (13), 2615-2618.

4. (a) GrÖBel, B.-T.; Seebach, D. *Synthesis* **1977,** 1977, (06), 357-402; (b) Seebach, D.; Geiß, K.-H.; Beck, A. K.; Graf, B.; Daum, H. *Chemische Berichte* **1972,** 105, (10), 3280-3300.

5. (a) Pascal, R. A.; Carter, M. L.; Johnson, M. R.; Ho, D. M. *Tetrahedron Letters* **1996,** 37, (45), 8125-8128; (b) Pascal, R. A.; Grossman, R. B. *The Journal of Organic Chemistry* **1987,** 52, (20), 4616-4617.

6. (a) Collins, M. S.; Carnes, M. E.; Nell, B. P.; Zakharov, L. N.; Johnson, D. W. *Nature Communications* **2016,** 7, 11052; (b) Collins, M. S.; Carnes, M. E.; Sather, A. C.; Berryman, O. B.; Zakharov, L. N.; Teat, S. J.; Johnson, D. W. *Chemical Communications* **2013,** 49, (59), 6599-6601.

7. Control experiments using benzyl mercaptan, $SbCl_3$ and I_2, in $CHBr_3$ solvent showed the reaction favors disulfide formation exclusively over thrithioorthoester, suggesting the cage formation provides a specific driving force for orthoester formation in this system.

8. (a) Valiulin, R. A.; Kutateladze, A. G. *The Journal of Organic Chemistry* **2008,** 73, (1), 335-338; (b) Tam, J. P.; Heath, W. F.; Merrifield, R. B. *Journal of the American Chemical Society* **1983,** 105, (21), 6442-6455; (c) Leriverend, C.; Metzner, P.; Capperucci, A.; Degl'Innocenti, A. *Tetrahedron* **1997,** 53, (4), 1323-1342.

9. Kay, E. R.; Leigh, D. A.; Zerbetto, F. *Angewandte Chemie International Edition* **2007,** 46, (1-2), 72-191.

Chapter IV

1. Fyfe, M. C. T.; Stoddart, J. F. *Accounts of Chemical Research* **1997,** 30, (10), 393-401.

2. Corbett, P. T.; Leclaire, J.; Vial, L.; West, K. R.; Wietor, J.-L.; Sanders, J. K. M.; Otto, S. *Chemical Reviews* **2006,** 106, (9), 3652-3711.

3. (a) Hu, L.; Schaufelberger, F.; Timmer, B. J. J.; Flos, M. A.; Ramström, O., Constitutional Dynamic Chemistry. In *Kirk-Othmer Encyclopedia of Chemical Technology*, ed.; pp 1-25; (b) Jin, Y.; Wang, Q.; Taynton, P.; Zhang, W. *Accounts of Chemical Research* **2014,** 47, (5), 1575-1586; (c) Rowan, S. J.; Cantrill, S. J.; Cousins, G. R. L.; Sanders, J. K. M.; Stoddart, J. F. *Angewandte Chemie International Edition* **2002,** 41, (6), 898-952.

4. Gorham, W. F. *Journal of Polymer Science Part A-1: Polymer Chemistry* **1966,** 4, (12), 3027-3039.

5. (a) Leung, D. H.; Fiedler, D.; Bergman, R. G.; Raymond, K. N. *Angewandte Chemie* **2004,** 116, (8), 981-984; (b) Zhang, M.; Xu, D.; Yan, X.; Chen, J.; Dong, S.; Zheng, B.; Huang, F. *Angewandte Chemie* **2012,** 124, (28), 7117-7121.

6. Yu, C.-Y.; Turner, M. L. *Angewandte Chemie* **2006,** 118, (46), 7961-7964.

7. (a) Collins, M. S.; Carnes, M. E.; Nell, B. P.; Zakharov, L. N.; Johnson, D. W. *Nature Communications* **2016,** 7, 11052; (b) Collins, M. S.; Phan, N.-M.; Zakharov, L. N.; Johnson, D. W. *Inorganic Chemistry* **2018,** 57, (7), 3486-3496; (c) Collins, M. S.; Shear, T. A.; Smith, E. K.; Strain, S. M.; Zakharov, L. N.; Johnson, D. W. *Chemistry – A European Journal* **2019,** 25, (58), 13290-13293.

8. (a) Phan, N.-M.; Zakharov, L. N.; Johnson, D. W. *Chemical Communications* **2018,** 54, (95), 13419-13422; (b) Shear, T. A.; Lin, F.; Zakharov, L. N.; Johnson, D. W. *Angewandte Chemie International Edition* **2020,** 59, (4), 1496-1500.

9. Montgomery, D. C., *Design and Analysis of Experiments*. ed.; John Wiley & Sons, Inc.: 2017.

10. Phan, N.-M.; Shear, T. A.; Zakharov, L. N.; Johnson, D. W. *European Journal of Organic Chemistry* n/a, (n/a).

11. (a) Allen, C. A.; Cangelosi, V. M.; Zakharov, L. N.; Johnson, D. W. *Crystal Growth and Design* **2009,** 9, (7), 3011-3013; (b) Cangelosi, V. M.; Pitt, M. A.; Vickaryous, W. J.; Allen, C. A.; Zakharov, L. N.; Johnson, D. W. *Crystal growth & design* **2010,** 10, (8), 3531-3536.

12. Carter, T. G.; Vickaryous, W. J.; Cangelosi, V. M.; Johnson, D. W. *Comments on Inorganic Chemistry* **2007,** 28, (3-4), 97-122.

13. (a) Fiedler, D.; Bergman, R. G.; Raymond, K. N. *Angewandte Chemie International Edition* **2006,** 45, (5), 745-748; (b) Ko, Y. H.; Kim, K.; Kang, J.-K.; Chun, H.; Lee, J. W.; Sakamoto, S.; Yamaguchi, K.; Fettinger, J. C.; Kim, K. *Journal of the American Chemical Society* **2004,** 126, (7), 1932-1933; (c) Ziegler, M.; Brumaghim, J. L.; Raymond, K. N. *Angewandte Chemie International Edition* **2000,** 39, (22), 4119-4121.

14. Bailey, T. S.; Henthorn, H. A.; Pluth, M. D. *Inorganic Chemistry* **2016,** 55, (24), 12618-12625.

15. Adams, R. D.; Perrin, J. L. *Journal of the American Chemical Society* **1999,** 121, (16), 3984-3991.

16. (a) Capozzi, G.; Lucchini, V.; Modena, G. *Reviews of Chemical Intermediates* **1979,** 2, (3), 347-375; (b) Capozzi, G.; Menichetti, S.; Nativi, C. *Encyclopedia of Reagents for Organic Synthesis* **2001**.

17. (a) Eglinton, G.; Lardy, I. A.; Raphael, R. A.; Sim, G. A. *Journal of the Chemical Society (Resumed)* **1964**, (0), 1154-1158; (b) Gleiter, R.; Rittinger, S.; Irngartinger, H. *Chemische Berichte* **1991,** 124, (2), 365-369.

Chapter V

1. Herbst, W.; Hunger, K., *Industrial organic pigments: production, properties, applications*. ed.; John Wiley & Sons: 2006.

2. Rajasingh, P.; Cohen, R.; Shirman, E.; Shimon, L. J.; Rybtchinski, B. *The Journal of organic chemistry* **2007,** 72, (16), 5973-5979.

3. Wu, J.; He, D.; Zhang, L.; Liu, Y.; Mo, X.; Lin, J.; Zhang, H.-j. *Organic letters* **2017,** 19, (19), 5438-5441.

4. Huang, C.; Barlow, S.; Marder, S. R. *The Journal of organic chemistry* **2011,** 76, (8), 2386-2407.

5. (a) Görl, D.; Zhang, X.; Würthner, F. *Angewandte Chemie International Edition* **2012,** 51, (26), 6328-6348; (b) Würthner, F.; Saha-Möller, C. R.; Fimmel, B.; Ogi, S.; Leowanawat, P.; Schmidt, D. *Chemical reviews* **2016,** 116, (3), 962-1052.

6. (a) Lang, E.; Würthner, F.; Köhler, J. *ChemPhysChem* **2005,** 6, (5), 935-941; (b) Yang, S. K.; Shi, X.; Park, S.; Doganay, S.; Ha, T.; Zimmerman, S. C. *Journal of the American Chemical Society* **2011,** 133, (26), 9964-9967; (c) Stöttinger, S.; Hinze, G.; Diezemann, G.; Oesterling, I.; Müllen, K.; Basché, T. *Nature nanotechnology* **2014,** 9, (3), 182.

7. (a) Vagnini, M. T.; Smeigh, A. L.; Blakemore, J. D.; Eaton, S. W.; Schley, N. D.; D'Souza, F.; Crabtree, R. H.; Brudvig, G. W.; Wasielewski, M. R. *Proceedings of the National Academy of Sciences* **2012,** 109, (39), 15651-15656; (b) Wasielewski, M. R. *Accounts of chemical research* **2009,** 42, (12), 1910-1921.

8. Eaton, S. W.; Shoer, L. E.; Karlen, S. D.; Dyar, S. M.; Margulies, E. A.; Veldkamp, B. S.; Ramanan, C.; Hartzler, D. A.; Savikhin, S.; Marks, T. J. *Journal of the American Chemical Society* **2013,** 135, (39), 14701-14712.

9. (a) Ramírez, M. G.; Pla, S.; Boj, P. G.; Villalvilla, J. M.; Quintana, J. A.; Díaz-García, M. A.; Fernández-Lázaro, F.; Sastre-Santos, Á. *Advanced Optical Materials* **2013,** 1, (12), 933-938; (b) Sadrai, M.; Bird, G. R. *Optics communications* **1984,** 51, (1), 62-64.

10. (a) Debije, M. G.; Verbunt, P. P. *Advanced Energy Materials* **2012,** 2, (1), 12-35; (b) Seybold, G.; Wagenblast, G. *Dyes and Pigments* **1989,** 11, (4), 303-317.

11. Langhals, H. *Heterocycles* **1995,** 1, (40), 477-500.
12. Wescott, L. D.; Mattern, D. L. *The Journal of organic chemistry* **2003,** 68, (26), 10058-10066.

13. Würthner, F. *Chemical communications* **2004**, (14), 1564-1579.

14. Ponnuswamy, N.; Cougnon, F. B. L.; Clough, J. M.; Pantoş, G. D.; Sanders, J. K. M. *Science* **2012,** 338, (6108), 783-785.

15. Huang, Y.; Yan, Y.; Smarsly, B. M.; Wei, Z.; Faul, C. F. *Journal of Materials Chemistry* **2009,** 19, (16), 2356-2362.

16. Huang, C. Perylene diimide-based materials for organic electronics and optical limiting applications. Georgia Institute of Technology, 2010.

17. Rogovik, V.; Gutnik, L. *Zhurnal Organicheskoi Khimii* **1988,** 24, (3), 635-639.

18. Würthner, F.; Stepanenko, V.; Chen, Z.; Saha-Möller, C. R.; Kocher, N.; Stalke, D. *The Journal of organic chemistry* **2004,** 69, (23), 7933-7939.

19. (a) Ahrens, M. J.; Fuller, M. J.; Wasielewski, M. R. *Chemistry of materials* **2003,** 15, (14), 2684-2686; (b) Boehm, A.; Arms, H.; Henning, G.; Blaschka, P. *Ger. Offen. DE* **1997,** 19547209; (c) de Craats, A. *Journal of Materials Chemistry* **2001,** 11, (7), 1789-1799; (d) Jones, B. A.; Ahrens, M. J.; Yoon, M. H.; Facchetti, A.; Marks, T. J.; Wasielewski, M. R. *Angewandte Chemie* **2004,** 116, (46), 6523-6526; (e) Zhao, Y.; Wasielewski, M. R. *Tetrahedron letters* **1999,** 40, (39), 7047-7050.

20. Qiu, W.; Chen, S.; Sun, X.; Liu, Y.; Zhu, D. *Organic letters* **2006,** 8, (5), 867-870.

21. Ball, M. L.; Zhang, B.; Xu, Q.; Paley, D. W.; Ritter, V. C.; Ng, F.; Steigerwald, M. L.; Nuckolls, C. *Journal of the American Chemical Society* **2018,** 140, (32), 10135-10139.

22. Weitz, R. T.; Amsharov, K.; Zschieschang, U.; Villas, E. B.; Goswami, D. K.; Burghard, M.; Dosch, H.; Jansen, M.; Kern, K.; Klauk, H. *Journal of the American Chemical Society* **2008,** 130, (14), 4637-4645.

23. An, Z.; Odom, S. A.; Kelley, R. F.; Huang, C.; Zhang, X.; Barlow, S.; Padilha, L. A.; Fu, J.; Webster, S.; Hagan, D. J. *The Journal of Physical Chemistry A* **2009,** 113, (19), 5585-5593.

24. Jones, B. A.; Facchetti, A.; Wasielewski, M. R.; Marks, T. J. *Journal of the American chemical society* **2007,** 129, (49), 15259-15278.

25. Ball, M.; Zhong, Y.; Fowler, B.; Zhang, B.; Li, P.; Etkin, G.; Paley, D. W.; Decatur, J.; Dalsania, A. K.; Li, H. *Journal of the American Chemical Society* **2016,** 138, (39), 12861-12867.

26. Barendt, T. A.; Myers, W. K.; Cornes, S. P.; Lebedeva, M. A.; Porfyrakis, K.; Marques, I.; Félix, V.; Beer, P. D. *Journal of the American Chemical Society* **2019,** 142, (1), 349-364.

27. (a) Collins, M. S.; Carnes, M. E.; Nell, B. P.; Zakharov, L. N.; Johnson, D. W. *Nature Communications* **2016,** 7, 11052; (b) Collins, M. S.; Carnes, M. E.; Sather, A. C.; Berryman, O. B.; Zakharov, L. N.; Teat, S. J.; Johnson, D. W. *Chemical Communications* **2013,** 49, (59), 6599-6601; (c) Phan, N. M.; Shear, T. A.;

Zakharov, L. N.; Johnson, D. W. *European Journal of Organic Chemistry* **2020,** 2020, (43), 6795-6800; (d) Shear, T. A.; Johnson, D. W. *Synlett*, (EFirst); (e) Shear, T. A.; Lin, F.; Zakharov, L. N.; Johnson, D. W. *Angewandte Chemie International Edition* **2020,** 59, (4), 1496-1500.

28. (a) Kota, R.; Samudrala, R.; Mattern, D. L. *The Journal of organic chemistry* **2012,** 77, (21), 9641-9651; (b) Wang, W.; Wang, L.; Palmer, B. J.; Exarhos, G. J.; Li, A. D. *Journal of the American Chemical Society* **2006,** 128, (34), 11150-11159; (c) Xu, B.; Xiao, X.; Yang, X.; Zang, L.; Tao, N. *Journal of the American Chemical Society* **2005,** 127, (8), 2386-2387.

29. Ball, M.; Fowler, B.; Li, P.; Joyce, L. A.; Li, F.; Liu, T.; Paley, D.; Zhong, Y.; Li, H.; Xiao, S. *Journal of the American Chemical Society* **2015,** 137, (31), 9982-9987.

30. Zheng, T.-C.; Burkart, M.; Richardson, D. E. *Tetrahedron Letters* **1999,** 40, (4), 603-606.

Chapter VI

1. Lees, W. J.; Whitesides, G. M. *The Journal of organic chemistry* **1993,** 58, (3), 642-647.

2. Bothe, M.; Orrillo, A. G.; Furlan, R. L.; von Delius, M. *Synlett* **2019,** 30, (17), 1988-1994.

3. Spenst, P.; Würthner, F. *Angewandte Chemie* **2015,** 127, (35), 10303-10306.